IDENTIFICATION OF WILD-TYPE KIRSTEN RAT SARCOMA (KRAS) AND ITS SIGNALLING PATHWAY IN IMMUNE EVASION IN HEPATOCELLULAR CARCINOMA

LEI MANG LENG

PhD

THE HONG KONG POLYTECHNIC UNIVERSITY

2024

The Hong Kong Polytechnic University
Department of Applied Biology and Chemical Technology

IDENTIFICATION OF WILD-TYPE KIRSTEN RAT SARCOMA (KRAS) AND ITS SIGNALLING PATHWAY IN IMMUNE EVASION IN HEPATOCELLULAR CARCINOMA

LEI MANG LENG

A thesis submitted in partial fulfilment of the requirements for the degree of Doctor of Philosophy

Oct 2023

CERTIFICATE OF ORIGINALITY

I hereby declare that this thesis is my own work and that, to the best of my knowledge and belief, it reproduces no material previously published or written, nor material that has been accepted for the award of any other degree or diploma, except where due acknowledgement has been made in the text.

_____(Signed)

LEI MANG LENG MARTINA (Name of Student)

Abstract

Hepatocellular carcinoma (HCC) is the third most lethal cancer and sixth most commonly diagnosed cancer worldwide. The landscape of advanced HCC treatments has been evolving rapidly in recent years. Systemic therapies have emerged from single-agent treatment combined with immune checkpoint inhibitors (ICIs) and molecular-targeted therapies such as atezolizumab-bevacizumab or durvalumab-tremelimumab. Although ICIs demonstrate tremendous promise for the treatment of HCC patients, their response rates are modest (~15%). This highlights the urgent need for identifying effective biomarkers to predict patient response. Therefore, understanding the immune evasive mechanism of HCC is urgently needed.

Increasing evidence indicates that oncogenic pathway activation is associated with generating an unfavourable tumour microenvironment with consequent immunotherapy resistance. Our study identified a critical oncogenic KRAS (Kirsten rat sarcoma viral oncogene homolog) signalling pathway involved in immune evasion in an antigen-expressing c-Myc^{OE} /Tp53^{KO} HCC mouse model by data-independent acquisition mass spectrometry (DIA-MS) proteomics. We identified that wild-type Kras was highly upregulated in immune-escaped tumours, with concurrent activation of its ligand-driven EGFR and its downstream MEK/ERK signalling. Likewise, endogenous Kras overexpression in this model led to an increase in tumour burden with shorter survival time of mice, implicating the regulatory role of KRAS signalling in immune evasion. Clinically, wild-type Kras was overexpressed in HCC at both mRNA and protein levels and associated with tumour recurrence and poorer patients' survival.

Using single-cell RNA sequencing (scRNA-seq) analysis, we demonstrated that wild-type KRAS hampered the recruitment of dendritic cells, leading to defective T-cell activity via suppression of the interferon (IFN) responses. Activation of KRAS/MEK/ERK signalling impaired HCC recognition by T cells via downregulation of major histocompatibility complex class I (MHC-I)-driven antigen presentation. To elucidate the underlying molecular mechanisms, we employed a novel *in vivo* CRISPR/Cas9 system targeting MEK1/2, a downstream effector of KRAS. MEK1/2 knockout reversed the immunosuppressive effects of wild-type KRAS, enhancing IFN responses, antigen presentation, and $CD8^+$ T cell recruitment.

Moreover, our study proposed a new combinational therapy targeting wild-type KRAS to enhance immunotherapy efficacy in HCC. The combination therapy involving the KRAS

inhibitor MRTX0902, MEK inhibitor trametinib, and anti-programmed cell death protein 1 (PD-1) treatment demonstrated increased intra-tumoral $CD8^+$ T cell infiltration and improved survival outcomes.

This data, together with the observation showing upregulation of this signalling pathway in PD-1-treated tumours, suggest a rational therapeutic strategy with a combination of KRAS inhibitor with ICIs.

(384 words)

Publications

1. **Lei MM**, Lee TK. Genetics: Gene expression (Encyclopedia of Gerontology and Population Aging, Springer Nature Switzerland AG 2019 D. Gu, M. E. Dupre (eds.)
2. **Lei MM**, Lee TK. Orchestrating the crosstalk between liver cancer cells and neutrophils via the CLCF1-mediated CXCL6/TGF-β axis. *Hepatology* 2021;73(5):1631-1633. (Impact Factor: 17.425)
3. **Lei MM**, Lee TK. Cancer stem cells: emerging key players in immune evasion of cancers. *Front Cell Dev Biol* 2021; 9: 692940. (Impact Factor: 6.684)
4. **Lei MM**[#], Leung CO[#], Lau EY#, Leung RW, Ma VW, Tong M, Lu YY, Huang CY, Zhu QH, Ng IO, Ma S, Lee TK. SCYL3, as a novel binding partner and regulator of ROCK2, promotes hepatocellular carcinoma progression. *JHep Rep* 2022;5(1):100604. (Impact Factor: 9.917)
5. Ho NP[#], Leung CO[#], Wong TL, Lau EY, **Lei MM**, Mok EH, Leung HW, Tong M, Ng IO, Yun JP, Ma S, Lee TK. The interplay of UBE2T and Mule in regulating Wnt/β-catenin activation to promote hepatocellular carcinoma progression. *Cell Death Dis* 2021;12(2):148. (Impact Factor: 8.469)
6. Leung HW[#], Lau EY[#], Leung CO, **Lei MM**, Mok EH, Ma V, Cho WC, Ng IO, Yun JP, Cai SH, Yu HJ, Ma S, Lee TK. NRF2/SHH signaling cascade promotes tumor-initiating cell lineage and drug resistance in hepatocellular carcinoma. *Cancer Lett* 2020; 476:48-56. (Impact Factor: 8.679)
7. Leung HW[#], Leung CO[#], Lau EY, Chung KPS, Mok EH, **Lei MM**, Leung RW, Tong M, Keng VW, Ma C, Zhao Q, Ng IO, Ma S, Lee TK. EPHB2 activates β-catenin to enhance cancer stem cell properties and drive sorafenib resistance in hepatocellular carcinoma. *Cancer Res* 2021;81(12): 3229-3240. (Impact Factor: 13.312)
8. Mok EH[#], Leung CO[#], Zhou L, **Lei MM**, Leung HW, Tong M, Wong TL, Lau EY, Ng IO, Ding J, Yun JP, Zhu HL, Lin CH, Yu J, Ma S, Lee TK. Caspase-3-induced SREBP2 activation drives drug resistance via promotion of cholesterol biosynthesis in hepatocellular carcinoma. *Cancer Res* 2022; 82 (17): 3102-3115. (Impact Factor: 13.312)
9. Leung CO, Yang Y, Leung RW, So KK, Guo HJ, **Lei MM**, Yun JP, Ma S, Zhao Q, Lee TK. Broad-spectrum kinome profiling identifies CDK6 upregulation as a driver of lenvatinib resistance in hepatocellular carcinoma. *Nat Commun* 2023;14(1):6699. (Impact Factor: 17.694)

Conference Presentations and Awards

1. ***ABCT Excellence Award 2023*** - Outstanding Postgraduate Student

2. **Lei MM**, Lee TK. 'Wild-type Kirsten rat Sarcoma (Kras) promotes immune escape via suppression of interferon-mediated immunity in Hepatocellular carcinoma.' The 13th Asia-Pacific Primary Liver Cancer Expert Meeting (APPLE), Seoul, Korea. 2023.
   This presentation was awarded the ***Young Investigator Award*** & ***Best Presentation Award*** (***The only awardee to receive both awards***).

3. **Lei MM**, Lee TK. 'Wild-type Kirsten rat Sarcoma (Kras) promotes immune escape via suppression of interferon-mediated immunity in Hepatocellular carcinoma.' PolyU Research Student Conference (PRSC), PolyU. 2023.
   This presentation was awarded the ***Best Presentation Award.***

4. **Lei MM**, Lee TK. 'Wild-type Kirsten rat Sarcoma (Kras) promotes immune escape via suppression of interferon-mediated immunity in Hepatocellular carcinoma.' 3rd ABCT Research Postgraduate Symposium in the Biology Discipline, PolyU
   This presentation was awarded the ***Best Oral Presentation Award.***

5. **Lei MM**, Leung CO, Ng IO, Lee TK. 'Overexpression of SCY1 Like Pseudokinase 3 (SCYL3) promotes tumor growth and metastasis via regulation of ROCK2 stability in hepatocellular carcinoma.' The 31st Conference of the Asian Pacific Association for the Study of the Liver (APASL), Coex, Seoul, Korea. 2022.
   This presentation was awarded the ***Travel Award.***

Scholarships

1. ***Higher Education (Merit scholarship)***, Education and Youth Development Bureau, Macau

2. Tigris Educational Fund 2023 - ***Graduate Student Travel Scholarship Award***, Tech Dragon Limited, Hong Kong

Acknowledgements

First and foremost, I would like to express my deepest gratitude to my supervisor, Prof. Terence Lee Kin Wah for his invaluable guidance and support throughout these four years. I am incredibly thankful for all the opportunities and trust he has placed in me since my very first day in this lab. His visionary mindset inspires me to confront challenges with curiosity and embrace the excitement of venturing into unchartered research topics. Despite his demanding schedule, he consistently responds to everyone's requests, offering timely and insightful guidance that gently nudges me back on track when I go too far. This delicate balance has fostered an environment of both independence and structured learning progress that I believe few postgraduates can have the privilege to experience. Your belief in my potential, the freedom to explore, and your courage in pushing the boundaries of research have left an indelible mark on my academic experience. Thank you for everything.

Special thanks to Prof. Stephanie Ma for her insightful advice and assistance, especially during the COVID-19 pandemic. Your dedication to your work has been a true inspiration, serving as a role model for me.

To Dr. Carmen Leung Oi Ning, thank you for taking care of all of us throughout these years and providing assistance when I needed it the most. Your encouragement and support have been a constant source of strength to me, making me feel safe. I genuinely hope that you achieve the aspirations you have set for yourself soon.

To my past and present labmates, Dr. Sherry Wu, Dr. Sara Ying, Dr. Huihai Yang, Dr. Shakeel Khan, Dr. Nicole Ho, Dr. Doris Leung, Dr. Etienne Mok, and Ms. Wing Ki Chau, for the cherished time spent together in the lab and things that I learnt from each of you. My night buddies, Ms. Rainbow Leung, Ms. Catherine Gu, Ms Candy Chu, Mr. Gregory Kenneth Muliawan and Ms. Mandy Chan, much appreciated for your warmest support and tolerance of my occasional bouts of craziness at the lab.

I would like to extend my sincere thanks to Dr. Heidi Ling and Mr. Nikolas Teo for their collaboration and shared dedication to advance our research. To Dr. Sirius Tse, Dr. So Pui Kin and other SOs for their valuable technical support on this project. Their contributions have enriched the depth and scope of this project. To Dr. Kwan Ho Tang, Dr. Carol Tong, Dr.

Johnson Ng, Dr. Eric Wong and Mr. Victor Ma for their generous knowledge sharing. To Ms Peggy Kwok, an incredibly helpful and experienced administrative staff in the department, for rescuing me from administrative work.

Lastly, I am deeply grateful for the endless support from my family and friends. Thank you for my parents' unconditional love in my whole life, and I love you beyond words. Many thanks to Dr. Bai Jin for her mentorship and guidance since my FYP project. Thank you, Stephanie, Angela, Candy and David for sending positive vibes to me, especially since I started my PhD. **Dr-to-be Katherine Chung** (in return to your salute) and Dr-to-be Thomas Lam, thank you for always listening to my 'daily' random ideas and having my back. I wish you two a fruitful and unforgettable postgraduate experience.

Thank you, C57BL/6!

This PhD journey is definitely challenging but rewarding. I am so blessed to have you all along with me. Thank you!

Table of Contents

List of Figures

List of Tables

List of Abbreviations

AASLD	American Association for the Study of Liver Diseases
AAV	Adeno-associated virus vectors
ALB	Albumin
APC	Antigen-presenting cell
APM	Antigen processing and presenting machinery
AREG	Amphiregulin
ARG1	Arginase 1
B2M	β2-microglobulin
BCLC	Barcelona Clinic Liver Cancer
B.I.D.	Bis in die; twice a day
BLAST	Basic Local Alignment Search Tool
CAF	Cancer-associated fibroblast
CAR-T	Chimeric antigen retrieval T cell
CCDNA	Covalently closed DNA
CCL	C-C motif chemokine ligand
CCND1	Cyclin D1
CDS	Coding Sequence
CRISPR	Clustered Regularly Interspaced Short Palindromic Repeats
CTL	Cytotoxic T cell
CTLA-4	Cytotoxic T lymphocyte–associated antigen 4
CTNNB1	β-catenin
CXCL	Chemokine (C-X-C motif) ligand
DAA	Direct-acting antiviral therapy
DAMP	Damage-associated molecular pattern
DC	Dendritic cell
DCR	Disease control rate
DDA	Data-dependent acquisition
DEG	Differentially expressed genes
DIA	Data-independent acquisition
DMEM	Dulbecco's Modified Eagle Medium
DUSP6	Dual-specificity phosphatase 6

EASL	European Association for the Study of the Liver
EGF	Epidermal growth factor
EGFR	Epidermal growth factor receptor
EPGN	Epithelial mitogen
EREG	Epiregulin
ERK	Extracellular signal-regulated kinase
FC	Fold Change
FDR	False discovery rate
FGFR	Fibroblast growth factor receptor
FN1	Fibronectin 1
GAP	GTPase-activating proteins
GATM	Glycine Amidinotransferase
GDC	Genomic Data Commons
GDP	Guanosine diphosphate
GEF	Guanine nucleotide exchange factor
GSEA	Gene Set Enrichment Analysis
GTP	Guanosine triphosphate
HB-EGF	Heparin-binding EGF like-growth factor
HBV	Hepatitis B virus
HCC	Hepatocellular carcinoma
HCD	High collision dissociation
HCV	Hepatitis C virus
HDV	Hepatitis D virus
HLA	Human leukocyte antigen
HRAS	Harvey-RAS
HTVI	Hydrodynamic tail vail injection
ICGC	International Cancer Genome Consortium
ICI	Immune checkpoint inhibitor
IDO	Indoleamine 2,3-dioxygenase
IFN	Interferon
IFN-γ	Interferon-gamma
IHC	Immunohistochemistry

IL	Interleukin
IP	Intraperitoneal
IRF	Interferon-regulatory factor
ISG	Interferon-stimulated gene
ISRE	Interferon-stimulated response element
IV	Intravenous
KC	Kupffer cell
KRAS	Kirsten rat sarcoma viral oncogene homolog
LAG-3	Lymphocyte-activation gene 3
LC-MS/MS	Liquid chromatography with tandem mass spectrometry
LPS	Lipopolysaccharide
MS	Mass spectrometry
MAMP	Microbial-associated molecular pattern
MDSC	Myeloid-derived suppressor cell
MEK	Mitogen-activated protein kinase kinase
MELD	Model for End-Stage Liver Disease
MHC	Major histocompatibility complex
MICA/B	MHC-I chain-related molecules A/B
MLL4	Mixed-lineage leukaemia 4
MWA	Microwave ablation
NAFLD	Non-alcoholic fatty liver disease
NASH	Non-alcoholic steatohepatitis
NES	Normalised enrichment score
NF-κB	Nuclear factor kappa-light-chain-enhancer of activated B cells
NGS	Next-generation sequencing
NK cell	Natural killer cell
NKT cell	Natural killer T cell
NLRC5	NLR Family CARD Domain Containing 5
NRAS	Neuroblastoma-RAS
NTC	Non-targeting control
ORR	Overall response rate
OVA	Ovalbumin

PC	Principal Component
PCA	Principal Component Analysis
PD-1	Programmed cell death protein 1
pDC	Plasmacytoid dendritic cells
PDGFR	Platelet-derived growth factor receptor
PD-L1	Programmed death-ligand 1
PEI	Percutaneous ethanol injection
PFS	Progression free survival
PMH	Primary mouse hepatocytes
Q.D.	Quater in die; every day
QPCR	Quantitative PCR
RAS	Rat sarcoma virus
RET	Rearranged during transfection
RFA	Radiofrequency ablation
RNA	Ribonucleic acid
ROS	Reactive oxygen species
RPMI1640	Roswell Park Memorial Institute 1640 Medium
RTK	Receptor Tyrosine Kinase
scRNA-seq	Single-cell RNA sequencing
SDS-PAGE	SDS- polyacrylamide gel electrophoresis
sgRNA	Single guide RNA
SIN	SIINFEKL
SIY	SIYRYYGL
SOS	Son of Sevenless homolog
STAT	Signal transducer and activator of transcription
STRIDE	Single Tremelimumab Regular Interval Durvalumab
SYT12	Synaptotagmin-12
TAA	Tumour-associated antigens
TACE	Transarterial chemoembolisation
TALEN	Transcription activator-like effector nuclease
TAM	Tumour-associated macrophage
TAP	Transporters associated with antigen processing

TCGA	The Cancer Genome Atlas
TCR	T cell receptor
TERT	Telomerase reverse transcriptase
TGF	Transforming growth factor
TIGIT	T cell immunoreceptors with immunoglobulin and ITIM domains
Th cell	T helper cell
TIM-3	T cell immunoglobulin domain and mucin domain 3
TIME	Tumour immune microenvironment
T.I.W.	three times per week
TLR4	Toll-like receptor 4
TNF-α	Tumour necrosis factor-α
Tp53	Tumour protein p53
Treg	Regulatory T cell
VEGF	Vascular endothelial growth factor
VEGFR	Vascular endothelial growth factor receptor
ZFN	Zinc finger nuclease
γδ T cell	Gamma delta T cell

Chapter 1. Introduction

1.1 Hepatocellular carcinoma (HCC)

The liver is an essential metabolic organ with a remarkable regenerative ability to sustain tissue homeostasis. In addition to modulating carbohydrate, protein, and lipid metabolism, the liver also removes waste products via bile production. Hepatocellular carcinoma (HCC) is the most common type of liver cancer worldwide. It accounts for 75-85% of primary liver cancers, 90% of which are associated with cirrhosis. When HCC develops, the liver fails to regenerate fully, and aberrant liver tissues are not eliminated.

1.1.1 Epidemiology of HCC

HCC is the third leading cause of malignancy-related mortality (8.3%) and the sixth most commonly diagnosed cancer worldwide. The incidence of HCC is the highest in Eastern Asia, South-Eastern Asia, and Western Africa (Figure 1.1). With regard to gender, the incidence and fatality rates of men are 2–3 times higher than those of women, with the highest prevalence in the 45–60 years age group (Sung et al., 2021). In terms of global incidence, there are around 850,000 newly diagnosed HCC cases and over 830,000 deaths annually (Figure 1.2). The prevalence of HCC in greater China alone accounts for about 50% and 45% of the global new liver cancer cases and related deaths, respectively (Zou et al., 2022). In Hong Kong, liver cancer is the third most lethal cancer (1530 reported cases), accounting for 10.3% of all cancer-related deaths (Census and Statistics Department, 2022). A report from the International Agency for Research on Cancer (2020) predicted that there would be more than a million cases of HCC by 2025.

Globally, Asian, elderly, and male populations are at the highest risk of HCC. However, the epidemiology of HCC is changing progressively. In recent years, the success of hepatitis B virus (HBV) vaccination and hepatitis C virus (HCV) antiviral treatment has resulted in a 20% decrease in the incidence rate and reduced mortality rate in ‘traditional’ high-risk areas, including Eastern Asia and Southeast Asia. Nevertheless, the prevalence of HCC and its related deaths in European and North American countries are consistently increasing. This can be attributed to the rapid development of non-alcoholic fatty liver disease (NAFLD) and non-alcoholic steatohepatitis (NASH) due to high fat and sugar intake in dietary habits. HBV-related HCC, which is prevalent in China, belongs to the proliferative subclass with poor differentiation and highly aggressive features. In contrast, HCV-, alcoholic-, and NASH-

associated HCCs in the West are characterised by moderate to well-differentiated cancers with low levels of vascular invasion.

The prognosis of HCC is poor, and most cases are detected at an advanced stage, resulting in high morbidity and mortality rates (Golabi et al., 2017). According to the BRIDGE study, approximately 9% and 55% of HCC cases in China were diagnosed at intermediate and advanced stages, respectively. In North America, 14% and 12% of patients were diagnosed at intermediate and advanced stages, respectively.

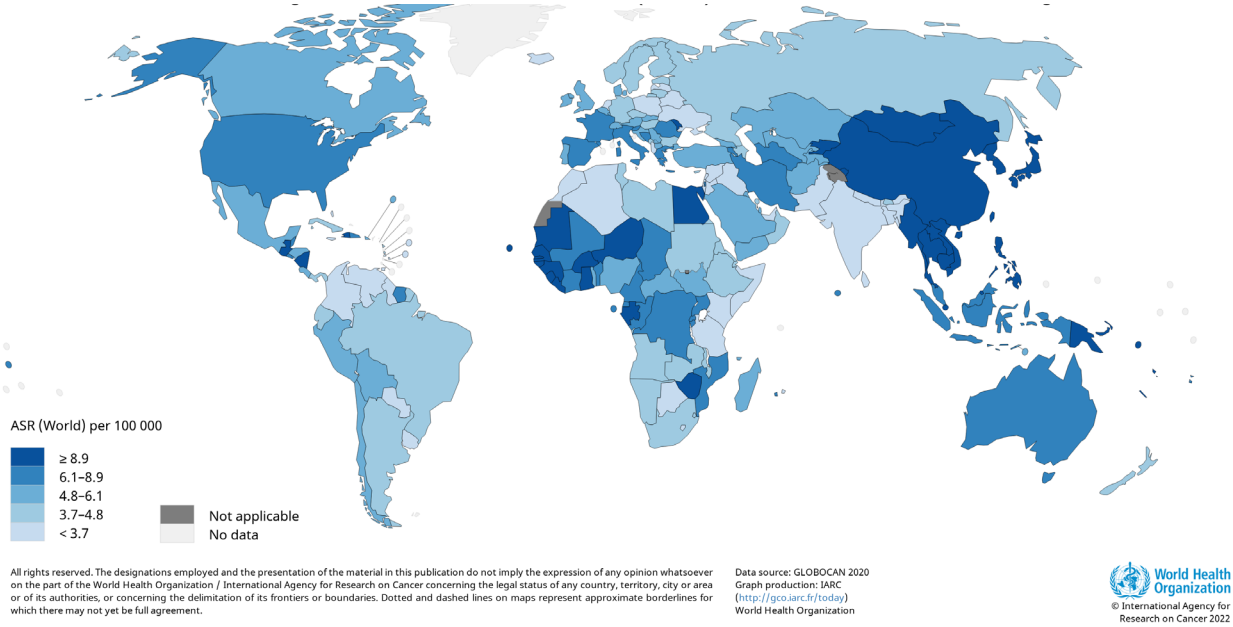

Figure 1.1 Global age-adjusted incidence rate of liver cancer in 2020. (W.H.O., 2020). Graph production: International Agency for Research on Cancer, World Health Organization.

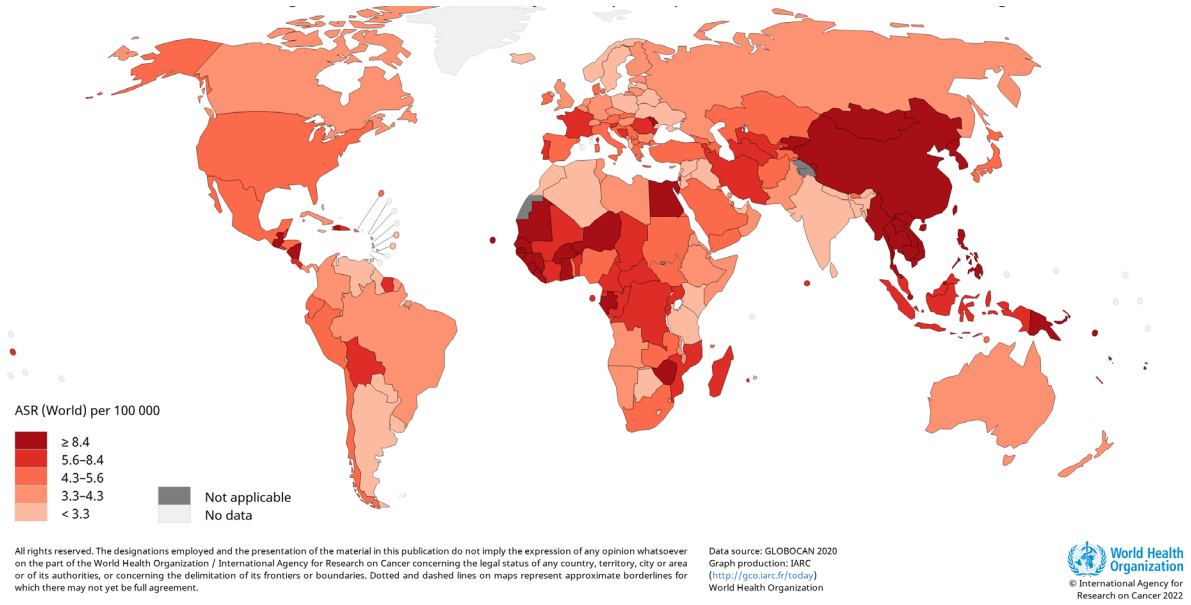

Figure 1.2 Global age-adjusted mortality rate of liver cancer in 2020. (W.H.O., 2020). Graph production: International Agency for Research on Cancer, World Health Organization.

1.1.2 Aetiology of HCC

Most cases of HCC arise from cirrhosis and chronic inflammation. The risk factors for HCC can be classified into four main categories: chronic viral infection, chemical exposure, metabolic syndrome, and chronic liver disease. Although the contribution of risk factors varies among regions, HBV and HCV remain dominant risk factors for HCC. Alcoholic- and NASH-related HCCs are becoming progressive risk factors for developing late-stage HCC. NAFLD is a growing risk factor, affecting 25% of the global population, particularly in Western countries. NAFLD is currently the leading cause of cirrhosis in the United States. About 20%-30% of NAFLD proceeds to NASH. The global incidence of NASH-associated HCCs surpasses that of HCV-related HCCs (25% versus 2.8%; Huang, El-Serag, & Loomba, 2021). Other risk factors for HCC include aflatoxin B1 intake, alcohol abuse, aristolochic acid exposure, diabetes mellitus, and tobacco use (Mohammadian et al., 2018).

1.1.2.1 Chronic viral infection

Chronic HBV, HCV, and hepatitis D (HDV) infections are the leading causes of HCC. Chronic hepatic viral infection disrupts the host immune system and promotes HCC progression via chronic inflammation, oxidative stress induction, and dysregulation of oncogenic signalling pathways. Chronic inflammation produces reactive oxygen species (ROS) and proinflammatory cytokines, which damage liver cells at genetic and metabolic levels, resulting in cell death. Repeated cell death and regeneration cycles increase the chance of chromosomal

instability and genetic mutations in hepatocytes, such as Telomerase reverse transcriptase (*TERT*) and β-catenin (*CTNNB1*), leading to HCC tumorigenesis. Viral proteins also activate cell signalling pathways that mediate cell growth and division and inhibit tumour suppressor genes and cell cycle checkpoints such as Tumour protein P53 (*TP53*) and retinoblastoma protein. The most commonly dysregulated oncogenic signalling pathways include Nuclear factor kappa-light-chain-enhancer of activated B cells (NF-κB), Wnt/β-catenin, RAF/MEK/ERK, and PI3K/AKT/mTOR pathways.

1.1.2.2 Hepatitis B virus (HBV)

HBV is a DNA virus transmitted vertically or through exposure to infectious blood or body fluids. This can result in both acute and chronic infections. Chronic HBV infection contributes to approximately 272,000 cases of HCC and 265,000 deaths. Approximately 3.5% of the global population is infected with HBV, with a high prevalence in Eastern and South-Eastern Asia. The lifetime risk of developing HCC in HBV carriers is 10 to 100-fold greater than that in non-infected individuals, approximately 9.6% and 60.2% for HBV carriers with positive HBsAg and double positivity for HBsAg and HBeAg, respectively.

HBV primarily affects the liver by integrating hepatitis B covalently closed DNA (ccDNA) into the host hepatocyte genome and replication, leading to liver damage, fibrosis, and cirrhosis. The principal mechanisms of HBV DNA integration in HCC progression include oncogene activation, dysregulation of tumour suppressor genes, production of truncated HBV proteins, and induction of chromosomal instability. The most frequently affected chromosomes include chromosomes 8p11, 10, and 17. Additionally, HBV integration can cause various genomic alterations in the early and late stages of HCC. Whole genome sequencing revealed that Synaptotagmin-12 (*SYT12*), Glycine Amidinotransferase (*GATM*), and Fibronectin 1 (*FN1*) are recurrent hotspots of early onset HBV-related HCCs, while Signal transducer and activator of transcription 1 (*STAT1*), Albumin (*ALB*), Mixed-lineage leukaemia 4 (*MLL4*), and *TERT* are commonly involved in the late-onset group (Yan et al., 2015). Cofactors, including demographic characteristics, viral infections, and environmental conditions such as aflatoxin exposure, diabetes, and obesity, also increase the risk of development among HBV carriers (El-Serag, 2012).

In recent decades, the incidence rates of HBV infection and associated HCC cases have been alleviated owing to the success of universal HBV vaccination of newborns and effective

treatment (Lin & Kao, 2021). The WHO has established a global target of a 90% vaccination rate to eradicate hepatitis B by 2030 (World Health Organisation., 2020). High-risk countries, including China, Mongolia, and Vietnam, have achieved >90% coverage of the HBV vaccination by 2020. In China, the Shanghai Hepatitis B Immunization Program has achieved great success, reducing HCC prevalence by 49.2% and 51.9% in males and females respectively (Yu et al., 2022). These findings prove that universal HBV vaccination in newborns is feasible with high coverage rates and effectively prevents both HBV infection and HCC in populations.

1.1.2.3 Hepatitis C virus (HCV)

HCV is a hepatotropic ribonucleic acid (RNA) virus. Hepatitis C affects approximately 1% of the global population, with a high prevalence in Northern America and Europe (Sun et al., 2021). Moreover, about 90 % of HCV-associated HCCs are preceded by liver cirrhosis, a risk factor for HCC progression (Gallage et al., 2021). Unlike HBV, HCV does not integrate into the host genome. The primary mechanisms of HCV in carcinogenesis involve persistent inflammation; dysregulation of mitogenic, angiogenic, and metastatic pathways; oxidative stress induction, and aberrant lipid metabolism. Currently, no vaccine is available for HCV. The introduction of direct-acting antiviral therapy (DAA) has altered the scenario of HCV-associated HCC. A sustained virologic response rate of over 90 % in DAA-treated HCV carriers reflects the effective eradication of HCV and is associated with a significant decline in the risk of HCC. Kanwal et al. (2017) reported that patients who developed sustained virologic response after receiving DAA, regardless of the cirrhotic background, are associated with a reduced risk for HCC compared to those who did not (0.9 vs 3.4 HCC per 100 person-years). However, the risk of HCC remains high in patients with advanced cirrhosis after DAA therapy and consistent HCC surveillance is required.

1.1.3 Molecular classification of HCC

HCC progression from cirrhosis involves a step-wise accumulation of somatic mutations and copy number variations in driver genes. Recent advances in next-generation sequencing (NGS) have enabled researchers to analyse genomes and identify driver gene mutations in HCC (Figure 1.3). The primary driver alterations can be categorised into telomere maintenance (*TERT*), cell cycle regulation (*TP53, CDKNA2, CCND1*), Wnt/β-catenin pathway (*CTNNB1, AXIN1*), RTK/RAS/ERK, and PI3K/AKT/mTOR pathways (*FGF19, VEGFA, RPS6KA3, PIK3CA, KRAS, NRAS*), oxidative stress (*NFE2L2, KEAP1*), and epigenetic modification

(*ARID1A, ARID2*). The most common driver gene is the reactivation of *TERT*, specifically in its promoter region, which is observed in approximately 60% of early HCC cases. In addition, some tumours show aberrant activation of the transforming growth factor-β (TGF-β) pathway or inactivating mutations in TGF-β related genes such as *SPTBN1*.

HCC was classified into 'proliferative' and 'non-proliferative' classes based on genetic, epigenetic and phenotypic properties. The proliferative class (~50%) is associated with poorer differentiation, aggressive tumours, frequent vascular invasion, and poor clinical outcomes. It is characterised by HBV aetiology and the activation of RTK/RAS/ERK, PI3K/AKT/mTOR, MET signalling, and chromosomal instability. The non-proliferative class (~50%) is associated with alcohol- or HCV-related HCC and comprises less aggressive, heterogeneous, and moderately differentiated tumours. Recent classifications by The Cancer Genome Atlas (TCGA) network further divided the molecular landscape into three integrative clusters: iCluster 1 and iCluster 3, representing two subclasses of the proliferative class, and iCluster 2, which belongs to the non-proliferative class. iCluster 1 demonstrated stem cell and progenitor markers like *EPCAM*. iCluster 3 was featured with *TP53* mutation and activation of Wnt/TGF-β signalling transduction. iCluster 2 showed a higher frequency of TERT promoter mutations and activation of Wnt/β-catenin signalling.

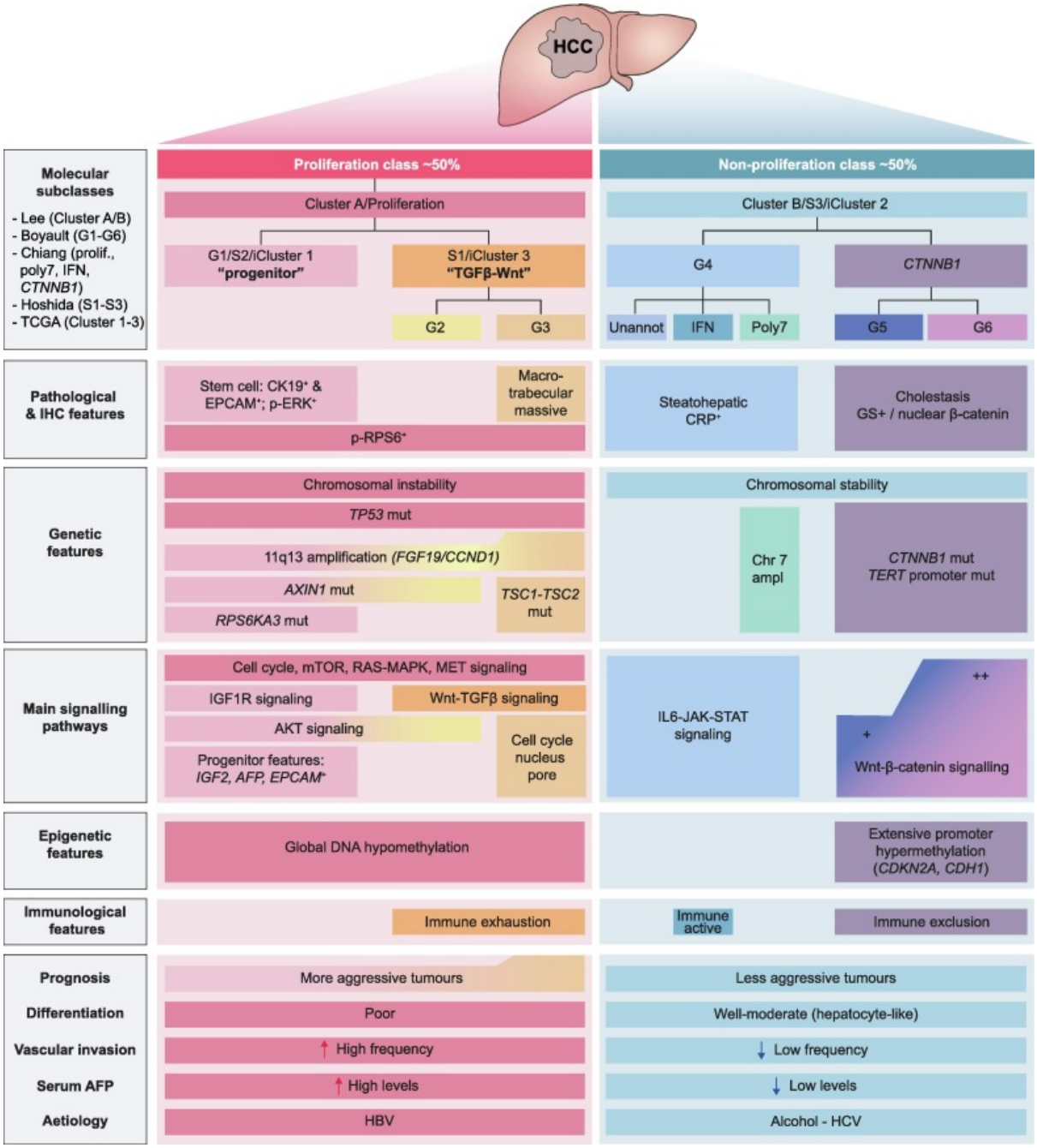

Figure 1.3 Molecular classification of HCC. (Rebouissou & Nault, 2020)

1.1.4 Treatment regimens for HCC

HCC is characterised by high heterogeneity in genetic, epigenetic, histopathological and immunological levels and the therapeutic options for HCC patients are determined by the tumour characteristics (Gallage et al., 2021). The Barcelona Clinic Liver Cancer (BCLC) staging system is considered a standard clinical staging system. It has been endorsed by the American Association for the Study of Liver Diseases (AASLD) and the European Association for the Study of the Liver (EASL). The BCLC staging system incorporates the size and number of tumours, liver function and patient performance status. HCC patients were classified into five stages: BCLC stage 0 to D with specific algorithms to guide treatment decisions.

Recently, the new 2022 BCLC strategy was updated in accordance with the advances in HCC treatment (Figure 1.4). These updates include the stratification of the heterogeneous BCLC-B group, the introduction of new immunotherapy options as the first-line treatment for patients with BCLC-C, and the consideration of liver transplant for individuals meeting the local extended liver transplant criteria or after successful downstaging with transarterial chemoembolisation (TACE). The concept of treatment-stage migration has also been introduced, which suggests the consideration of treatment for a more advanced stage when first-line treatment is not feasible due to patient profile or disease progression.

The most effective curative treatment for HCC is available when the disease is detected early. According to the staging system, resection, liver transplantation, and local ablation are the standard treatments for patients with Stage A HCC. However, liver cancer is often asymptomatic or lacks obvious symptoms, leading to late-stage diagnosis. Additionally, the 5-year recurrence rate of HCC patients after resection is about 70%, while most HCC relapses result in a more advanced tumour stage (Lacaze & Scotté, 2015). Patients at the intermediate stage (Stage B) preferentially receive TACE as first-line treatment. Systemic therapies are administered to intermediate- and advanced-stage HCCs (Stage C). In recent years, systemic therapies have emerged from single-agent treatment to combining immune checkpoint inhibitors with molecular-targeted therapies. Sorafenib remained the primary first-line treatment for advanced HCCs for the past decade. In 2020, the FDA approved a combination of atezolizumab and bevacizumab (targeting Programmed death-ligand 1; PD-L1 and Vascular endothelial growth factor; VEGF) for patients with advanced HCC without systemic therapy experience. Recently, the HIMALAYA trial demonstrated the superiority of Single Tremelimumab Regular Interval Durvalumab (STRIDE) regimen over sorafenib, providing a

new and promising first-line treatment option. In this section, the currently available treatments and limitations are discussed.

1.1.4.1 Hepatic resection

Hepatectomy remains the standard treatment for patients with resectable HCC (BCLC: Early stage A). The criteria for liver resection depend on the quality of the underlying liver parenchyma and the extent of resection. Liver resection is recommended for patients with a single tumour, a tumour size of less than 3 cm and no cirrhotic background. The subsequent 5-year survival rate of patients undergoing liver resection can be as high as 70%. The perioperative death after liver resection is lower than 5%, yet the risk of liver decompensation ranges from 10% to 12%. Liver decompensation can be predicted by the extent of hepatectomy, portal hypertension and the Model for End-Stage Liver Disease (MELD) score >9. The latest EASL guidelines did not exclude surgery for patients with portal hypertension if the patient has a MELD score <9, but emphasised a higher risk of liver decompensation and associated mortality. However, the recurrence rate of HCC within five consecutive years is about 70%.

1.1.4.2 Liver transplantation

Liver transplantation provides the best long-term benefits for patients, with a 5-year survival rate of over 70% and a recurrence rate of less than 10%. It enables the removal of both detectable and undetectable intrahepatic lesions while simultaneously addressing the underlying liver disease. Thus, liver transplantation offers a better choice of treatment over liver resection. However, liver transplantation is limited by the supply of available organs, the need for immunosuppression over a lifetime, and the high dropout rates of patients awaiting available transplants. The Milan criteria, published in 1996, defined the standard of liver transplantation as patients with a single tumour <5 cm or 3 cm in diameter at most or up to three lesions. Downstaging therapies, such as locoregional or systemic therapies, have been suggested to reduce the patient's tumour burden to fit the Milan criteria. The successful rates of downstaging treatments range from 24% to 90%, yet generate significant posttransplant outcomes with low recurrence rates. Therefore, the 2022 BCLC guidelines updated the suggestion of liver transplant for BCLC-B HCC patients who met the Milan criteria after receiving downstaging treatments.

1.1.4.3 Local ablation treatment

For early-stage patients who are not eligible for resection or liver transplantation, ablation treatment is the standard approach. Ablation induces tumour necrosis through radiofrequency ablation (RFA), microwave ablation (MWA) or percutaneous ethanol injection (PEI). Although RFA remains the first-line technique for ablation with an over 90% complete response, MWA is now replacing RFA due to its ability to ablate larger lesions ranging from 3 to 5 cm. Ablation is the recommended treatment choice for individuals with very early-stage HCC (solitary HCC <2 cm) and Child-Pugh stage A liver disease who are unsuitable candidates for liver transplantation. Studies have shown that ablation can result in a long-term survival comparable to that of surgical resection. For patients with multinodular early-stage HCC (<3 nodules, all <3 cm) and who cannot receive liver transplants, the latest BCLC guidelines recommended ablation over resection.

1.1.4.4 Transarterial chemoembolisation (TACE)

Arterial-directed therapies targeting the tumour blood vessels derived from the hepatic artery have become the primary treatment for intermediate-stage BCLC-B patients with multiple nodules. TACE is recommended among individuals with no angiogenic and metastatic HCC. TACE combines chemotherapeutic drugs such as doxorubicin and radio-opaque agent Lipiodol or drug-eluting beads to block the tumour blood supply from the hepatic artery and facilitate the drug delivery to the tumour site. The survival benefits of TACE and drug-eluting beads-TACE treatment can be achieved up to over 28 and 44 months respectively.

1.1.4.5 Systemic therapy

HCC is characterised by its heterogeneity and numerous genomic alterations affecting multiple signalling pathways, including Wnt/β-catenin, Sonic hedgehog, Notch, RAF/MEK/ERK, PI3K/AKT/mTOR, and VEGF signalling. Targeting these aberrant molecular activations has demonstrated therapeutic benefits in patients with HCC.

Sorafenib has stood as the sole effective systemic therapy for advanced HCC (BCLC-C group) since its first launch in 2007. Nevertheless, sorafenib offers only marginal improvements in survival compared to the best supportive care. Patients with advanced HCC still experience poor survival rates (<15% with a five-year survival rate; Wang & Li, 2019). In recent years, significant advances in the development and approval of new systemic therapies have changed

the systemic treatment landscape of advanced HCC, providing numerous options for first- and second-line therapies. The 2022 BCLC guidelines updated the first-line treatment with the combined use of atezolizumab and bevacizumab, as well as durvalumab-tremelimumab, in front of the use of sorafenib or lenvatinib if feasible. Currently approved second-line therapies, such as regorafenib, cabozantinib, ramucirumab, and a combination of nivolumab and ipilimumab, have been explicitly assessed in patients with prior sorafenib treatment. When the second-line and combinational therapies fail to cure the tumour, clinical trials of the potential therapeutic targets are recommended. Regrettably, supportive care from family and friends remains the sole treatment option for patients with terminal HCC.

1.1.4.5.1 Atezolizumab and bevacizumab

In the 2022 BCLC guidelines, atezolizumab (anti-PD-L1) and bevacizumab (anti-VEGF) became the standard of first-line treatment for advanced HCCs with no prior systemic therapy. This was the first combinational treatment of molecular-targeted drugs and immunotherapy approved by the FDA. In the IMBrave150 clinical trial, atezolizumab and bevacizumab offered better progression-free (6.8 months versus 4.3 months for sorafenib) and overall survival benefits (67.2% versus 54.6% of overall survival rate at 12 months; Finn et al., 2020). Moreover, analyses comparing the IMbrave150 and HIMALAYA trials indicated that atezolizumab-bevacizumab showed a better overall response rate (29.8% vs 20.1%) and less risk of related mortality (34% vs 22%) than durvalumab-tremelimumab when compared to sorafenib.

1.1.4.5.2 Durvalumab and Tremelimumab

Durvalumab (anti-PD-L1) and tremelimumab (anti-cytotoxic T lymphocyte–associated antigen 4; CTLA-4) were approved by the FDA after the combinational immune checkpoint inhibitors (ICIs) showed a superior outcome over sorafenib (overall survival 16.4 months vs 13.8 months). In the phase III HIMALAYA trial, the STRIDE regimen was adopted to treat 782 patients with advanced HCCs. This regimen enables tremelimumab to induce the proliferation of $CD4^+$ and $CD8^+$ T cells, thereby increasing the effectiveness of subsequent PD-L1 inhibition by durvalumab. A remarkable 36-month overall survival rate was achieved in 30.7% of patients. Patients who followed the STRIDE regimen developed fewer grade 3-4 adverse events than those who received sorafenib (25.8% vs. 36.9%). Durvalumab was also evaluated as a single-agent therapy in the trial and demonstrated no inferior survival outcome compared to sorafenib.

In addition, the STRIDE regimen offers an alternative for those who are ineligible for atezolizumab-bevacizumab.

1.1.4.5.3 Sorafenib

Sorafenib was the initial FDA-approved multi-kinase inhibitor, among several others, used to treat advanced-stage HCC since 2007. It is an orally active multi-kinase inhibitor, that effectively targets Receptor Tyrosine Kinase (RTK) receptors, for example, vascular endothelial growth factor receptor (VEGFR), platelet-derived growth factor receptor (PDGFR), and drivers of cell proliferation, such as RAF kinase. In the SHARP trial, the response rate of sorafenib was only 12%, plus the overall survival benefit offered by sorafenib was only three months more than placebo (10.7 months versus 7.9 months, HR 0.69; 95% CI 0.55–0.87; $P < 0.001$). Nevertheless, grade 3-4 adverse events, including anorexia, diarrhoea and weight loss, were reported in half of the sorafenib-treated patients, leading to a withdrawal rate of ~15% (Llovet et al., 2021).

1.1.4.5.4 Lenvatinib

Lenvatinib is a receptor tyrosine kinase inhibitor which targets VEGFR1-3, fibroblast growth factor receptors (FGFR1-4), PDGFR-α, rearranged during transfection (RET) and KIT receptors. It was associated with a better performance than sorafenib, with a response rate of 42%. In addition, an improved median overall survival of 13.6 months was attained by lenvatinib compared to 12.3 months for sorafenib in the REFLECT trial (Kudo et al., 2018). The frequency of grade >3 adverse events was higher in lenvatinib-treated patients than in sorafenib-treated patients (57% vs. 49%).

1.1.4.5.5 Second-line treatments

When first-line treatments fail to cure advanced HCCs or develop resistance to drugs, second-line therapies are introduced as alternative therapeutic options for patients. Tyrosine kinase inhibitors such as regorafenib and cabozantinib, the anti-VEGF monoclonal antibody ramucirumab, and the combination of nivolumab and ipilimumab are recommended for post-sorafenib-treated patients.

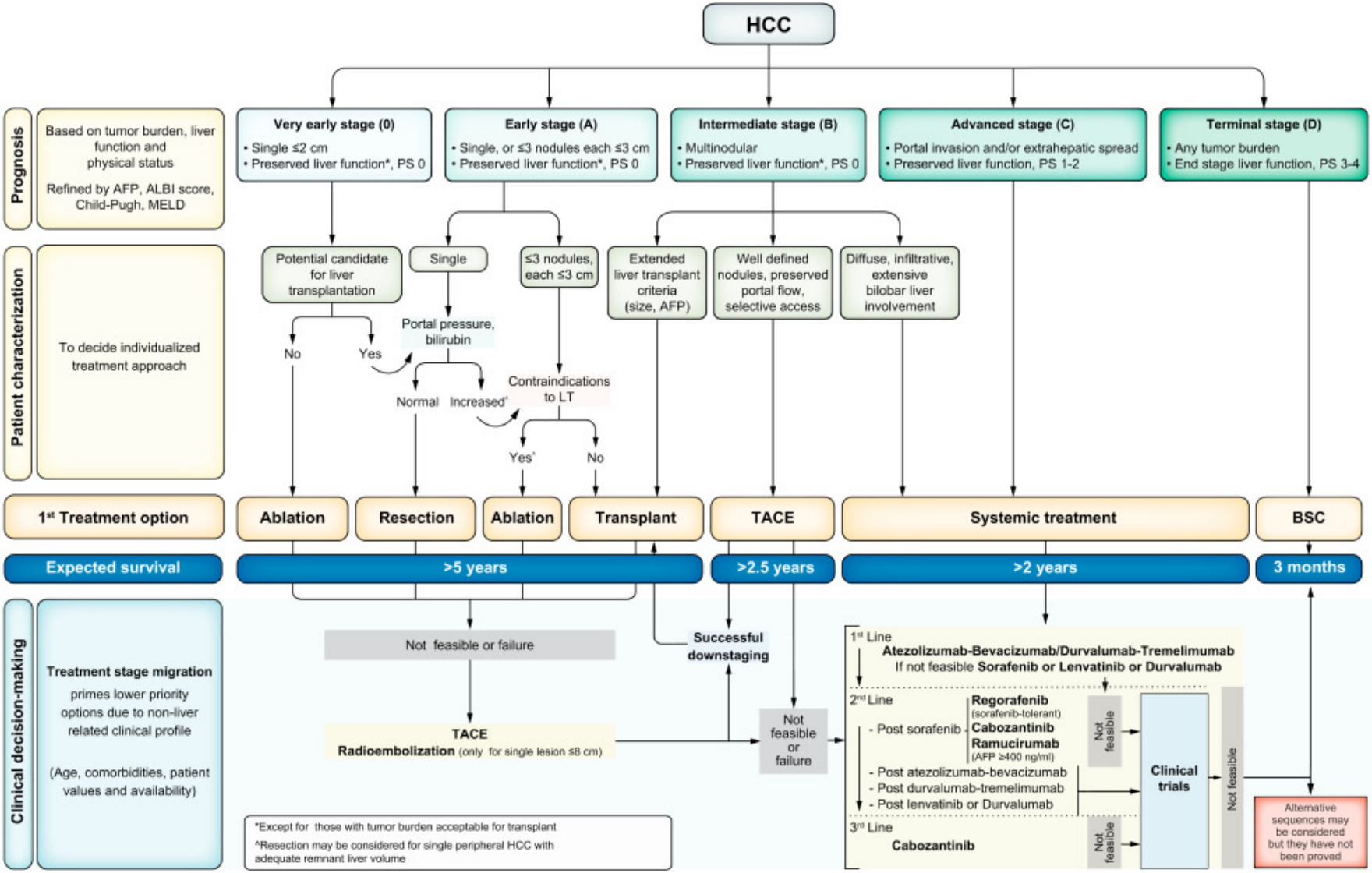

Figure 1.4 Treatment strategy for HCC based on the BCLC staging system in 2022. (Reig et al., 2022)

1.2 Liver immunology

The liver is a 'tolerogenic' organ due to its chronic exposure to various antigens in numerous physiological processes. These include filtering pathogens in the blood and purification of toxic wastes and foreign agents from gastrointestinal traits. Tolerance has been developed in innate and adaptive immune responses to prevent autoimmune damage from non-specific antigens, while adequate immunosurveillance is still required for pathogenic infection and malignant cells. The liver possesses the highest population of resident macrophages (Kupffer cells; KCs) in the body and has a high abundance of antigen-presenting dendritic cells (DCs), natural killer cells (NK cells), natural killer T cells (NKT cells), and gamma delta (γδ) T cells. It is characterised by a greater ratio of $CD8^+$ T cells to $CD4^+$ T cells than that in the periphery. In the context of a healthy adult liver, these liver-resident immune populations play crucial roles in modulating inflammation and preserving organ homeostasis. Pattern recognition receptor expressed by hepatocytes and KCs binds to microbial-associated molecular patterns (MAMPs) and damage-associated molecular patterns (DAMPs) in the blood from the portal vein of the liver. These immunogenic molecules are then phagocytosed and degraded by KCs and hepatocytes. Blood detoxification regulates the rest of the body from an excess immune response and establishes a unique immunosuppressive microenvironment within the liver. Consequently, immune tolerance arises from intricate interactions between liver-resident cells and peripheral leukocytes, resulting in the limited or incomplete activation of $CD4^+$ and $CD8^+$ T cells. The immunosuppressive environment is sustained by a complicated cytokine milieu characterised by basal proinflammatory cytokines (interleukin; IL-2, IL-7, IL-12, IL-15, and IFN-γ), which are offset by anti-inflammatory cytokines (IL-10, IL-13, and TGF-β).

1.2.1 Cancer-immunology and the 'cancer-immunity cycle'

The first concept of 'immuno-oncology' can be traced back to Dr. William B. Coley, the Father of Immunotherapy, who utilised the immune system for sarcoma cancer treatment in the late 19^{th} century. The idea of immuno-oncology aims at boosting the host's sole immune system to combat cancer. Various immunotherapies have been developed based on the cancer–immunity cycle, as suggested by Chen and Mellman in 2013 (Figure 1.5). The 7-step framework depicts a series of stepwise events by which the immune system recognises the cancer cell antigens and eradicates cancer cells.

The cancer-immunity cycle begins with oncogenesis, in which the transformation of normal cells into cancer cells leads to the release of neoantigens. The tumour-associated antigens

(TAAs) are captured by antigen-presenting cells (APCs), for example, DCs (Step 1). DCs then process the TAAs and present the peptides that bind to major histocompatibility complex (MHC)-I and -II to T cells (Step 3). The priming of effector T cells triggers the activation of effector T cell response against TAAs (Step 3). These TAAs are now recognised as foreign antigens. The activated effector T cells migrate to the tumour site (Step 4) and infiltrate the tumour (Step 5). Activated T cells recognise the foreign TAAs and bind specifically to cancer cells through the interaction between T-cell receptors, and MHC-I is present on the cancer cell surface (Step 6). Ultimately, T cells eliminate target cancer cells (Step 7). The dying cancer cells release additional TAAs and continue the cycle. As each cycle progresses, more antigens are released, leading to an expanded immune response over time.

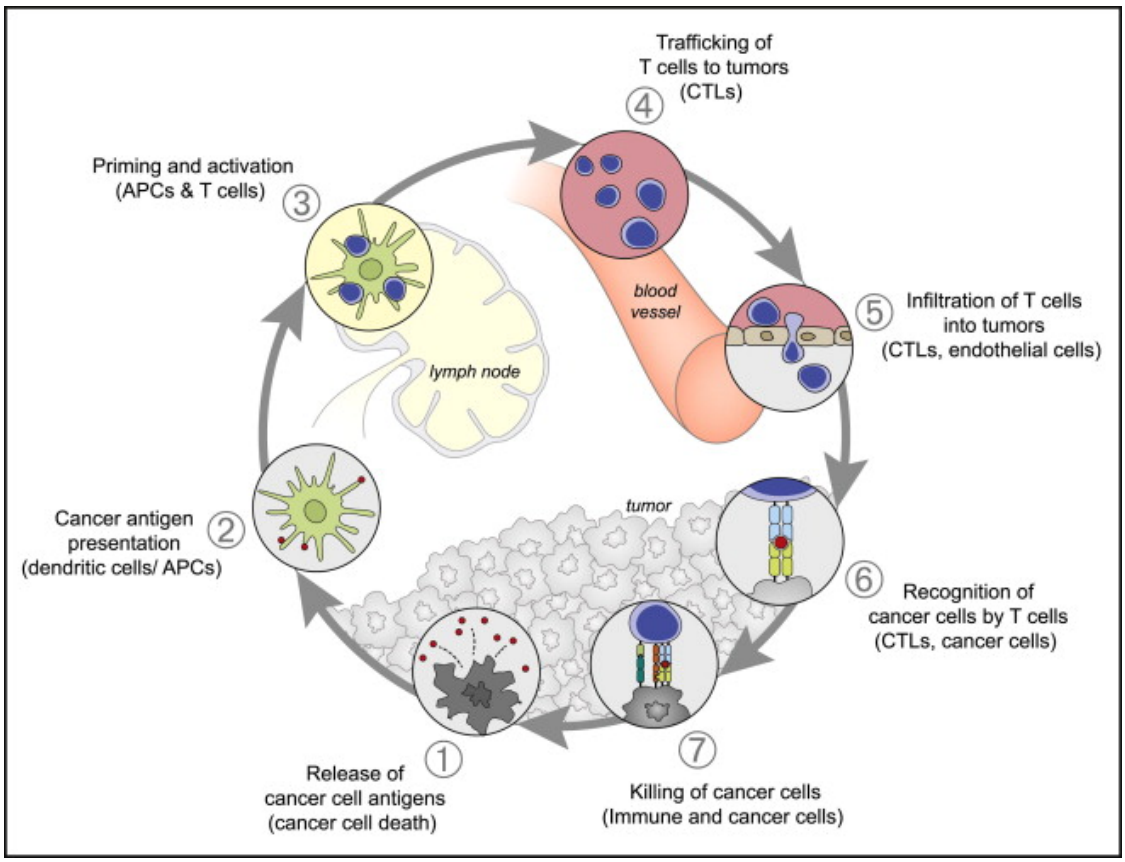

Figure 1.5 The cancer immunity cycle. (Chen and Mellman, 2013)

1.2.2 Immunotherapy

Immunotherapies have been pioneered in cancer treatments in recent decades (Figure 1.6). Various immunotherapies have been developed: ICIs, adoptive cell transfer therapy, chimeric antigen retrieval T cell (CAR-T) therapy, as well as therapeutic vaccines. Currently, the inhibitory therapeutics targeting immune checkpoints PD-1/PD-L1 and CTLA-4 demonstrated the most significant progress in immunotherapy. Atezolizumab-bevacizumab and the STRIDE regimen have become the front-line treatments for successful outcomes in the IMbrave150 and HIMALAYA trials. Recently, the MORPHEUS-liver study demonstrated that the addition of tiragolumab (ICI that targets T cell immunoreceptors with immunoglobulin and ITIM domains (TIGIT)) in standard-of-care atezolizumab plus bevacizumab resulted in improved ORR (42.5% vs 11.1%) and progression free survival (PFS; 11.1 months vs 4.2 months), compared to control arms. Tiragolumab is thus suggested to be a potential enhancer of atezolizumab and bevacizumab. Other immuno-oncology therapeutic targets include T cell immunoglobulin domain and mucin domain 3 (TIM-3), and lymphocyte-activation gene 3 protein (LAG-3).

Despite the latest remarkable advances, only a few patients could obtain long-lasting clinical benefits; thus, substantial therapeutic challenges remain. In the Checkmate 459 trial, the response rate to anti-PD-1/PD-L1 treatment was only 15% (Yau et al., 2019). Furthermore, about 30% of HCCs demonstrated intrinsic resistance to ICIs (Kim et al., 2021). The non-responders of ICIs developed accelerated tumour progression, deteriorated liver functions and poor prognosis (Mohr et al., 2021). The main reason for the unresponsiveness to ICIs can be attributed to the non-specificity in provoking an immune response due to the significant inter- and intra-tumoral heterogeneity and lack of tumour antigens (Sharma, Hu-Lieskovan, Wargo, & Ribas, 2017). Using single-cell RNA sequencing (scRNA-seq), Ma et al. (2019) linked the heterogeneity at levels of tumour cells, tumour microenvironment and patient prognosis. This study identified differentiated intra-tumoral heterogeneity based on the expression of cancer stemness genes. Tumours with high heterogeneity were correlated with worse clinical outcomes and weaker cytotoxic characteristics. In addition, the lack of reliable predictive markers limits the efficacy of immunotherapy (Gallage et al., 2021).

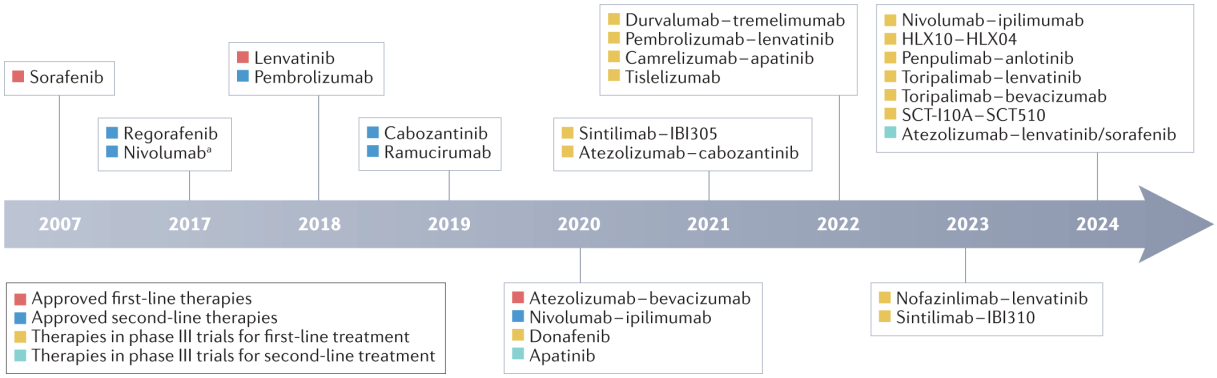

Figure 1.6 Evolving systemic therapeutics for advanced HCCs. (Yang et al., 2023)

1.2.3. Immune evasive mechanism of HCC

Chronic inflammation in the liver, often associated with underlying liver diseases like cirrhosis and hepatitis, contributes to immune dysfunction and loss of tolerance towards tumour antigens (Figure 1.7). Aberrant antigen presentation in chronic inflammation is mediated by alterations in APCs and excessive expressions of co-inhibitory molecules. Such a typical inflammatory environment, characterised by immunosuppression via IL-10 and TGF-β release produced by KCs, myeloid-derived suppressor cells (MDSCs) and regulatory T cells (Tregs), is beneficial for the onset of HCC. Immune evasion occurs throughout the tumorigenesis, progression and later metastasis of HCC (Nguyen et al., 2022). It is generally accepted as the consequence of the failure of immune surveillance, attributed to the dysfunctional tumour immune microenvironment (TIME). It is a complex process involving multiple strategies the tumour employs to evade immune surveillance.

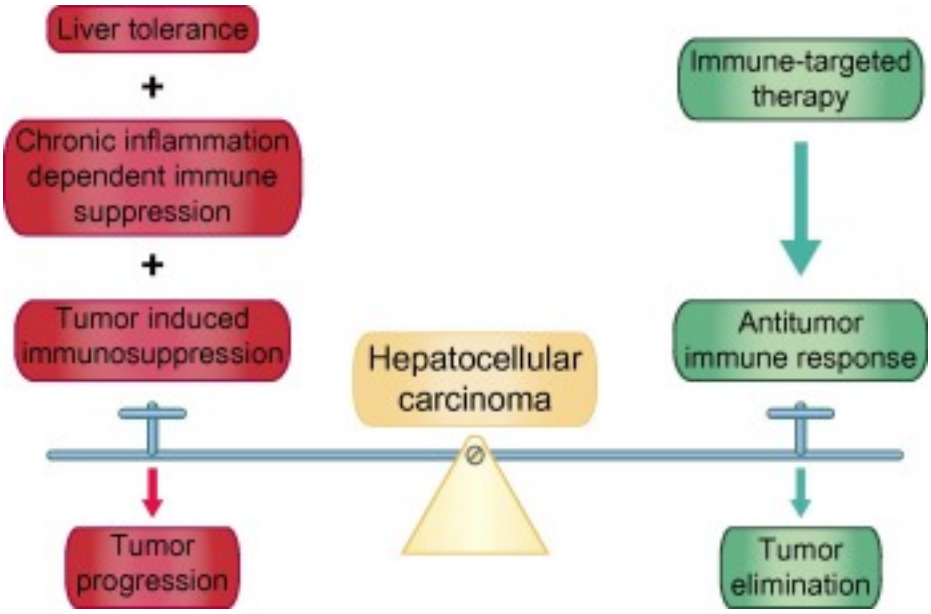

Figure 1.7 The counteracting forces regulate the balance between tumour progression and tumour elimination. (Makarova-Rusher et al., 2015)

1.2.3.1 Tumour intrinsic mechanisms of immune evasion

Tumour intrinsic mechanism of immune escape can be attributed to (1) inadequate T cell response due to deficit antigen processing and presenting machinery (APM) and MHC-I downregulation; (2) activation of oncogenic WNT/β-catenin signalling pathway; (3) activation of RAF/MEK/ERK and PI3K/AKT/mTOR signalling cascades; 4) disruption of intrinsic interferon-gamma (IFN-γ) signalling pathway.

(1) Inadequate T cell response due to deficit APM and MHC-I downregulation

Downregulation of MHC-I is commonly found in 40-90% of human cancers and is often associated with worse prognosis and unsatisfactory ICI response rate. High human leukocyte antigen (HLA) class I expression is an independent prognostic factor for HCC. It is associated with $CD3^+$ cell infiltration and lower recurrence rate (Umemoto et al., 2015). The importance of MHC-I downregulation in cancer is correlated with the number of tumour-infiltrating lymphocytes, and thus, T cell-mediated cytotoxicity. The complex machinery of MHC-I can be dysregulated at the genetic, epigenetic, transcriptional or post-translational levels.

Dysfunctional MHC-I regulation can be classified into soft and hard lesions, based on MHC-I expression. In contrast, the former is therapeutically treatable, and the latter is intractable due to somatic deficits (Taylor & Balko, 2022). Soft lesions in MHC-I can be created via epigenetic, transcriptional, and post-transcriptional silencing, autophagy degradation, and activation of the ERK pathway. NF-κB, STATs, Interferon-regulatory factors (IRFs), and NLR Family CARD Domain Containing 5 (NLRC5) are interferon (IFN) pathway-related MHC-I transactivators. Downregulation of both type I and II IFN pathways or suppression of these critical regulators leads to downregulation of MHC-I. Furthermore, activation of the ERK pathway negatively influences MHC-I expression by suppressing STAT1 and IRF activity. The expression of APM genes can also be downregulated through epigenetic silencing, such as the hypermethylation of NLRC5 and the promoter region of MHC-I. A panel of microRNAs has been reported to suppress the expression of MHC-I chain-related molecules A/B (MICA/B) in HCC at the post-transcriptional level (Wu et al., 2014). The downregulation of MHC-I expression via these mechanisms could be reversed by a potential combination of inhibitors, such as MEKi and HDACi, combined with ICIs.

Somatic defects, such as loss of heterozygosity, mutations in APM components and MHC-I heavy chain, and IFN pathway defects, lead to hard lesions in MHC-I expression. Loss of heterozygosity of the HLA allele, observed in 17% of multifocal HCC cases, impairs the ability of the MHC to present neoantigens (Dong et al., 2020). Lei et al., (2018) reported HLA class I antigen loss with underlying deletion across β2-microglobulin (*B2M*) locus and HLA class I heavy chain defects in 50% of sarcomatoid HCC cell lines. A genome-wide association study on HBV-related HCC suggested a correlation between genetic variants in *HLA-DQ* and *STAT4* and the risk of HCCs (Jiang et al., 2013). Moreover, a comprehensive whole genome analysis revealed 9.1% *JAK1* mutations and 45.5% alterations in the JAK/STAT pathway in the HCCs (Kan et al., 2013). Loss of function mutations in the JAK/STAT pathway leads to the downregulation of the regulators of APM components, such as NLRC5 and IRFs.

(2) Activation of oncogenic WNT/β-catenin signalling pathway

In an analysis of gene expression profiles of HCC patients, the 'CTNNB1 mutation' gene signature was characterised by immune exclusion (cold tumour) (Kurebayashi et al., 2018). The CTNNB1 mutation group showed lower T cell enrichment with downregulation of T cell chemoattractant C-C motif chemokine ligand 4 (CCL4) (Sia et al., 2017). Activation of the WNT/β-catenin signalling pathway in the murine HCC model was recently reported to promote immune escape and resistance against anti-PD-1 therapy (de Galarreta et al., 2019). Via downregulating Ccl5, WNT/β-catenin signalling exploits anti-tumour $CD8^+$ T cell response and suppresses dendritic cell recruitment. Over 30% of HCC patients carrying the CTNNB1 mutant are predicted to resist the anti-PD-1 treatment (Pinyol et al., 2019). Moreover, a clinical analysis using NGS for genotype HCC patients undergoing ICIs revealed that activated WNT HCCs were associated with shorter PFS (Harding et al., 2019). In this study, 50% of wild-type CTNNB1 patients developed a response to anti-PD-1 or anti-PD-L1 therapy, whereas none of the ten patients with CTNNB1 activation responded. Collective data suggest that CTNNB1 alteration could represent a novel biomarker for ICI prognosis in HCC patients. Intriguingly, a recent clinical trial found no inferiority in the overall response to ICIs in HCC tumours with β-catenin activation. Ogawa et al. (2022) reported that no significant difference was found in the overall response rate (ORR: 8% vs 12.5%), PFS (6.6 vs 7.6 months) and disease control rate (DCR: 68% vs 87.5%) between HCC patients carrying wild-type and mutant CTNNB1 in the treatment of atezolizumab-bevacizumab. The comparable survival outcomes between the patient groups with wild-type and mutant CTNNB1 showed that combining atezolizumab-

bevacizumab might improve immunosuppressive TIME influenced by *CTNNB1* mutation. In the latest immunogenomic classification of HCC published in 2023, Montironi et al. further divided patients with activated CTNNB1 into 'immune-excluded' and 'immune-like' subclusters. About two-thirds of the patients with *CTNNB1* mutations have immune exclusion. In contrast, one-third have high immune infiltrates due to the domination of high IFN signalling and type I antigen-presenting genes. These two distinct patterns in *CTNNB1* mutation are associated with differentiated immune evasive mechanisms and might explain the comparable response rates of the wild-type and mutant CTNNB1 groups upon ICI treatment. More investigations are needed to confirm the reliability of using WNT/CTNNB1 mutation status as a biomarker for ICI response.

(3) Activation of RAF/MEK/ERK and PI3K/AKT/mTOR signalling cascades

In the transcriptome-based classification of HCC, the proliferative group of HCC was characterised by the activation of RAF/MEK/ERK, PI3K/AKT/mTOR and MET signalling. Loss of PTEN, which leads to PI3K/AKT activation, also correlates with resistance to the ICIs (Peng et al., 2016). In a murine melanoma model, deficient Pten expression, which activates PI3K signalling, led to decreased T cell infiltration to the tumour site and consequently impaired T cell-mediated tumour killing. In melanoma patients, PTEN loss was linked to reduced T cell infiltration within tumours, resulting in a less favourable response to anti-PD-1 immunotherapy. Currently, there is no published evidence suggesting that PTEN promotes immune escape in HCC. Nevertheless, PTEN alterations have been observed in 7% of human HCC patients, making it a potential therapeutic target. Further research is required to determine whether tumour-specific loss of PTEN leads to immune escape in HCC.

ERK signalling is activated in over 50% of HCC cases, leading to unrestrained cell proliferation. Few studies have reported the functional role of ERK signalling in HCC. Yet, the mechanisms of ERK-induced immune escape are widely reported in other cancers, such as lung cancer, colon cancer and melanoma. As the downstream signalling of oncogenic Rat sarcoma virus (RAS), MEK/ERK induces the expression of PD-L1 on tumour cells. This increases PD-1/PD-L1 levels, leading to T-cell exhaustion and apoptosis. In the presence of activated ERK, epidermal growth factor (EGF) induces the secretion of cytokine IL-10 and TGF-β and recruits Tregs and tumour-associated macrophages (TAMs) to the tumour site, aggravating the immunosuppressive TIME (Salaroglio et al., 2019). Furthermore, activation of the ERK

pathway negatively influences MHC-I expression by suppressing IFN signalling, as explained above.

(4) Disruption of intrinsic interferon-gamma (IFN-γ) signalling pathway

In the immunogenomic classification of HCC patients, ~65% of HCC cases belong to the 'non-inflamed' class, characterised by downregulated IFN signalling and low immune activation (Montironi et al., 2023). The other ~35% of HCC cases presented with high IFN signalling and an increased number of checkpoint molecules. As previously described, a defective IFN-γ signalling pathway leads to dysfunctional antigen presentation and MHC-I downregulation in tumour cells. IFN-γ also affects cell-mediated anti-tumour responses by inducing the production of the T-cell chemoattractants chemokine (C-X-C motif) ligand 9 (CXCL9), CXCL10, and CXCL11 for immune activation (Gallage et al., 2021; Kaplan et al., 1998). Low IFN-γ expression is associated with poor prognosis and advanced tumour stage in HCC patients. IFN-γ, released from T cells infiltrating the tumour, activates the JAK/STAT1/IRF1 pathway to induce PD-L1 in tumour cells. Li et al. (2018) reported a synergistic effect of tumour necrosis factor-α (TNF-α) on IFN-γ-induced PD-L1 expression in HCC cells via upregulation of IFN-γ receptors. Moreover, the loss of IFN-γ pathway molecules correlates with resistance to anti-CTLA-4 and anti-PD-1/PD-L1 treatments in melanoma (Spranger & Gajewski, 2018). IFN-γ is a multifunctional cytokine with anti-proliferative and anti-apoptotic properties (Jhunjhunwala et al., 2021).

1.2.3.2 Tumour extrinsic mechanisms of immune evasion

Crosstalk between tumour cells and the TIME is also a critical factor for immune escape in HCC. The immunosuppressive TIME acts as an external driver of immune evasion via (1) the presence of immunosuppressive immune cells; (2) promoting T cell exhaustion via upregulation of co-inhibitory signals; (3) disruption of extrinsic IFN-γ signalling pathways; (4) metabolically hostile tumour microenvironment; (5) gut microbiota that suppresses the immune microenvironment.

(1) Presence of immunosuppressive immune cells and cytokines

Cytotoxic $CD8^+$ T cells, $CD4^+$ T cells, and NK cells collaborate to maintain immune surveillance. In contrast, the abundance of immune cells in HCC, such as MDSCs, Tregs, and TAMs, contributes to immune evasion and promotes tumour progression. MDSCs are a

heterogeneous population of immature myeloid cells with strong immunosuppressive activity. MDSCs are recruited via the similar chemotactic mechanisms as their myeloid counterparts, which involve CCL2, CCL5, CXCL1, CXCL5, CXCL6, CXCL8, CXCL6, CXCL8, CXCL12. Several cytokines, such as IL-6, IL-1β, GM-CSF, G-CSF, VEGF and MCP-1, have also been reported to induce MDSC accumulation in preclinical models of HCC. MDSCs impede the proliferation and activation of effector T cells via depriving essential amino acids and secretion of immunosuppressive VEGF, TGF-β, Indoleamine 2,3-dioxygenase (IDO) and arginase 1 (Arg1). They also disrupt T cell receptor (TCR) signalling via releasing reactive oxygen and nitrogen species. The ligand of the immune checkpoint TIM-3, Galectin-9 expressed on MDSCs, binds to TIM-3 on T cells, leading to T cell exhaustion. Moreover, the presence of a high abundance of MDSCs in HCC promotes the transformation of naïve T cells into Tregs and drives their development via IL-10, TGF-β and CD40-CD40L interaction. MDSCs can impair the cytotoxicity of NK cells by interacting with them through the NKp30 receptor, and they can also interact with Kupffer cells to enhance the expression of PD-L1.

Tregs maintain autoimmune tolerance by inhibiting the excessive immune response in a healthy liver. However, the hyperactivation of Tregs exploits the T cell-mediated immune response. Tregs can be recruited by various chemokines, including CXCR3-CXCL9/CXCL10/CXCL11-CXCR3, CCL3/CCL4/CCL5-CCR5, CCL17/CCL22-CCR4, CCL20-CCR6 and CCL27-CCR10 (Ozga, Chow & Luster, 2021), and is activated by the binding of TCR with IL-10 and TGF-β. Tregs damage the cytotoxicity of $CD8^+$ T cells via the release of granzyme A, B, and perforin, and inhibition of TNF-α and IFN-γ. Qiu et al. (2020) suggested a role for Annexin A2 in promoting immune escape via recruitment of Treg cells in HCC. Furthermore, Treg cells constitutively express immune checkpoints PD-1, CTLA-4, and TIM-3 and secrete inhibitory molecules, including IL-10 and TGF-β.

TAMs originate from circulating bone marrow-derived monocytes and are mainly recruited by the CCL2-CCR2 and CCL5-CCR5 axes. The presence of high levels of TAMs with a high ratio of M2 to M1 polarisation has been linked to poor prognosis in HCC (Dong et al. 2019; Fu et al. 2019). Similar to MDSCs, M2-polarised TAMs induce the immunosuppressive factors IL-10, TGF-β, VEGF, IDO, and Arg1. In HCC, M2-TAMs are the primary cellular sources of PD-L1. The regulation of PD-L1 expression in TAMs differs from that in tumour cells. It is primarily induced by TNF-α and is upregulated by GM-CSF and IL-10 (Glorieux et al., 2021). Tumour cells can also upregulate the expression of PD-L1 in TAMs via NF-κB and STAT3-

related pathways (Zhang et al. 2020). A report revealed that Hedgehog signalling could induce PD-L1 on M2-TAMs in the HCC (Petty et al., 2021). Lu et al. (2022) suggested that glycolytic metabolism is involved in PD-L1 upregulation on tumour macrophages, and the blockade of PD-L1 restores the antitumorigenic properties of macrophage. Intriguingly, Zong et al. (2019) reported that IL-1β secreted by M1-TAMs could induce PD-L1 expression in HCC tumour cells via transcription factor p65 and IRF1 (Zong et al., 2019). TAMs also promote T cell exhaustion by upregulating TIM-3 on the cell surface, further promoting TAM-mediated HCC progression via the NF-κB/IL-6 axis (Yan et al. 2015). TAMs also interact with other immunosuppressive cells, including Tregs and MDSCs. TAMs contribute to immune evasion through the secretion of CCL17, CCL18, and CCL22, which attracts $CCR4^+$ and $CCR8^+$ Treg cells (Ozga et al., 2021). MDSCs also can transform into M2-TAMs. Crosstalk between TAMs and MDSCs further exacerbates immunosuppression in the TIME via the positive feedback production of IL-10 by MDSCs and reduced production of IL-6 and IL-12 by macrophages. The alteration of cytokines favours the development of T helper 2 (Th2) cells, orchestrating type 2 immune response. The co-culture of MDSCs and macrophages subsequently decreases MHC-II expression in macrophages, thereby impeding their antigen presentation function.

(2) Promoting T cell exhaustion via upregulation of co-inhibitory signals

The effector function of T cells is balanced between the co-stimulatory and co-inhibitory signals to prevent an excessive immune response. Under normal conditions, T cells transiently induce inhibitory receptor expression upon activation. However, under chronic antigen presentation and prolonged T cell activation, increasing co-inhibitory molecules expressed on the T cell surface drives T cell exhaustion. T cell exhaustion is strongly correlated with a poor prognosis in HCC. Exhausted T cells are characterised by increased checkpoint co-inhibitory receptors, reduced expression of anti-tumour cytokines, production of tumour-promoting chemokines, and high apoptosis rates; the more co-inhibitory receptors expressed by T cells, the more serious the dysfunction.

The PD-1/ PD-L1 interaction has been widely studied and has become the first target of cancer immunotherapy. A large number of $PD\text{-}1^+$ $CD8^+$ T cells within the tumour indicates a poor prognosis and an increased likelihood of recurrence (Shi et al., 2011). Overexpression of PD-L1 suggests a high risk of operative recurrence in patients with HCC (Qiang Gao et al., 2009; Tan et al., 2022). PD-1 is expressed by activated T cells, NK cells, Tregs, DCs, and monocytes. It interacts with PD-L1 on tumour cells or TAMs and promotes $CD8^+$ T cell apoptosis (Lauko

et al., 2021). In addition, PD-1/ PD-L1 interaction inhibits T cell infiltration and reduces anti-tumour cytokines, including TNF-α, IFN-γ and IL-2. CTLA-4 is constitutively expressed by Treg cells and activated T cells. By competing with the co-stimulatory receptor CD28 for binding to CD80 and CD86, CTLA-4 prevents T cell proliferation in HCC (Seidel et al., 2018; Freed-Pastor et al., 2021). TIM-3 is expressed in $CD4^+$ and $CD8^+$ TILs, TAMs, and NK cells. Its interaction with the ligand galectin-9 leads to T cell dysfunction, while its presence on Treg cells enhances its suppressive activity.

(3) Disruption of extrinsic IFN-γ signalling pathways

Disruption of the IFN-γ signalling pathway also exerts an extrinsic influence on TIME and promotes immune evasion. IFN-γ is primarily produced by $CD4^+$ and $CD8^+$ cells during the adaptive immune response. It plays an essential role in the induction of cytolytic activity in cytotoxic T cells (CTLs), most likely by affecting the expression of the IL-2 receptor. Autocrine IFN-γ stimulation on $CD4^+$ T cells promotes adaptive immune response by augmenting cell survival and cytokine secretion during T cell activation. IFN-γ is also secreted by human invariant NKT cells and γδ T cells to promote tumour-associated antigen-specific CTL responses. For CTL responses, the induction of MHC-I and transporters associated with antigen processing (TAP) can be elicited by IFN-γ stimulation of target cancer cells and APCs. Besides regulating MHC-mediated antigen presentation pathways, IFN-γ fosters the development of type 1 T helper cell (Th1) responses, leading to anti-microbial effects. As a Th1 cytokine, IFN-γ triggers M1-polarised differentiation of the anticancer macrophage phenotype but not tumour-promoting M2 macrophages with immunosuppressive properties.

(4) Metabolically hostile tumour microenvironment

In the TIME, hypermetabolic tumour cells interfere with immune cell functions by depriving nutrients, such as glucose and amino acids, and producing oxidative stress and immunosuppressive metabolites. In the context of enhanced aerobic glycolysis, the tumour consumes excessive glucose. This leads to limited glucose supply and lactate accumulation in the TIME. Glucose constraints hamper IFN-γ production and effector T cell functions. In contrast, immunosuppressive Tregs uptake lactate to fuel their survival via the tricarboxylic acid cycle. In addition, lactate promotes M2 polarisation in TAM, MDSC differentiation and induction of PD-L1 expressions, aggravating the immunosuppression. Amino acid deprivation, for example, glutamine deficiency, inhibits effector T cell activation and Th1 differentiation. Yet, the low glutamine level favours Treg production and M2-TAM polarisation. Arg1 also

converts arginine to ornithine, impairs $CD8^+$ T cell's cytotoxicity, and leads to arginine deprivation.

The TIME is also characterised by increased lipogenesis. Immune cells absorb excessive lipids via binding to CD36, which results in high oxidative stress. This promotes T-cell dysfunction and ferroptosis. Moreover, immunosuppressive metabolites IDO released by TAMs, and MDSCs, promote immune evasion via catalysing the conversion of tryptophan to kynurenine. The tryptophan depletion leads to T cell anergy, and the kynurenine aggregation upregulates PD-1 expression in T cells. Hyperactive IDO also contributes to resistance to ICIs in HCC (Brown et al., 2018).

(5) Gut microbiota that suppresses the immune microenvironment

The gut microbial microenvironment of HCC plays a significant role in immune evasion mechanisms. Microbial activation of Toll-like receptor 4 (TLR4) promotes the formation of an immunosuppressive tumour microenvironment. Bacterial lipopolysaccharide (LPS)-induced TLR4 activation could stimulate hepatocytes to express CXCL1 and recruit $CXCR2^+$ polymorphonuclear MDSCs. *Fusobacterium* recognised by TLR4 regulates the IL-6/STAT3/C-MYC signalling pathway, facilitating TAM polarisation into the M2 phenotype. Microbial dysbiosis increases the levels of immunogenic substances, such as LPS and lipoteichoic acid. High levels of LPS have been detected in HCC patients, promoting immune tolerance and tumorigenesis. Microbial dysbiosis also damages intracellular tight junctions and enhances immune cell exposure to toxic substances. Dysbiosis-driven chronic inflammation can trigger oxidative stress and alter the expression of pathogen recognition receptors, thereby contributing to HCC development and immune evasion. Some microbes, such as the Fap2 protein of *Fusobacterium mucleatum,* interact with the inhibitory checkpoint ligands TIGIT or CEACAM1 to protect tumours from the immune attack of NK cells and T cells. However, other bacteria such as *Bifidobacterium* and *Akkermansia muciniphila* can enhance the efficacy of PD-1 blockade and facilitate immune cell activity (Sivan et al., 2015; Zheng et al., 2019).

The combination of these immune evasion mechanisms allows HCC to evade recognition and elimination by the immune system, enabling tumour growth, progression, and resistance to conventional therapies.

1.3 Introduction of KRAS (Kirsten rat sarcoma viral oncogene homolog) signalling

KRAS (Kirsten rat sarcoma viral oncogene homolog) is a proto-oncogene that encodes small GTPase transductor protein KRAS. It was first identified as a viral oncogene in the Kirsten Rat Sarcoma virus. Along with Harvey-RAS (HRAS) and neuroblastoma-RAS (NRAS), KRAS belongs to the RAS family, which shares functional small GTPases. KRAS protein is derived into two splice variants, KRAS 4A and KRAS 4B, while KRAS 4B is the common form of KRAS. The KRAS protein is comprised of 189 amino acids, with a molecular weight of 21.6kDa.

KRAS protein is a GTPase, which acts as an on-off switch and converts the nucleotide guanosine triphosphate (GTP) into guanosine diphosphate (GDP). Through the regulation of GDP-GTP exchange, KRAS is responsible for the cytoplasmic transduction of extracellular stimuli from cell surface growth factor receptors to intracellular signalling through on-off control by GTP binding. Under physiological conditions, KRAS-GTPase is active, binds to GTP, and is inactive when bound to GDP. The transition between GTP and GDP is catalysed by the guanine nucleotide exchange factor (GEF) and opposing GTPase-activating proteins (GAPs). GEF binds to KRAS-GTPase and catalyses the release of GDP, allowing the binding of GTP due to its higher cytosolic ratio to GDP. GTP binding to KRAS-GTPases leads to the release of GEF, which activates another KRAS-GTPase. GAP acts as an antagonist that inactivates KRAS-GTPases by promoting GTP hydrolysis. Son of Sevenless homologs (SOSs), which are RAS-GEF proteins, catalyse the KRAS nucleotide exchange of GDP to GTP, enabling the RAS in an active GTP-bound state.

KRAS is responsible for the regulation of cell proliferation and survival pathways (Figure 1.8). Upon activation of RTK receptors, such as epidermal growth factor receptor (EGFR), by growth factor stimulation, KRAS switches from GDP to GTP-bound states and activates downstream signalling via the RAF/MEK/ERK, PI3K/AKT/mTOR, and RALGEF/RAL/NF-κB pathways (Neel et al., 2011; Martinelli et al., 2017; Degirmenci, Wang & Hu, 2020; Prior, Hood & Hartley, 2020). RAF/MEK/ERK signalling is a canonical downstream target of KRAS signalling. It plays a role in the regulation of cell proliferation, differentiation, inflammation, apoptosis, and migration. PI3K/AKT/mTOR is another downstream signalling pathway of KRAS. It is crucial for cell proliferation, differentiation, apoptosis, and metabolic activities such as glucose transport. RAL/GDS-mediated signal transduction induces alterations in membrane trafficking and vesicle formation.

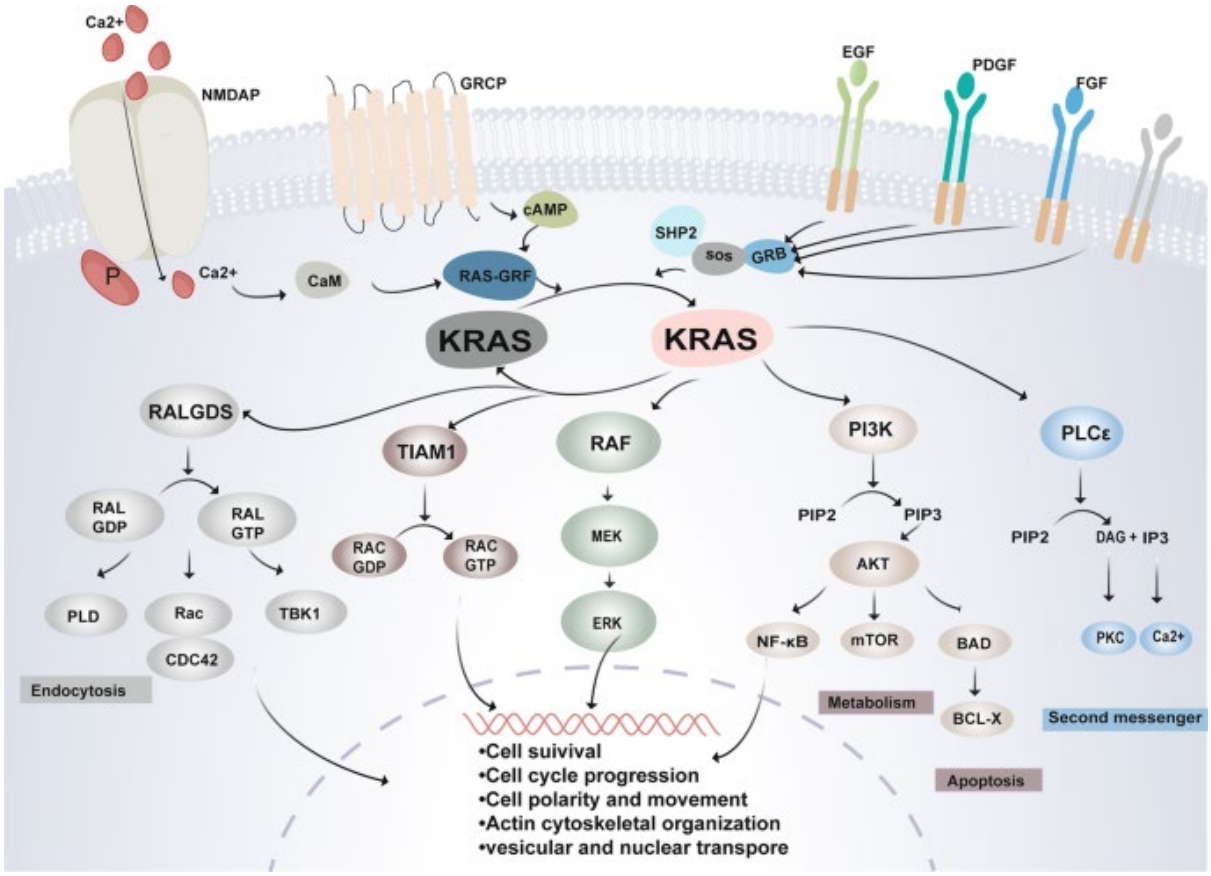

Figure 1.8 Schematic diagram of KRAS activation and downstream signalling pathways. (Huang, Guo, Wang, & Fu, 2021)

1.3.1 The role of KRAS signalling in cancer

RAS is frequently mutated in cancers (~30%), and KRAS mutations account for 86% of RAS mutations (Liu, Wang, & Li, 2019). Common mutation sites of KRAS are G12C, G12D, G12V, and G13D. KRAS mutations contribute to 25% of all human malignancies, with a high dominance in pancreatic cancer (90%), colorectal cancer (40%), and lung cancer (32%). However, most (~80%) HCC patients carry wild-type KRAS and KRAS mutations in only 7% of liver cancer (Turhal et al., 2015). Despite the low mutation rate of KRAS in HCC, wild-type KRAS expression was elevated in HCC at the mRNA and protein levels. Dysregulation of KRAS in HCC could be attributed to the aberrant regulation of non-coding RNA (Dietrich et al., 2018; Ghafouri-Fard et al., 2022). Wild-type KRAS expression is associated with HCC progression, advanced tumour size and poor prognosis. KRAS signalling aggravates steatosis progression in HCC. Activation of KRAS is significantly enhanced in the high-fat diet-induced HCC mouse model (Xu et al., 2019). Interestingly, the expression of KRAS is proportional to the number of tumour nodules induced, implicating its oncogenic role. It was reported that only

5% activation of RAS-GTPase is efficient in fully activating ERK (Hallberg, Rayter, & Downward, 1994). Hence, RAF/MEK/ERK and PI3K/AKT/mTOR signalling pathways are activated in ~50% of HCC; both of them are essential to drive tumour resistance in HCC (Dietrich et al., 2018). The RalGEF pathway has also been implicated in carcinogenesis and tumour progression.

Interestingly, wild-type KRAS and mutant KRAS interact with each other to mediate KRAS-driven cancer. Wild-type KRAS antagonises mutated KRAS and exhibits growth-inhibitory effects in cancer. The inhibitory effect is attributed to wild-type and mutant KRAS competition for membrane localisation, mutual regulator and downstream signalling, and the dimerisation capacity of wild-type KRAS with mutant KRAS. However, this inhibition is often overcome by the gain or loss of the KRAS gene in cancer, resulting in allelic imbalance and promoting tumour fitness (Burgess et al., 2017). Moreover, studies have shown that wild-type KRAS contributes to the development of acquired resistance and impairs the response to inhibition of mutant KRAS and its downstream ERK pathway (Cox et al., 2014; Ambrogio et al., 2018). This is probably partly due to the inhibition of mutant KRAS and its signalling, leading to the reactivation of RAS pathways mediated by wild-type KRAS (Ryan et al., 2020). It has been suggested that rapid feedback reactivation is driven by multiple RTKs, which induce wild-type KRAS, HRAS, or NRAS activity and the subsequent reactivation of downstream signalling. Interestingly, the loss of wild-type KRAS enhances the sensitivity of KRAS-mutant cells to MEK inhibitors (Burgess et al., 2017). Dietrich et al., (2018) reported the role of wild-type Kras in contribution to the acquired resistance to sorafenib in HCC. Sorafenib-mediated inhibition of the RAF/ERK pathway, upregulated wild-type Kras expression and its downstream Akt activation induced the resistance to sorafenib and promoted tumorigenesis. Direct inhibition of Kras desensitised sorafenib-resistant HCC cells and suppressed their proliferation.

1.3.2 The role of KRAS in immune evasion

Oncogenic KRAS exerts various immunomodulatory effects in the tumour microenvironment, promoting tumour progression. KRAS remodels and reprograms surrounding stromal cells and immune cells via the secretion of IL-6, IL-8, CCL9, IL-23, and GM-CSF. KRAS-induced IL-6 stimulates the activation of JAK1/ STAT3, contributing to the reoccurrence of pancreatic cancer, and induces ROS through activation of the ERK pathway. IL-8 has been found to be a

downstream transcriptional target of the KRAS-mediated MEK/ERK and PI3K/AKT signalling cascades. Binding of IL-8 to CXCR2 promotes inflammation by recruiting neutrophils to the tumour site in lung cancer. In addition, activation of CXCR2 signalling recruits cancer-associated fibroblasts (CAFs) to secrete pro-tumorigenic cytokines and recruit MDSCs to the tumour (Pylayeva-Gupta et al., 2012).

Moreover, KRAS signalling promotes immune evasion by suppressing the IFN response (Mugarza et al., 2022). Upon KRAS activation, the TIME is characterised by the recruitment of immunosuppressive monocytes and neutrophils. Inhibition of the IFN pathway leads to APC activation and subsequently reduces T cell infiltration. In contrast, Kras inhibition rescues the APC activation and synergises the effect of ICIs in immunogenic tumours. Previous studies have associated oncogenic KRAS with the decreased expression of MHC- I molecules (Atkins et al., 2004). Restoring this immune evasion mechanism can enhance T cell recognition, making tumour cells more vulnerable to cytotoxic $CD8^+$ T cell response.

KRAS mediates T cell exhaustion by regulating the intrinsic characteristics of tumour cells. The upregulation of PD-L1 expression in KRAS tumours is also considered one of the immune escape mechanisms in mutated KRAS-driven lung cancers (Chen et al., 2017). It was reported that ERK signalling and STAT3 but not AKT signalling participated in the induction of PD-L1 expression in the KRAS mutated lung cancer (Sumimoto et al., 2016). The MEK/ERK signalling stabilised PD-L1 mRNA via phosphorylating and suppressing the activity of AU-rich binding protein tristerrolin by MK2 kinase (Coelho et al., 2017). A study reported that activated $KRAS^{G12V}$ adopted a redox mechanism and enhanced PD-L1 expression by increasing the ROS production and FGFR1 expression (Glorieux et al., 2021). Clinical data showed that 80.4% of NSCLC patients with KRAS mutation expressed PD-L1, compared to 61.9% in those with wild-type KRAS (Lauko et al., 2021). Evidence has shown that KRAS cooperates with other oncogenes and promotes immune evasion. The co-occurrence of TP53/KRAS has also been reported to enhance PD-L1 expression in lung adenocarcinoma Field exclusively (Dong et al., 2017). A pancreatic cancer study identified the CD155/ TIGIT axis as the crucial immune evasion mechanism in pancreatic organoids with mutated KRAS and loss of TP53 background (Freed-Pastor et al., 2021). Co-activation of MYC and KRAS initiates immunosuppressive stroma for tumorigenesis by promoting PD-L1 mRNA and exclusion of B, T, and NK cells via IL-23 and CCL9 cytokines (Kortlever et al., 2017).

Moreover, KRAS inhibits T cell activity via ERK signalling and secretion of IL-10 and TGF-β. These findings suggest the importance of KRAS in the regulation of antitumour immunity.

1.4 Aim of study

The rapid development of the therapeutic landscape in advanced HCCs can be attributed to two critical breakthroughs in disease research: (1) the development of novel systemic therapeutics and (2) the significance of patient selection in clinical trials. Numerous molecular-targeted agents and ICIs are being tested as single-agent therapies with potential predictive biomarkers for advanced HCCs. However, a single agent of anti-PD-1 treatment only resulted in a 15-20% response rate in phase II and III trials (Yau et al., 2019). Furthermore, approximately 30% of HCCs develop adverse outcomes with ICIs (Kim et al., 2021). In the absence of predictive biomarkers to identify patients who will benefit the most from immunotherapy, combinational strategies of targeted therapies and ICIs offer promising treatment options for HCCs. In the revised 2022 BCLC strategy, the combinational therapies of atezolizumab-bevacizumab or durvalumab-tremelimumab (STRIDE regimen) have become the first-line treatment for advanced HCC patients. The promising survival outcomes in the IMbrave150 and HIMALAYA trials shed new light on the potential of developing combinational therapies.

Nevertheless, with regard to several front-line combinations available, there are currently no biomarkers that would help identify the optimal treatment option for patients nor predict the outcomes for patients upon receiving the treatment. In addition, the multifactorial aetiological setting of patients complicates disease management. Therefore, further biomarker development to select patients eligible for immunotherapy treatment is urgently needed. Taking into account these questions, there is a need to understand better the immune evasive mechanisms of HCC, as well as the intrinsic and acquired resistance to ICIs.

1.5 Hypothesis

We hypothesise that the intrinsic oncogenic signalling pathway plays a crucial role in driving immune evasion in HCC, and its suppression may enhance the therapeutic efficacy of current immune checkpoint therapy.

1.6 Objectives of this study

1. To identify the intrinsic oncogenic pathway crucial for immune escape in an antigen-expressing c-Myc-lucOS^{OE}/Tp53^{KO} HCC mouse model.
2. To evaluate the clinical relevance and functionally characterise the role of the intrinsic oncogenic pathway in immune evasion in HCC.
3. To investigate the molecular mechanism by which the intrinsic oncogenic pathway mediates immune evasion.
4. To evaluate the therapeutic efficacy of targeting the intrinsic oncogenic pathway in combination with ICI for effective HCC treatment.

Chapter 2. Materials and Methods

2.1 Study design

This study aims to examine the effect of wild-type KRAS activation in HCC. We used the immunocompetent murine HCC model induced by hydrodynamic tail vail injection (HTVI) in the context of c-Myc^{OE}/Tp53^{KO} and c-Myc-lucOS^{OE}/Tp53^{KO} background. We also assessed the effects of SOS1 inhibitor MRTX0902 in non-blinded randomised studies (alone or in combination with ICI) on mouse survival. Endpoints were predefined and not modified throughout the study, and mice whose death could not be attributed to liver tumours were excluded from the study. Other *in vivo* experiments were to examine the TIME of murine models by combining data-independent acquisition mass spectrometry (DIA-MS), scRNA-seq and flow cytometry data. Sample size was chosen empirically based on the results of previous studies, outliers, with more than 3 standard deviations away from the mean, were excluded from these analyses.

2.2. Materials

Cell line	Growth medium	Source	Pathological condition
Hep55.1c	DMEM	Cell Line Service (Eppelheim, Germany)	Mouse HCC
Hepa-1,6	DMEM	Gift from Prof. Stephanie Ma (HKU, Hong Kong)	Mouse HCC
RIL-175	RPMI1640	Gift from Prof. Stephanie Ma (HKU, Hong Kong)	Mouse HCC

Table 2.1 List of murine HCC cell lines.

Gene	Forward primer (5'-3')	Reverse primer (5'-3')
18S	GCAATTATTCCCCATGAACG	GGGACTTAATCAACGCAAGC
β-actin	CCTGAGCGCAAGTACTCTGTGT	GCTGATCCACATCTGCTGGAA
Ccl3	CCAAGTCTTCTCAGCGCCATA	GATGAATTGGCGTGGAATCTTC
Ccl5	AGATCTCTGCAGCTGCCCTCA	GGAGCACTTGCTGCTGGTGTAG
Ccnd1	TCAAGTGTGACCCGGACTG	ATGTCCACATCTCGCACGTC
Cxcl9	CGAGGCACGATCCACTACAA	AGGCAGGTTTGATCTCCGTT
Cxcl10	GCCGTCATTTTCTGCCTCAT	GCTTCCCTATGGCCCTCATT

Cxcl11	CCGAGTAACGGCTGCGACAAAG	CCTGCATTATGAGGCGAGCTTG
Dusp6	CTCGGATCACTGGAGCCAAAAC	TCTGCATGAGGTACGCCACTGT
Egf	AGCATACTCAGCGTCACAGC	GCAGGACCGGCACAAGTC
Gapdh	AGGTCGGTGTGAACGGATTTG	TGTAGACCATGTAGTTGAGGTCA
Irf1	TCCAAGTCCAGCCGAGACACTA	ACTGCTGTGGTCATCAGGTAGG
Irf2	AATTCCAATACGATACCAGGGCT	GAGCGGAGCATCCTTTTCCA
Irf7	GAGCGAAGAGAGCGAAGAGG	GGCCCACAGTAGATCCAAGC
Irf9	GCCGAGTGGTGGGTAAGAC	GCAAAGGCGCTGAACAAAGAG
Kras	GTTGGAGCTGGTGGCGTAGG	CTCCTCTTGACCTGCTGTGTCG
Stat1	GCCTCTCATTGTCACCGAAGAAC	TGGCTGACGTTGGAGATCACCA
Stat2	TCCTGCCAATGGACGTTCG	GTCCCACTGGTTCAGTTGGT

Table 2.2 List of primer sequences for qPCR.

Gene	Sequence (5'-3')
Map2k1	CATTCTAGTGAACTCACGTG
Map2k2	GTGCAACTCGCCCTACATCG
NTC	GAAACACCGGGTCTTCGAGAAGACCT

Table 2.3 List of sgRNA sequences.

Target	Experiment	Condition	Catalogue Number	Source
α-tubulin	Western blot	1:5000	#T9026	Merck (New Jersey, USA)
β-actin	Western blot	1:5000	#A5316	Millipore Sigma (Massachusetts, USA)

CD8α	Immunofluorescence	1:500	#98941	Cell Signaling Technology (Massachusetts, USA)
CD11c	Immunofluorescence	1:500	#97585	Cell Signaling Technology (Massachusetts, USA)
CD279 (anti-Pd-1)	*In vivo* blocking of Pd-1	200μg	#BE0146	Bio X Cell (Lebanon, NH, USA)
CXCL9	Immunofluorescence	1:2000	#ab137792	Abcam (Cambridge, UK)
EGF	Western blot	1:1000	#sc-374255	Santa Cruz Biotechnology (Texas, USA)
pEGFR	Immunohistochemistry Immunofluorescence Western blot	1:100 1:100 1:1000	#sc-81488	Santa Cruz Biotechnology (Texas, USA)
EGFR	Western blot	1:1000	#sc-373746	Santa Cruz Biotechnology (Texas, USA)
H-2Kb	Flow cytometry	1:200	#116505	BioLegend (California, USA)
H-2Kb/ SIINFEKL	Immunofluorescence	1:200	#141606	BioLegend (California, USA)
IgG2a, κ Isotype	Flow cytometry	1:200	#400207	BioLegend (California, USA)
IgG2a, κ Isotype	In vivo blocking	200μg	#BE0089	Bio X Cell (Lebanon, NH, USA)
KRAS	Immunofluorescence	1:100	#sc-30	Santa Cruz Biotechnology (Texas, USA)
KRAS	Immunohistochemistry	1:200	#LS-B4683	LifeSpan BioSciences (Seattle, USA)
pERK1/2 (Thr202/Tyr204)	Immunohistochemistry Immunofluorescence Western blot	1:500 1:500 1:1000	#9101	Cell Signaling Technology (Massachusetts, USA)
ERK	Western blot	1:1000	#9102	Cell Signaling Technology (Massachusetts, USA)
MHC-I	Western blot	1:500	#sc-59200	Santa Cruz Biotechnology (Texas, USA)
pMEK1/2 (Ser217/221)	Western blot	1:1000	#9154	Cell Signaling Technology (Massachusetts, USA)

MEK1/2	Western blot	1:1000	#9122	Cell Signaling Technology (Massachusetts, USA)
RAS	Western blot	1:1000	#05-516	Millipore Sigma (Massachusetts, USA)

Table 2.4 List of antibodies.

Reagents	Source
BrightGreen 2X qPCR MasterMix	Applied Biological Materials (Vancouver, Canada)
cOmplete™ EDTA-free protease inhibitor cocktail	Roche (Basel, Switzerland)
Dimethyl sulfoxide (DMSO)	Millipore Sigma (Burlington, Massachusetts, USA)
EasyPep™ MS Sample Prep Kits	Thermo Fisher Scientific (Waltham, Massachusetts, USA)
Murine Epidermal Growth Factor	Millipore Sigma (Burlington, Massachusetts, USA)
Gateway™ LR Clonase™ II Enzyme mix	Invitrogen™, ThermoFisher Scientific (Waltham, Massachusetts, USA)
MHC Class I Pentamers SIINFEKL	ProImmune, Inc (Oxford, UK)
MRTX0902	MedChemExpress (Monmouth Junction, New Jersey, USA)
Opal 4-Color Manual IHC Kit	Akoya Biosciences (Massachusetts, USA)
PhosSTOP™	Roche (Basel, Switzerland)
PrimeScript™ RT Reagent Kit	Takara (Shiga, Japan)
Puromycin	Millipore Sigma (Burlington, Massachusetts, USA)
QIAprep Plasmid Midi Kit	Qiagen (Maryland, USA)
RAS Activation Assay Kit	Millipore Sigma (Burlington, Massachusetts, USA)
Recombinant Murine IFN-γ	PeproTech, Inc. (Cranbury, NJ, USA)

Sulfobutylether-β-Cyclodextrin (SBE-β-CD)	MedChemExpress (Monmouth Junction, New Jersey, USA)
Trametinib	MedChemExpress (Monmouth Junction, New Jersey, USA)
TRIzol® Reagent	Invitrogen™, Thermo Fisher Scientific (Waltham, Massachusetts, USA)
U0126	LC Laboratory (Woburn, MA, USA)
Western Bright ECL HRP substrate	Advansta (San Jose, California, USA)

Table 2.5 List of reagents.

2.3 Methods

2.3.1 Animals

C57BL/6 mice were bred by The University of Hong Kong and The Chinese University of Hong Kong. They were then housed under specific-pathogen-free conditions at Centralised Animal Facilities at The Hong Kong Polytechnic University.

2.3.2 Cell lines and cell culture

The murine HCC cell lines listed in Table 2.1 were maintained in Dulbecco's Modified Eagle Medium (DMEM) or Roswell Park Memorial Institute 1640 Medium (RPMI1640) with high glucose and L-glutamine (Gibco, Invitrogen) supplemented with 10% heat-inactivated fetal bovine serum (Gibco, Invitrogen) and 100 mg/mL penicillin-streptomycin (Thermo Fisher Scientific) at 37C in a humidified chamber containing 5% CO_2.

The Hep55.1c cell line stably expressing KRAS was selected and maintained in DMEM containing puromycin (2 μg/mL). The culture medium was refreshed every two days. All cell lines used in this study were obtained between 2013 and 2016, and they were regularly authenticated by morphologic observation and AuthentiFiler STR (Invitrogen) as well as tested for the absence of mycoplasma contamination (MycoAlert, Lonza). Cells were used within 20 passages after thawing.

2.3.3 Molecular cloning

pT3-EF1A-c-Myc-lucOS was a gift from Amaia Lujambio (Addgene plasmid #129776 ; http://n2t.net/addgene:129776 ; RRID:Addgene_129776). To examine the role of Kras in HCC tumorigenesis and progression, pT3-EF1A-Kras (5,698 base pair; bp) was generated for HTVI. The complete coding sequence of mouse Kras (NM_021284; 567 bp) was generated in the pDONR^{TM}-221 vector (Hitrobio Biotechnology, Beijing, China) and inserted into the pT3-EF1A vector using Gateway^{TM} LR Clonase^{TM} (Thermo Fisher Scientific, Massachusetts, USA). For *in vivo* MEK1/2 knockout, the px330-sgTp53-sgMap2k1-sgMap2k2 (9,373 bp) was composed by Genscript Biotech, USA. The single guide RNA (sgRNA) sequences targeting mouse MEK1 (sgMap2k1:CATTCTAGTGAACTCACGTG) and MEK2 (sgMap2k2: GTGCAACTCGCCCTACATCG) referenced from Mouse CRISPR Knockout Pooled Library (Brie) were cloned into CRISPR/Cas9 vector expressing sgTp53 (px330-sgTp53). In the control plasmid, a sequence of non-targeting control (sgNTC: GAAACACCGGGTCTTCGAG

AAGACCT) was added to the sites of sgMap2k1 and sgMap2k2 in the px330-sgTp53 plasmid.

2.3.4 Establishment of hydrodynamic tail vein c-Myc-luc^{OE}/Tp53^{KO} and c-Myc-lucOS^{OE}/Tp53^{KO} HCC mouse models

Six to eight-week-old male wild-type C57BL/6 mice were used. 15μg of plasmids pT3-EF1A-c-Myc-luc encoding human c-MYC with luciferase expression or pT3-EF1A-c-Myc-lucOS encoding c-MYC with exogenous antigens and CRISPR/Cas9 vector expressing sgTp53 (px330-sgTp53) along with SB13 transposase expressing vector (CMV-SB13) in a ratio of 25:1 were diluted in saline (in a volume ratio 10% of the mouse weight), filtered through 0.22 μm filter and injected into the lateral tail vein of C57BL/6 mice within 5-7 seconds. The constructs used in this study showed long-term expression of genes via HTVI. In order to investigate the effect of KRAS activation in anti-tumour T cell response, pT3-EF1A-Kras, pT3-EF1A-c-Myc-lucOS, px330-sgTp53 and pCMV-SB13 were injected into the mice hepatocytes. In the control, c-Myc-lucOS^{OE}/Tp53^{KO}/EV group, the same amount of empty vector pT3-EF1A was added instead of Kras expressing plasmid to maintain the consistent transfection efficiency of c-Myc and sgTp53 plasmids. To assess the effect of MEK inhibition, the px330-sgp53-sgMap2k1-sgMap2k2 and the same amount of its NTC control px330-sgp53-sgNTC were injected into the mice hepatocytes in the combination of pT3-EF1A-Kras, pT3-EF1A-c-Myc-lucOS and CMV-SB13. To monitor the tumour growth, mice were administered with 100 mg/kg D-luciferin (Gold Biotechnology) via intraperitoneal (IP) injection 5 minutes before bioluminescent imaging (Perkin-Elmer IVIS Lumina Series III Pre-clinical In Vivo Animal Imaging Systems) at defined time points.

The study protocol was approved by and performed in accordance with the Committee of the Use of Live Animals in Teaching and Research at the Hong Kong Polytechnic University (Hong Kong, P.R. China).

2.3.5 Combinational therapy of MRTX0902, trametinib and anti-PD-1 treatments

The c-Myc-lucOS^{OE}/Tp53^{KO}/Kras HCC mouse model was induced in C57BL/6 mice via HTVI, as described in section 2.3.4. The two-week treatment commenced on day 6 after HTVI. The mice were administered the SOS1 inhibitor MRTX0902 (5 mg/kg q.d.; MedChemExpress) via intravenous (IV) injection, coupled with a daily oral administration of trametinib (0.2 mg/kg b.i.d.; MedChemExpress), and anti-PD-1 (200 μg t.i.w.; Bio X Cell) through IP injection.

Tumour growth was monitored using bioluminescence imaging at specific time points. The tumour tissues were harvested for gene and protein expression analyses.

2.3.6 Liquid chromatography with tandem mass spectrometry (LC-MS/MS) analysis

Mouse tumour samples were homogenised and extracted in lysis buffer with Universal Nuclease at 4°C using Precellys Evolution tissue homogeniser and Cryolys cooling (Bertin Technologies). The tissue lysates were centrifuged at 16,000 g for 10 minutes. After protein concentration measurement, 100 µg of protein samples were reduced and digested using EasyPep™ MS Sample Prep Kits (Thermo Fisher Scientific) according to the manufacturer's instructions. The peptide samples were dried using Refrigerated CentriVap Vacuum Concentrators with Cold Traps (Labconco) and resuspended in 100 µl of 0.1% formic acid (FA) in water for LC-MS/MS analysis.

LC-MS/MS analyses were performed on an Orbitrap Fusion Lumos Tribrid Mass Spectrometer (Thermo Fisher Scientific) coupled with UltiMate 3000 RSLCnano System (Thermo Fisher Scientific). A 1mm × 5 mm trap cartridge and a C18 analytical column (75 µm × 250 mm, 2 µm, 100Å) (Acclaim PepMap, ThermoFisher Scientific, USA) were employed for heat-trapping and LC separation respectively. Mobile phases A and B consisted of 0.1% FA in water and 0.1% FA in 100% Acetonitrile (ACN), respectively. Peptides were first trapped for 10 minutes with 100% A with a flow rate of 10µl/min, followed by separation with a flow rate of 300nL/minute: mobile phase B at 2% in 0-10 minutes (trapping time), 2-6% in 10-12 minutes; 6-20% in 12-82 minutes 20-30% in 82-92 minutes, 30-90% in 92-100 minutes and held until 105minutes, and returned to 2% at 105 minutes and maintained until 120 minutes. Both trapping and LC separation were performed in a column oven maintained at 50°C.

Data were collected separately in modes of data-dependent acquisition (DDA) and DIA-MS. The spray voltage and ion transfer tube temperature were maintained at 2,300 V and 300°C respectively, throughout all acquisition. In both acquisition modes, an MS scan with an m/z range of 400-1,500 was performed with an orbitrap resolution of 60,000 maximum injection time of 20 milliseconds and standard AGC target. In DDA mode, precursors with charge states 2-7 were selected for MS/MS analysis with normalised high collision dissociation (HCD) energy of 30%. Dynamic exclusion time was set as 40s. Data-dependent MS/MS spectra were acquired using the orbitrap analyser with a resolution of 7,500 maximum injection target of 30

milliseconds and standard AGC target. The cycling time of each DDA cycle was set to be 3 seconds. In DIA mode, the precursor was fragmented using HCD energy of 32%. The isolation window was set to be 20 m/z in a 400-1500 precursor range, i.e., in a total of 55 scan events in each cycle. MS/MS spectra were acquired using an orbitrap analyser with a resolution of 30,000 scan range of 200-2,000 m/z and maximum injection time of 50ms.

2.3.7 Immunohistochemical analysis of Kras in HCC specimens

Sections were deparaffinised in xylene and rehydrated in graded alcohols and distilled water. Slides were processed for antigen retrieval by a standard microwave heating technique in Tris-EDTA buffer. Endogenous peroxidase activities were quenched using 3% hydrogen peroxide. The sections were immersed in serum free-protein block solution (DAKO). Specimens were subsequently incubated with the antibodies listed in Table 2.4 for mouse HCC samples and human HCC tissue microarray. The sections were then washed thoroughly and incubated with anti-rabbit Envision^{TM} HRP-conjugated secondary antibody (DAKO). Positive signals were visualised using the Liquid DAB+ Substrate-Chromogen System (DAKO). Sections were counterstained with Mayer's haematoxylin and examined using a light microscope. For quantitation of KRAS expression in a tissue microarray, the stained sections were assessed with no prior knowledge of the clinicopathological data for the patients. For intensity (I), each specimen was individually scored from 0 to 1, 0 represents weak and belongs to the "low expression" group; while 1 represents strong and belongs to the "high expression".

2.3.8 Single-cell RNA sequencing (scRNA-seq) analysis

The workflow of scRNA-seq preparation is shown in Figure 5.1. Tumour tissues of c-Myc-luc^{OE}/Tp53^{KO}/EV and c-Myc-luc^{OE}/Tp53^{KO}/Kras were freshly harvested and subjected to enzymatic dissociation. Tumour cells were dissociated in a dissociation buffer containing 0.1 g/ml Collagenase IV and 10mg/ml DNaseI, by the gentleMACS™ dissociator with the programme of liver dissociation and incubated at 37°C. The supernatant was filtered with a 70 µm cell strainer and centrifuged at 600 g for 10 minutes. The supernatant was discarded and subjected to 40%- 80% percoll purification. The cell pellet was resuspended in 40% percoll solution and was carefully transferred to a tube containing 80% percoll solution. The 40% - 80% percoll solution was centrifuged at 1,200 g for 25 minutes at 20°C with no brake. After centrifugation, the middle colourless immune cell layer was transferred to a new tube for red blood cell lysis. The suspension was centrifuged at 700 g for 5 minutes, and the pellet was resuspended in FACS buffer, and immune cells were counted. The cells were stained with anti-

CD45-APC antibody and then LIVE/DEAD™ FixableNear-IR Dead Cell Stain. IgG2bκ was used as a control for anti-CD45 antibody. After washing, the stained cells proceeded to cell sorting for $CD45^+$ immune cells with high viability by BD FACS Aria III cell sorter. The sorted samples were sent for scRNA-seq analysis. Single-cell transcriptomics of tumour tissues was performed using 10X Genomics droplet-based technology, which incorporates microfluidics with DNA barcoding and bioinformatics software (Cell Ranger). Total mRNA from each living $CD45^+$ immune cell was then captured, labelled with unique barcodes, and profiled with RNA sequencing. The alterations in the number of immune cells and their transcriptomic profiles were analysed using the Seurat package in R.

2.3.9 Immune profiling by flow cytometry

Mouse liver samples of c-Myc-lucOS^{OE}/Tp53^{KO}/EV and c-Myc-lucOS^{OE}/Tp53^{KO}/Kras were chopped into small chips in 6-well culture plates containing T cell medium and subjected to enzymatic dissociation as previously described in the preparation procedure of section 2.3.6. scRNA-seq analysis. The cells were subjected to 40%-80% percoll purification for immune cell extraction and then red blood cell lysis. A million cells/samples were seeded into each well of a V-shaped 96 plate. The staining mix for surface staining was added to each well for 20 minutes at 4°C (Table 2.6). The cells were then fixed and permeabilised with eBioscience™ Foxp3/Transcription Factor Staining Buffer Set (#00-5523-00, Invitrogen™) for 30 minutes. The staining mix for intracellular staining was added to each well for 20 minutes at 4°C. After washing, the stained cells were resuspended in FACS buffer and analysed by BD LSRFortessa™ Cell Analyzer.

Markers	Colour channels	Targets/ Functions	Dilution	Source
CD3	BV785	T cell	1:100	Biolegend
CD4	PercP-Cy5.5	CD4 T cell	1:300	Biolegend
CD8a	AF700; FITC; BV421	CD8 T cell	1:100; 1:200; 1:100	Biolegend
CD11b	FITC	Myeloid Cell	1:300	Biolegend
CD11c	APC	Conventional Dendritic Cell	1:100	Biolegend
CD16/32	-	Fc Blocking	1:100	Biolegend
CD19	PE	B cell	1:200	Biolegend
CD44	BV711	Activation marker	1:200	Biolegend
CD45	APC-Cy7	Leukocyte	1:500	Biolegend
CD49b	PE	NK cell	1:50	Biolegend
CD69	BV785	Activation marker	1:100	Biolegend
F4/80	BV605	Macrophage	1:100	Biolegend
Live/Dead	BV510	Viability	1:100	Biolegend
Ki-67	AF700	Proliferation	1:100	Biolegend
LAG-3	BV421	Immune checkpoint	1:50	Biolegend
Ly6C	AF700	Monocytes	1:700	Biolegend
Ly6G	BV711	Neutrophil	1:300	Biolegend
I-A/I-E	PE-Cy7	MHC class II	1:100	Biolegend
PD-1	PE-Cy7	Immune checkpoint	1:100	Biolegend
MHC Class I Pentamers SIINFEKL	PE	H-2Kb SIINFEKL Ovalbumin (257-264)	1:100	ProImmune
TCR-beta	BV650; PercP-Cy5.5	T cell	1:100; 1:200	Biolegend
TIM-3	BV605	Immune checkpoint	1:200	Biolegend

Table 2.6 Immune profiling panel for flow cytometry analysis.

2.3.10 Multiplexed immunohistochemistry in HCC specimens

Multiplexed immunohistochemistry was performed using Opal 4-Color Manual IHC Kit (#NEL810001KT, Akoya Biosciences). Sections were deparaffinised in xylene and rehydrated in decreasing graded alcohols and distilled water. Slides were processed for antigen retrieval by a standard microwave heating technique in 1X AR9 Tris-EDTA buffer (pH9.0, #AR900250ML, Perkin Elmer) for 15 minutes. Endogenous peroxidase activities were quenched using 3% hydrogen peroxide for 10 minutes at room temperature. The sections were immersed in the blocking/antibody diluent (#ARD1001EA, Perkin Elmer) for 30 minutes at room temperature. The specimens were subsequently incubated with the antibodies listed in Table 2.4. The sections were then washed thoroughly and incubated with Opal polymer HRP Ms+Rb for 30 minutes at room temperature. After a brief wash with 1xTBST, Opal 520, 570 and 690 fluorophores (1:200) were applied for 15 minutes. Staining steps were repeated for each antibody staining. A final stripping step was performed in 1x AR6 sodium citrate buffer (pH 6.0) in a microwave oven for 15 minutes. The section slides were cooled down and stained with DAPI solution (1:1000).

2.3.11 GTP-RAS activation assay

Tumour samples were homogenised and lysed using Magnesium Lysis Buffer and the protein concentration of each sample was measured. The non-tumour liver tissue from naïve mice was used for positive and negative controls for the RAS activation assay. The activated RAS level of 2 mg lysates of each sample was measured using the RAS activation assay kit (#17-218, EMD Millipore). The activated GTP-bound RAS was pulled down by RAF which was conjugated to agarose beads. The eluates were analysed by immunoblotting and probed with anti-RAS antibody (# 05-516, Sigma-Aldrich).

2.3.12 RNA extraction and quantitative PCR (qPCR) analysis

Total RNA from murine samples was extracted using TRIzol® Reagent (Invitrogen, Waltham, MA). Samples were lysed for 30 seconds and paused for 2 minutes using Precellys Evolution tissue homogeniser and Cryolys cooling (Bertin Technologies). Homogeniser cycles were repeated twice. Chloroform (Merck, Kenilworth, NJ) was added and mixed with a ratio of 1:5 to the volume of TRIzol® Reagent. The chloroform-TRIzol mixture was centrifuged at 13,300 rpm for 30 minutes at 4°C for phase separation. The top aqueous layer was withdrawn and transferred to a new tube. 500 µl of 100% isopropanol (Merck, Kenilworth, NJ) was added to

the aqueous layer and incubated at 4°C for 20 minutes for RNA precipitation. After incubation, the solution was centrifuged at 13,300 rpm for 20 minutes at 4°C to collect RNA pellets. The supernatant was discarded, and the pellet was washed twice with 1ml of 75% ethanol (Merck, Kenilworth, NJ) and centrifuged at 10,000 rpm for 15 minutes at 4°C. The pellet was air-dried at room temperature and resuspended in UltraPure™ distilled water (Invitrogen, Waltham, MA). RNA concentration was measured with NanoDrop™ One/One^{C} Microvolume UV-Vis Spectrophotometer (Thermo Scientific) and kept at -80°C for long-term storage. cDNA was synthesised using the PrimeScript RT Reagent Kit (Takara) according to the manufacturer's instructions. The mixture was incubated at 37°C for 15 minutes, followed by 85°C for 5 seconds for cDNA production. The cDNA was diluted with UltraPure™ Distilled Water to make a 10-fold dilution and was stored at -20°C. The cDNA samples were mixed with Bright Green 2X qPCR Master Mix (Applied Biological Materials Inc., Canada) in accordance with the manufacturer's instructions. The PCR analysis was performed using QuantStudio 7 Flex Read Time PCR System (Applied Biosystems) with primers specific to the sequences of genes of interest, which are provided in Table 2.2. Relative expression differences were calculated using $2^{-\Delta\Delta}C_{\mathrm{T}}$ method with reference to housekeeping genes β-actin or Gapdh.

2.3.13 Western blot analysis

Tumour samples were homogenised at 4°C using Precellys Evolution tissue homogeniser and Cryolys cooling (Bertin Technologies) and extracted using either RIPA buffer supplemented with a protease inhibitor cocktail and phosphatase inhibitors (Roche). Protein lysates were separated by SDS-polyacrylamide gel electrophoresis (SDS-PAGE) and transferred to a polyvinylidene difluoride membrane (Millipore) for western blot analysis. Primary antibodies listed in Table 2.4 were incubated at 4°C overnight. After washing, the membrane was incubated with horseradish peroxidase-conjugated anti-mouse or rabbit antibody (GE HealthCare). The signals were visualised using the enhanced chemiluminescence method. Blot images were quantified by densitometry using ImageJ software.

2.3.14 Bioinformatics and statistical analysis

2.3.14.1 MS data analysis of label-free DDA and DIA proteomics

The acquired label-free DDA data of c-Myc-luc^{OE}/Tp53^{KO} HCC and c-Myc-lucOS^{OE}/Tp53^{KO} HCC samples (n=5/ group) were imported to Spectronaut 14 software (Biognosys) for the generation of a spectral library. The DIA data were imported to the DDA library-based DIA analysis and searched against the mouse UniProt database (release 2022_01, 23rd Feb 2022). The BGS Factory Settings (default setting) was adopted for the DIA analysis. In parallel, the DDA data of the same set of tumour samples were analysed using Progenesis QI for Proteomics (QIP, Waters Corp., USA) with Mascot Server 2.4 (Matrix Science, United Kingdom) for protein identification. The precursor ion mass tolerance and fragmentation tolerance were set as 10 ppm and 0.05 Da for the database search, respectively. The maximum number of modifications per peptide was three. Carbamidomethylation of cysteine was set as a fixed modification, and oxidation of methionine and N-terminal acetylation were set as variable modifications. The enzyme was specified as trypsin with up to two missed cleavages allowed. The false discovery rate for peptide matches and proteins was adjusted to 1%.

2.3.14.2 Pathway analysis by Gene Set Enrichment Analysis (GSEA)

In the MS analysis, the average values of the log2 ratio of c-Myc-lucOS^{OE}/Tp53^{KO} compared to c-Myc-lucOS^{OE}/Tp53^{KO} HCC samples (n=5/group), with the q-value $\leq$ 0.05 were input to Gene Set Enrichment Analysis (GSEA) software_4.2.3. In the TCGA-LIHC cohort, 372 HCC samples were divided into groups with low (n=228) and high (n=144) wild-type KRAS expression, according to mean KRAS expression and input into GSEA software. The H: hallmark gene sets database from Molecular Signatures Database Collections (MSigDB) was used in the pathway analysis and with a false discovery rate (FDR) <0.25, which was considered to be significantly enriched and suitable for further investigation of the biological processes involved (Subramanian et al., 2005).

2.3.14.3 Statistical analysis

Statistical significance of qPCR, flow cytometry, and immunohistochemistry results were analysed by Student's t-test using GraphPad Prism. The displayed results showed the means and the standard deviations, and those with p-values less than 0.05 were considered statistically significant (* $p<0.05$, ** $p<0.01$, *** $p<0.001$ and **** $p<0.0001$). All tests are two-sided. Data point was excluded if it deviated from the mean with more than 3 standard deviations.

Investigators were not blinded to the group allocation during the experiment and when assessing the outcome in all experiments including animal experiments. There is no estimate of variation within each group of data. Variance is similar between the groups that are being statistically compared. Chi-square test was employed to examine the correlation of KRAS with tumour relapse in HCC samples. Kaplan-Meier survival analysis was used to test the overall survival and disease-free survival, and a log-rank test was used to determine the statistical significance; these analyses were carried out using SPSS 21 software.

Chapter 3. DIA proteomic analysis identified KRAS signalling is enriched in c-Myc-lucOS^{OE}/Tp53^{KO} HCC mice model

3.1 Introduction

In cancer immunology, the immune response to cancer is often conceptualised with the cancer immunity cycle, as suggested by Chen and Mellman (2013; Figure 1.5). In addition to the reactivation of cytotoxic $CD8^+$ T cell response, the current direction of therapeutic strategies targets more than one step of anti-tumour response within the immunity cycle, for example, antigen presentation, priming to the T cell, T cell infiltration and activation. In this context, combinational therapies would offer a synergistic effect for enhancing the anti-tumour immune response. Thus, understanding the interactions between the tumour cells and the other components of the immunity cycle is of utmost importance.

In order to identify the oncogenic pathway that mediates immune escape in HCC, a suitable immunocompetent HCC model for studies on immune surveillance is required. The *in vivo* system of endogenous T cell response in genetically engineered mice was first designed by DuPage et al. (2011). In that model, the introduction of exogenous antigens, including the 2c T cell receptor epitope SIYRYYGL (SIY) and two antigens from ovalbumin (OVA)-SIINFEKL (SIN, OVA257-264) and OVA323-339 – fused to the C-terminus of luciferase of the Lenti vector (Lenti-LucOS), mimicked the TAAs. The expression of TAAs enhances the immunogenicity of the tumour and recruits the cytotoxic T cell infiltration into the tumour site, leading to a delay in tumour progression.

Ovalbumin is a well-characterised source of adjuvants for subunit vaccines, which are constantly challenged by poor immunogenicity. T cells recognise the antigens by binding to the peptides that are presented by the MHC-I. The peptide epitopes OVA257-264 and OVA323-339 induced both humoral and cellular immune responses in the host immune system. SIINFEKL (the amino acid sequence of epitope OVA257-264) is a class I (Kb)-restricted peptide epitope of OVA. This peptide can be recognised by cytotoxic T cell lymphocytes and subsequently induces a peptide-specific T cell response (Rötzschke et al., 1991; Hulseberg et al., 2010). OVA323-339 encompasses a peptide epitope that binds to MHC-II I-A(d) and is responsible for T cell activation (McFarland et al., 1999).

The Lenti-LucOS model revealed the dynamic nature of immune surveillance and enabled tracking of antigen-specific endogenous T cells during tumorigenesis (DuPage et al., 2011). It was later introduced into HTVI-induced c-Myc-$lucOS^{OE}$/$Tp53^{KO}$ HCC in immunocompetent mice by de Galarreta et al. (2019). In this study, β-catenin activation was found to promote

immune evasion and resistance to anti-PD-1 treatment in HCC cells. The findings in the murine model provided a mechanistic explanation of immune exclusion to the clinical data where more than 30% of CTNNB1 mutants are predicted to resist the anti-PD-1 therapy (Pinyol et al.2019). Moreover, the introduction of exogenous antigens was also employed to investigate T cell exhaustion in the AKT/NRAS HCC murine model (Liu et al., 2018).

Clinically, TAA-specific $CD8^+$ T cell responses naturally occur in HCC patients and contribute to the T cell repertoire. Moreover, the breadth of these responses is positively correlated to patient survival (Flecken et al., 2014). These findings support the development of the LucOS model as a suitable immunocompetent HCC mouse model to study the immunology of HCC.

3.2 Experiment design

(1) An immunocompetent murine HCC model was established with the gene transfer of two commonly altered genes in HCC: *MYC* (12%) and *TP53* (32%) in the TCGA-LIHC cohort (Cerami et al., 2012). Utilising the concept of immune surveillance, T cell epitope antigens SIYRYYGL (SIY), SIINFEKL (SIN, OVA257-264), and OVA323-339 were fused to the C-terminus of an oncogenic c-Myc-expressing plasmid. The plasmids were introduced into the hepatocytes of the C57BL/6 mice via HTVI. Intravascular pressure within the inferior vena cava increases upon tail vein injection of the plasmid mixture. The injected solution enters the heart and induces cardiac congestion, which pushes the solution back in the retrograde direction. The solution flew into the liver via the hepatic vein and caused swelling of the liver and an increase in the permeability of the hepatocytes, thus transferring the genes into the hepatocytes. In the antigen-expressing c-Myc-lucOS^{OE}/Tp53^{KO} HCC tumour, the T cell epitope peptides were expressed and bound to MHC molecules on the surface of the tumour cells. This increased the immunogenicity of the mouse model and enhanced the anti-tumour CD8^{+} immune response.

(2) The tumour tissues of c-Myc-luc^{OE}/Tp53^{KO} and immune-escaped c-Myc-lucOS^{OE}/Tp53^{KO} were harvested and analysed by DIA label-free proteomics. The MS data was further analysed using GSEA software to identify the intrinsic oncogenic pathway enriched in the immune-escaped tumour.

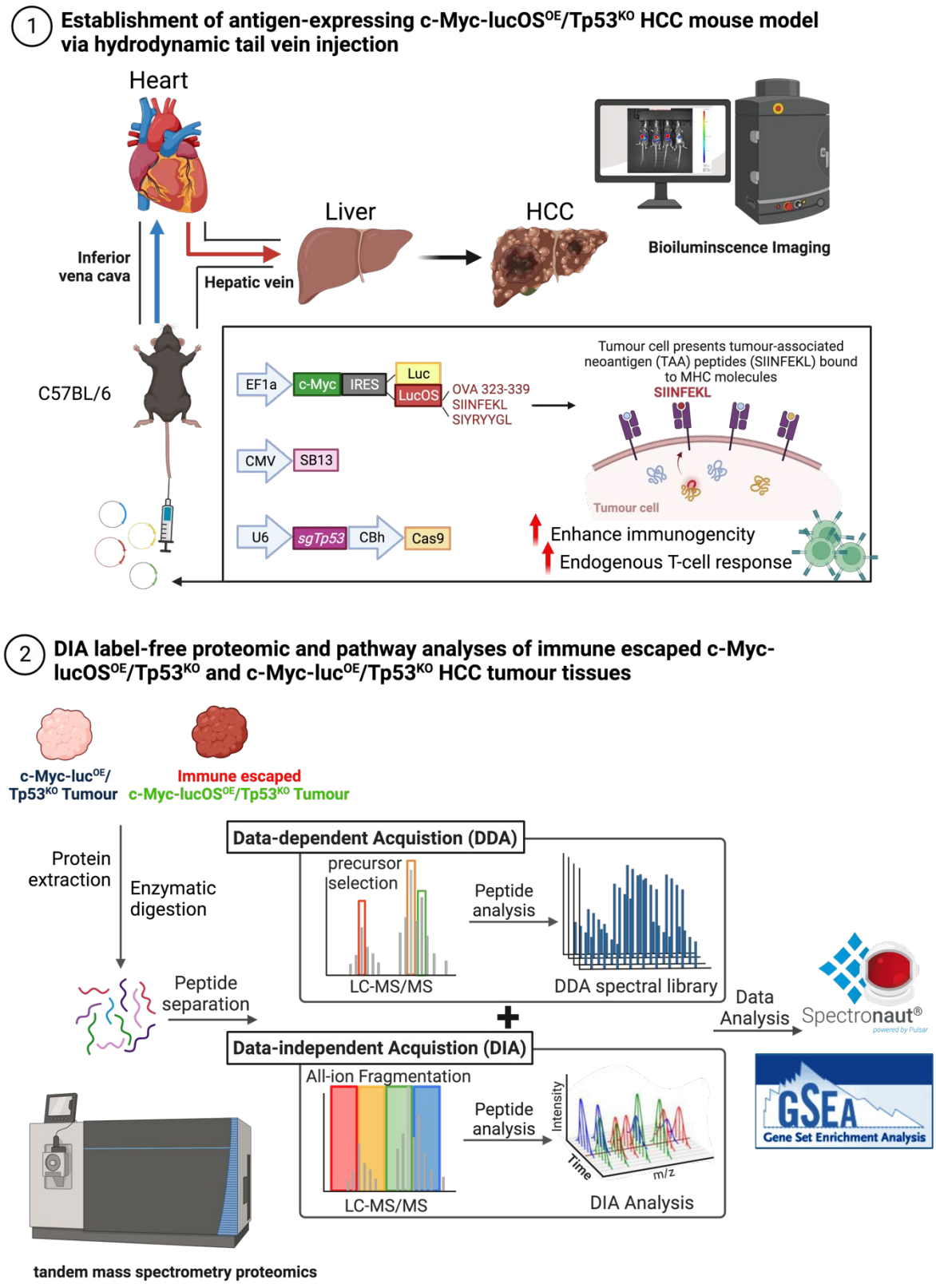

Figure 3.1 An outline of the experiment design to investigate the intrinsic oncogenic pathway that mediates the immune escape in the c-Myc-lucOS^{OE}/Tp53^{KO} HCC mouse model

3.3 Results

3.3.1 Expression of exogenous antigens delays tumour progression in c-Myc-lucOS^{OE}/Tp53^{KO} HCC mice model

To establish an HCC murine model, two of the most commonly altered genes, c-Myc and Tp53, were selected as the oncogene background. In the TCGA-LIHC cohort, oncogene *MYC* was amplified in 12% of the patients, while the deletion or mutation of tumour suppressor *TP53* was attributed to 32% of HCC cases (Cerami et al., 2012; Figure 3.2A). In the control group, plasmids encoding sgTp53, SB13 and c-Myc with luciferase (c-Myc-luc) were injected into the mice, and the tumour growth was monitored by bioluminescence imaging. The tumour continued to grow, as shown in the luciferase signals on day 12 and day 29 (Figure 3.2B&C). All the mice presented gross liver tumours, with a median survival of 42 to 48 days (Figure 3.2D). In the antigen-expressing c-Myc-lucOS^{OE}/Tp53^{KO} group, the same amount of c-Myc-lucOS, sgTp53, and SB13-expressing plasmids were injected into the mice. The expression of the exogenous T cell antigens caused a reduction in tumour progression. The luciferase signals of the antigen-expressing lucOS group were lower than those of the control group on day 12 and continued to decrease on day 29. The majority of mice did not develop any tumours within 60 days (Figure 3.2B&C). However, the anti-tumour T cell response failed to clear the tumour cells in all mice, and some of them (about 2 out of 10 mice) eventually escaped the immune system and developed tumours (Figure 3.2D).

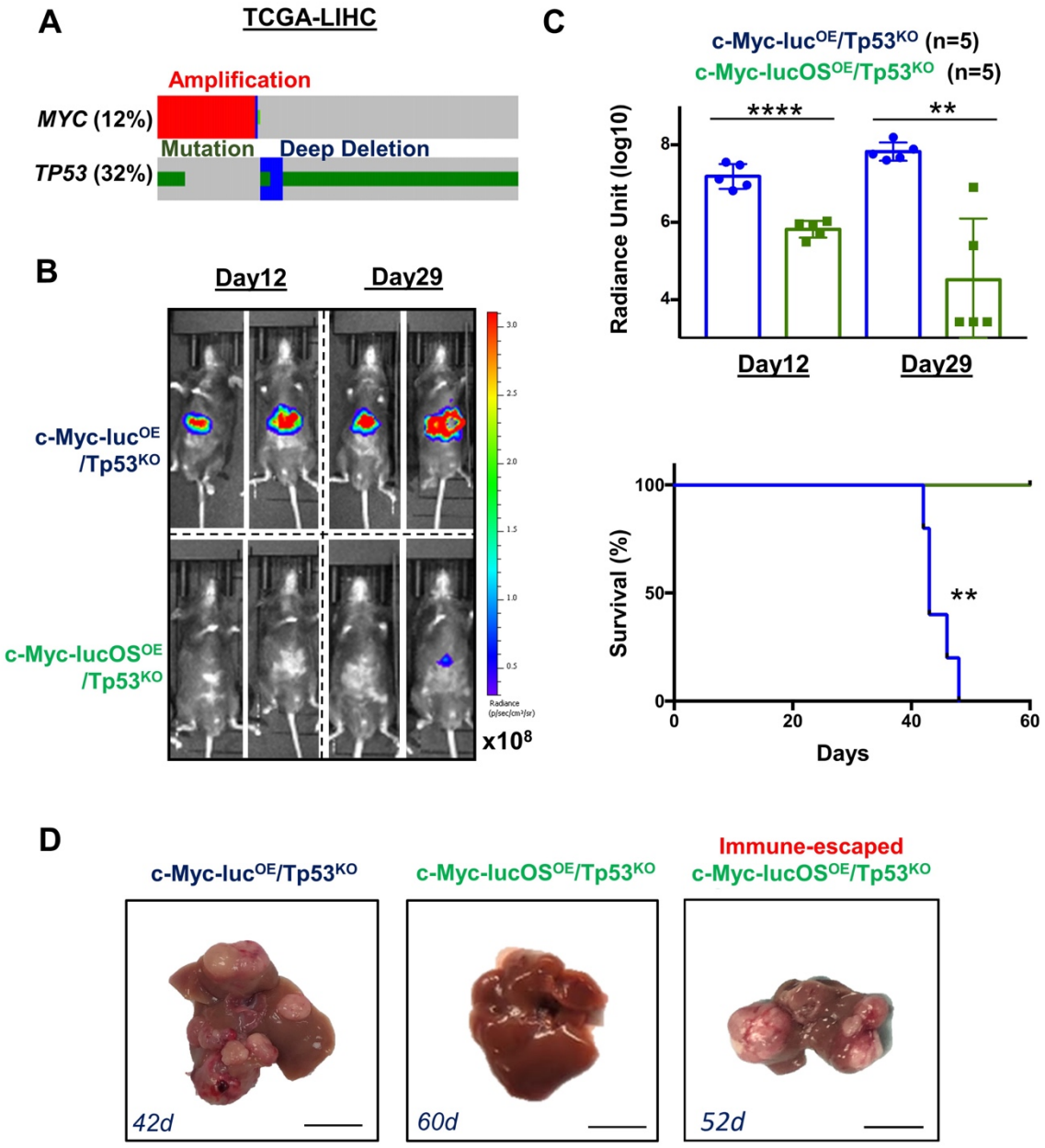

Figure 3.2 Expression of exogenous antigens delays tumour progression in c-Myc-lucOS^{OE}/Tp53^{KO} HCC mouse model.

(**A**) Genomic alterations of oncogene *MYC* (12%) and tumour suppressor gene *TP53* (32%) in the TCGA-LIHC cohort (n=372 samples). Oncogenic plasmids of two commonly altered genes in HCC, c-Myc, and Tp53 were introduced into the hepatocytes of mice via HTVI to induce HCC. (**B**) Representative bioluminescence images of c-Myc-luc^{OE}/Tp53^{KO} and c-Myc-lucOS^{OE}/Tp53^{KO} on day 12 and day 29 after HTVI. The scale bar for the luciferase signal was shown. Quantification of normalised luciferase signal at days 12 and 29 after injection of vectors (n = 5 per group). (**C**) Exogenous T cell-specific antigens expression caused a reduction in the luciferase signal and resulted in tumour delay. The majority of the mice did not develop

any tumours, with a significant survival benefit. However, the clearance of tumour cells was incomplete in all mice, and some of the tumours (2 out of 10) eventually escaped the immune system. (**D**) Representative images of c-Myc-luc^{OE}/Tp53^{KO}, c-Myc-lucOS^{OE}/Tp53^{KO} and immune-escaped c-Myc-lucOS^{OE}/Tp53^{KO} livers.

3.3.2 DIA proteomic analysis identified oncogenic KRAS signalling enriched in immune-escaped c-Myc-lucOS^{OE}/Tp53^{KO} HCC mice model

To investigate the intrinsic oncogenic pathway enriched in the immune-escaped tumour, c-Myc-luc^{OE}/Tp53^{KO} and immune-escaped c-Myc-lucOS^{OE}/Tp53^{KO} tumour tissues were harvested for DIA proteomics. A total of 4515 differentially expressed proteins with a q-value <0.05 were identified in the DIA proteomics. In the analysis, the Principal Component Analysis (PCA) showed 37.53% variability between the two groups in the first principal component (PC1) and 18.99% in PC2 (Figure 3.3A). The volcano plot of the proteomic analysis (Figure 3.3B) revealed that the top differentially expressed proteins, for example, Slc2a1 (Log2 Fold Change (FC): 3.69, p<0.01), Igf2bp1 (Log2FC:3.38, p<0.01), Anxa2 (Log2FC: 3.11, p<0.01), Plaur (Log2FC: 2.91, p<0.01), Itga3 (Log2FC: 2.76, p<0.01) and Itgam (Log2FC: 2.67, p<0.01), enriched in the c-Myc-lucOS^{OE}/Tp53^{KO} groups were associated with immune infiltration in cancer (Elcheva et al., 2023; Li et al., 2021; Liu et al., 2021; Liu et al., 2022; Ning, Li, & Wang, 2023; Schmid et al., 2018). The enrichment of these marker genes further confirmed that the expression of the antigens enhanced immunogenicity.

The proteomic data was further analysed by GSEA to examine the enrichment of oncogenic pathways in immune-escaped tumours using the H: Hallmark gene sets database (MSigDB v2022.1.Hs; Subramanian et al., 2005). Nine gene sets were significantly enriched at a nominal p-value <0.05 in the c-Myc-lucOS^{OE}/Tp53^{KO} group, while four gene sets were significantly enriched in the c-Myc-luc^{OE}/Tp53^{KO} group (Figure 3.3C). Immune-related pathways such as coagulation, complement, and IL2/ STAT5 signalling were significantly enriched in c-Myc-lucOS^{OE}/Tp53^{KO}, ensuring the activation of the immune response in the lucOS group. Among the enriched pathways in the immune-escaped group, oncogenic KRAS signalling (HALLMARK_KRAS_SIGNALLING_UP) was ranked fifth with a normalised enrichment score (NES) of 2.11. Nevertheless, it was the top oncogenic pathway enriched in the immune-escaped group. Moreover, Kras (Log2FC:1.44, p<0.05) and its downstream effector Cyclin D1 (Ccnd1; Log2FC:2.915, p<0.05) were upregulated in protein levels in immune-escaped c-Myc-lucOS^{OE}/Tp53^{KO} tumours (Figure 3.3B). qPCR analysis also confirmed the upregulated Kras mRNA expression in immune-escaped tumours (Figure 3.3D).

To validate that the KRAS signalling pathway was activated in immune-escaped tumours, immunohistochemical (IHC) analyses for the upstream phospho-epidermal growth factor receptor (pEGFR) and downstream phospho-extracellular signal-regulated kinase (pERK1/2) were performed (Figure 3.3F). Higher expressions of pEGFR, KRAS and pERK1/2 were found in immune-escaped tumours, with a colocalisation of KRAS and pERK1/2, confirming the activation of EGFR/KRAS/ERK signalling in immune-escaped c-Myc-lucOS^{OE}/Tp53^{KO} HCC (Figure 3.3F).

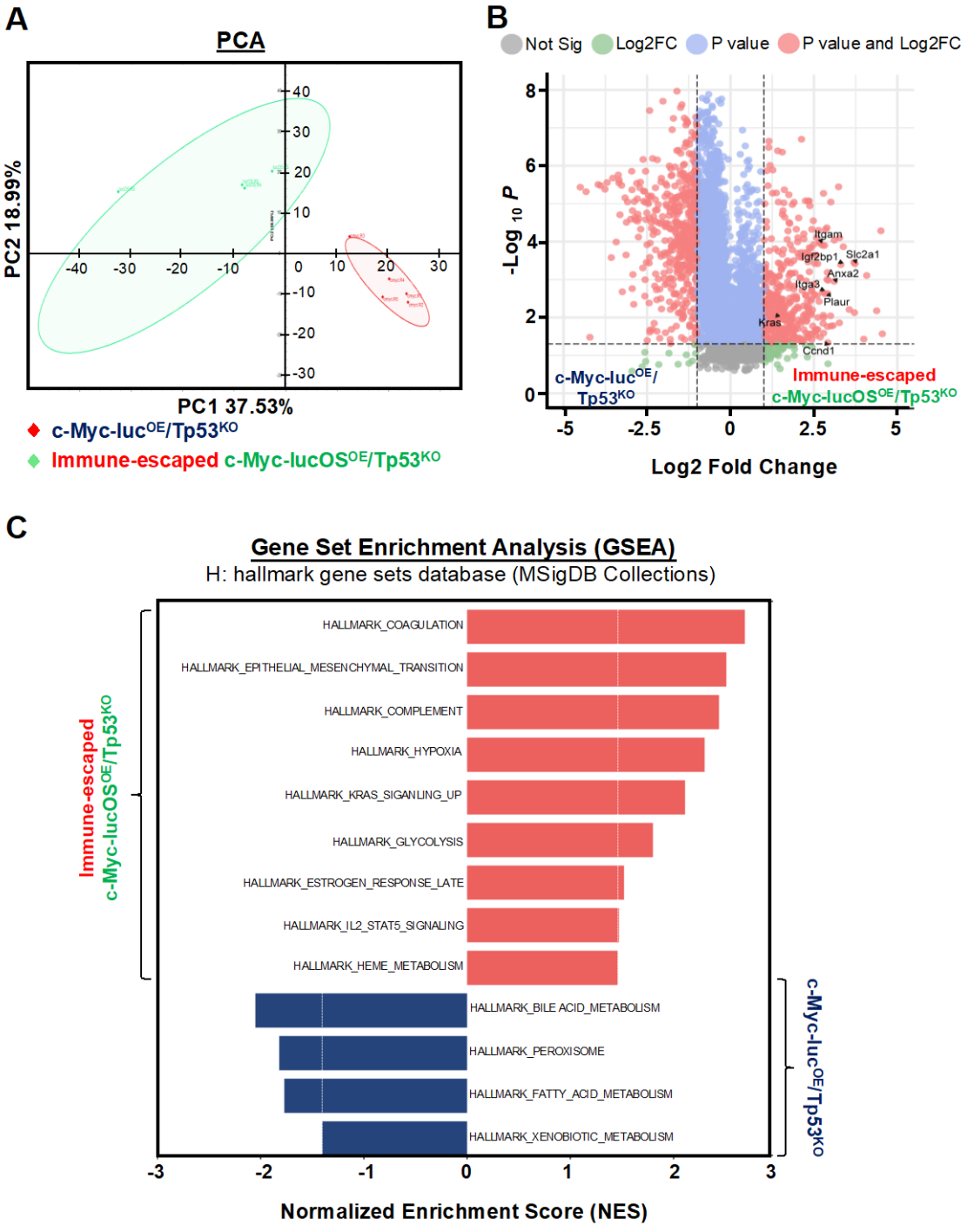
A
PCA
PC2 18.99%
PC1 37.53%
c-Myc-luc^OE/Tp53^KO
Immune-escaped c-Myc-lucOS^OE/Tp53^KO
B
Not Sig
Log2FC
P value
P value and Log2FC
-Log 10 P
Log2 Fold Change
Itgam
Igf2bp1
Slc2a1
Anxa2
Itga3
Plaur
Kras
Ccnd1
c-Myc-luc^OE/ Tp53^KO
Immune-escaped c-Myc-lucOS^OE/Tp53^KO
C
Gene Set Enrichment Analysis (GSEA)
H: hallmark gene sets database (MSigDB Collections)
HALLMARK_COAGULATION
HALLMARK_EPITHELIAL_MESENCHYMAL_TRANSITION
HALLMARK_COMPLEMENT
HALLMARK_HYPOXIA
HALLMARK_KRAS_SIGANLING_UP
HALLMARK_GLYCOLYSIS
HALLMARK_ESTROGEN_RESPONSE_LATE
HALLMARK_IL2_STAT5_SIGNALING
HALLMARK_HEME_METABOLISM
HALLMARK_BILE ACID_METABOLISM
HALLMARK_PEROXISOME
HALLMARK_FATTY_ACID_METABOLISM
HALLMARK_XENOBIOTIC_METABOLISM
Immune-escaped c-Myc-lucOS^OE/Tp53^KO
c-Myc-luc^OE/Tp53^KO
Normalized Enrichment Score (NES)

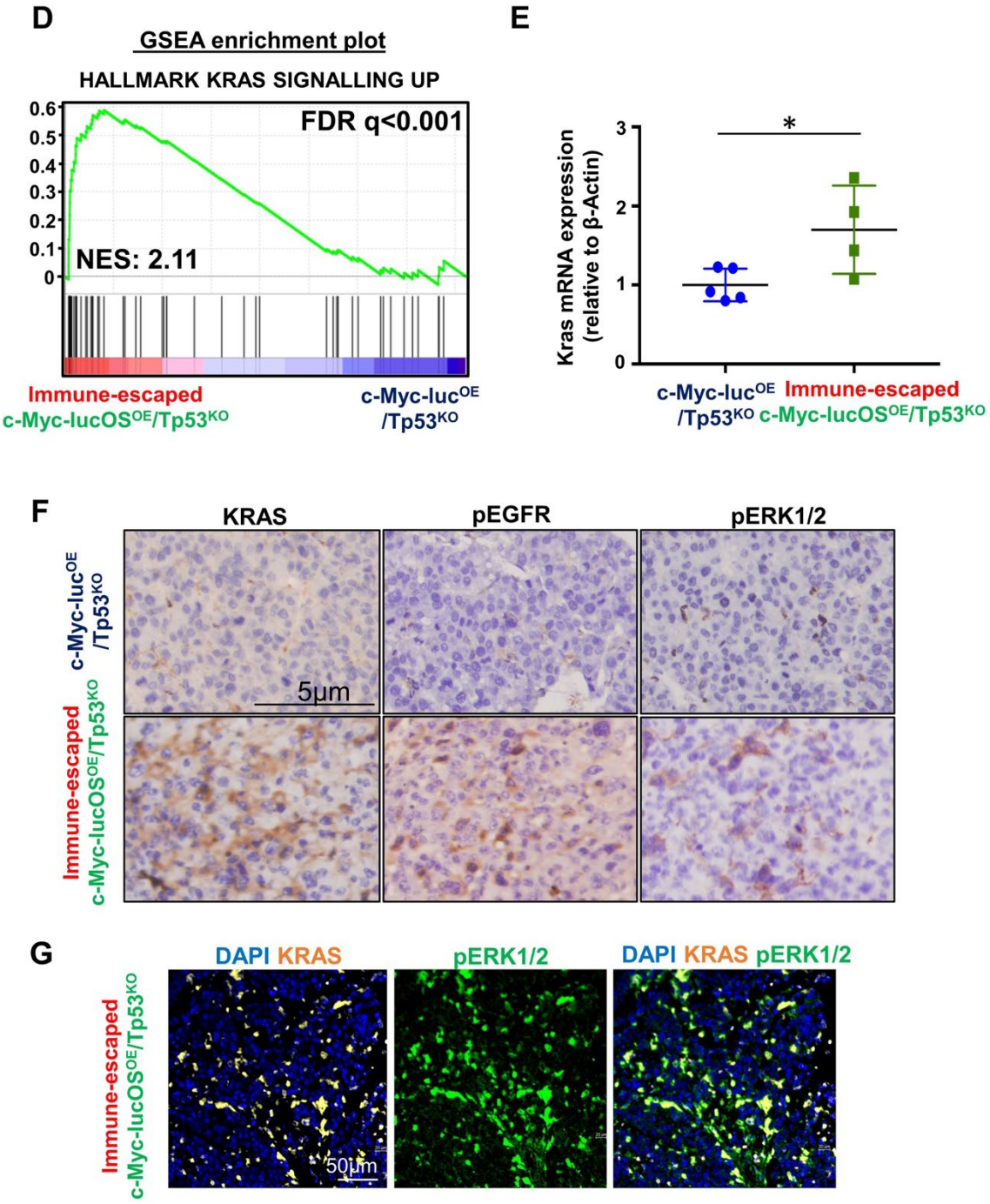

Figure 3.3 DIA proteomic analysis identified oncogenic KRAS signalling enriched in the immune-escaped c-Myc-lucOS^{OE}/Tp53^{KO} HCC mouse model.

(**A**) Principal component analysis (PCA) plot showing the clusters of c-Myc-luc^{OE}/Tp53^{KO} (n=5) and immune-evaded c-Myc-lucOS^{OE}/Tp53^{KO} tumour tissues (n=5) in DIA-MS proteomics. PC1 and PC2 explained 37.53% and 18.99% of the variability between the two groups, respectively. (**B**) Volcano plot of the proteomic analysis revealed that Kras (Log2FC:1.44, $p<0.05$) and its downstream effector Cyclin D1 (Ccnd1; Log2FC:2.915, $p<0.05$) were upregulated in immune escaped c-Myc-lucOS^{OE}/Tp53^{KO} tumours. Marker genes related to immune infiltration, e.g. Itga3 were also upregulated in immune-escaped tumours, further confirming that endogenous expression of the antigens enhances immunogenicity. (**C**) GSEA pathway analysis (H: hallmark gene sets database from MSigDB Collections) compared the c-

Myc-luc^{OE}/Tp53^{KO} and immune-escaped c-Myc-lucOS^{OE}/Tp53^{KO} tumour tissues. (**D**) Oncogenic KRAS signalling pathway (NES: 2.11, FDR q<0.01) was enriched in c-Myc-lucOS^{OE}/Tp53^{KO} tumours. Red: c-Myc-lucOS^{OE}/Tp53^{KO}, blue: c-Myc-luc^{OE}/Tp53^{KO} (**E**) qPCR confirmed the upregulated Kras mRNA expression in immune-escaped tumours. (n=5; * p<0.05, t-test). (**F**) Immunohistochemistry analysis demonstrated that EGFR/KRAS/ ERK1/2 signalling was activated in immune-escaped c-Myc-lucOS^{OE}/Tp53^{KO} HCC. (**G**) Multiplexed immunofluorescence showed the colocalisation of Kras and pERK1/2 expression in c-Myc-lucOS^{OE}/Tp53^{KO} tumour tissue.

3.4 Discussion

In this study, the HCC murine model was induced by HTVI, which generates endogenous and heterogeneous liver-specific tumours and better mimics the characteristics of HCC patients. Unlike orthoptic or ectopic transplantation of the primary tumour cells or cell line, the autochthonous tumour undergoes the process of tumorigenesis and avoids the unnecessary immune response that could be provoked by the introduction of foreign cells into the liver. As HTVI is performed in 6 to 8-week-old adult mice, it avoids problems that might occur during the development of traditional transgenic mice (Gu & Lee, 2022). Moreover, the transfection efficiency of HTVI is around 10- 40% of hepatocytes, leading to a small population of cells undergoing genetic alteration, which resembles the initiation of human HCC.

C-Myc and Tp53 were selected as the oncogenic background of the HCC model in this study due to their frequent genetic alteration in HCC. The co-occurrence of dysregulation of *MYC* and *TP53* in HCC was found in 6.5% of the patients. Overexpression of *c-Myc* is broadly observed in solid tumours, often caused by genomic amplification at chromosome 8q24.1. It is frequently detected in patients with advanced liver fibrosis and strongly correlates with cirrhosis and HCC progression (Nevzorova et al., 2013). C-Myc is a crucial driver of immune evasion as its overexpression is associated with the suppression of innate immunity and MHC-I antigen presentation, leading to inadequate $CD8^+$ T cell infiltration. The disruption of Tp53 has been reported to promote immune escape via the perturbation of APM and suppression of the immunogenicity of the tumour (Wang et al., 2013; Zhu et al., 1999). Loss of p53 function also damaged T cell response via the recruitment of immunosuppressive myeloid and Treg populations (Bezzi et al., 2018). Studies have also reported the crosstalk between Myc and Tp53 in promoting HCC progression and suppressing the TIME (Blagih, Buck, & Vousden, 2020; Kawate et al., 1999). Thus, the c-Myc-luc^{OE}/$Tp53^{KO}$ HCC model has low immunogenicity and was previously reported to be unresponsive to anti-PD-1 therapy (Chiu et al., 2020).

TAA-specific $CD8^+$ T cell responses occur naturally in HCC patients and characterise part of the normal T cell repertoire (Flecken et al., 2014). Moreover, the efficacy of these responses correlates with patient survival. The introduction of the exogenous antigens SIYRYYGL (SIY), SIINFEKL (SIN, OVA257-264), and OVA323-339 in the c-Myc-luc^{OE}/$Tp53^{KO}$ model increased its immunogenicity and aroused a TAA-specific anti-CD8 T cell response. Our findings supported that the induction of T cell response was able to eliminate the tumour cells

and delay the tumour progression. Intriguingly, the T cell immune response was not complete and failed to eradicate the tumour cells in all mice. This observation aligns with previously reported findings in the lung cancer model (DuPage et al., 2011). Immune escape could be attributed to the capability of the cancer immunoediting (Dupage et al., 2012). Through the gradual selection of clones with loss of antigen expression or presentation on MHC-I, tumour cells were edited to become less immunogenic and thus led to dysfunctional T cell response. It is also possible that in our model, a small population of tumour cells, which downregulated the MHC-I expression on their cell surface, survived the attack of cytotoxic T cells and expanded in the liver. Yet, the underlying mechanism of incomplete anti-tumour response remains unknown. Besides defective antigen presentation, tumour cells evade host immune defence through various methods, including impaired T cell activation, infiltration, and accumulation of immunosuppressive molecules and cells in the TIME (Chen & Mellman, 2017; Figure 3.4).

In addition to $CD8^+$ T cell-mediated immune surveillance, $CD4^+$ T cells also play an important role in assisting the anti-tumour immune response via MHC-II antigen processing. Novel autochthonous mouse models incorporated with the expression of CD4-specific neoantigens were also established to examine the role of $CD4^+$ in the T-cell dysfunction (Westcott et al., 2021). By inducing the endogenous $CD4^+$ cells, the number of functional tumour-specific $CD8^+$ was significantly enhanced, leading to a reduced tumour burden in the mouse model. This highlighted the importance of the intricate coordination of $CD8^+$ cells and other immune cells in eliciting the anti-tumour response.

To investigate the underlying mechanism of immune-evaded tumours, we performed a DIA-MS analysis to examine the proteomic profile of tumour tissues. In contrast to DDA-MS, DIA-MS offers a broader spectrum of protein identification and a higher reproducibility and accuracy in the quantification of protein levels (Bichmann et al., 2021). This is because, in DIA-MS, all the peptides within a defined mass-to-charge (m/z) window in the MS1 scan are fragmented for the second stage of tandem MS analysis (MS2). In DDA-MS, only the top precursor peptides (the highest abundance in MS1) are subjected to fragmentation for MS2 (Figure 3.1). Furthermore, the MS/MS data acquisition in DIA occurs in parallel across peptides. Therefore, the consequent MS spectra are highly multiplexed and avoid the under-representation of low-abundant proteins.

Our proteomic data demonstrated the successful induction of the immunogenicity of the model, evidenced by the upregulation of the immune infiltration-related proteins, including Slc2a1, Igf2bp1, Anxa2, Plaur and Itgam (Figure 3.3B). GSEA analysis also revealed the activation of immune-related pathways in the immune-escaped group. This hinted at the possibility of other oncogenic pathways in exploiting the immune surveillance in these immune-escaped mice. In the pathway analysis, the oncogenic KRAS signalling pathway was enriched in the lucOS group with an upregulation of one of its downstream effectors Ccnd1 (Figure 3.3B&C). The data was further validated by the qPCR and IHC analysis, suggesting that the KRAS signalling was turned on upon the upstream activation.

Moreover, the lipid metabolism-related pathways, including the bile acid, peroxisome and fatty acid metabolisms, were enriched in the c-Myc-luc^{OE}/Tp53^{KO} HCC. Increasing demand for local glucose and oxygen is one of the hallmarks of the tumour microenvironment. Lipids are the primary energy source for both tumour and immune cells in the hypoxic and glucose-deficient tumour milieu. Indeed, lipid metabolism reprogramming influenced the anti-tumour immune response and the responsiveness to the immunotherapy (Feng et al., 2023; Wang et al., 2023). Intracellular fatty acid facilitated CD8$^+$ T cells' lipid metabolism and preserved their effector functions via activation of PPARα (Wang et al., 2020). Depletion of lipids in CD8$^+$ T cells inhibited their proliferation and cytotoxicity and promoted T cell exhaustion (Vergnes et al., 2013). In addition, the immunogenicity of DCs is associated with the level of lipid content. The higher lipid-containing DCs are immunogenic as they possess a higher capacity for robust antigen presentation and enhance the endogenous cytotoxic T cells (Ibrahim et al., 2012). DCs with high lipid compositions tend to produce higher levels of integrins, co-stimulatory molecules, pro-inflammatory cytokines and chemokines (Dong & Bullock, 2014). Dysregulated lipid metabolism in DCs could make the cells tolerogenic, promoting immune evasion in HCC (Herber et al., 2010). Therefore, it could be possible that the downregulated lipid metabolism impeded the functions of the immune cells and elicited an adequate immune response in immune-escaped tumours.

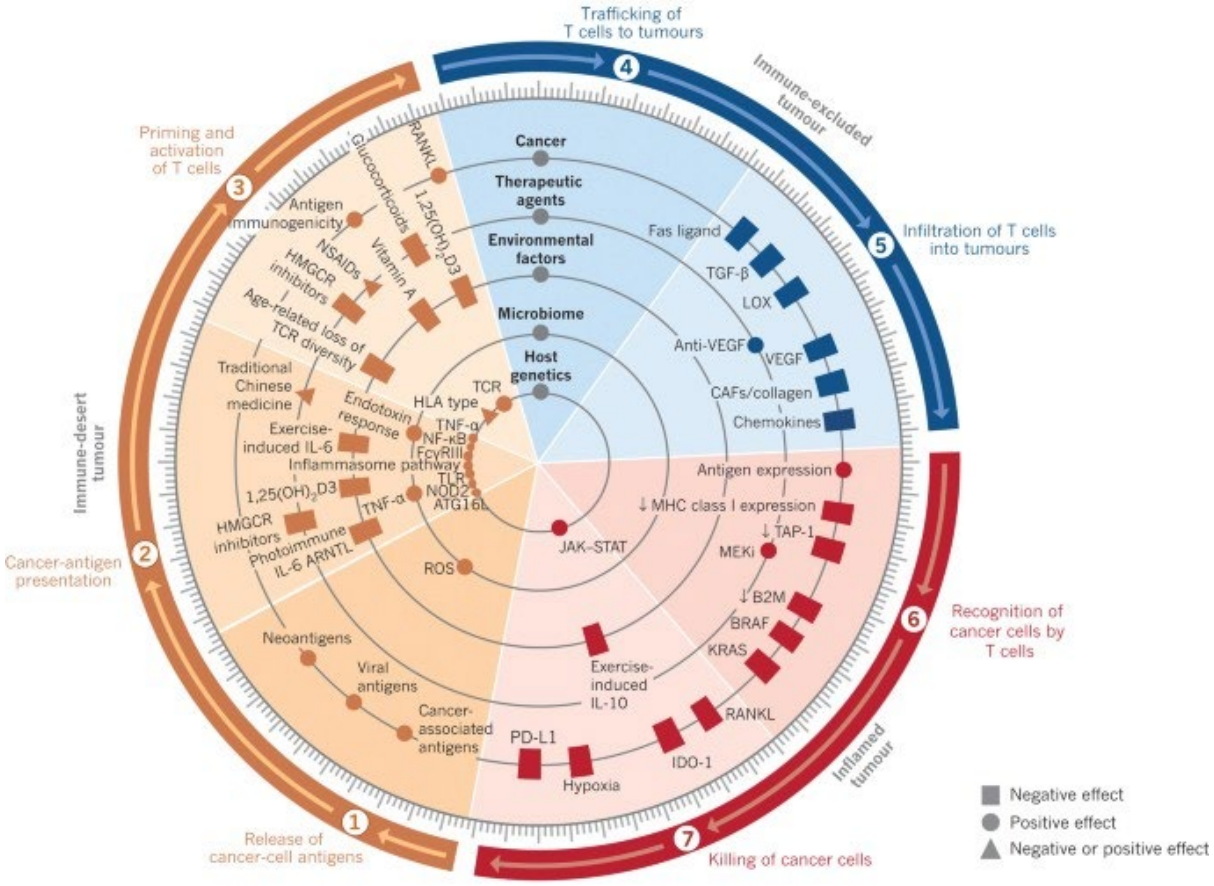

Figure 3.4 Factors affecting the different processes in the cancer-immunity cycle.
(Chen & Mellman, 2017)

Chapter 4. Wild-type Kras overexpression promotes immune evasion in c-Myc-lucOS^{OE}/Tp53^{KO} HCC mice model

4.1 Introduction

In Chapter 3, the DIA-MS result showed that wild-type Kras expression and KRAS signalling were enriched in the immune-escaped c-Myc-lucOS^{OE}/Tp53^{KO} HCC tumours. As a result, we hypothesise that KRAS signalling promotes immune evasion. Activation of KRAS signalling is often observed in cancers that harbour high levels of KRAS mutation, such as pancreatic, colorectal and non-small cell lung cancers. However, KRAS is rarely mutated in HCC. The functional role of KRAS in HCC has not been elucidated, nor does it affect immune response. Due to the scarcity of current knowledge on the role of wild-type KRAS in HCC and our previous findings in immune escaped c-Myc-lucOS^{OE}/Tp53^{KO} tumours, we selected wild-type Kras as our target in this study.

In this chapter, we first examined the clinical relevance of KRAS in HCC-related cohorts. To investigate the role of wild-type Kras in HCC, we composed a Kras-overexpressing plasmid pT3-EF1a-Kras, which enables an endogenous overexpression of wild-type Kras via HTVI, in our *in vivo* c-Myc-luc^{OE}/Tp53^{KO} HCC mouse model. We further validated if wild-type Kras modulates the anti-tumour T cell response and exploits the immune surveillance using the antigen-expressing c-Myc-lucOS^{OE}/Tp53^{KO} model. Moreover, we aimed to elucidate molecular mechanisms by which oncogenic KRAS signalling is able to evade immune responses in the context of HCC.

4.2 Experiment design

(1) The clinical relevance and significance of KRAS in HCC were examined in liver cancer cohorts using the International Cancer Genome Consortium (ICGC) Data Portal (https://dcc.icgc.org/) and Genomic Data Commons (GDC) Data Portal (https://portal.gdc.cancer.gov/). The keyword "KRAS" was searched regarding mutation rate, gene expression by stage, expression comparison between normal/ cancerous tissues, and survival analysis. An in-house HCC human tissue microarray was examined for KRAS protein expression, recurrence and survival analyses.

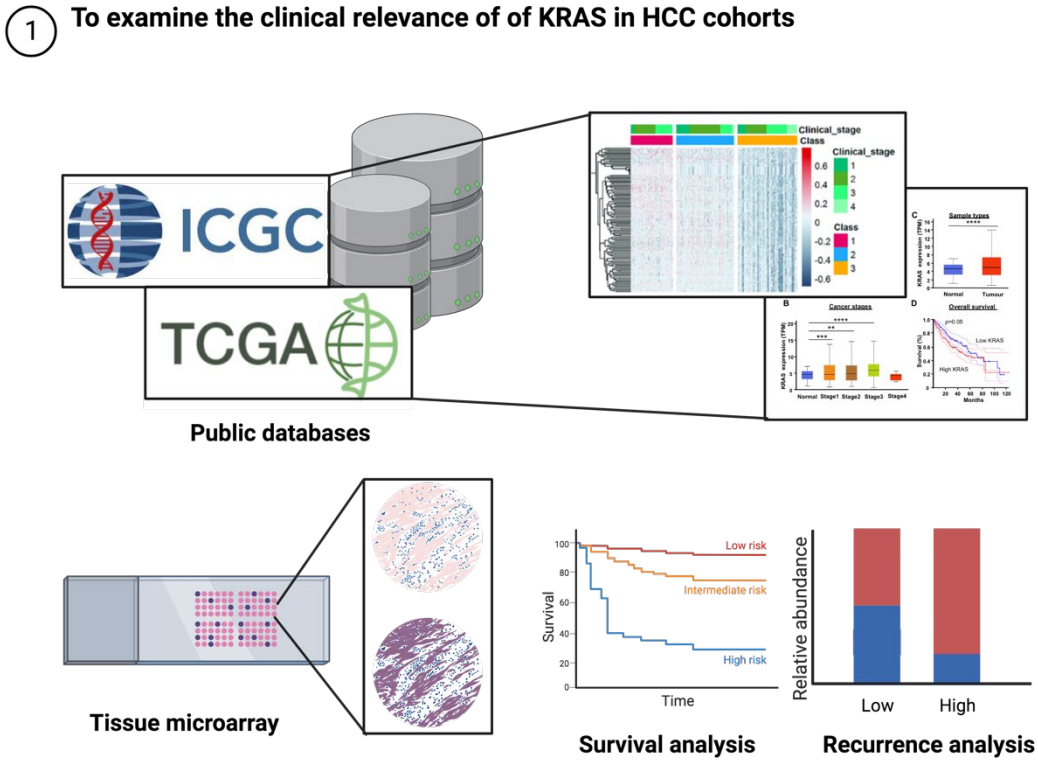

Figure 4.1 An outline of the workflow to examine the clinical relevance of KRAS in HCC patients

The diagram summarises the methods used to evaluate the clinical relevance of KRAS in HCC patients. Online databases, including ICGC and TCGA cohorts, were explored in the search for the gene KRAS. IHC analysis was performed using tissue microarray of the HCC tissue samples, followed by survival and recurrence analyses.

(2) The wild-type Kras overexpressing plasmid was cloned as described in the Method section. The plasmids expressing c-Myc or c-Myc with T cell antigens (c-Myc-lucOS), sgTp53, transposase SB13 and Kras were introduced into the hepatocytes of the C57BL/6 mice via HTVI. The intravascular pressure within the inferior vena cava increased upon the tail vein injection of the plasmid mixture. The injected solution entered the heart and induced cardiac congestion, which pushed the solution back in the retrograde direction. The solution flew into the liver via the hepatic vein and caused swelling of the liver and an increase in the permeability of the hepatocytes, thus transferring the genes into the hepatocytes. To monitor tumour growth, the mice were subjected to bioluminescence imaging at certain time points. The tumour tissues were harvested for various gene and protein expression analyses, including qPCR, western blot, IHC, and RAS activation assay.

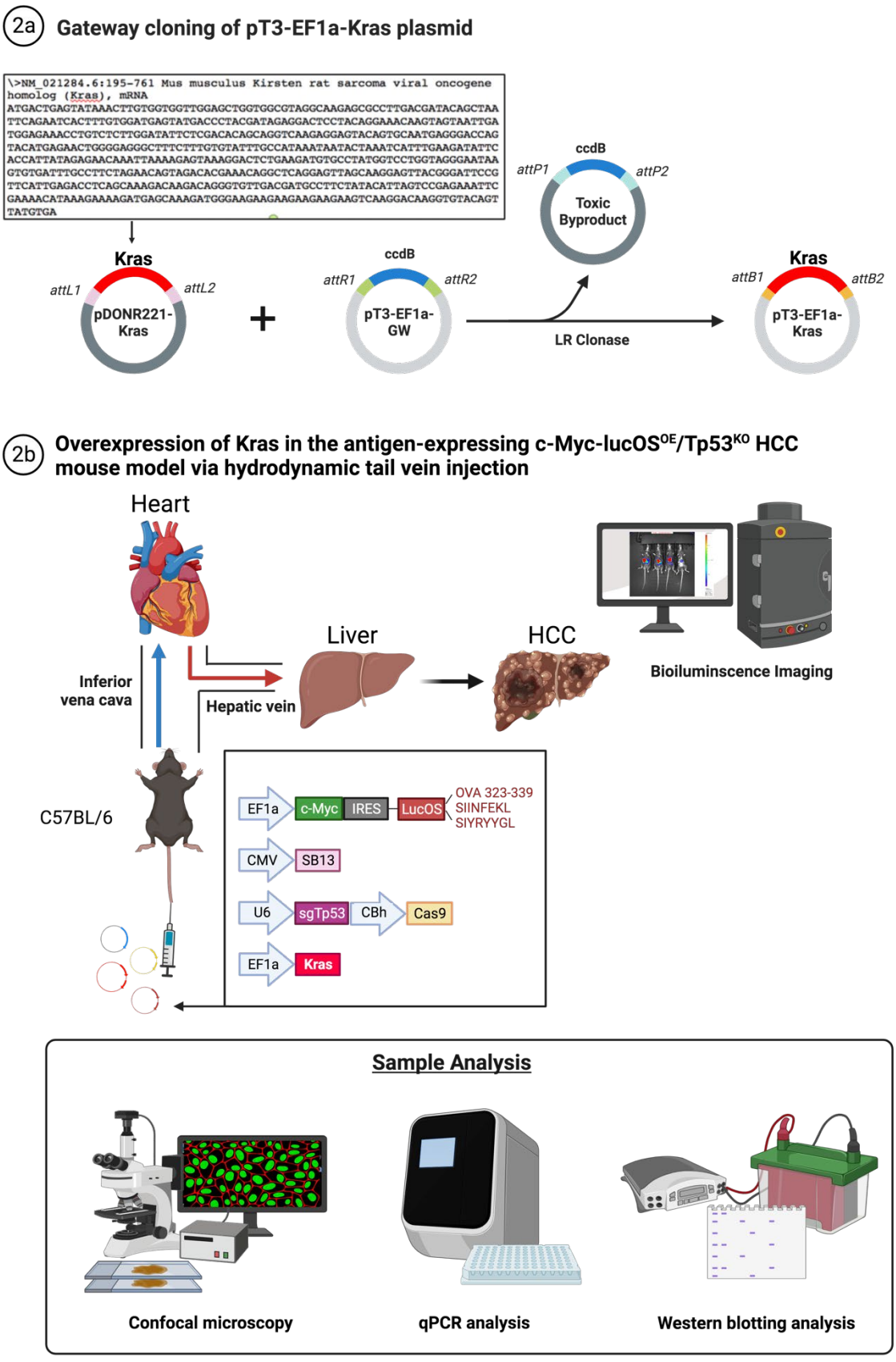

Figure 4.2 A summary of the construction of plasmid pT3-EF1a-Kras and the experimental design of establishing c-Myc-lucOS^{OE}/Tp53^{KO}/Kras HCC mouse model

4.3 Results

4.3.1 Wild-type KRAS expression is upregulated in HCC samples in mRNA and protein levels and is correlated with poor prognosis

Unlike other cancer types, *KRAS* mutation is rare in liver cancer. In the TCGA-LIHC cohort containing 372 primary HCC tumours, the frequency of *KRAS* mutation only accounts for about 1.33% of cases (Figure 4.3A). The rate of *KRAS* mutation ranges from 2.54% to 17.83% in other cohorts (Table 4.1) from countries, including France, China, and Japan. In the TCGA-LIHC cohort, wild-type KRAS expression is significantly upregulated in primary HCC tumours (median expression: 4.93 transcripts per million (TPM)) compared to 50 normal liver tissue samples (median expression: 4.6 TPM; Figure 4.3B). A stepwise upregulation of KRAS mRNA expression was also observed according to the cancer stages in the primary HCC tumour cohort (Figure 4.3C). The median expression of 4.65 TPM at stage 1 to 5.9 TPM at stage 3. (Normal: median expression: 4.6 TPM, n= 50; stage 1: median expression: 4.65, n=168; stage 2: median expression: 4.9 TPM, n=84; stage 3: median expression: 5.9 TPM, n=82; stage 4: median expression: 4.29; n=6). The overall survival rate of HCC patients with high KRAS expression was significantly lower than those of patients with low KRAS expression ($p=0.049$; log-rank test; Figure 4.3D). Immunohistochemical staining analysis of a tissue microarray with 50 clinical HCC samples was performed to compare the KRAS expression at the protein level (Figure 4.3E). Patients with high KRAS expression had a higher chance of experiencing HCC relapse (~76%; Figure 4.3F). The disease-free survival rate of HCC patients with high KRAS overexpression was significantly lower than those of patients with low KRAS expression (*** $p<0.001$; log-rank test), as well as the overall survival rate (Figure 4.3G). All in all, wild-type KRAS expression is enhanced in HCC and is correlated with tumour stage, poor prognosis, and survival.

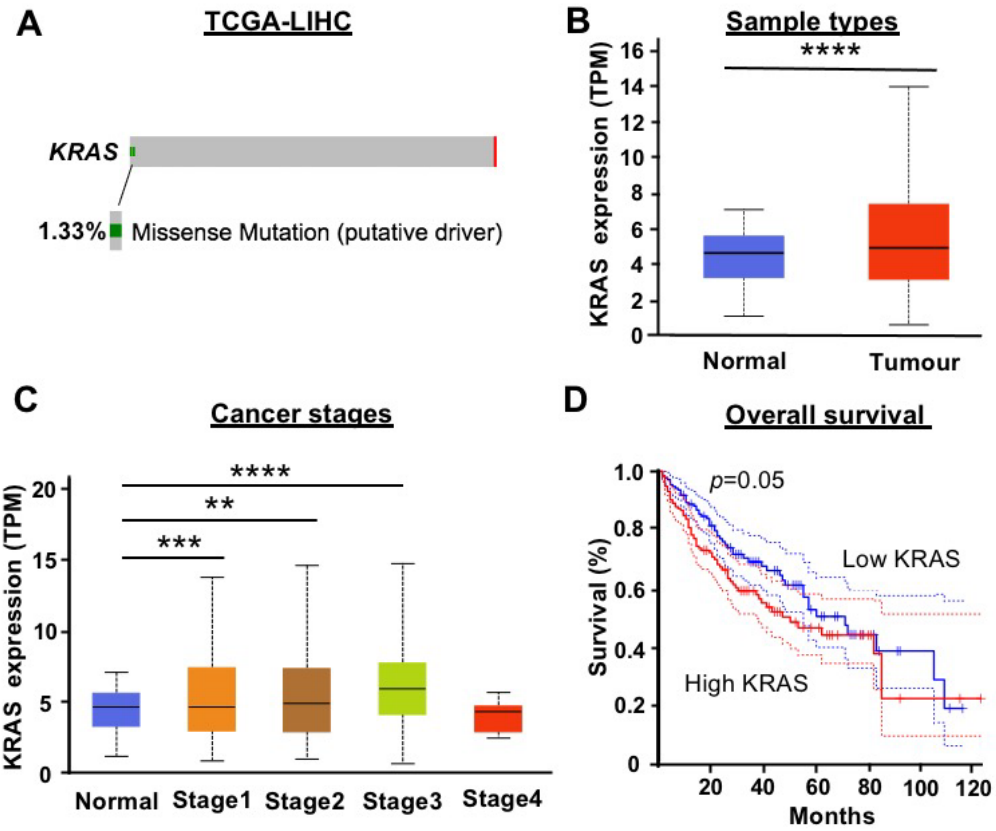
A
TCGA-LIHC
KRAS
1.33%
Missense Mutation (putative driver)
B
Sample types
****
KRAS expression (TPM)
Normal
Tumour
C
Cancer stages
****
**
***
KRAS expression (TPM)
Normal
Stage1
Stage2
Stage3
Stage4
D
Overall survival
p=0.05
Low KRAS
High KRAS
Survival (%)
Months

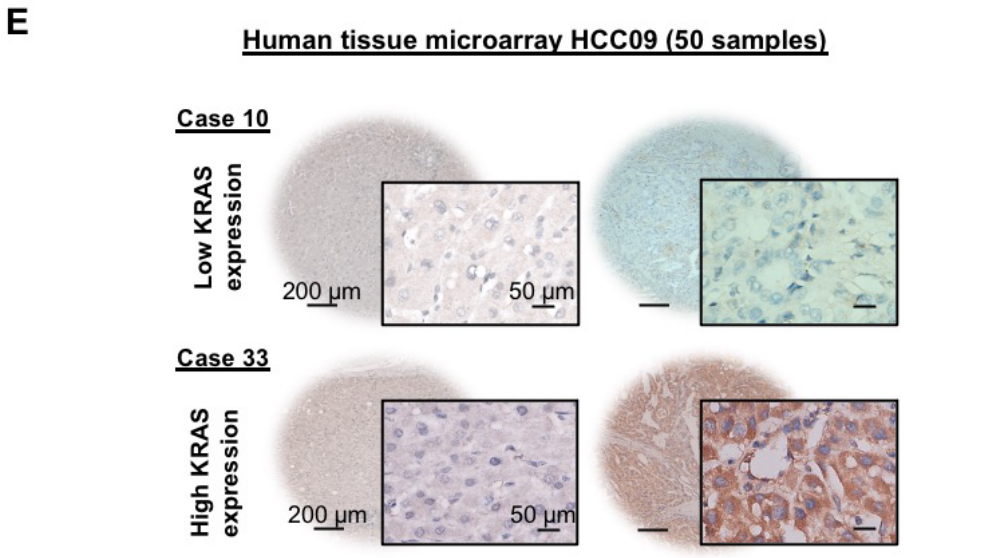
E
Human tissue microarray HCC09 (50 samples)
Case 10
Low KRAS expression
200 µm
50 µm
Case 33
High KRAS expression
200 µm
50 µm

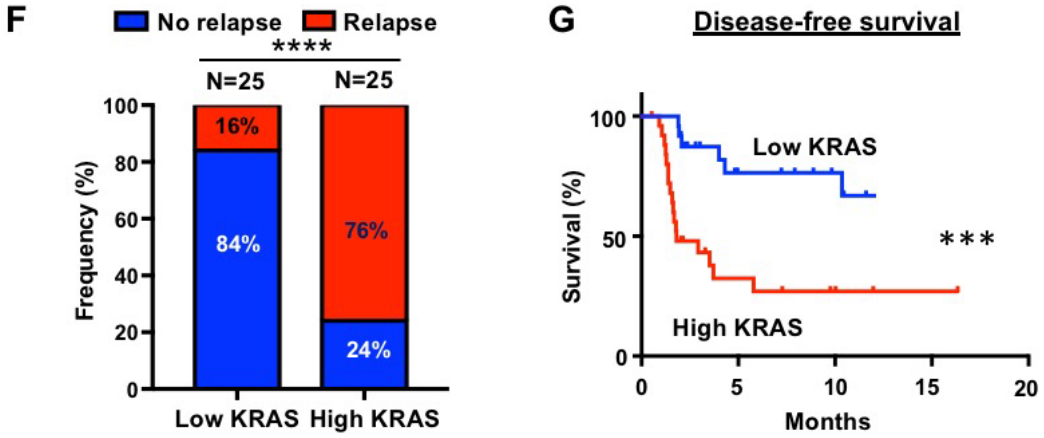

Figure 4.3 Wild-type KRAS expression is upregulated in HCC samples in mRNA and protein levels, and is correlated with poor prognosis.
(A) Genomic alterations of *KRAS* (<1% mutation) found in the TCGA-LIHC cohort (n=372 samples). **(B)** Analysis of the dataset showed upregulation of KRAS mRNA expression (372 primary HCC tumours compared with 50 normal samples; **** p<0.0001, t-test). **(C)** A stepwise upregulation of KRAS mRNA expression according to the cancer stages was observed in the TCGA-LIHC cohort compared to 50 normal samples (stage 1: n=168, stage 2: n=84, stage 3: n=82, stage 4: n=6; ** p<0.01, *** p<0.001, **** p<0.0001, t-test). (**D**) The overall survival rate of HCC patients with high KRAS overexpression was significantly lower than that of patients with low KRAS expression (p=0.049; log-rank test). (**E**) Immunohistochemical staining of a tissue microarray comparing KRAS expression in 50 clinical HCC samples. Scale bar = 50 µm. Representative cases of HCC with low KRAS expression (Case #10) and high KRAS expression (Case #33) are shown. **(F & G)** High KRAS expression is correlated with a higher chance of HCC relapse (~76%) in 50 HCC samples (**** p<0.0001, t-test). Error bars indicate the mean ± SD. The disease-free survival rate of HCC patients with high KRAS overexpression was significantly lower than that of patients with low KRAS expression (*** p<0.001; log-rank test).

Project	Tumour Subtype	Number of participants	*KRAS* Mutations	Percentage of *KRAS* Mutations
LIHC-US,TCGA	HCC	372	5	1.33%
LINC-JP	HCC (Virus associated)	394	8	2.54%
LICA-FR	HCC (Secondary to alcohol and adiposity)	252	9	3.57%
LICA-CN	HCC (HBV-associated)	402	46	10.70%
LIRI-JP	HCC (Virus associated)	258	53	17.83%

Table 4.1 *KRAS* is rarely mutated in HCC.
The table demonstrated the frequency of the mutation rate of *KRAS* in liver cancer datasets associated with diverse aetiological factors, including TCGA-LIHC, LICA-France (LICA-FR), LINC-Japan (LINC-JP), LICA-China (LICA-CN) and LIRI-Japan (LICA-JP).

4.3.2 Successful establishment of a Kras overexpressing plasmid pT3-EF1a-Kras and the functional role of Kras in c-Myc-luc^{OE}/Tp53^{KO} HCC

As described in the Method section, we constructed plasmid pT3-EF1a-Kras (Appendix 1). Briefly, the coding sequence of mouse Kras (NM_021284) was cloned into the donor vector pDONR-221. Subsequently, the Kras coding sequence was inserted into the vector pT3-EF1a-GW using the Gateway^{TM} cloning method facilitated by LR Clonase^{TM}. DNA electrophoresis confirmed the size of the plasmid pT3-EF1a-Kras. As shown in Figure 4.4A, a clear single band of pT3-EF1a-Kras (cut by the digestion enzyme XhoI) was observed at a calculated size of 5.7kb. The insertion of the Kras fragment was confirmed by DNA sequencing using the EF1a forward primer (Figure 4.4B). The result of the Basic Local Alignment Search Tool (BLAST) showed a 100% identity with the Kras mRNA sequence.

The plasmid pT3-EF1a-Kras was injected into the hepatocytes of mice with plasmids expressing sgTp53, SB13, and c-Myc. The luciferase signals of both groups were comparable on day 12 (Figure 4.4C), indicating equal transfection efficiency and expression of the c-Myc plasmid in both groups. On day 22, there was a drastic increase in luciferase expression among Kras mice compared to that in EV mice, indicating faster tumour growth in Kras-overexpressing mice. All the Kras overexpressed mice presented gross liver tumours with higher tumour weight, with a median survival of 24 to 37 days (Figure 4.4D&E&F). These findings confirmed that Kras overexpression promotes HCC progression. To validate this *in vivo* system, both the c-Myc-luc^{OE}/Tp53^{KO}/EV and c-Myc-luc^{OE}/Tp53^{KO}/Kras tumour tissues were harvested to evaluate Kras expression. QPCR analysis showed an increase in Kras mRNA expression in Kras overexpressing tumours (Figure 4.5A), while western blot confirmed the upregulation of KRAS in the protein level (Figure 4.5B). Immunohistochemistry staining analyses showed high and specific expression of KRAS in c-Myc-luc^{OE}/Tp53^{KO}/Kras tumour tissues (Figure 4.5C). A GTP-RAS activation assay (Figure 4.5D) was performed to examine *in vivo* RAS activation in both groups. The Ras signalling switches between an active GTP-bound state and an inactive GDP-bound state. GTP-RAS was pulled down by binding to the RAS-binding domain in RAF1. Western blot demonstrated a significantly higher expression of RAS-GTP at 21kDa in the Kras tumour sample compared to the EV tumour sample and naive non-tumour liver tissue. This implies that RAS signalling was activated upon wild-type Kras overexpression.

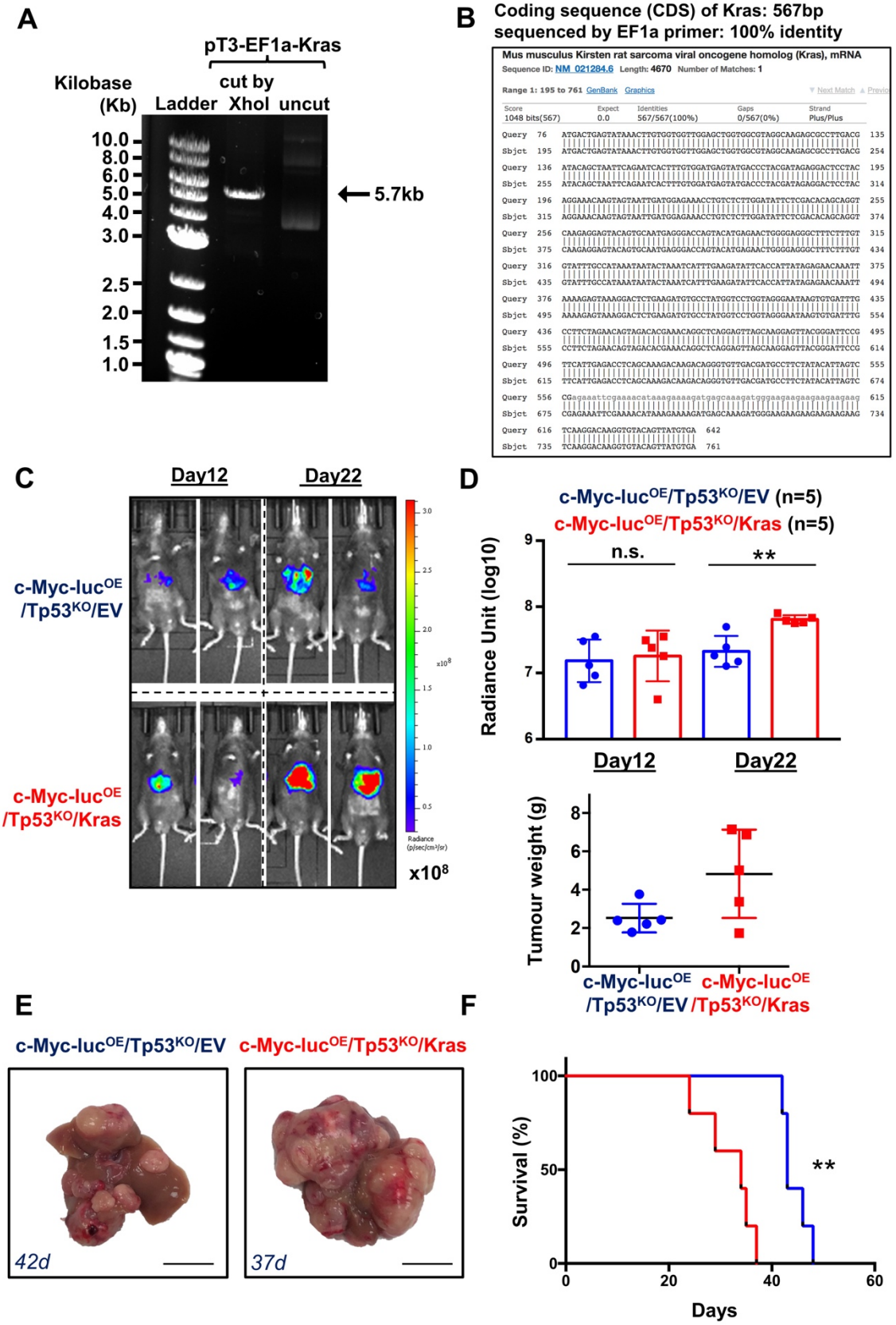
A
pT3-EF1a-Kras
cut by
Kilobase (Kb)
Ladder
XhoI
uncut
10.0
8.0
6.0
5.0
4.0
3.0
2.5
2.0
1.5
1.0
5.7kb
B
Coding sequence (CDS) of Kras: 567bp sequenced by EF1a primer: 100% identity
Mus musculus Kirsten rat sarcoma viral oncogene homolog (Kras), mRNA
Sequence ID: NM_021284.6 Length: 4670 Number of Matches: 1
Range 1: 195 to 761 GenBank Graphics
Score 1048 bits(567)
Expect 0.0
Identities 567/567(100%)
Gaps 0/567(0%)
Strand Plus/Plus
Query 76 ATGACTGAGTATAAACTTGTGGTGGTTGGAGCTGGTGGCGTAGGCAAGAGCGCCTTGACG 135
Sbjct 195 ATGACTGAGTATAAACTTGTGGTTGGAGCTGGTGGCGTAGGCAAGAGCGCCTTGACG 254
Query 136 ATACAGCTAATTCAGAATCACTTTGTGGATGAGTATGACCCTACGATAGAGGACTCCTAC 195
Sbjct 255 ATACAGCTAATTCAGAATCACTTTGTGGATGAGTATGACCCTACGATAGAGGACTCCTAC 314
Query 196 AGGAAACAAGTAGTAATTGATGGAGAAACCTGTCTCTTGGATATTCTCGACACAGCAGGT 255
Sbjct 315 AGGAAACAAGTAGTAATTGATGGAGAAACCTGTCTCTTGGATATTCTCGACACAGCAGGT 374
Query 256 CAAGAGGAGTACAGTGCAATGAGGGACCAGTACATGAGAACTGGGGAGGGCTTTCTTTGT 315
Sbjct 375 CAAGAGGAGTACAGTGCAATGAGGGACCAGTACATGAGAACTGGGGAGGGCTTTCTTTGT 434
Query 316 GTATTTGCCATAAATAATACTAAATCATTTGAAGATATTCACCATTATAGAGAACAAATT 375
Sbjct 435 GTATTTGCCATAAATAATACTAAATCATTTGAAGATATTCACCATTATAGAGAACAAATT 494
Query 376 AAAAGAGTAAAGGACTCTGAAGATGTGCCTATGGTCCTGGTAGGGAATAAGTGTGATTTG 435
Sbjct 495 AAAAGAGTAAAGGACTCTGAAGATGTGCCTATGGTCCTGGTAGGGAATAAGTGTGATTTG 554
Query 436 CCTTCTAGAACAGTAGACACGAAACAGGCTCAGGAGTTAGCAAGGAGTTACGGGATTCCG 495
Sbjct 555 CCTTCTAGAACAGTAGACACGAAACAGGCTCAGGAGTTAGCAAGGAGTTACGGGATTCCG 614
Query 496 TTCATTGAGACCTCAGCAAAGACAAGACAGGGTGTTGACGATGCCTTCTATACATTAGTC 555
Sbjct 615 TTCATTGAGACCTCAGCAAAGACAAGACAGGGTGTTGACGATGCCTTCTATACATTAGTC 674
Query 556 CGagaaattcgaaaacataaagaaaagatgagcaaagatgggaagaagaagaaagaaggag 615
Sbjct 675 CGAGAAATTCGAAAACATAAAGAAAAGATGAGCAAAGATGGGAAGAAGAAGAAGAAGAAG 734
Query 616 TCAAGGACAAGGTGTACAGTTATGTGA 642
Sbjct 735 TCAAGGACAAGGTGTACAGTTATGTGA 761
C
Day12
Day22
c-Myc-luc^OE /Tp53^KO/EV
c-Myc-luc^OE /Tp53^KO/Kras
Radiance (p/sec/cm²/sr)
x10^8
D
c-Myc-luc^OE/Tp53^KO/EV (n=5)
c-Myc-luc^OE/Tp53^KO/Kras (n=5)
n.s.
**
Radiance Unit (log10)
Day12
Day22
Tumour weight (g)
c-Myc-luc^OE /Tp53^KO/EV
c-Myc-luc^OE /Tp53^KO/Kras
E
c-Myc-luc^OE/Tp53^KO/EV
c-Myc-luc^OE/Tp53^KO/Kras
42d
37d
F
Survival (%)
**
Days

Figure 4.4 Wild-type Kras overexpression promotes tumour growth in c-Myc-luc^{OE}/Tp53^{KO} model

(A) DNA electrophoresis of the pT3-EF1a-Kras plasmid. Lane 1: Ladder, Lane 2: pT3-EF1a-Kras plasmid digested with XhoI. Lane 3: uncut pT3-EF1a-Kras plasmid. **(B)** The DNA sequencing result of the pT3-EF1a-Kras plasmid confirmed the mouse Kras sequence was successfully cloned into the plasmid. **(C)** Overexpression of wild-type Kras in the c-Myc-luc^{OE}/Tp53^{KO} model promoted tumour development. Representative bioluminescence images on days 12 and 22 of c-Myc-luc^{OE}/Tp53^{KO}/EV and c-Myc-luc^{OE}/Tp53^{KO}/Kras after HTVI. The scale bar for the luciferase signal is shown. **(D)** Quantification of normalised luciferase signals on days 12 and 22 after HTVI (n=5 per group, ** $p<0.01$, t-test). The tumour weight of the c-Myc-luc^{OE}/Tp53^{KO}/Kras group was higher than that of the c-Myc-luc^{OE}/Tp53^{KO}/EV group. **(E)** Representative images of c-Myc-luc^{OE}/Tp53^{KO}/EV and c-Myc-luc^{OE}/Tp53^{KO}/Kras livers. **(F)** A significant reduction in survival was observed in the Kras group, with a median survival of 30 days (** $p<0.01$; log-rank test).

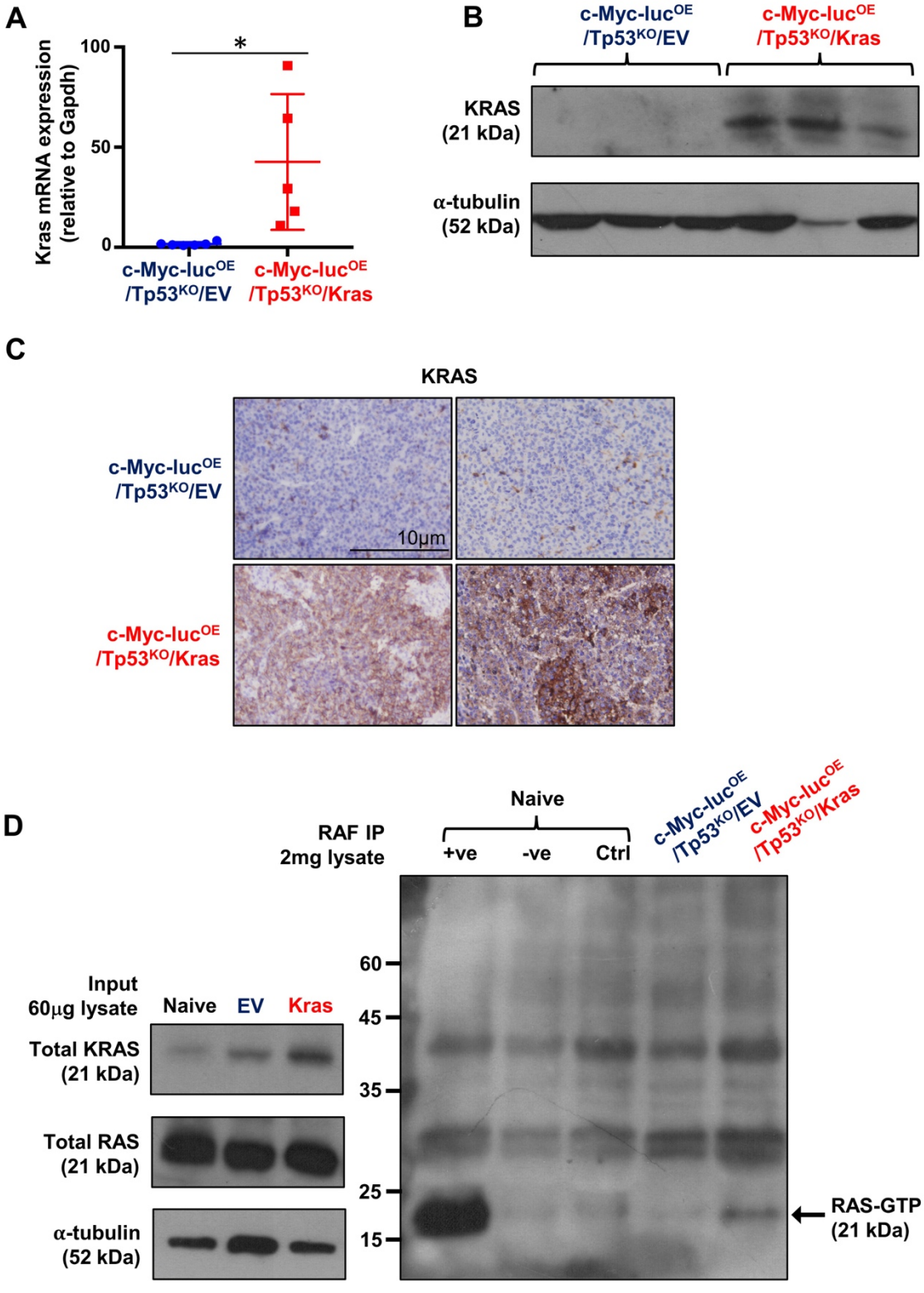
A
Kras mRNA expression (relative to Gapdh)
100
50
0
*
c-Myc-luc^OE /Tp53^KO/EV
c-Myc-luc^OE /Tp53^KO/Kras
B
c-Myc-luc^OE /Tp53^KO/EV
c-Myc-luc^OE /Tp53^KO/Kras
KRAS (21 kDa)
α-tubulin (52 kDa)
C
KRAS
c-Myc-luc^OE /Tp53^KO/EV
c-Myc-luc^OE /Tp53^KO/Kras
10μm
D
Naive
RAF IP 2mg lysate
+ve
-ve
Ctrl
c-Myc-luc^OE /Tp53^KO/EV
c-Myc-luc^OE /Tp53^KO/Kras
Input 60μg lysate
Naive
EV
Kras
Total KRAS (21 kDa)
Total RAS (21 kDa)
α-tubulin (52 kDa)
60
45
35
25
15
RAS-GTP (21 kDa)

Figure 4.5 Kras overexpression in c-Myc-luc^{OE}/Tp53^{KO} model confirmed at mRNA and protein levels.
(A) QPCR analysis revealed significantly enhanced wild-type Kras mRNA expression in livers injected with Kras compared to the control (* $p<0.05$, t-test). **(B)** Western blot analysis showed an increase in Kras protein expression in c-Myc-luc^{OE}/Tp53^{KO}/Kras tumours compared to the control c-Myc-luc^{OE}/Tp53^{KO}/EV group. Three representative samples were shown. **(C)** Immunohistochemical staining demonstrated overexpression of Kras in c-Myc-luc^{OE}/Tp53^{KO}/Kras tumours. Two representative samples were shown. Scale bar = 10 μm. **(D)** GTP-Ras activation assay demonstrated that Ras was activated upon Kras overexpression in the c-Myc-luc^{OE}/Tp53^{KO} /Kras tumour.

4.3.3 Wild-type Kras overexpression abolishes the anti-tumour T cell response and promotes immune evasion in c-Myc-lucOS^{OE}/Tp53^{KO} model

To validate the hypothesis that KRAS signalling promotes immune evasion, we overexpressed wild-type Kras in the c-Myc-lucOS^{OE}/Tp53^{KO} HCC model. On day 9, the luciferase signals of the c-Myc-lucOS^{OE}/Tp53^{KO}/Kras group were higher than those of the c-Myc-lucOS^{OE}/Tp53^{KO}/EV group (Figure 4.6A). Aligned to the previous findings in c-Myc-lucOS^{OE}/Tp53^{KO}/EV group, the luciferase signals of c-Myc-lucOS^{OE}/Tp53^{KO}/EV mice reduced on day 22 as the expression of the exogenous T cell antigens caused a delay in tumour progression (Figure 4.6B). The majority of the mice did not develop any tumours (Figure 4.6C). In contrast, the c-Myc-lucOS^{OE}/Tp53^{KO}/Kras tumours continued to grow, as reflected by the luciferase signals on day 22. All of the mice escaped the immune surveillance induced by the exogenous antigens and developed tumours. The survival benefits of the OS system were exploited (Figure 4.6B). QPCR analysis of the harvested tumours validated the overexpression of wild-type Kras in the c-Myc-lucOS^{OE}/Tp53^{KO}/Kras group (Figure 4.6D). Furthermore, we would like to confirm whether the overexpression of wild-type Kras leads to changes in its downstream signalling. In wild-type Kras overexpressed tissue, downstream ERK1/2 was phosphorylated with colocalisation to Kras expression (Figure 4.6E). All these findings conclude that the wild-type Kras overexpression in c-Myc-lucOS^{OE}/Tp53^{KO} HCC drives immune evasion via KRAS/ERK1/2 activation.

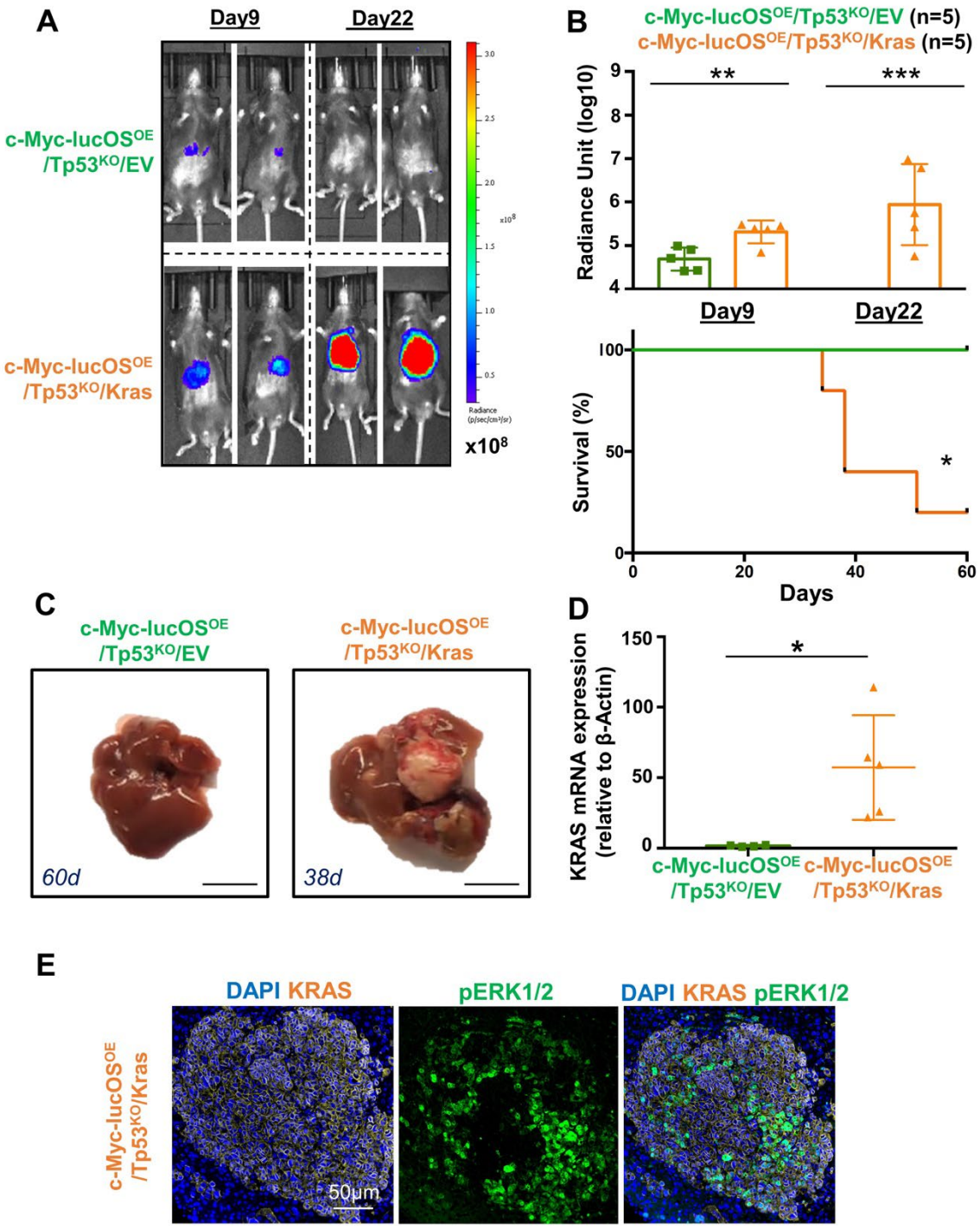

Figure 4.6 Wild-type Kras overexpression abolishes the anti-tumour T cell response and promotes immune evasion in c-Myc-lucOS^{OE}/Tp53^{KO} model

(A) Representative bioluminescence images on days 9 and 22 of c-Myc-lucOS^{OE}/Tp53^{KO}/EV and c-Myc-lucOS^{OE}/Tp53^{KO}/Kras after HTVI. The scale bar for the luciferase signal is shown. **(B)** Quantification of normalised luciferase signals at days 9 and 22 after HTVI (n=5 per group, ** $p<0.01$, *** $p<0.001$, t-test). All c-Myc-lucOS^{OE}/Tp53^{KO}/Kras mice developed tumours and exploited the survival benefits of T cell-specific antigens (* $p<0.05$, t-test). **(C)** Representative images of c-Myc-lucOS^{OE}/Tp53^{KO}/EV and c-Myc-lucOS^{OE}/Tp53^{KO}/Kras livers. **(D)** QPCR

analysis confirmed the wild-type Kras mRNA overexpression in livers injected with Kras expressing plasmid, compared to the control (n=5; * $p<0.05$, t-test). **(E)** In wild-type Kras overexpressed tissue, downstream ERK1/2 was phosphorylated with colocalisation to Kras expression. Scale bar = 50μm.

To investigate the upstream signalling that turned on the KRAS signalling, we sought the upstream ligands and receptors that play a role in c-Myc-lucOS^{OE}/Tp53^{KO}/Kras tumours. RTK signalling modulates proliferation and survival via KRAS activation. Upon the binding of an RTK ligand to the receptor, the receptor dimerises and activates the downstream signalling cascade. Previous findings in Chapter 3 revealed that EGFR is phosphorylated with the activation of KRAS and pERK1/2 in immune escaped c-Myc-lucOS^{OE}/Tp53^{KO} tumours. There are various RTK ligands which bind to EGFR (Figure 4.7A). This includes amphiregulin (Areg), epiregulin (Ereg), Egf, epithelial mitogen (Epgn), heparin-binding EGF like-growth factor (Hb-Egf) and Tgf-α. Among them, Egf was found to be upregulated in both c-Myc-lucOS^{OE}/Tp53^{KO}/EV and c-Myc-lucOS^{OE}/Tp53^{KO}/Kras groups (Figure 4.7B). Western blot analysis (Figure 4.7C) showed that the expressions of EGF precursor were increased in both c-Myc-lucOS^{OE}/Tp53^{KO}/EV and c-Myc-lucOS^{OE}/Tp53^{KO}/Kras groups, aligned with the upregulated expressions of pEGFR in these two groups. Alongside, the expressions of downstream pERK1/2 in both c-Myc-lucOS^{OE}/Tp53^{KO}/EV and c-Myc-lucOS^{OE}/Tp53^{KO}/Kras groups were upregulated. In c-Myc-lucOS^{OE}/Tp53^{KO}/Kras groups, the overexpression of Kras led to a higher expression of pERK1/2. This implies that the Kras overexpression further activates the downstream pERK1/2 signalling pathway. Immunohistochemical staining (Figure 4.7D) demonstrated the colocalisation of pEGFR, pERK1/2 and KRAS in both of the OS-expressing groups. All these data indicate that, upon the stimulation from upregulated EGF, wild-type Kras overexpression promotes immune evasion and cancer progression via the activation of EGFR/KRAS/ERK signalling in the context of c-Myc-lucOS^{OE}/Tp53^{KO} HCC.

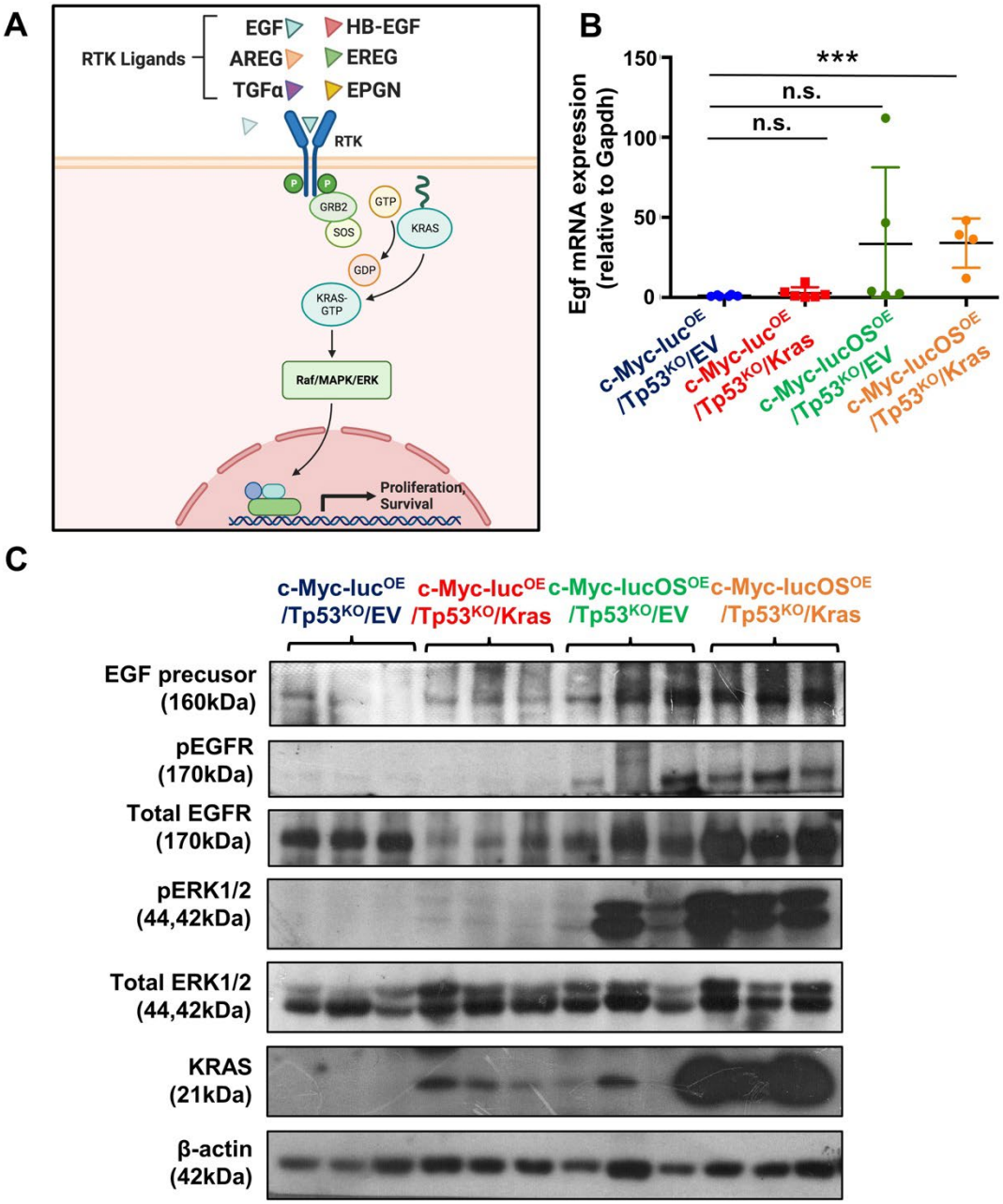
A
RTK Ligands
EGF
AREG
TGFα
HB-EGF
EREG
EPGN
RTK
GRB2
SOS
GTP
KRAS
GDP
KRAS-GTP
Raf/MAPK/ERK
Proliferation, Survival
B
Egf mRNA expression (relative to Gapdh)
150
100
50
0
***
n.s.
n.s.
c-Myc-luc^OE /Tp53^KO/EV
c-Myc-luc^OE /Tp53^KO/Kras
c-Myc-lucOS^OE /Tp53^KO/EV
c-Myc-lucOS^OE /Tp53^KO/Kras
C
c-Myc-luc^OE /Tp53^KO/EV
c-Myc-luc^OE /Tp53^KO/Kras
c-Myc-lucOS^OE /Tp53^KO/EV
c-Myc-lucOS^OE /Tp53^KO/Kras
EGF precusor (160kDa)
pEGFR (170kDa)
Total EGFR (170kDa)
pERK1/2 (44,42kDa)
Total ERK1/2 (44,42kDa)
KRAS (21kDa)
β-actin (42kDa)

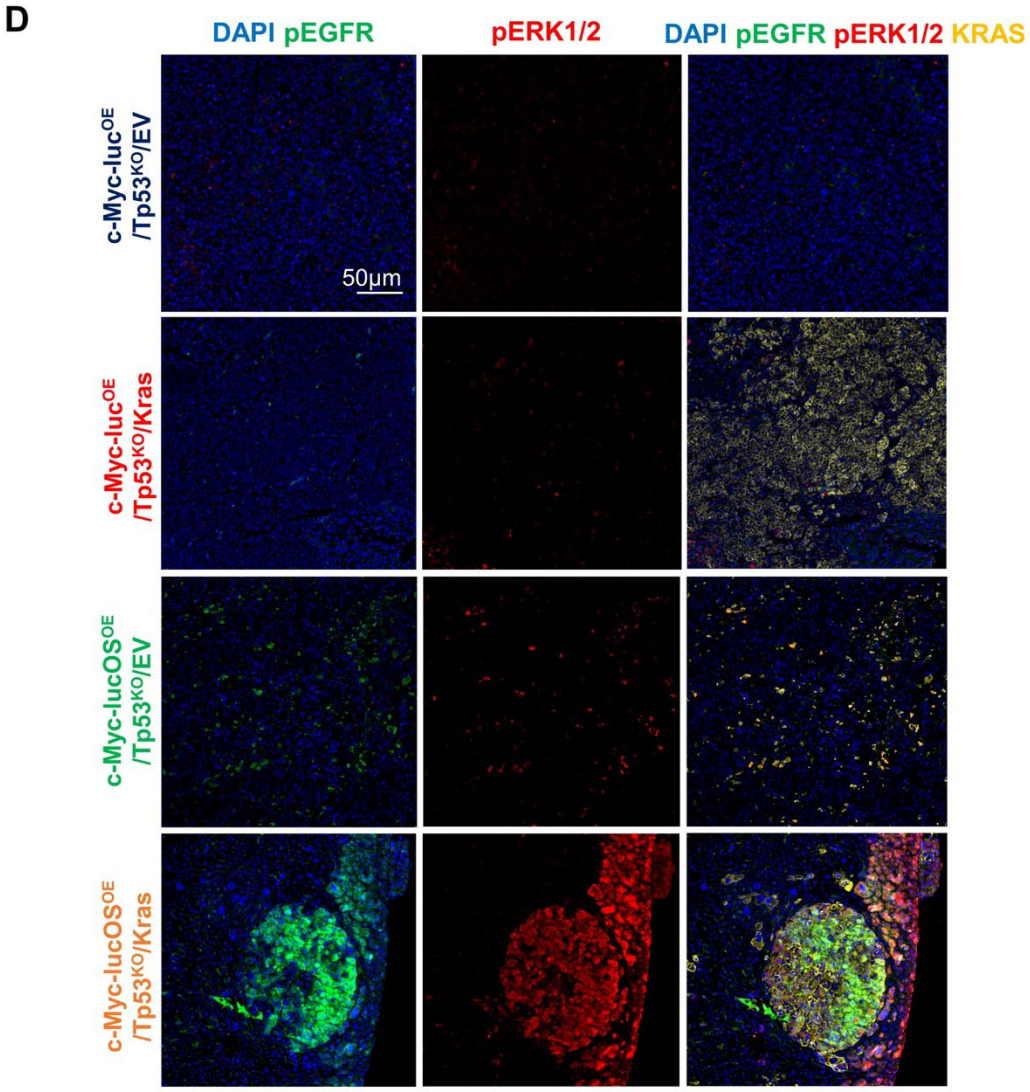

Figure 4.7 EGF is upregulated and activates EGFR/KRAS/ERK signalling in immune escaped c-Myc-lucOS^{OE}/Tp53^{KO} mice

(A) Diagram showed the RTK signalling cascade. RTK ligands include AREG, EREG, EGF, EPGN, HB-EGF, and TGF-α. Upon binding of the RTK ligand to RTK receptors, the receptors dimerise and activate the downstream signalling pathway. **(B)** QPCR revealed that Egf is upregulated in c-Myc-lucOS^{OE}/Tp53^{KO}/EV and c-Myc-lucOS^{OE}/Tp53^{KO}/Kras tissues. (*** $p<0.001$; t-test). **(C & D)** Western blotting and multiplexed immunofluorescence demonstrated that EGF/EGFR/KRAS/ERK signalling is enriched in immune-escaped c-Myc-lucOS^{OE}/Tp53^{KO}/EV and c-Myc-lucOS^{OE}/Tp53^{KO}/Kras tumours.

4.4 Discussion

In Chapter 3, the DIA-MS showed that wild-type Kras expression and KRAS signalling were enriched in immune-escaped c-Myc-lucOS^{OE}/Tp53^{KO} HCC tumours. KRAS is considered one of the most common oncogenic drivers of numerous cancers. Oncogenic KRAS signalling has been widely studied in cancers with a high *KRAS* mutation rate, such as pancreatic cancer, NSCLC, and colorectal cancer. However, to date, the role of KRAS and its molecular mechanism in HCC remain largely unknown.

To understand the genetic profile of KRAS in HCC patients, we accessed liver cancer cohorts using the online public databases ICGC and GDC Data Portal. The majority of HCC cases carry wild-type KRAS, and KRAS mutations are found in only about 1.33% - 17.83% of HCC patients. Nevertheless, upregulated wild-type KRAS expression was observed in HCC tumours compared to normal liver tissue, with an increasing trend in the staging of HCC. Moreover, patients with higher wild-type KRAS expression are associated with a higher chance of tumour relapse and poor survival. In terms of molecular classification, HCC, characterised by the activation of RAS/ERK signalling, was classified into the proliferative subset (Rebouissou & Nault, 2020). Our *in vivo* overexpression of wild-type Kras in the c-Myc-lucOS^{OE}/Tp53^{KO} model also confirmed the pro-tumorigenic and proliferative properties of Kras. Altogether, these results suggested that Kras, notwithstanding its mutation status, exerts a tumour-promoting effect in HCC. Dietrich et al. (2018) first reported that wild-type KRAS expression was elevated in HCC and was correlated to HCC progression and poor prognosis. Enhanced KRAS expression in HCC contributes to acquired resistance to sorafenib via activation of RAF/ERK signalling.

The major objective of this study is to elucidate the intrinsic oncogenic pathway that modulates immune evasion and contributes to resistance to immunotherapy. Therefore, we hypothesised that wild-type Kras, via activation of its downstream signalling, acts as an immune evasive mechanism in HCC. To validate our hypothesis, we overexpressed wild-type Kras in the context of c-Myc-lucOS^{OE}/Tp53^{KO}. Interestingly, all mice escaped immune surveillance and exploited the survival benefit of exogenous T cells. In wild-type Kras-overexpressing tumours, we confirmed that the upstream pEGFR and downstream pERK1/2 were activated. This indicated that wild-type KRAS activation drives immune escape in HCC, via activation of RAF/ERK signalling.

Wild-type KRAS activation functions differently from mutated KRAS, which leads to constitutive activation and downstream ERK-dependent pathways. In the case of wild-type KRAS, it activates upon the phosphorylation of the upstream EGFR. The activation of wild-type KRAS signalling can be mediated by the TIME rich in cytokines and growth factors (Berasain & Avila, 2014). EGF, which is an EGFR ligand, was found to be upregulated in the c-Myc-lucOS^{OE}/Tp53^{KO} models. In other reports, EGF was expressed in highly malignant HCC, and its aberrant expression was associated with poor prognosis and intrahepatic metastasis (Ito et al., 2001; Liu et al., 2018). Other RTK ligands, including Areg, Ereg, Hb-Egf, and Tgf-α, have also been reported to be upregulated in HCC (Castillo et al., 2006; Moon et al., 2006). However, in our study, EGF was the predominant EGFR ligand.

These results raise a question about the source of EGF. Apart from HCC tumour cells, EGF is also induced by immune cells such as CAFs and TAMs (Figure 4.8; Leonardi et al., 2012). In the OS model, the expression of T cell antigens enhanced immunogenicity and induced immune cell infiltration. The DIA-MS result showed that the gene marker of macrophages Itgam (Log2FC: 2.67, $p<0.01$) was upregulated in c-Myc-lucOS^{OE}/Tp53^{KO}, compared to c-Myc-luc^{OE}/Tp53^{KO} tumour. This finding suggests that infiltrating macrophages, which are recruited by the expression of antigens and act as APCs, may be the source of EGF. Further experiments, such as immunohistochemical analysis of EGF expression in c-Myc-lucOS^{OE}/Tp53^{KO} tissues, are needed to confirm the source of EGF.

Currently, the mechanism by which wild-type KRAS mediates immune evasion in HCC has yet to be explored. As described in Figure 3.4, the adaptive immune response is a series of multifactorial actions that depend on proper cooperation between the TIME components (Chen & Mellman, 2017). Mutant KRAS is a pivotal driver of immune evasion in cancers. KRAS and other molecules in the KRAS signalling, i.e. MEK and BRAF are correlated with inadequate recognition of tumour cells by T cells in cancer. In addition, oncogenic KRAS has been reported to affect the recruitment of immunosuppressive neutrophils, CAFs, and monocytes, suppress antigen presentation pathways, and promote T cell exhaustion (Chen et al., 2017; Mugarza et al., 2022; Pylayeva-Gupta et al., 2012). Furthermore, KRAS mutation has a negative clinical correlation with cytotoxic CD8$^+$ T cell infiltration in colorectal cancer and exhibited poor response in ICI and adoptive T cell therapies (Liu et al. 2023).

In the next chapter, we aim to dissect the effect of wild-type Kras overexpression on the TIME and the underlying mechanisms by which KRAS activation affects the adaptive immune response.

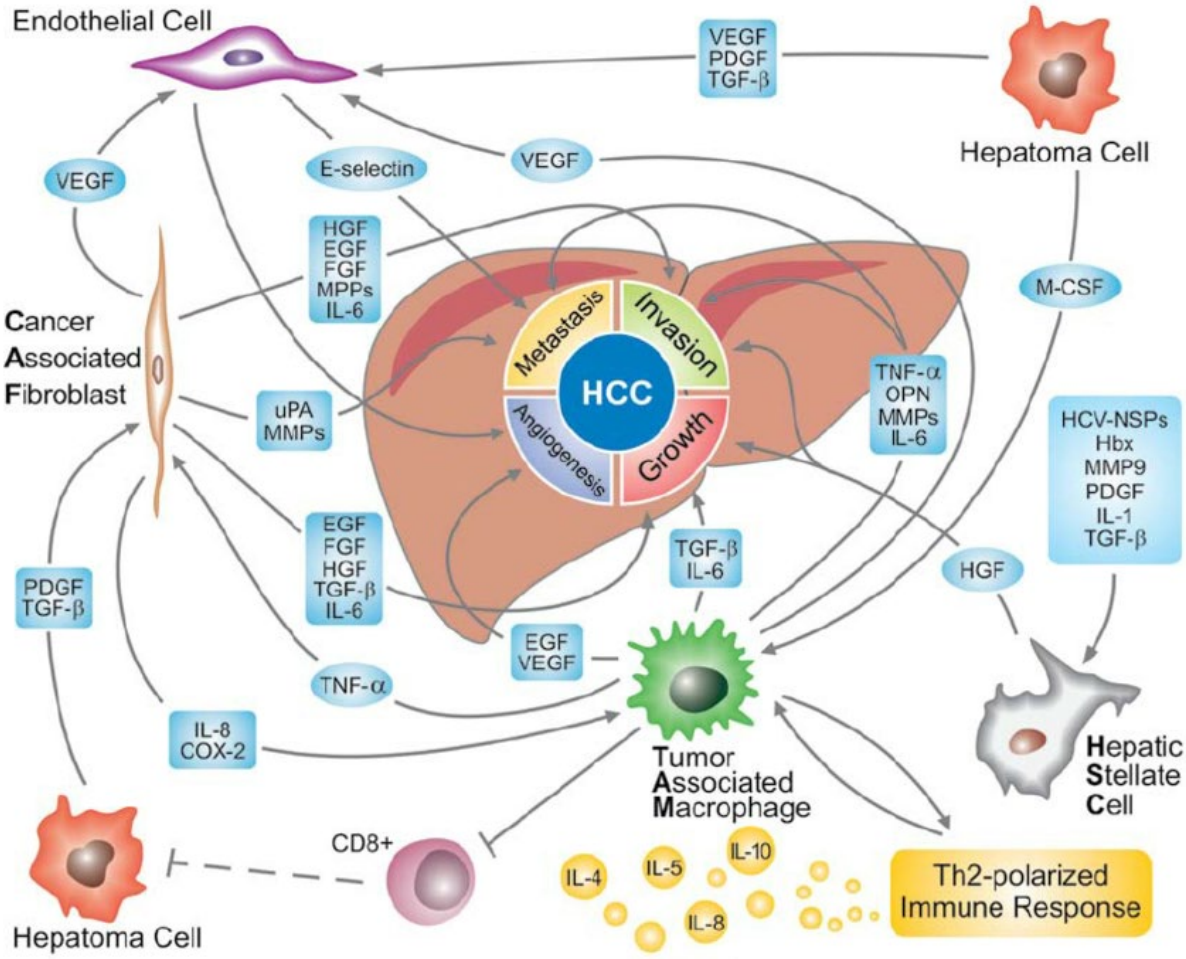

Figure 4.8 The interplay between HCC tumour cells and the TIME. (Leonardi et al., 2012)

Chapter 5. Wild-type Kras overexpression dampens the extrinsic IFN response and antigen presentation in the tumour microenvironment

5.1 Introduction

In Chapter 4, we have shown that wild-type Kras overexpression modulates immune escape via KRAS/ERK signalling activation. Endogenous wild-type Kras overexpression in the c-Myc-lucOS^{OE}/Tp53^{KO} model led to an increase in tumour burden with a shorter survival time in mice, implicating the regulatory role of wild-type Kras in immune evasion. In this chapter, we aimed to investigate the effect of wild-type Kras overexpression on the TIME of c-Myc-luc^{OE}/Tp53^{KO} HCC and the underlying mechanisms by which KRAS activation is involved in HCC immune evasion.

To decipher the influence of wild-type Kras overexpression in the TIME, we sorted CD45^{+} immune cells for scRNA-seq analysis to compare the immune landscape of the wild-type Kras overexpressed tumour and the control group. scRNA-seq is one of the latest high throughput technologies to reveal expression profiles at individual cell levels within the tumour milieu. This immune profile not only provides insights into cellular heterogeneity but also elucidates the relationships between different types of immune cells within the tumour, which could be obscured by traditional bulk RNA sequencing.

Next, we conducted flow cytometry immune profiling to examine the changes in immune populations within the cancer-immunity cycle induced by the overexpression of wild-type Kras. Furthermore, we investigated whether the expression of wild-type Kras exerts a similar immunomodulatory effect in the HCC clinical cohort.

5.2 Experiment design

(1) The workflow of scRNA-seq preparation is shown in Figure 5.1, and the procedure is described in the Method section. Briefly, tumour tissues of c-Myc-luc^{OE}/Tp53^{KO}/EV and c-Myc-luc^{OE}/Tp53^{KO}/Kras were freshly harvested and subjected to enzymatic dissociation. After dissociation and percoll purification, cells were sorted with CD45^{+} surface staining and sent for scRNA-seq analysis. Single-cell transcriptomics of tumour tissues was performed using 10X Genomics droplet-based technology, which incorporates microfluidics with DNA barcoding and bioinformatics software (Cell Ranger). The alterations in the number of immune cells and their transcriptomic profiles were analysed using the Seurat package in R.

(2) To study how wild-type Kras modulates the anti-tumour T cell response, the immune profiles of c-Myc-lucOS^{OE}/Tp53^{KO}/EV and c-Myc-lucOS^{OE}/Tp53^{KO}/Kras livers were compared. The liver tissues were harvested and dissociated into a single-cell suspension by enzymatic digestion. The detailed procedure of multi-channel flow cytometry is described in the Method section. An immune panel with markers of various immune cell targets was selected for the multi-channel flow cytometry analysis (Table 2.6).

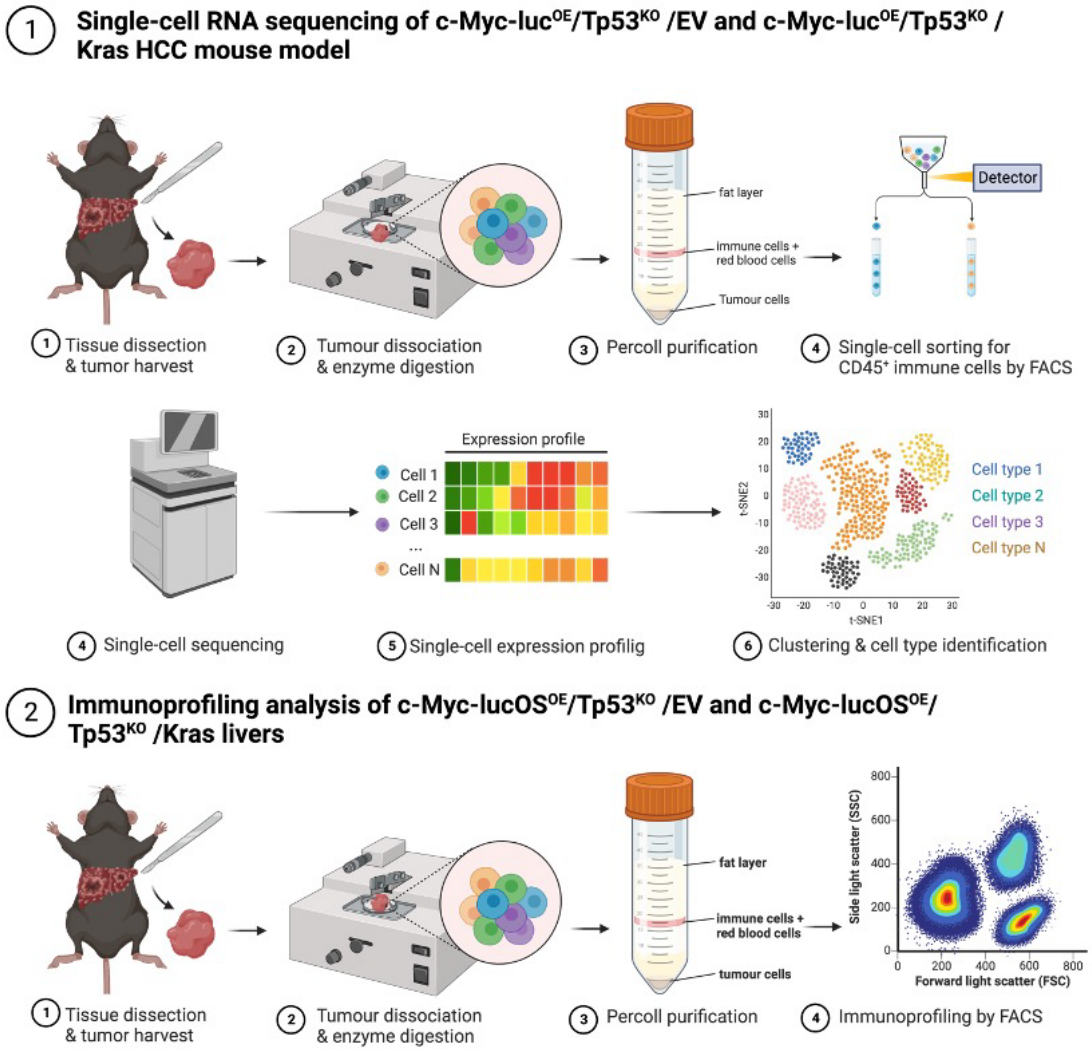

Figure 5.1 An outline of the workflow of sample preparation for scRNA-seq analysis and flow cytometry immune profiling.

5.3 Results

5.3.1 scRNA-seq revealed that Kras dampens IFN responses and antigen presentation in the TIME

In scRNA-seq, the TIME of c-Myc-luc^{OE}/Tp53^{KO}/EV and c-Myc-luc^{OE}/Tp53^{KO}/Kras tumours were compared. The raw sequencing data were subjected to a standard pre-processing workflow and normalisation in the Seurat package. Low-quality or dying cells with low sequencing depth, low genetic content, or mitochondrial contamination were filtered out based on quality control metrics. The criteria for the number of unique genes detected in each cell and the percentage of reads that mapped to the mitochondrial genome were set to <200 and <10%, respectively (Figure 5.2A).

Cells were grouped into clusters based on the identified variable features and then visualised using the principal component (PC) with a set value of 18. Cell clusters were defined based on the differentially expressed genes (DEGs) specific to each cluster in comparison to the others (Figure 5.2B). Major immune cell components such as T cells, NK cells, B cells, neutrophils, plasmacytoid dendritic cells (pDCs), monocytes/macrophages (Mo/Mac), DCs, mast cells, endothelial cells, and MDSCs were annotated based on the expression of their respective immune markers (Figure 5.2C). The number of cells in each immune cell cluster was compared (Figure 5.2D&E). The immune composition of Kras-overexpressing tumours exhibited lower infiltration of T cells, NK cells, and pDCs and a higher abundance of B cells. Both NK cells and pDCs play roles in the innate immune response, contributing to the initiation of primary anti-tumoral immunity in the early stages of infection. In contrast, T cells are predominant components of the adaptive immune system. GSEA pathway analysis was employed to compare enriched pathways within the immune clusters of Kras-overexpressing tumours and the control. The heatmap revealed that oncogenic Kras exerts an immunosuppressive effect on the TIME, leading to the downregulation of antigen processing and presentation, IFN responses, and leukocyte activation (Figure 5.2F).

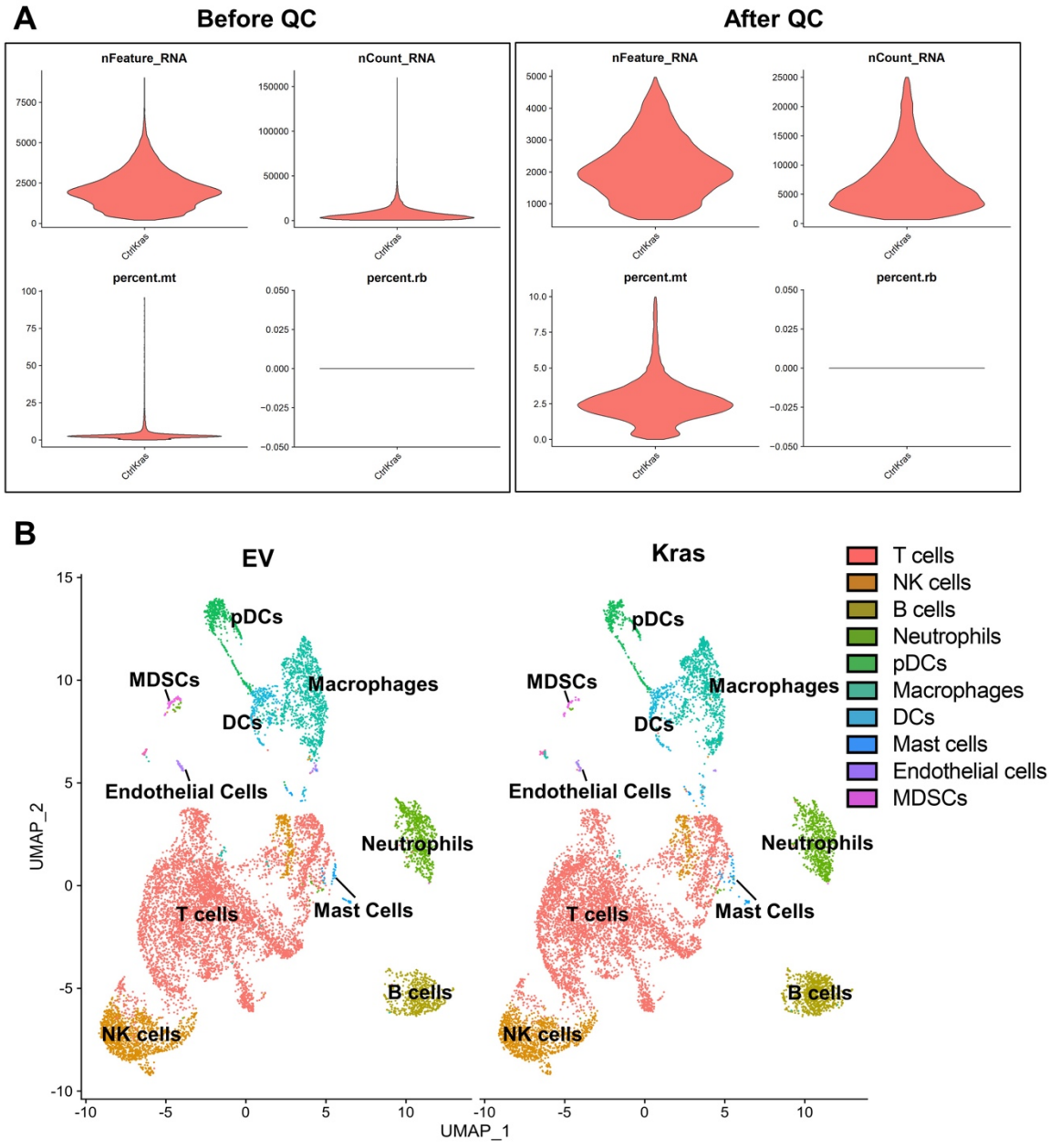
A
Before QC
After QC
nFeature_RNA
nCount_RNA
percent.mt
percent.rb
CtrlKras
B
EV
Kras
pDCs
MDSCs
Macrophages
DCs
Endothelial Cells
Neutrophils
T cells
Mast Cells
B cells
NK cells
UMAP_1
UMAP_2
T cells
NK cells
B cells
Neutrophils
pDCs
Macrophages
DCs
Mast cells
Endothelial cells
MDSCs

C

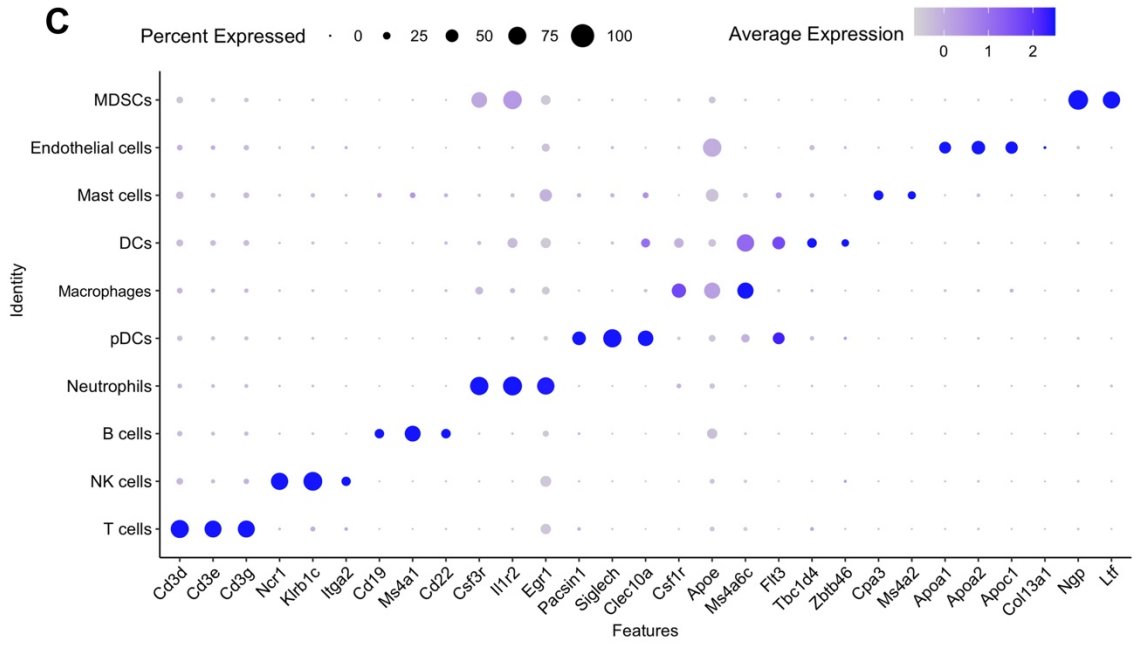

D

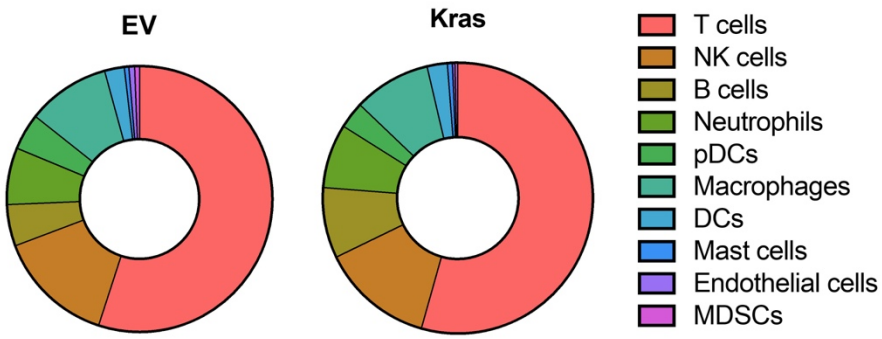

E

Annotation	EV	Kras
T cells	5904	5682
NK cells	1534	1409
B cells	542	881
Neutrophils	742	801
pDCs	474	333
Macrophages	1083	965
DCs	259	253
Mast cells	59	64
Endothelial cells	75	31
MDSCs	64	36
Total	10719	10426

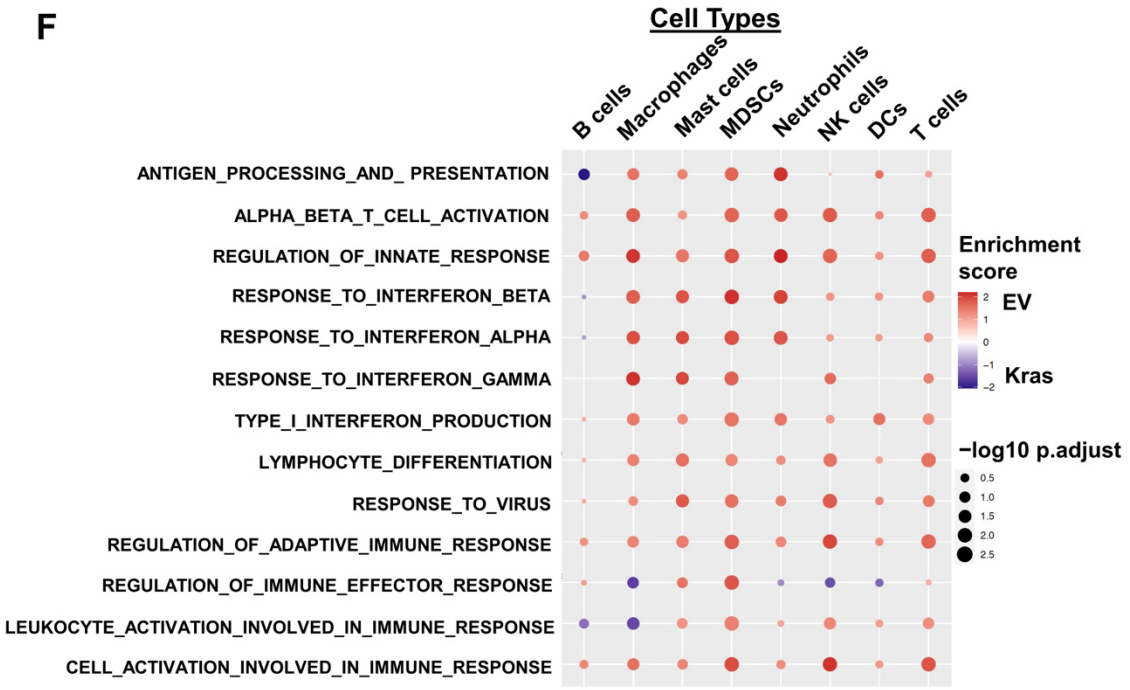

Figure 5.2 scRNA-seq analysis revealed that wild-type Kras dampens IFN responses and antigen presentation in the tumour milieu.
(A) Raw scRNA-seq data required standard quality control, which filtered out low-quality or dying cells with a low gene content and mitochondrial contamination. Violin plots represent the number of genes (nFeature_RNA), the number of reads (nCount_RNA), the percentage of mitochondrial genes (percent.mt), and the percentage of ribosomal gene reads (percent.rb) detected in each cell before and after QC. **(B)** UMAP visualised and compared the TIME of c-Myc-luc^{OE}/Tp53^{KO}/EV and c-Myc-luc^{OE}/Tp53^{KO}/Kras tumours. **(C)** The dot plot showed the gene markers for defined cell types located on UMAP. **(D&E)** The pie chart and table compared the cell number of each immune cell cluster. **(F)** Heatmap indicated several mechanisms through which oncogenic Kras exerts an immunosuppressive effect on the TIME. These mechanisms include downregulation of antigen processing and presentation, IFN responses, and leukocyte activation.

Since the pathway analysis indicated impairment of antigen presentation function upon wild-type Kras overexpression, we proceeded to investigate the major antigen-presenting compartments in the TIME. Professional APCs present antigens bound to MHC proteins on their surfaces to T cells. The primary types of professional APCs include DCs, macrophages, and B cells. The pathways "HALLMARK_INTERFERON_ALPHA_RESPONSE" and "HALLMARK_INTERFERON_GAMMA_RESPONSE" were enriched in the DC population of the EV group with NES of 1.59 ($p<0.001$) and 1.49 ($p=0$), respectively (Figure 5.3A). Notably, the genes enriched in these two GSEA hallmark gene sets, including Jak1, Jak2, Stat1, and Irf7, displayed lower expression levels in the DCs of the Kras-overexpressed group (Figure 5.3B). The expression of IFN-induced antigen-presenting machinery components, such as Nlrc5, CD47, B2m, Tap1, and Ciita, was also found to be lower in the Kras group (Figure 5.3D). Hence, we deduced that the downregulation of "KEGG: Antigen processing and presentation" (NES: 1.52, $p<0.01$) is a consequence of suppressed IFN responses (Figure 5.3C).

Macrophages, another type of professional APCs, also exhibited downregulation in "HALLMARK_INTERFERON_ALPHA_RESPONSE" and "HALLMARK_INTERFERON_GAMMA_RESPONSE" with NES of 2.16 ($p<0.001$) and 2.13 ($p<0.001$), respectively (Figure 5.4A). In the Kras-overexpressed group, IFN-related genes such as Jak2, Stat1, and Irf7, were downregulated (Figure 5.4B). Additionally, the levels of IFN-inducible chemokines Cxcl9 and Cxcl10, which facilitate lymphocyte chemotaxis, were lower in the Kras-overexpressed group. KEGG: Antigen processing and presentation", along with associated APM components, were downregulated in the Kras-overexpressed group (Figure 5.4C&D).

Since T cells are the primary focus of this study, an in-depth T cell cluster analysis was conducted. T cell population was extracted and further subclustered into distinct subsets based on the expressions of their representative genes (Figure 5.5A&B&C). GSEA pathway analysis (Figure 5.2F) previously showed suppressed IFN responses and downregulated activation in the T cell cluster. Consistent with earlier findings, the count of IFN-stimulated $CD8^+$ T cells was lower in the Kras group (Figure 5.5 F&G). Regarding the impact on activation, the reduced number of effector memory $CD8^+$ T cells and higher abundance of naïve $CD8^+$ T cells in the Kras group imply reduced T cell activation (Figure 5.5G).

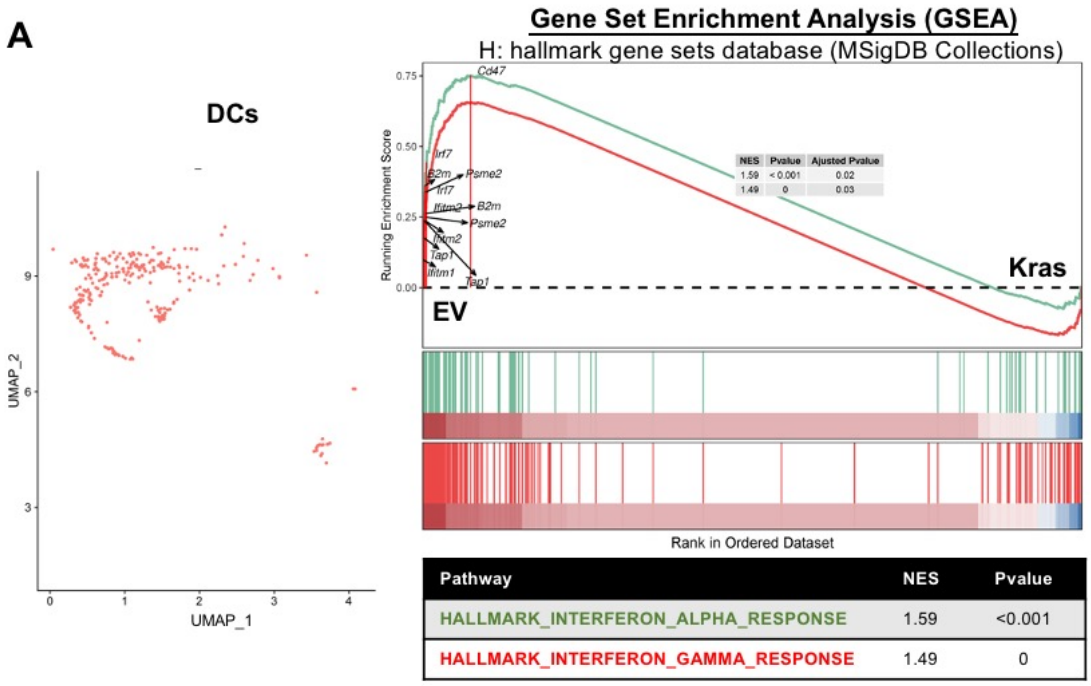

Pathway	NES	Pvalue
HALLMARK_INTERFERON_ALPHA_RESPONSE	1.59	<0.001
HALLMARK_INTERFERON_GAMMA_RESPONSE	1.49	0

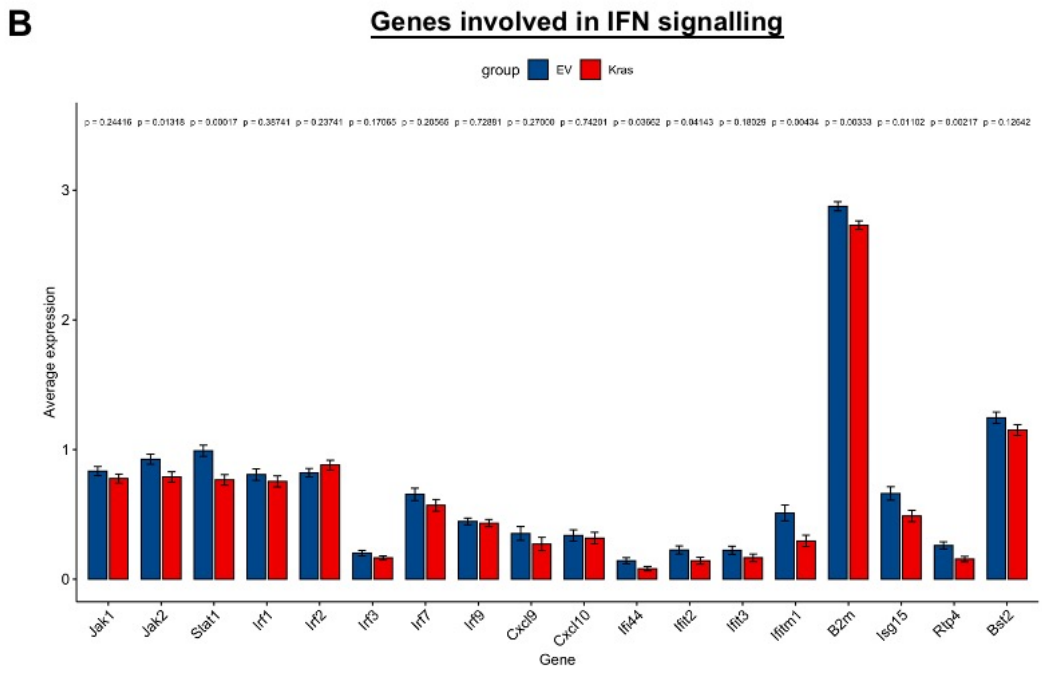

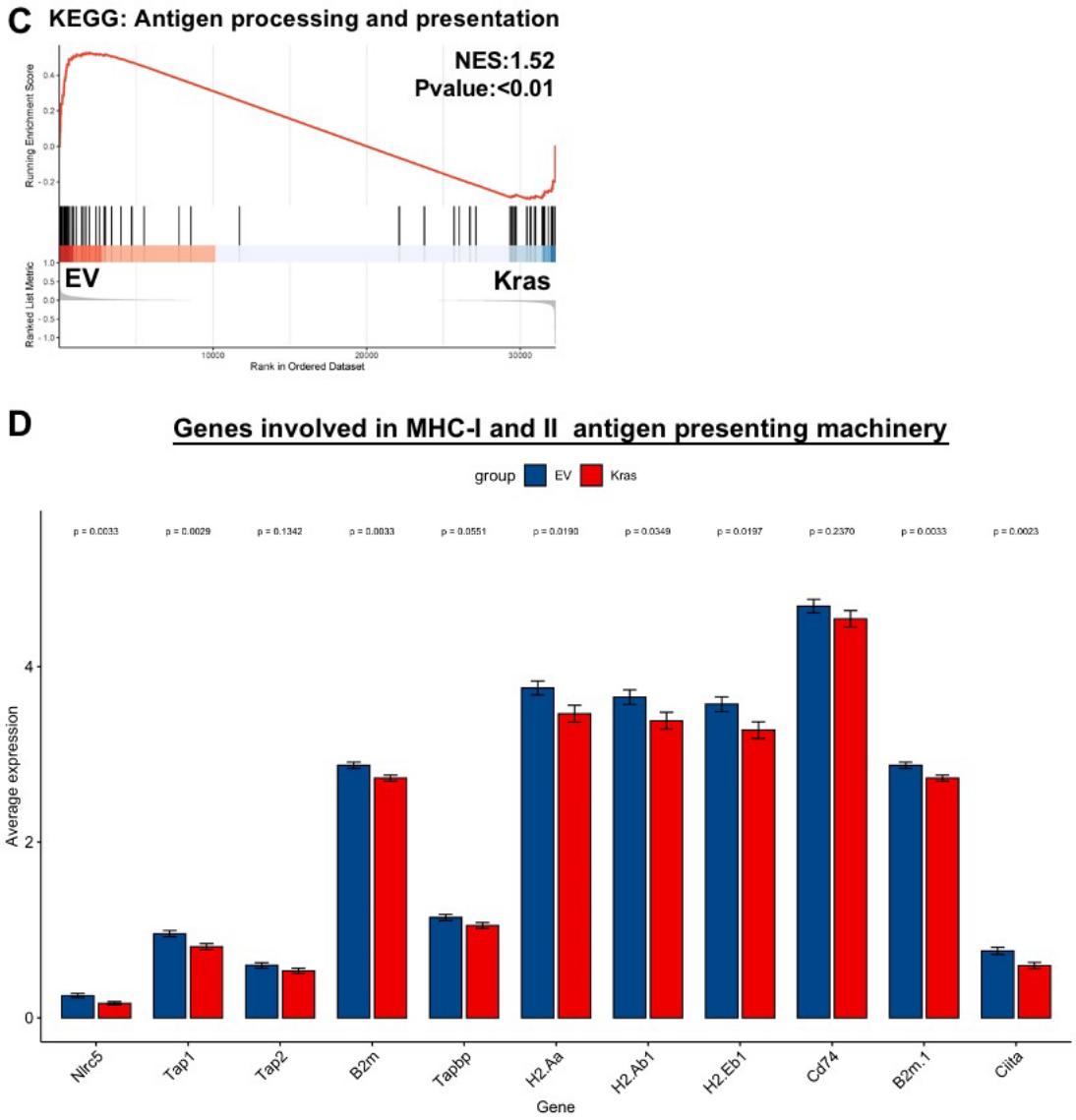

Figure 5.3 DCs exhibit reduced IFN responses and antigen presentation in wild-type Kras overexpressing tumours.
(A) UMAP presenting the DC population in the TIME. GSEA pathway analysis (H: hallmark gene sets database from MSigDB Collections) demonstrated that DCs in c-Myc-luc^{OE}/Tp53^{KO}/EV were enriched with "HALLMARK_INTERFERON_ALPHA_RESPONSE" (NES:1.59, p<0.001) and "HALLMARK_INTERFERON_GAMMA_RESPONSE" (NES:1.49, p=0). **(B)** Genes related to IFN signalling, for example, Jak1, Jak2, Stat1, and Cxcl9, were downregulated in the Kras-overexpressed group. **(C)** GSEA enrichment plot demonstrated that DCs in the control EV group are enriched with "KEGG: Antigen processing and presentation" (NES:1.52, p <0.01), suggesting that DCs in the Kras-overexpressed group exhibit impaired antigen presentation capabilities. **(D)** Representative genes of the antigen-presenting machinery were downregulated in the Kras overexpressed group.

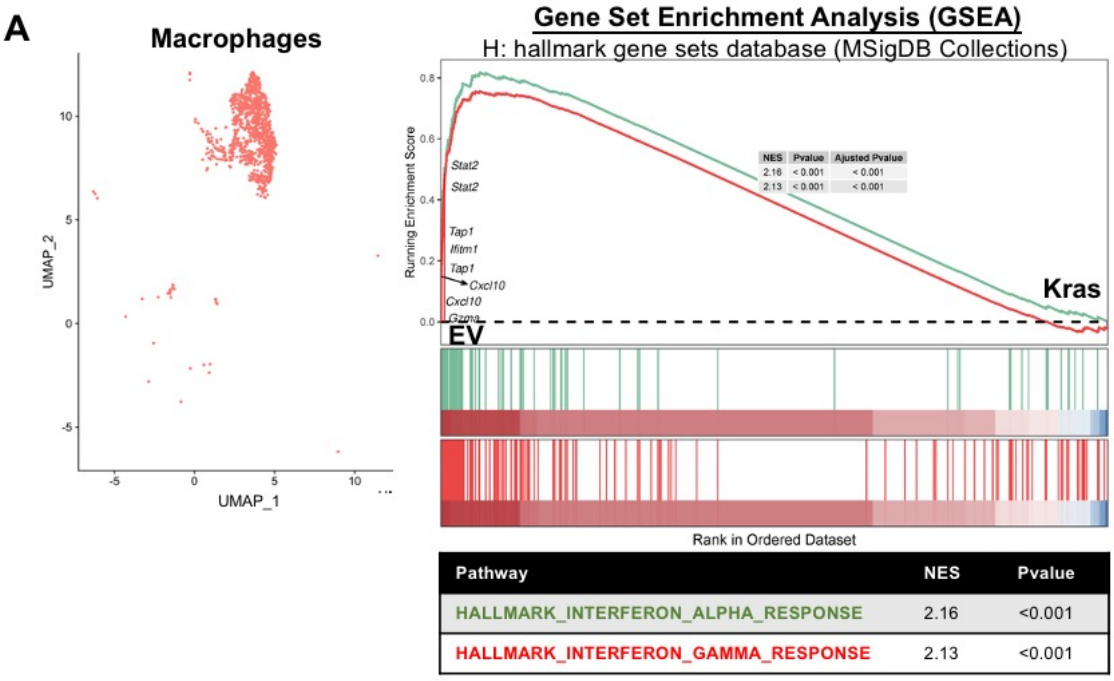

Pathway	NES	Pvalue
HALLMARK_INTERFERON_ALPHA_RESPONSE	2.16	<0.001
HALLMARK_INTERFERON_GAMMA_RESPONSE	2.13	<0.001

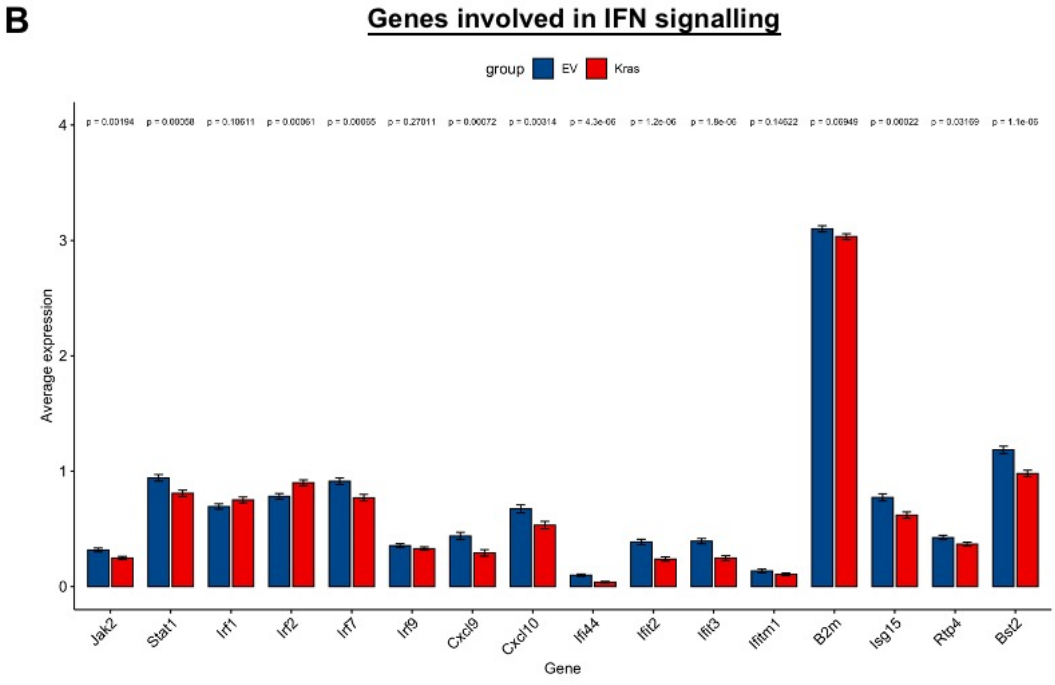

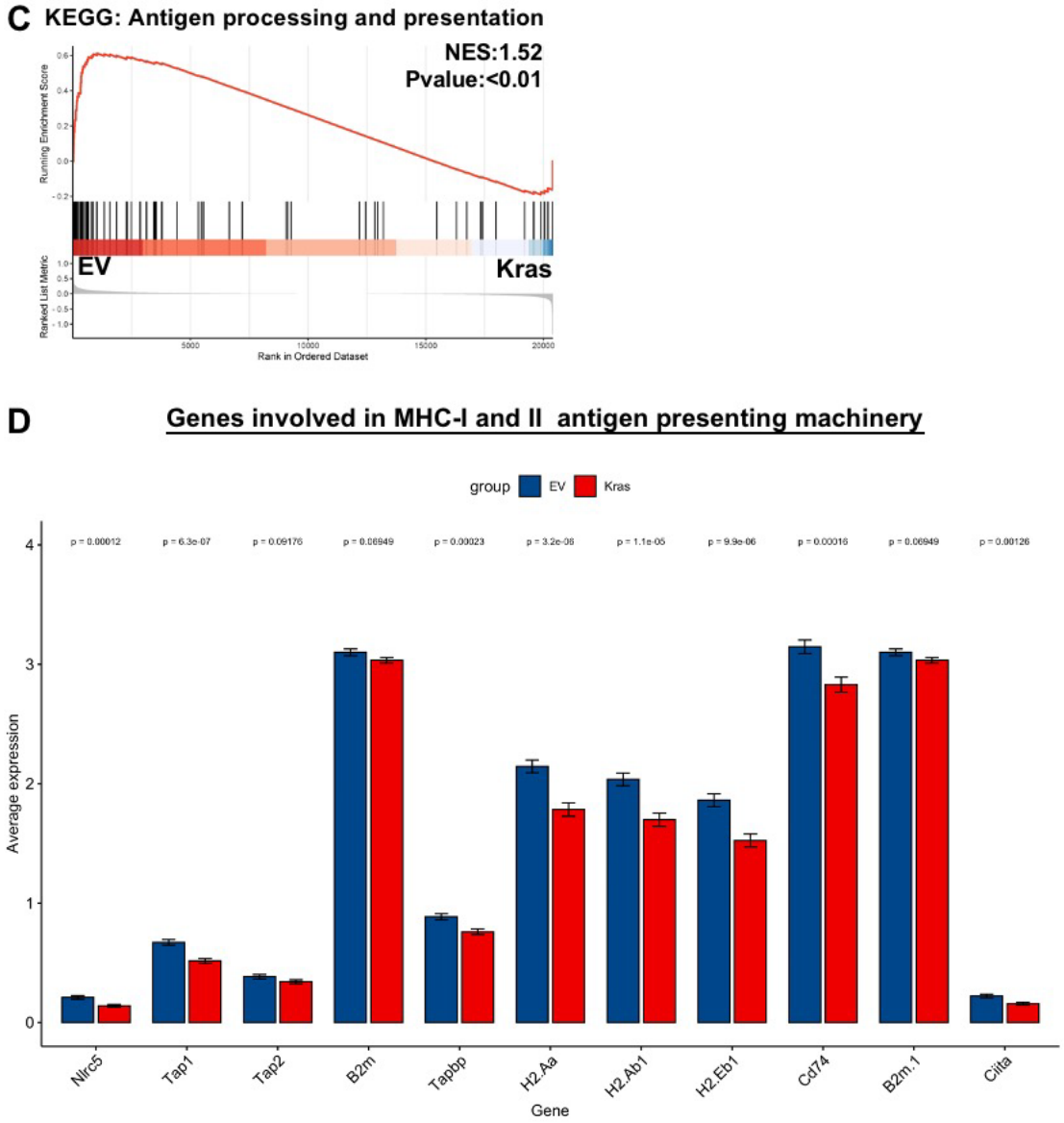

Figure 5.4 Macrophages exhibit reduced IFN responses and antigen presentation in wild-type Kras overexpressed tumours.
(A) UMAP presenting macrophage population in the TIME. GSEA pathway analysis (H: hallmark gene sets database from MSigDB Collections) demonstrated that macrophages in c-Myc-luc^{OE}/Tp53^{KO}/EV are enriched with "HALLMARK_INTERFERON_ALPHA_ RESPONSE" (NES:2.16, p<0.001) and "HALLMARK_INTERFERON_GAMMA_ RESPONSE" (NES:2.13, p<0.001). **(B)** Genes related to IFN signalling, for example, Jak2, Stat1, Cxcl9, and Cxcl10, were downregulated in the Kras-overexpressed group. **(C)** GSEA enrichment plot demonstrated that macrophages in the control EV group are enriched with "KEGG: Antigen processing and presentation" (NES:1.52, p<0.01), indicating that macrophages in the Kras overexpressed group exhibit impaired antigen presentation capabilities. **(D)** Representative genes of antigen-presenting machinery were downregulated in the Kras-overexpressed group.

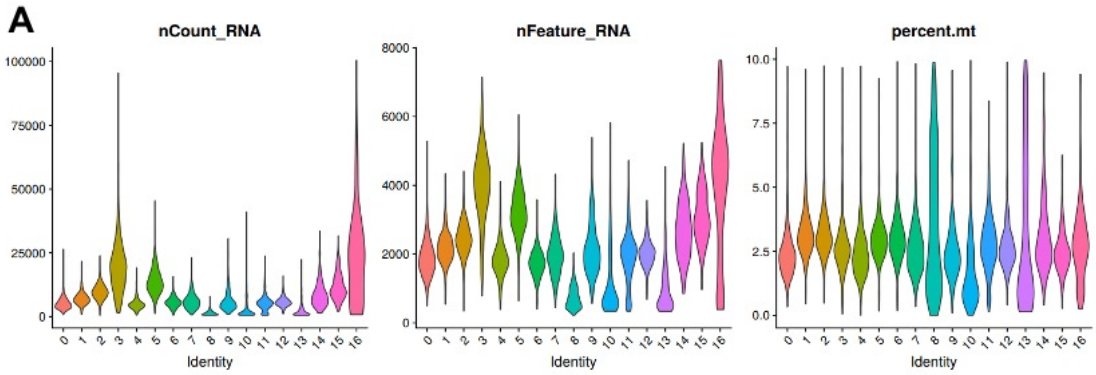

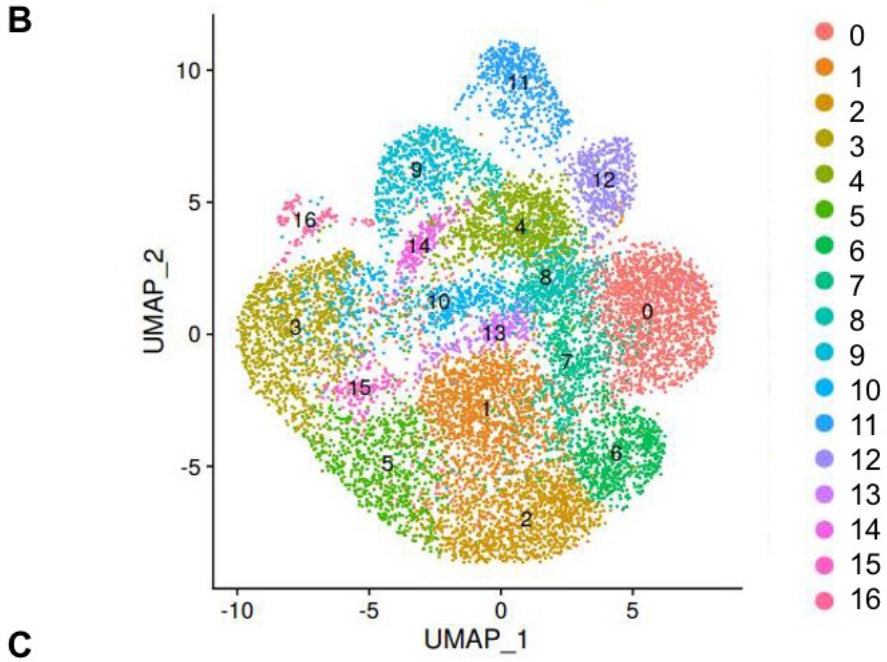

C

Cluster ID	Cluster name	Representative genes	Functional properties
Cluster-0	CD8-c1-Gzmk	Cd3d, Cd3e, Cd3g, Cd8a, Cd8b1, Gzmk, Ccl4, Ccl5	effector memory T cells
Cluster-1	NKT-c1-Klrb1c	Cd3d, Cd3e, Cd3g, Klrb1c	natural killer T cells
Cluster-2	CD8-c2-Lef1	Cd3d, Cd3e, Cd3g, Cd8a, Cd8b1, Ccr7, Sell, Lef1	naïve T cells
Cluster-3	CD8-c3-Mki67	Cd3d, Cd3e, Cd3g, Cd8a, Cd8b1, Mki67, Stmn1	proliferative T cells
Cluster-4	CD4-c1-Icos	Cd3d, Cd3e, Cd3g, Cd4, Cd40lg, Cxcr3, Icos, Ctla4, Pdcd1	follicular helper T cells
Cluster-5	CD8-c4-Sell	Cd3d, Cd3e, Cd3g, Cd8a, Cd8b1, Sell,	naïve T cells
Cluster-6	CD8-c5-Ccr7	Cd3d, Cd3e, Cd3g, Cd8a, Cd8b1, Ccr7, Sell, Lef1	naïve T cells
Cluster-7	CD8-c6-Isg15	Cd3d, Cd3e, Cd3g, Cd8a, Cd8b1, Ifit3, Ifit1, Isg15	Interferon-stimulated T cells
Cluster-8	T-c1-Malat1	Cd3d, Cd3e, Cd3g, Malat1, Neat1	tolerant T cells
Cluster-9	CD4-c2-Foxp3	Cd3d, Cd3e, Cd3g, Cd4, Foxp3, Ctla4	regulatory T cells
Cluster-10	CD8-c7-Stmn1	Cd3d, Cd3e, Cd3g, Cd8a, Cd8b1, Mki67, Stmn1, Ube2c	proliferative T cells
Cluster-11	γδT-c1-Trdc	Cd3d, Cd3e, Cd3g, Trdc, Trdv4	gamma delta T cells
Cluster-12	NKT-c2-Cxcr6	Cd3d, Cd3e, Cd3g, Klrb1c,Ccr2, Cxcr6, Il7r	natural killer T cells
Cluster-13	NK-c1-Ncr1	Ncr1, Tyrobp, Gzma	natural killer cells
Cluster-14	CD4-c3-Pdcd1	Cd3d, Cd3e, Cd3g, Cd4, Pdcd1, Lag3, Havcr2	exhausted T cells
Cluster-15	CD8-c8-Pclaf	Cd3d, Cd3e, Cd3g, Cd8a, Cd8b1, Mki67, Stmn1, Ube2c, Pclaf	proliferative T cells
Cluster-16	Doublet	Cd3d, Cd3e, Cd3g, Igkc, Cd79a, Cd79b	Doublet

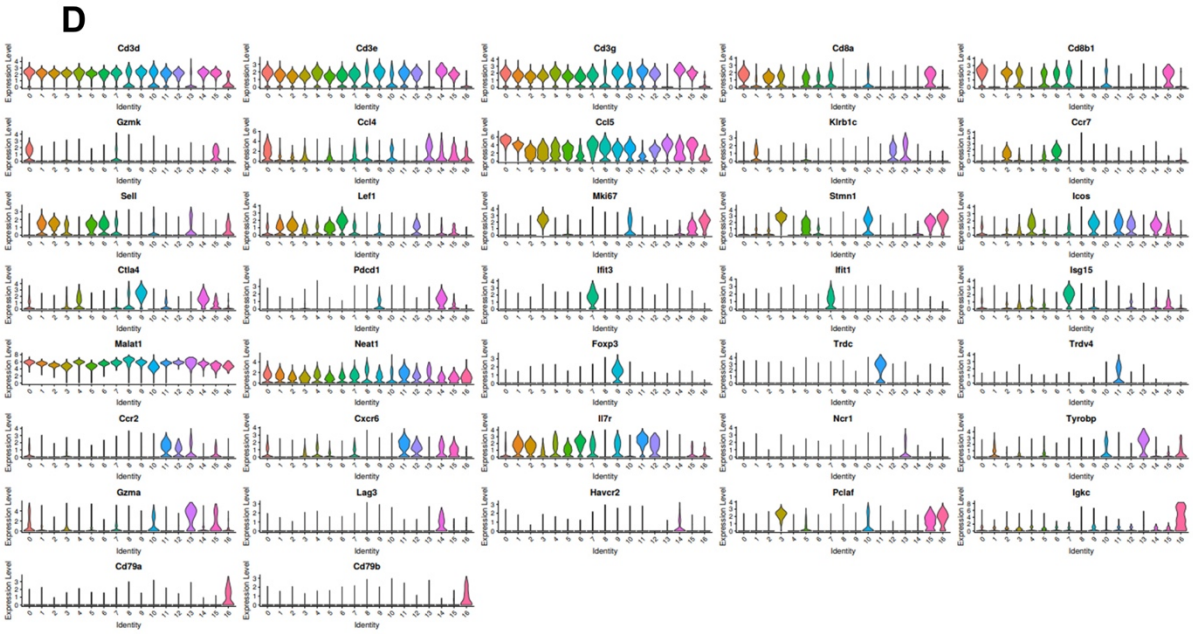
D
Cd3d
Cd3e
Cd3g
Cd8a
Cd8b1
Gzmk
Ccl4
Ccl5
Klrb1c
Ccr7
Sell
Lef1
Mki67
Stmn1
Icos
Ctla4
Pdcd1
Ifit3
Ifit1
Isg15
Malat1
Neat1
Foxp3
Trdc
Trdv4
Ccr2
Cxcr6
Il7r
Ncr1
Tyrobp
Gzma
Lag3
Havcr2
Pclaf
Igkc
Cd79a
Cd79b
Expression Level
Identity

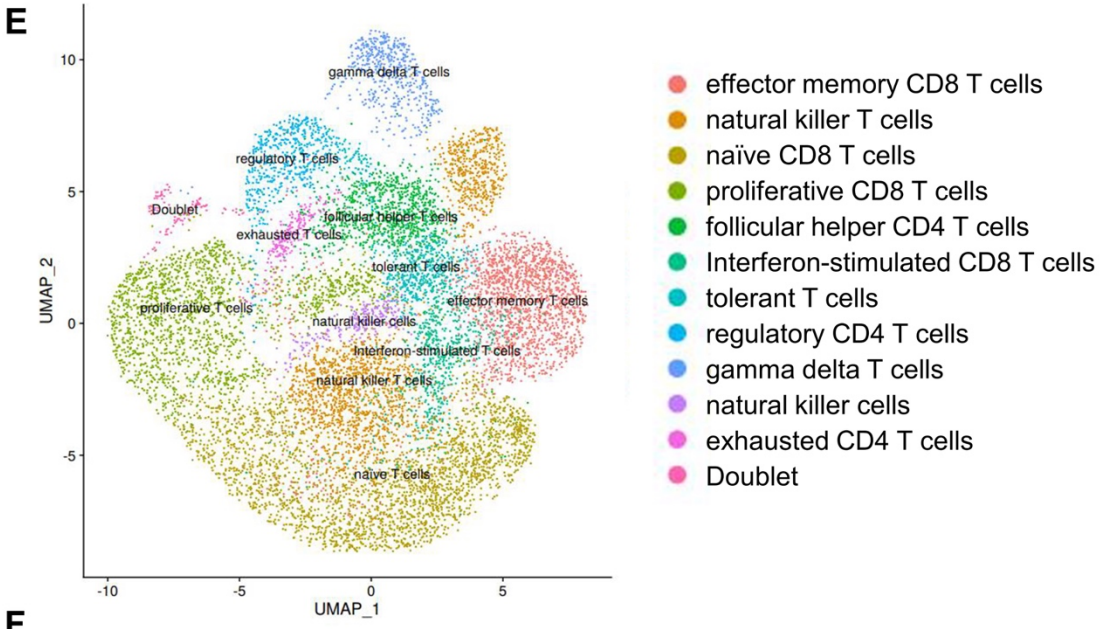
E
gamma delta T cells
regulatory T cells
Doublet
follicular helper T cells
exhausted T cells
tolerant T cells
effector memory T cells
proliferative T cells
natural killer cells
Interferon-stimulated T cells
natural killer T cells
naïve T cells
UMAP_2
UMAP_1
10
5
0
-5
-10
effector memory CD8 T cells
natural killer T cells
naïve CD8 T cells
proliferative CD8 T cells
follicular helper CD4 T cells
Interferon-stimulated CD8 T cells
tolerant T cells
regulatory CD4 T cells
gamma delta T cells
natural killer cells
exhausted CD4 T cells
Doublet

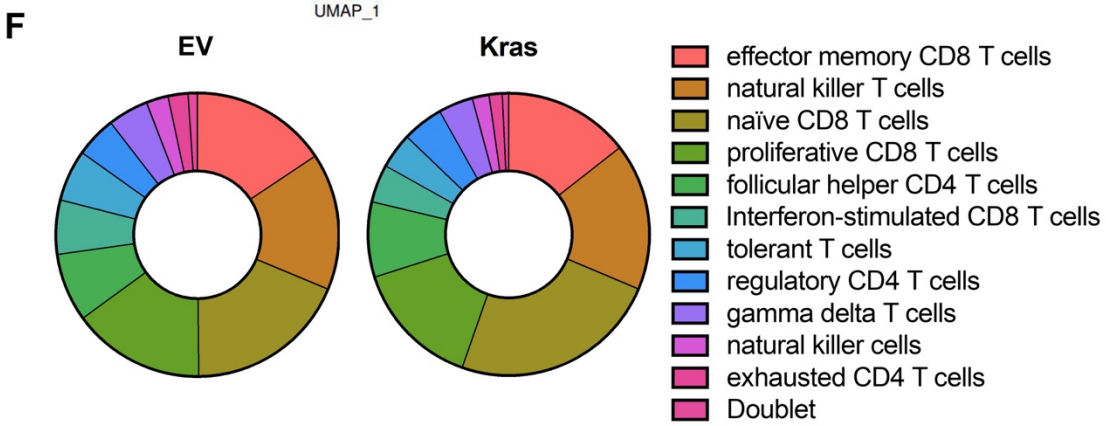
F
EV
Kras
effector memory CD8 T cells
natural killer T cells
naïve CD8 T cells
proliferative CD8 T cells
follicular helper CD4 T cells
Interferon-stimulated CD8 T cells
tolerant T cells
regulatory CD4 T cells
gamma delta T cells
natural killer cells
exhausted CD4 T cells
Doublet

G

Annotation	EV	Kras
effector memory CD8 T cells	927	827
natural killer T cells	927	964
naïve CD8 T cells	1102	1375
Proliferative CD8 T cells	898	842
follicular helper CD4 T cells	461	493
Interferon-stimulated CD8 T cells	366	248
tolerant T cells	348	233
regulatory CD4 T cells	278	269
gamma delta T cells	274	228
natural killer cells	150	110
exhausted CD4 T cells	135	86
Doublet	63	43

Figure 5.5 scRNA-seq analysis revealed that wild-type Kras dampens T cell activation in the TIME.
(A) Violin plots presenting the number of genes (nFeature_RNA), the number of reads (nCount_RNA) and the percentage of mitochondrial gene (percent.mt) detected in T cell populations after quality control. **(B&C)** UMAP and table presenting different T cell clusters with representative markers. **(D)** Violin plots showing the expression of representative genes in each T cell population. **(E)** UMAP presenting defined T cell populations after grouping. **(F&G)** Pie chart and table comparing the cell number of each T cell cluster.

5.3.2 Wild-type KRAS activation promotes immune evasion via suppression of DC and T cell recruitment to the tumour site

To study how wild-type Kras modulates the anti-tumour T cell response, we performed flow cytometry using the c-Myc-lucOS^{OE}/Tp53^{KO} HCC model. T cell and myeloid cell antibody panels with the dilution of antibodies are listed in the Method section (Table 2.6). The immunophenotyping panel covers the major cell types in the TIME, including B cells, DCs, Neutrophils, NK cells, Monocytes, Macrophages, T cells, CD4$^+$ T cells, CD8$^+$ T cells, and antigen SIINFEKL-specific CD8$^+$ T cells. The gating strategy and cell type definitions are shown in Figure 5.6. Pro5® MHC I Pentamer-SIINFEKL (ProImmune, UK) was used to detect and separate the SIINFEKL-specific CD8 T$^+$ cells. The design of five MHC peptide complexes in the pentamer enhances the avidity interaction with the TCR receptor.

To determine the optimal timepoint for immune profiling, we monitored the bioluminescence signals and changes in SIINFEKL-specific CD8$^+$ T cells in c-Myc-lucOS^{OE}/Tp53^{KO}/EV and c-Myc-lucOS^{OE}/Tp53^{KO}/Kras mice during the first two weeks after HTVI (Figure 5.7A&B). The luciferase signals between the two groups were similar, and no SIINFEKL-specific CD8$^+$ T cells were detected in the first week. In the second week, the signals of c-Myc-

lucOS^{OE}/Tp53^{KO}/EV group began to decrease, indicating the elicitation of an anti-tumour immune response. This was further supported by the detection of SIINFEKL-specific CD8^{+} T cells in both groups. Hence, we performed the immune profiling in the second week after HTVI.

In comparison to naïve mice, elevated levels of immune cells including DCs, T cells, NK cells and monocytes were observed in the c-Myc-lucOS^{OE}/Tp53^{KO} HCC model (Figure 5.7C). This validated the induction of an immune response through the overexpression of antigens in the lucOS model. In c-Myc-lucOS^{OE}/Tp53^{KO}/Kras livers, the number of DCs was significantly lower than that in the control EV group. DCs play a crucial role in priming and activating T cells in an adaptive immune response. Moreover, the overall composition of T cells was diminished in c-Myc-lucOS^{OE}/Tp53^{KO}/Kras livers. The number of CD4^{+} T cells decreased from 17% to 13%, and that of CD8^{+} T cells decreased from 29% to 20% in the Kras-overexpressed group. Both CD4^{+} and CD8^{+} T cells exhibited lower activation (CD44^{+}) rates. Intriguingly, the number of SIINFEKL-specific CD8^{+} T cells in the Kras group was approximately one-third that in the control group, suggesting an insufficient CD8^{+} T cell response. These findings indicate that Kras overexpression impairs the recruitment of DCs and T cells to the tumour site. No difference was observed in the number of NK cells between the two groups. However, the levels of monocytes, macrophages, and neutrophils were higher in c-Myc-lucOS^{OE}/Tp53^{KO}/Kras livers. This finding implies that wild-type Kras overexpression induced the infiltration of myeloid cells to the tumour site.

Furthermore, we investigated the expression of cytokines and chemokines between the c-Myc-lucOS^{OE}/Tp53^{KO}/EV and c-Myc-lucOS^{OE}/Tp53^{KO}/Kras tumour cells using qPCR analysis. The expression of Ccl3 was significantly higher in the Kras group (Figure 5.7D), suggesting that the upregulated recruitment of myeloid cells, including monocytes, macrophages, and neutrophils, is possibly mediated by Ccl3 expression. Interestingly, the expressions of Ccl5, Cxcl9, and Cxcl11 were significantly downregulated in the Kras group. Ccl5, Cxcl9 and Cxcl11 are IFN-inducible inflammatory chemokines (Ozga et al., 2021). Ccl5 is responsible for the recruitment of DCs, whereas Cxcl9 and Cxcl11 act as chemoattractants for T cells at the tumour site (Gao et al., 2019; López et al., 2018). Thus, we measured the expression of IFN-related genes in the tumour cells. Consistent with our hypothesis, the expression of Stat1, Stat2, Irf1, Irf2 and Irf9 was downregulated in c-Myc-lucOS^{OE}/Tp53^{KO}/Kras tumours. In summary, we concluded that wild-type KRAS activation, via suppression of extrinsic IFN

responses, led to impaired recruitment of DCs and T cells to the TIME and reduced T cell activation.

Furthermore, we investigated whether there was a correlation between IFN responses and KRAS expression in the clinical data (Figure 5.8A). In the TCGA-LIHC cohort (n=372 samples), patients were divided into low (n=228) and high (n=144) KRAS expression groups based on mean KRAS expression. GSEA pathway analysis was performed to compare the enriched pathways between the low and high KRAS expression groups (Figure 5.8B). "HALLMARK_INTERFERON_ALPHA_RESPONSE" (NES:1.49, p=0) was enriched in the low KRAS expression group, while "HALLMARK_INTERFERON_GAMMA _RESPONSE" showed no significant difference in the enrichment between the two groups. With regards to the regulation of DC recruitment, the expression of DC-related transcripts BATF3 and ITGAE (CD103) was negatively correlated with KRAS expression, in accordance with the expression level of KRAS.

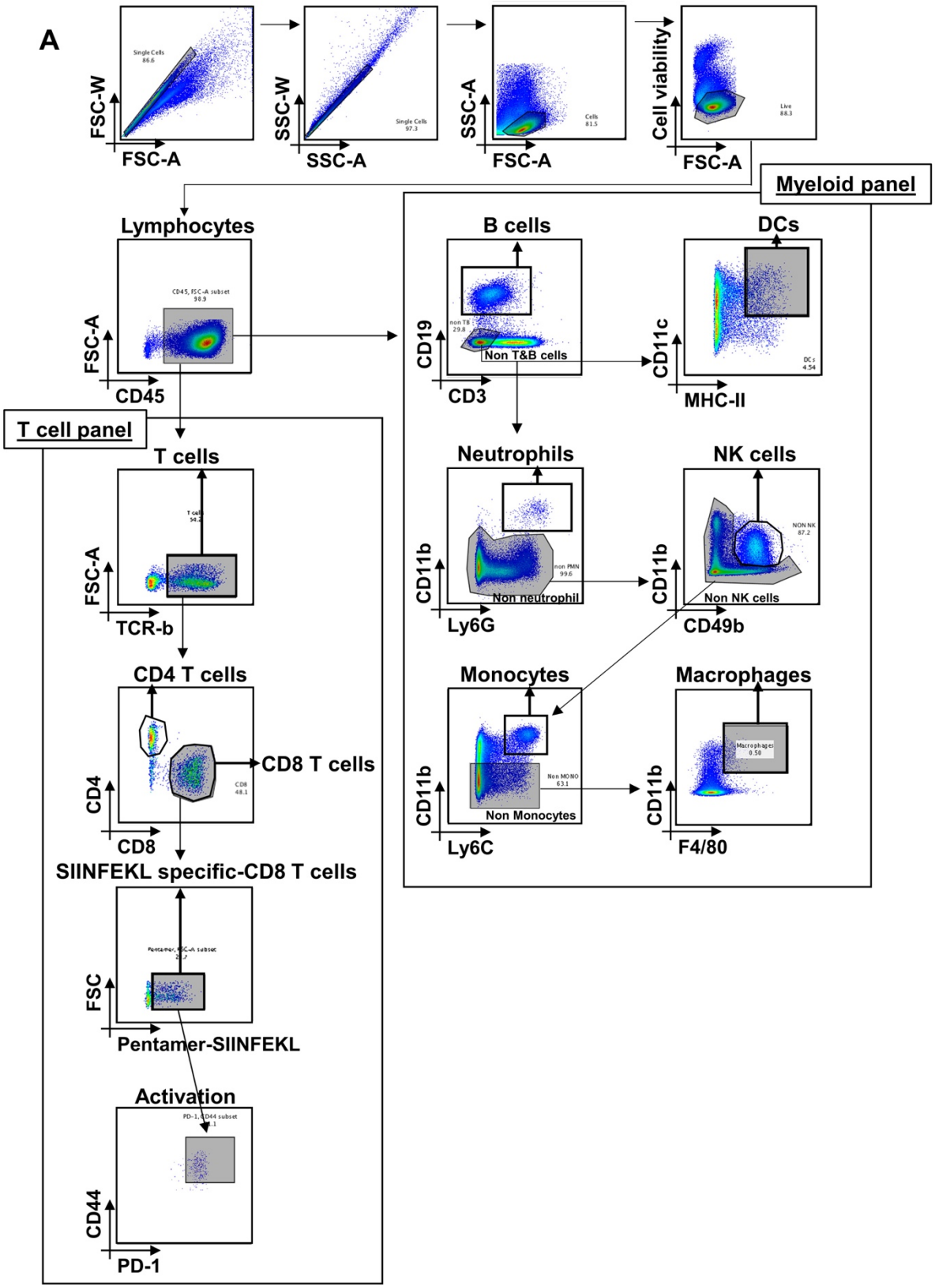
A
FSC-W
FSC-A
Single Cells
86.6
SSC-W
SSC-A
Single Cells
97.3
SSC-A
FSC-A
Cells
81.5
Cell viability
FSC-A
Live
88.3
Myeloid panel
Lymphocytes
FSC-A
CD45
CD45, FSC-A subset
98.9
B cells
CD19
CD3
non T&B
29.8
Non T&B cells
DCs
CD11c
MHC-II
DCs
4.54
T cell panel
T cells
FSC-A
TCR-b
T cells
94.2
Neutrophils
CD11b
Ly6G
non PMN
99.6
Non neutrophil
NK cells
CD11b
CD49b
NON NK
87.2
Non NK cells
CD4 T cells
CD4
CD8
CD8 T cells
CD8
48.1
Monocytes
CD11b
Ly6C
Non MONO
63.1
Non Monocytes
Macrophages
CD11b
F4/80
Macrophages
0.58
SIINFEKL specific-CD8 T cells
FSC
Pentamer-SIINFEKL
Activation
CD44
PD-1
PD-1, CD44 subset
1.1

B

Definition of cell types in Immunoprofiling	
T cells	$CD45^+TCR\text{-}b^+$
CD4 T cells	$CD45^+TCR\text{-}b^+\ CD4^+$
CD8 T cells	$CD45^+TCR\text{-}b^+\ CD8^+$
SIINFEKL specific-CD8 T cells	$CD45^+TCR\text{-}b^+\ CD8^+Pentamer\text{-}SIINFEKL^+$
B cells	$CD45^+\ CD19^+$
DCs	$CD45^+\ CD11c^+MHC\text{-}II^+$
Neutrophils	$CD45^+\ CD11b^+Ly\text{-}6G^+$
NK cells	$CD45^+\ CD11b^+CD49b^+$
Monocytes	$CD45^+\ CD11b^+Ly\text{-}6G^-Ly\text{-}6C^+$
Monocyte-derived macrophages	$CD45^+\ CD11b^+Ly\text{-}6G^-Ly\text{-}6C^+F4/80^+$

Figure 5.6 Flow cytometry immune profiling comparing the immune cell composition of c-Myc-lucOS^{OE}/Tp53^{KO}/EV and c-Myc-lucOS^{OE}/Tp53^{KO}/Kras livers.
(A) Diagram demonstrating the gating strategy of T cell and myeloid panels. **(B)** The table listed the definition of the cell types in immune profiling.

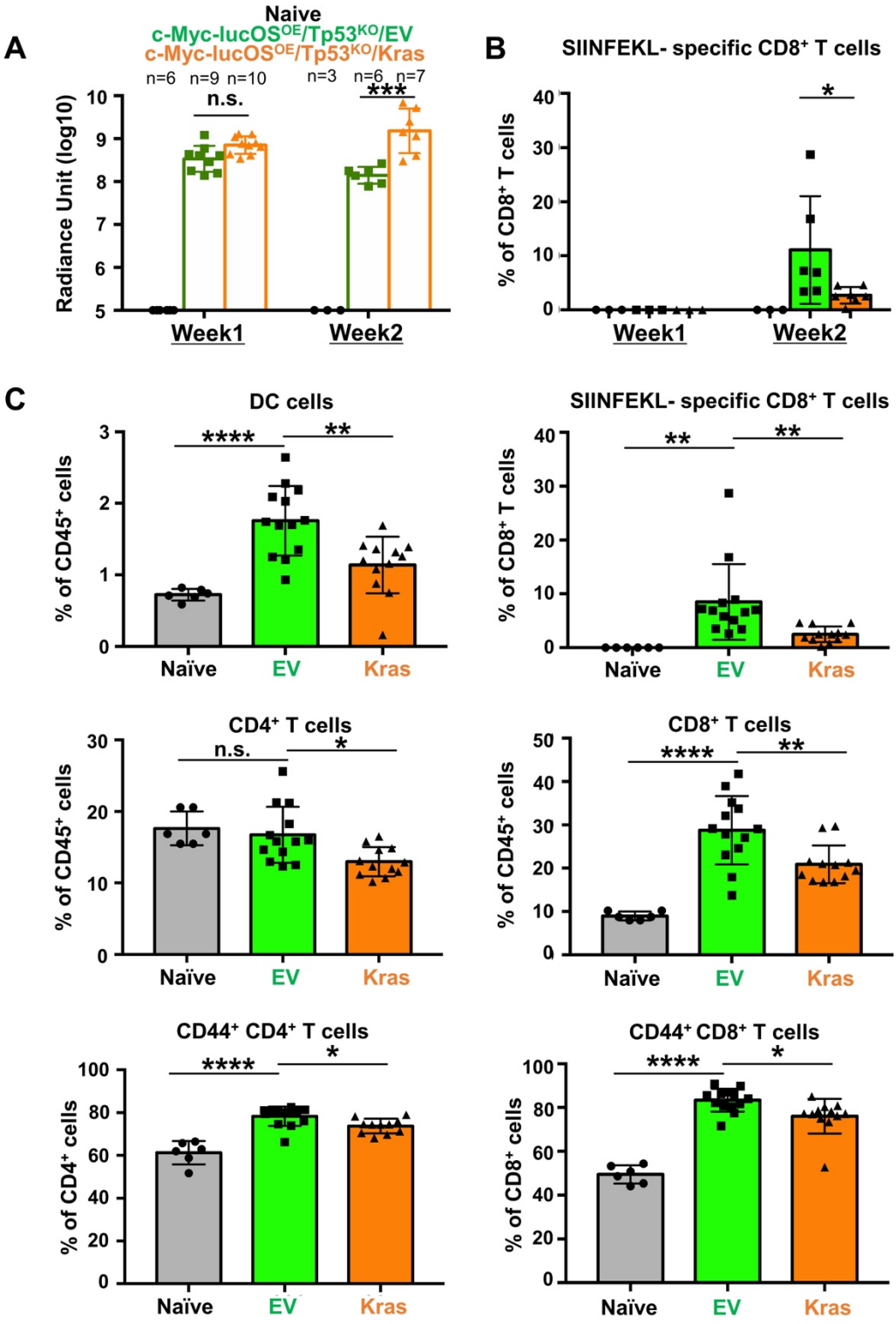
A
Naive
c-Myc-lucOS^OE/Tp53^KO/EV
c-Myc-lucOS^OE/Tp53^KO/Kras
n=6 n=9 n=10
n=3 n=6 n=7
n.s.
***
Radiance Unit (log10)
Week1
Week2
B
SIINFEKL- specific CD8+ T cells
*
% of CD8+ T cells
Week1
Week2
C
DC cells
****
**
% of CD45+ cells
Naïve
EV
Kras
SIINFEKL- specific CD8+ T cells
**
**
% of CD8+ T cells
Naïve
EV
Kras
CD4+ T cells
n.s.
*
% of CD45+ cells
Naïve
EV
Kras
CD8+ T cells
****
**
% of CD45+ cells
Naïve
EV
Kras
CD44+ CD4+ T cells
****
*
% of CD4+ cells
Naïve
EV
Kras
CD44+ CD8+ T cells
****
*
% of CD8+ cells
Naïve
EV
Kras

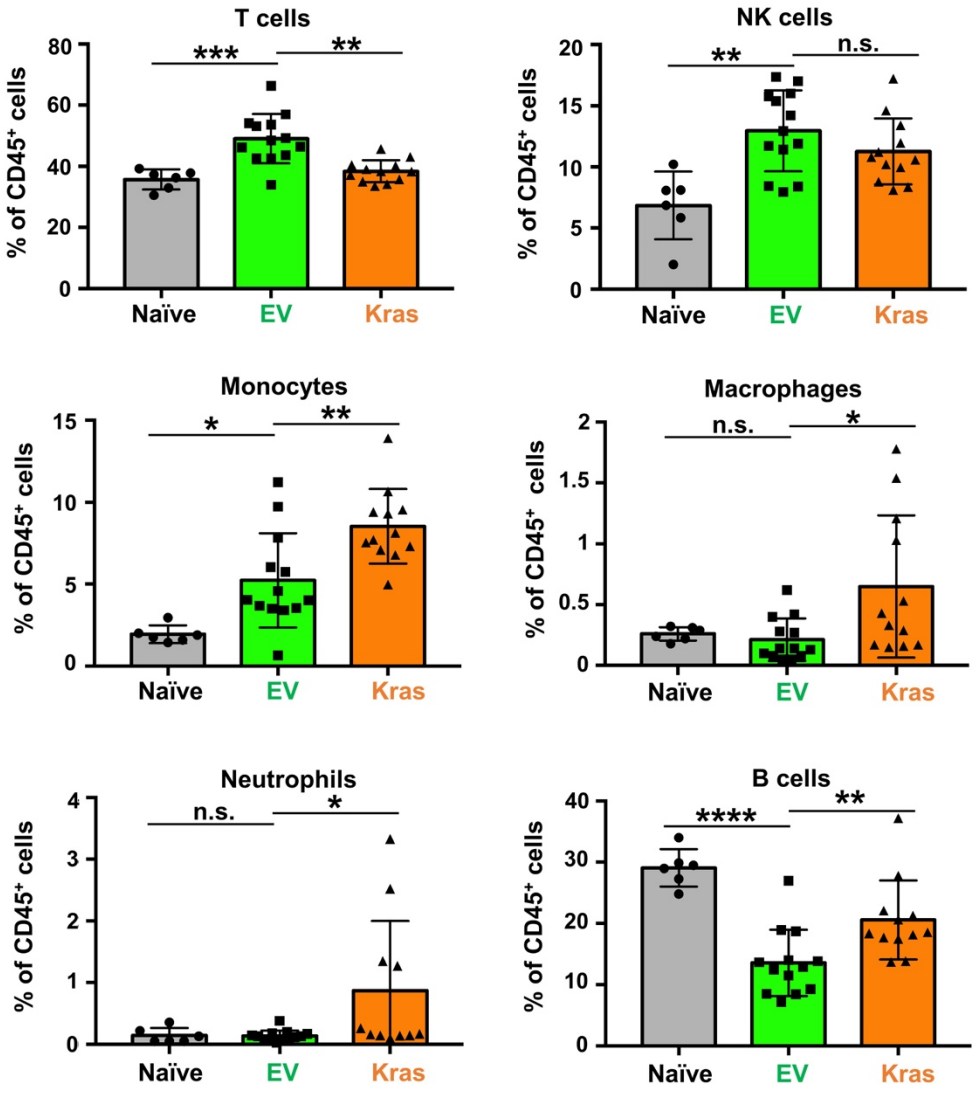
T cells
% of CD45+ cells
***
**
Naïve
EV
Kras
NK cells
n.s.
Monocytes
Macrophages
Neutrophils
B cells
****

D

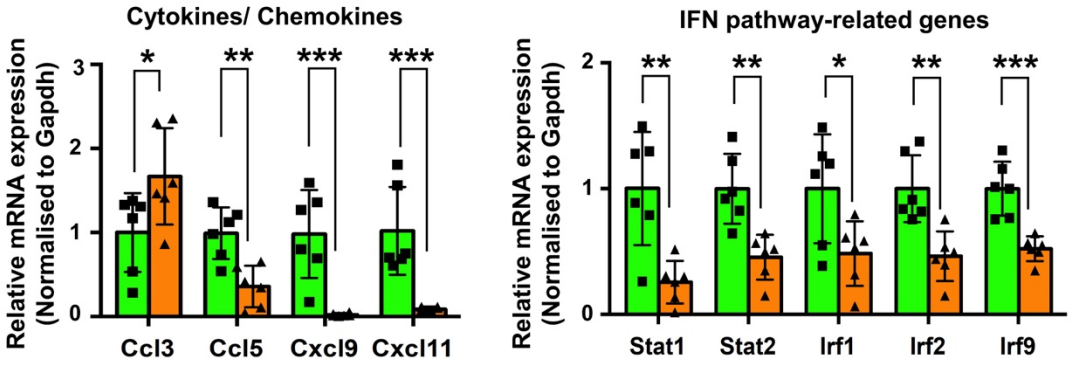
Cytokines/ Chemokines
Relative mRNA expression (Normalised to Gapdh)
Ccl3
Ccl5
Cxcl9
Cxcl11
IFN pathway-related genes
Stat1
Stat2
Irf1
Irf2
Irf9

Figure 5.7 Immune profiling demonstrated suppression of DC and T cell recruitment in Kras-overexpressed mice

(A) Quantification of normalised luciferase signals of c-Myc-lucOS^{OE}/Tp53^{KO}/EV and c-Myc-lucOS^{OE}/Tp53^{KO}/Kras in week one and week two after HTVI (*** $p<0.001$, t-test). **(B)** Flow cytometry compared the number of SIINFEKL-CD8^{+} T cells in the control EV and Kras groups (* $p<0.05$, t-test). **(C)** In c-Myc-lucOS^{OE}/Tp53^{KO}/Kras livers, DCs, CD4^{+}, CD8^{+} and SIINFEKL-specific CD8^{+} T cells were significantly reduced (naïve, n=6; EV, n=13; Kras, n =12; * $p<0.05$, ** $p<0.01$, *** $p<0.001$, **** $p<0.0001$, t-test). **(D)** qPCR analysis revealed downregulation of IFN-inducible chemokines Ccl5, Cxcl9, and Cxcl11 in c-Myc-lucOS^{OE}/Tp53^{KO}/Kras livers. Apart from the downregulated extrinsic IFN response in the TIME, Kras overexpression also repressed the intrinsic IFN signalling cascade in tumour cells. qPCR analysis revealed downregulated expression of IFN pathway genes in the Kras group (n = 6 per group; *$p<0.05$, **$p<0.01$, ***$p<0.001$, t-test).

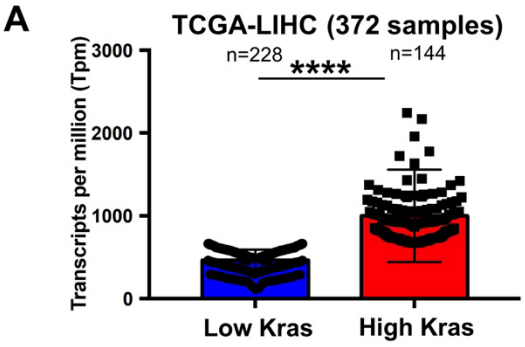

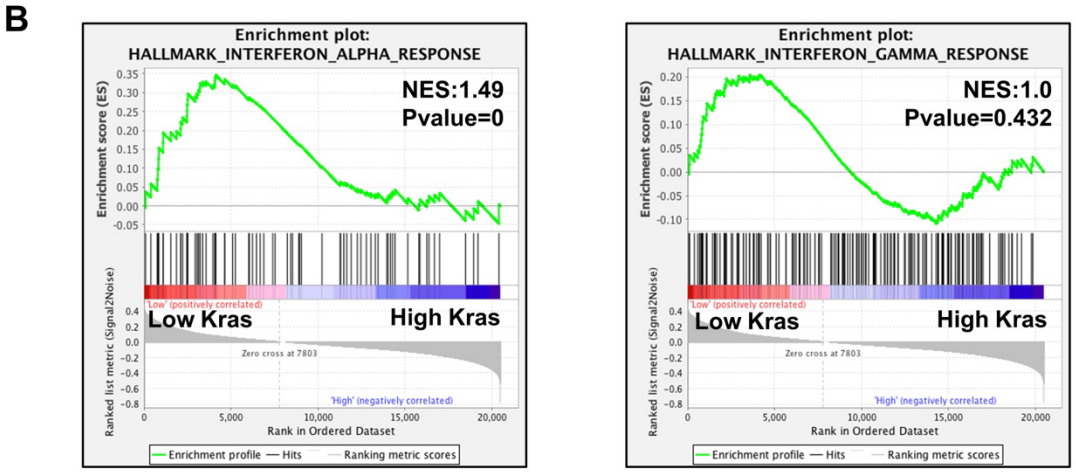

C

TCGA-LIHC (372 samples)			
Gene_Symbol	**Low (n=124)**	**Intermediate (n=124)**	**High (n=124)**
KRAS	370.29	594.29	1045.39
BATF3 (DCs)	31.89	27.64	23.81
ITGAE (CD103/ T cell infiltration)	215.87	252.06	202.02

Figure 5.8 TCGA-LIHC cohort showed that KRAS expression is negatively associated with IFN response.
(A) Patients in the TCGA-LIHC cohort (n=372 samples) were divided into groups with low (n=228) and high (n=144) wild-type KRAS expression, according to mean KRAS expression. **(B)** GSEA pathway analysis (H: hallmark gene sets database from MSigDB Collections) demonstrated that patients with low KRAS expression were enriched with "HALLMARK_INTERFERON_ALPHA_RESPONSE" (NES:1.49, p=0). **(C)** The TCGA-LIHC cohort (n=372 samples) showed a negative correlation between KRAS expression and DC-related genes.

5.4 Discussion

In this chapter, we have gained a deeper understanding of how wild-type Kras reprogrammes the immune landscape in a c-Myc^{OE}/Tp53^{KO} HCC background (Figure 5.9). Upon wild-type Kras overexpression, the TIME became more immunosuppressive, characterised by the repression of interferon-alpha/beta (type I IFN) and gamma (type II IFN) responses. The downregulated IFN responses led to inadequate recruitment of DCs and T cells, attributed to the decline in Ccl5, Cxcl9, and Cxcl11 expression. In addition to suppressing DC and T cell recruitment, both type I and type II IFNs modify the immune response by regulating APC function (Gessani et al., 2014). Our scRNA-seq data revealed that professional APCs, DCs, and macrophages exhibited lower antigen-presenting capacities in Kras overexpressed mice. The downregulated IFN responses affected the downstream APM-related genes, such as B2m, Tap1, Tap2, Nlrc5, and Ciita. The decreased expressions of MHC-I and MHC-II on APCs, in turn, affect T cell priming and activation, consistent with the observations from our immune profiling results. These immune evasive mechanisms disrupted the recruitment of antigen SIINFEKL-specific CD8^{+} T cells, ultimately leading to the failure of immunosurveillance.

Meanwhile, we also examined the clinical relevance of KRAS expression in suppressing the IFN response. Consistent with the findings in our mouse model, we found an inverse correlation between IFN response and KRAS expression in the TCGA cohort. Also, the KRAS expression was inversely associated with the expression of DC-related genes.

The impact of oncogenic KRAS signalling extends beyond the tumour cells to the TIME (Carvalho et al., 2018). Oncogenic KRAS not only aggravates the tumour-promoting properties of immune cells, but also induces immune evasion, escaping from the immunosurveillance (Kortlever et al., 2017). Indeed, the modulation of tumour-associated immune responses by KRAS signalling occurs during the recruitment, activation, and differentiation of immune cells.

Oncogenic KRAS was reported to inhibit the expression of STAT1 and STAT2, interfering with STAT-dependent transcription in colon cancer (Klampfer et al., 2003). Since STAT1 and STAT2 are pivotal transcription factors that promote crucial anti-tumour immunity, their direct inhibition resulted in reduced responsiveness to IFN-γ, downregulation of MHC molecules, limited T cell infiltration, and T cell exhaustion (Lal et al., 2018; Li et al., 2018). Mechanistically, upon IFN-dependent activation of the cognate receptor, STAT1 and STAT2 bind to IRF9 to form the ISGF3 complex (Platanitis et al., 2019). The ISGF3 complex then

binds to a promoter sequence called interferon-stimulated response element (ISRE) of an interferon-stimulated gene (ISG), for example, IRFs. In response to type I IFN and ISGF3 activation, IRF1 and IRF7 become activated and induce the expression of proinflammatory genes, such as CCL5, CXCL9, CXCL10, and CXCL11, by binding to ISREs in hepatocytes (Cremer, Ghysdael & Vieillard, 2002; Forero et al., 2019; Jilg et al., 2014). CCL5 is crucial for DC recruitment into the tumours (de Galarreta et al., 2019; Kohli, Pillarisetty & Kim, 2022). Type II IFN, which is predominantly released by T and NK cells in response to IL-12, also regulates CXCL9, CXCL10, and CXCL11 expression via IRFs (Billiau & Matthys, 2009; Lal et al., 2018). The CXCR3 receptor ligands CXCL9, CXCL10, and CXCL11 mediate the recruitment of $CXCR3^+$ T cells to solid cancers (Whiting et al., 2007). Notably, the concentration of these ligands is associated with increased lymphocyte infiltration and improved survival in several cancers (Denkert et al., 2010; Specht et al., 2009; Suyama et al., 2005). Inverse correlations between oncogenic KRAS/ERK signalling and intra-tumoral $CD8^+$ T cell infiltration have been reported in clinical data and immunocompetent mouse models (Kemp et al., 2023; Lal et al., 2018; Liu et al., 2023; Loi et al., 2016). Another frequently deregulated gene in cancers, Myc, has also been reported to cooperate with Kras in evading T- and NK-cell immunity via suppression of the type I IFN pathway in pancreatic cancer (Muthalagu et al., 2020).

Indeed, oncogenic KRAS has been shown to confer resistance to ICB therapy via suppression of the IFN response in other cancers (Liao et al., 2020; Mugarza et al., 2022). In colorectal cancer, mutated KRAS hinders IRF2, promoting MDSC recruitment to the TIME via the CXCL3/CXCR2 axis, leading to resistance to anti-PD-1 therapy (Liao et al., 2020). Intriguingly, repression of IRF2-mediated IFN responses was also observed in a cell line carrying wild-type Kras. This evidence further supported our hypothesis that KRAS, regardless of the mutation status, induces immunosuppression via inhibiting IFN responses. On the other hand, inhibition of KRAS signalling has been shown to upregulate IFN signalling, effectively reversing immunosuppression driven by KRAS (Mugarza et al., 2022). Treatment of DCs with type I IFN and type II IFN has also demonstrated the potential to enhance tumour eradication and improve immunotherapy efficacy (Cauwels et al., 2018; Garris et al., 2018).

As most reports have focused on the regulatory role of mutant KRAS in the TIME, our study generated new insights into the role of wild-type KRAS and potential resistance mechanisms arising in the cancer immunology of HCC.

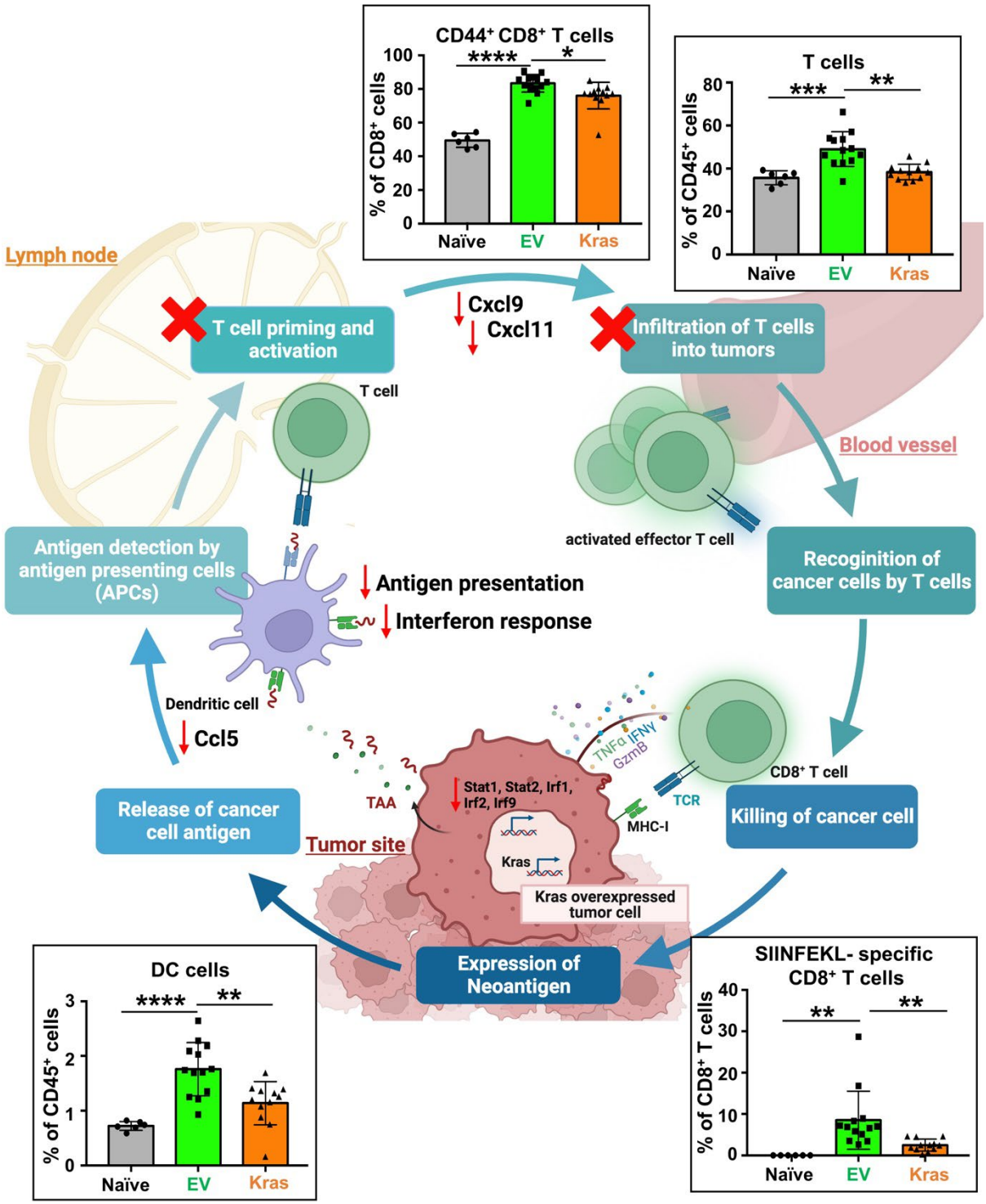

Figure 5.9 Diagram summarising the immunosuppressive functions of wild-type Kras overexpression in the TIME

Chapter 6. Wild-type Kras overexpression suppresses the MHC-I expression in the c-Myc-lucOS^{OE}/Tp53^{KO} HCC mice model

6.1 Introduction

In Chapter 5, our investigation revealed that the overexpression of wild-type Kras contributes to the formation of an immunosuppressive TIME. This occurs because of suppressed IFN responses, leading to compromised antigen presentation by APCs and impaired T cell activation. The reduced expression of the chemoattractants such as Ccl5, Cxcl9, and Cxcl11 further hampered the recruitment of DCs and T cells. These orchestrated immune evasion strategies exploited the survival benefits brought by the antigens.

In addition to defective APCs and T cell recruitment, tumour cells can escape antigen-dependent recognition from T cell-mediated killing. Loss of MHC-I is one of the key intrinsic mechanisms by which tumour cells avoid $CD8^+$ T cell recognition (Dupage et al., 2012; Jongsma et al., 2021). The MHC-I antigen processing machinery, normally induced in response to IFN, can be dysregulated at the genetic, epigenetic, transcriptional, and post-translational levels (Taylor & Balko, 2022). The transcription of MHC-I is governed by IFN-related NF-κB, STATs, IRFs, and NLRC5 (Chang et al., 1992; Lorenzi et al., 2012; Yoshihama et al., 2016). Downregulation of both type I and II IFN pathways or suppression of these critical regulators leads to the downregulation of MHC-I (Fenton et al., 2021; Kriegsman et al., 2019; Sade-Feldman et al., 2017).

Mutant RAS/ERK signalling has been reported to suppress the tumour cell immunogenicity and contribute to immunotherapy resistance by impairing IFN-responsive MHC-I expression in cancers (Gettinger et al., 2017; Klampfer et al., 2003; Salaroglio et al., 2019; Taylor & Balko, 2022; Zhao et al., 2021). In this chapter, we explored the correlation of wild-type Kras and MHC-I in HCC. The regulation of wild-type Kras on MHC-I was validated through *in vivo* and *in vitro* experiments. Murine HCC cell line Hep55.1c was subjected to wild-type Kras overexpression to examine the alteration of MHC-I expression.

6.2 Experiment design

(1) The clinical correlation between KRAS and MHC-I-related genes in HCC was examined in the TCGA-LIHC cohort.

(2) To study how wild-type Kras modulates MHC-I expression, c-Myc-lucOS^{OE}/Tp53^{KO}/Kras livers were harvested and analysed with western blot and IHC.

(3) *In vitro* experiments were performed to examine the effect of wild-type KRAS signalling on MHC-I expression. The wild-type Kras-overexpressing plasmid was cloned as described in the Method section. Murine HCC cell lines were examined for wild-type Kras expression. The cell line with the lowest wild-type Kras level was selected for wild-type Kras overexpression. IFN-γ treatment (50ng/ml) was added to induce the MHC-I H-2Kb expression. EGF was added at a concentration of 5nM and 10nM to the cell line to examine alterations in MHC-I expression.

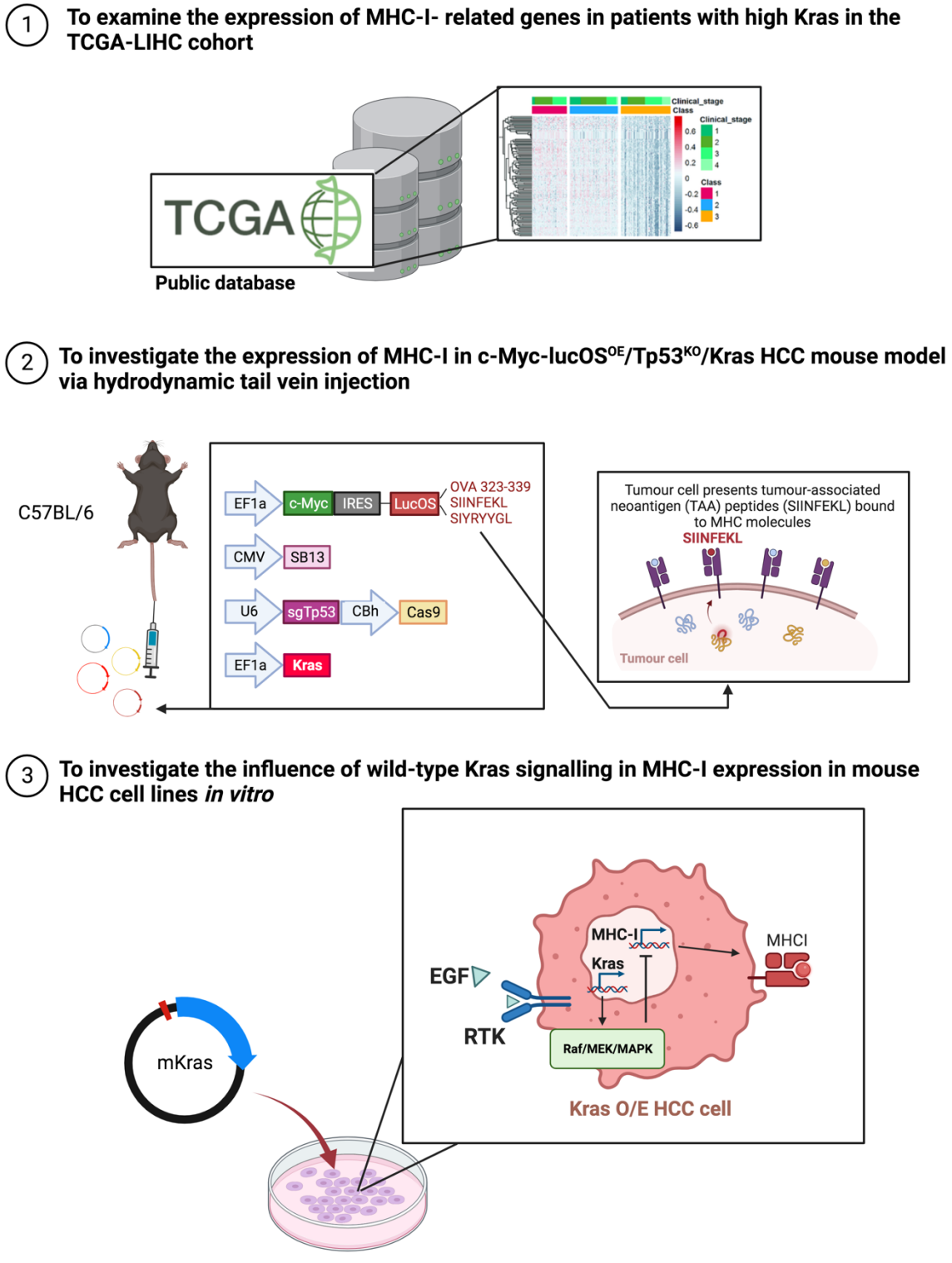

Figure 6.1 An outline of the workflow to examine the regulatory role of wild-type Kras in MHC-I expression.

6.3 Results

6.3.1 TCGA-LIHC cohort shows a negative correlation between Kras expression and MHC-I–related genes

The negative regulation of oncogenic KRAS/ERK signalling in APM components, which leads to defects in the MHC-I antigen processing pathway, has been widely reported in colorectal, lung, and breast cancers, and intrahepatic cholangiocarcinoma (Atkins et al., 2004; El-Jawhari et al., 2013; Franklin et al., 2020; Taylor & Balko, 2022; Wabitsch et al., 2021). Hence, we examined whether wild-type KRAS expression also correlates with the expression of MHC-I and APM components in the HCC clinical data.

In the TCGA-LIHC cohorts (n=372 samples), the heatmap (Figure 6.2A&B) showed that the transcription level of wild-type KRAS was negatively correlated with the expression of major (HLA-A, HLA-B, HLA-C) and minor (HLA-E, HLA-F, HLA-G, HLA-H) MHC-I genes, as well as the APM components such as B2M, TAP1, TAP2, and CD74. HCC patients were further separated into groups with low, intermediate, and high levels of KRAS, and the expression of HLA-A, HLA-B, and CD74 was significantly inversely associated with the expression of wild-type KRAS.

We then observed MHC-I expression in the lucOS model. Western blot (Figure 6.2C) demonstrated a significant downregulation in the protein expression of MHC-I in the c-Myc-lucOS^{OE}/Tp53^{KO}/Kras tumours, compared to the EV control, whereas no significant difference was observed between the c-Myc-luc^{OE}/Tp53^{KO}/EV and c-Myc-luc^{OE}/Tp53^{KO}/Kras groups. Multiplexed immunofluorescence (Figure 6.2D) further confirmed this observation, showing a decreased expression of H-2Kb/SIINFEKL in c-Myc-lucOS^{OE}/Tp53^{KO}/Kras. The H-2Kb/SIINFEKL antibody specifically detects the ovalbumin-related peptide SIINFEKL bound to H-2Kb of MHC-I. In c-Myc-lucOS^{OE}/Tp53^{KO}/Kras tumour, the pERK1/2 level was upregulated upon wild-type Kras overexpression, aligned with earlier findings. Interestingly, the expressions of pERK1/2 and H-2Kb/SIINFEKL were mutually exclusive, with no colocalisation observed. This observation is consistent with other studies that, the KRAS/ERK activation suppresses the expression of MHC-I (El-Jawhari et al., 2013; Franklin et al., 2020; Loi et al., 2016).

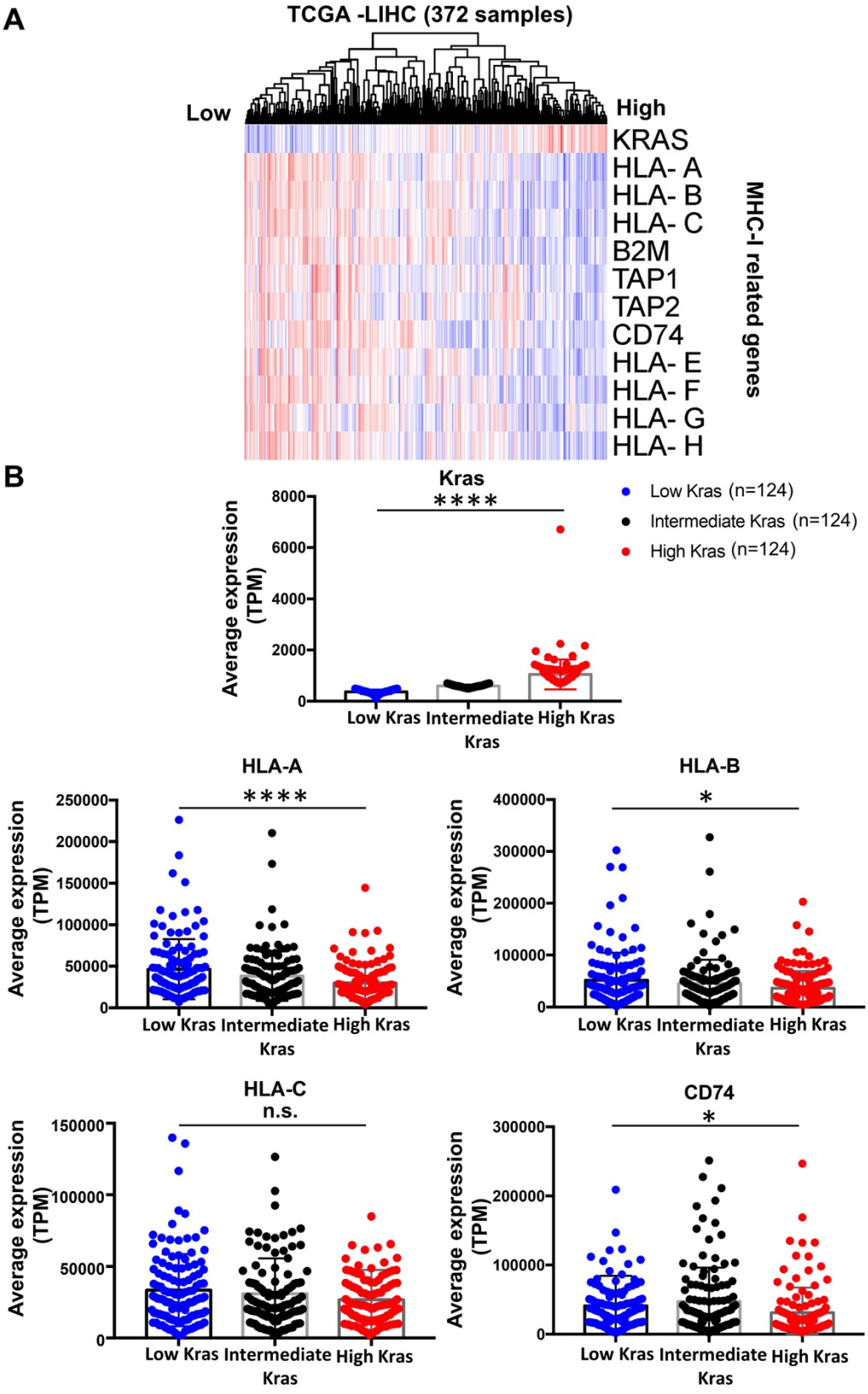
A
TCGA -LIHC (372 samples)
Low
High
KRAS
HLA- A
HLA- B
HLA- C
B2M
TAP1
TAP2
CD74
HLA- E
HLA- F
HLA- G
HLA- H
MHC-I related genes
B
Kras
****
Low Kras (n=124)
Intermediate Kras (n=124)
High Kras (n=124)
Average expression (TPM)
8000
6000
4000
2000
0
Low Kras Intermediate High Kras
Kras
HLA-A
****
250000
200000
150000
100000
50000
0
HLA-B
*
400000
300000
200000
100000
HLA-C
n.s.
150000
CD74
*
300000

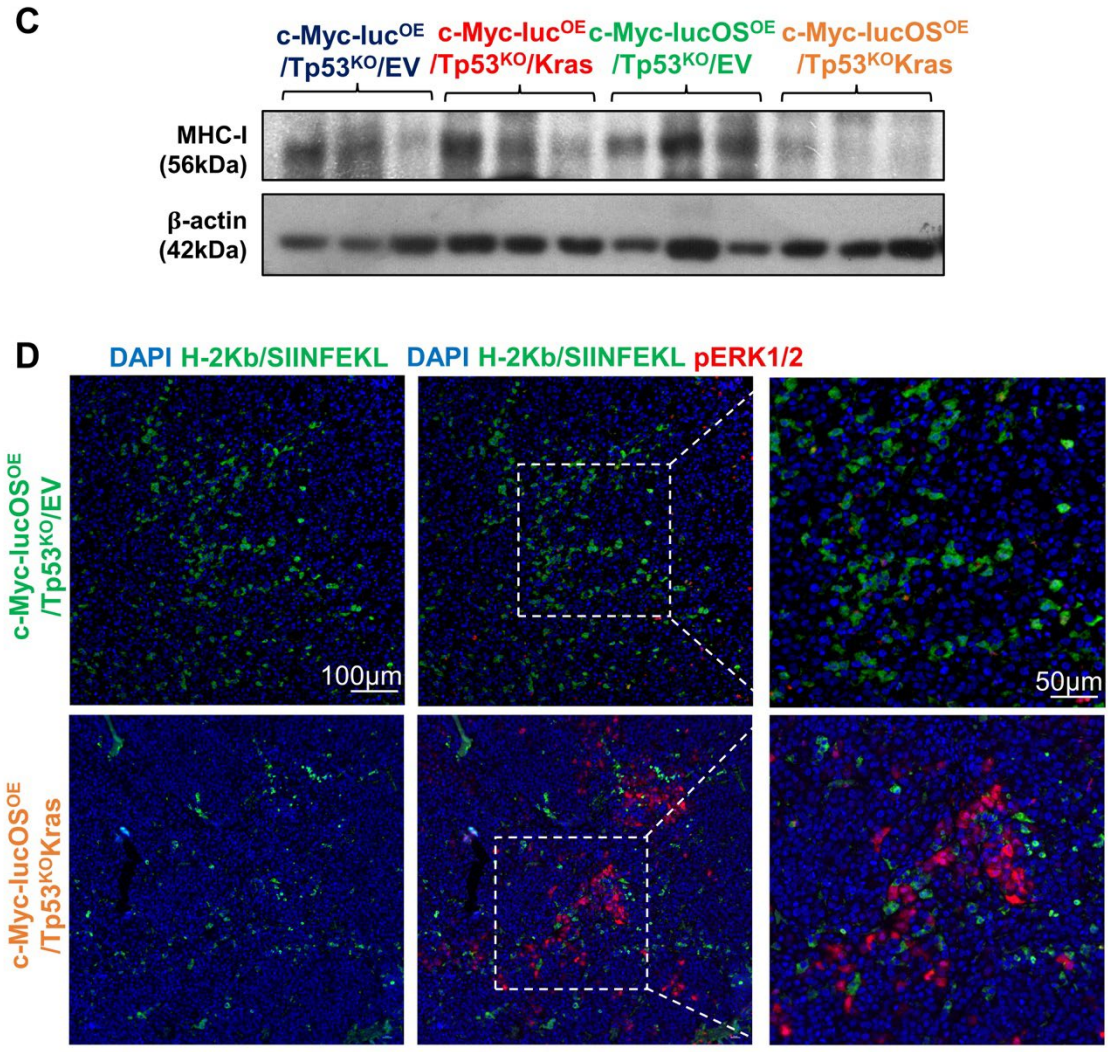

Figure 6.2 A negative correlation between Kras expression and MHC-I-related genes is found in clinical data and *in vivo* c-Myc-lucOS^{OE}/Tp53^{KO}/Kras model.
(A&B) Heatmap and plots showing a negative association between KRAS and antigen presentation-related genes (MHC-I and APM components; * $p<0.05$, **** $p<0.0001$, t-test). **(C)** Western blot demonstrated downregulation of MHC-I expression in c-Myc-lucOS^{OE}/Tp53^{KO}/Kras tumours. **(D)** Multiplexed immunofluorescence showed that in Kras-overexpressed tissue, the expression of H-2Kb/SIINFEKL was downregulated and did not co-localise with pERK1/2 expression. Scale bar = 50μm, 100 μm.

6.3.1 *In vitro* experiments confirmed the negative regulatory role of wild-type Kras in MHC-I antigen presentation

We assessed wild-type Kras expression through western blot and qPCR analysis in a cell line panel comprising primary mouse hepatocytes (PMHs) and murine HCC cell lines Hep55.1c,

Hepa-1,6 and RIL-175 (Figure 6.3A&B). Both the mRNA and protein levels of wild-type Kras are higher in all the mouse HCC cell lines than in the PMHs, consistent with the earlier observation of elevated wild-type KRAS levels in human HCC tissues (Figure 4.3). Among the three murine HCC cell lines, Hepa-1,6 and RIL-175 exhibit high protein expressions of wild-type KRAS, whereas Hep55.1c cells display a low level of wild-type KRAS. Since RIL-175 was derived from $HRAS^{V12}$ $p53^{-/-}$ hepatic tumours, it is not suitable for studying wild-type Kras (Zender et al., 2005). Hepa-1,6 cells, characterised by high protein levels of wild-type KRAS and pERK1/2 and low levels of MHC-I proteins, were selected as a model for inhibiting ERK1/2 (Figure 6.3B; Chen et al., 2016; Cheng et al., 2022).

Flow cytometry analysis (Figure 6.3B) first validated the low surface level of H-2Kb protein in the Hepa-1,6 cell line. Following treatment with IFN-γ (50ng/ml) for 24 hours, the surface expression of H-2Kb increased by approximately one-fold compared with that of the control. Treatment of Hepa-1, 6 cells with the ERK inhibitor U0126 (10μM) induced a six-fold increase in H-2Kb expression and further augmented the effect of IFN-γ-induced H-2Kb expression. This confirmed that ERK activation suppresses MHC-I expression and the blockade of ERK reverses this suppression.

The Hep55.1c cell line, characterised by low wild-type KRAS protein levels, was chosen as a model for wild-type Kras overexpression (Figure 6.3A). A plasmid, pLVX-flag-Kras, expressing wild-type Kras, was established (Appendix 2). Hep55.1c cell line was infected with the lentivirus expressing wild-type Kras and subjected to puromycin selection to generate a stable wild-type Kras overexpressed (Kras O/E) Hep55.1c cell line. After confirming Kras overexpression via western blot (Figure 6.4A), both control EV and Kras O/E groups were subjected to EGF treatment (5 and 10 nM) for 24 hours. Without IFN-γ stimulation, H-2Kb surface expression of Hep55.1c was minimal. With IFN-γ stimulation (50ng/ml), flow cytometry showed that wild-type Kras overexpression had a suppressive effect on H-2Kb surface expression (Figure 6.4B). Both the EV and Kras O/E groups showed a decrease in H-2Kb expression in a dose-dependent manner with EGF treatment for both 24 and 48 hours. The 48-hour treatment with EGF showed higher suppression of H-2Kb expression in the Kras O/E group. H-2Kb expression in the 10nM EGF-treated Kras O/E group was approximately 10% lower than that in the untreated EV. This result indicates that the activation of KRAS signalling inhibits IFN-induced MHC-I expression in HCC.

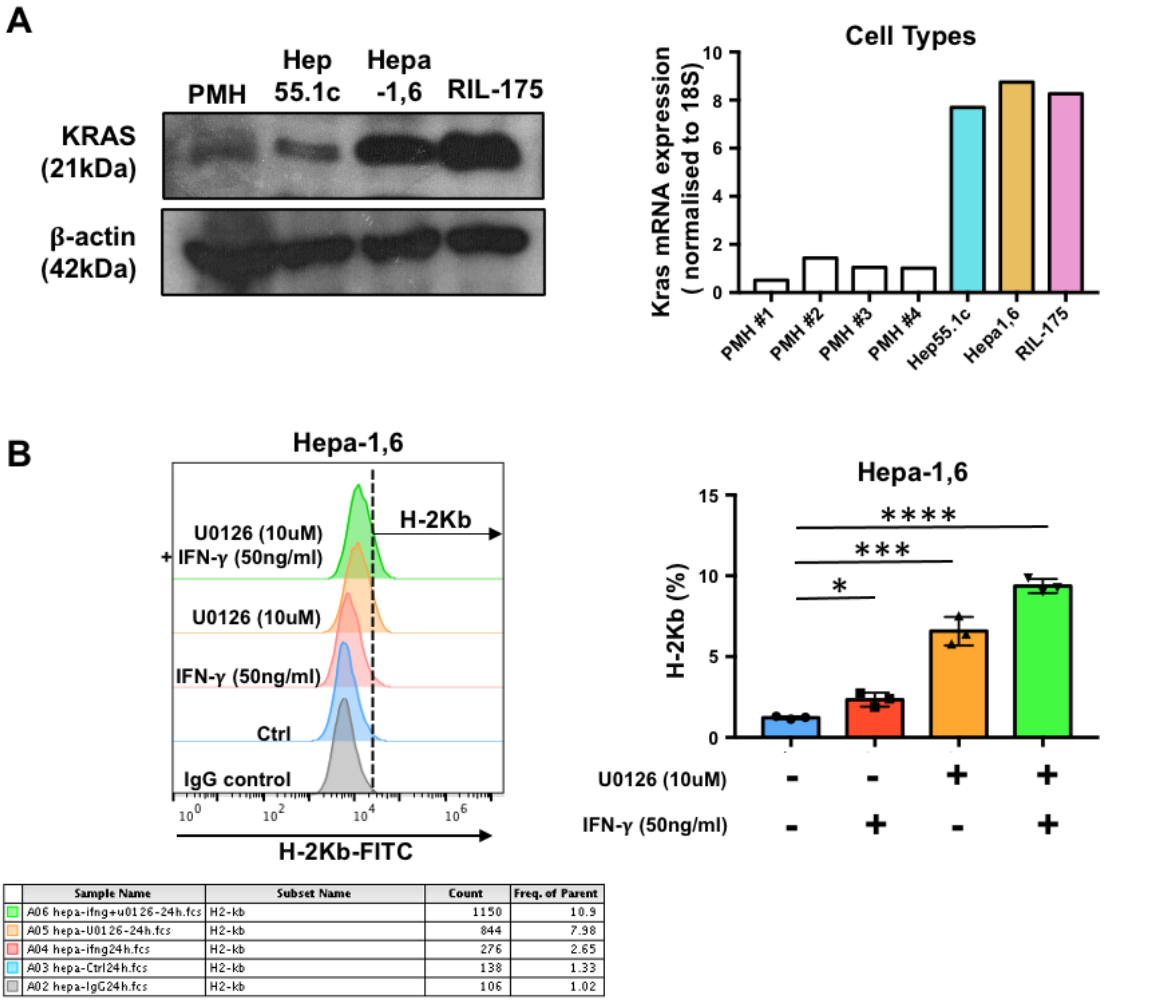

	Sample Name	Subset Name	Count	Freq. of Parent
	A06 hepa-ifng+u0126-24h.fcs	H2-kb	1150	10.9
	A05 hepa-U0126-24h.fcs	H2-kb	844	7.98
	A04 hepa-ifng24h.fcs	H2-kb	276	2.65
	A03 hepa-Ctrl24h.fcs	H2-kb	138	1.33
	A02 hepa-IgG24h.fcs	H2-kb	106	1.02

Figure 6.3 *In vitro* experiments confirmed that ERK1/2 inhibition enhances H-2Kb expression on the tumour surface in HCC.
(A) A cell line panel of mouse HCC cell lines and PMHs comparing wild-type Kras expression at both the mRNA and protein levels. The wild-type Kras expressions were higher in mouse HCC cell lines than in PMHs. **(B)** The Hepa-1,6 cell line was subjected to pharmacological inhibition of pERK1/2 using U0126 (10μM), IFN-γ treatment (50ng/ml), and combined treatment for 24 hours. Flow cytometry revealed that ERK1/2 inhibition upregulated the surface expression of H-2Kb and further enhanced IFN-γ-induced H-2Kb expression (* $p<0.05$, *** $p<0.01$, **** $p<0.0001$, t-test).

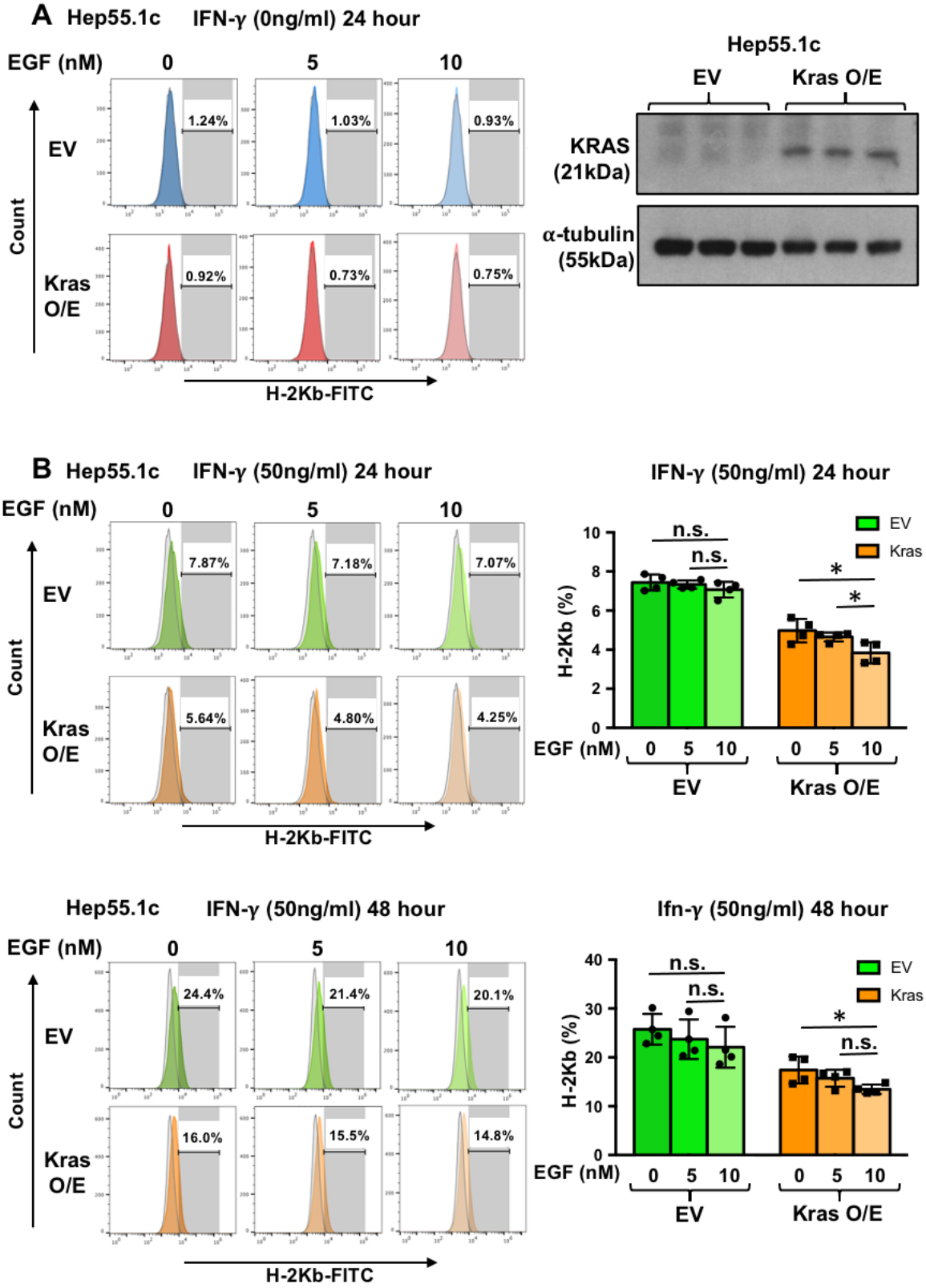
A Hep55.1c IFN-γ (0ng/ml) 24 hour
EGF (nM) 0 5 10
EV
Kras O/E
Count
1.24%
1.03%
0.93%
0.92%
0.73%
0.75%
H-2Kb-FITC
Hep55.1c
EV
Kras O/E
KRAS (21kDa)
α-tubulin (55kDa)
B Hep55.1c IFN-γ (50ng/ml) 24 hour
7.87%
7.18%
7.07%
5.64%
4.80%
4.25%
IFN-γ (50ng/ml) 24 hour
H-2Kb (%)
n.s.
n.s.
*
*
EV
Kras
Hep55.1c IFN-γ (50ng/ml) 48 hour
24.4%
21.4%
20.1%
16.0%
15.5%
14.8%
Ifn-γ (50ng/ml) 48 hour

Figure 6.4 Activation of wild-type KRAS signalling downregulates H-2Kb expression in the Hep55.1c cell line.
(A) Western blot confirmed the overexpression of wild-type Kras in the Hep 55.1c cells. Flow cytometry analysis revealed downregulation of H-2Kb expression in both EV and Kras overexpressed (Kras O/E) clones after treatment with EGF (5 and 10nM) for 24 hours. **(B)** H-2Kb expression in the EV and Kras O/E groups was induced after IFN-γ treatment (50ng/ml) for 24 and 48 hours, while H-2Kb expression in the Kras O/E group was less than that in the EV group. EGF treatment (5 and 10nM) reduced IFN-γ-induced H-2Kb expression in a dose-dependent manner in both groups. Activation of wild-type Kras overexpression further downregulated H-2Kb expression in the Kras O/E group (* $p<0.05$, t-test).

6.4 Discussion

In this chapter, we have examined the negative regulatory effect of wild-type Kras on MHC-I expression at three different levels. First, we observed a clinical correlation between wild-type KRAS and MHC-I-related genes in the TCGA-LIHC cohort. Subsequently, we validated the reduced MHC-I expression as well as downregulated antigen presentation on MHC-I molecules in our *in vivo* c-Myc-lucOS^{OE}/Tp53^{KO}/Kras model. Finally, using an *in vitro* HCC cell line model, we consolidated the suppressive effect of wild-type Kras overexpression and the activation of its downstream signalling on IFN-induced MHC-I expression.

Mutation in KRAS or other mutational activation of ERK signalling has been reported to repress the transcription of MHC-I molecules or dampen the molecules essential for peptide loading (Figure 3.4; Chen & Mellman, 2017; Gettinger et al., 2017; Klampfer et al., 2003). The mechanisms involved in KRAS-driven MHC-I downregulation are mediated by the suppression of IFN signalling (El-Jawhari et al., 2013; Klampfer et al., 2003). The reduction in STAT1, STAT2, and IRF9 expression suppresses the expression of APM components, such as TAP1, TAP2, TAPBP, and B2M, resulting in a loss of MHC-I. These alterations attenuate the immunogenicity in tumours and reduce the killing of cancer cells via turning down the recognition of tumour cells by T cells. Blockade of oncogenic KRAS or MEK inhibition reactivated STAT signalling and induced MHC-I expression in tumour cells (Franklin et al., 2020; Kemp et al., 2023; Loi et al., 2016). Downregulation of ERK signalling by the tyrosine kinase inhibitor regorafenib or MEK inhibitor trametinib augmented IFN-γ/ STAT1- mediated HLA Class I expression in human HCC cell lines (Takahashi et al., 2021).

Loss of MHC-I by tumour cells is associated with poor clinical outcomes (Atkins et al., 2004; Garrido et al., 2016; Leone et al., 2013). Downregulation of antigen presentation by MHC-I is associated with resistance to immunotherapy in several cancer types (Gettinger et al., 2017; Sade-Feldman et al., 2017; Zaretsky et al., 2016). Transcriptional downregulation of MHC-I and the 'master regulators' NLRC5/CITA correlates with a compromised response to ICI in melanoma (Lee et al., 2020; Yoshihama et al., 2021). Reduced MHC-I expression was associated with primary resistance to anti-CTLA4 treatment in CheckMate 069 cells (Rodig et al., 2018). In addition, the loss of the B2M gene also shaped a suppressive immune landscape with less immune infiltration, contributing to resistance to the immunotherapy (Zhao et al., 2021). MHC protein expression also determines the acquired resistance to ICI and tumour relapse. Dupage et al. (2012) suggested that under the selective pressure of T cells, tumour cells

were capable of reducing tumour antigen presentation on MHC-I and became less immunogenic in an immunogenic lung mouse model. This immunoediting process enabled the tumour cells to escape from the recognition by T cells and led to tumour relapse. The immunoediting process of tumour cells has also been observed in a study of Merkel cell carcinoma patients who developed acquired resistance after receiving combination immunotherapy (Paulson et al., 2018). scRNA-seq of the relapsed tumours revealed transcriptional loss of HLA genes as a consequence of dense $CD8^+$ T cell immunologic pressure.

In conclusion, this chapter provides a mechanistic insight into how the suppressed tumour-intrinsic IFN response affects MHC-I expression. This finding enhances our understanding of how wild-type Kras promotes immune evasion in HCC.

Chapter 7. *In vivo* CRISPR/Cas9-mediated MEK1/2 knockout rescues the immunosuppressive effects brought by the wild-type Kras overexpression in the c-Myc-lucOS^{OE}/Tp53^{KO}/Kras HCC mice model

7.1 Introduction

In the previous chapters, we revealed the immunosuppressive role of wild-type Kras in c-Myc-lucOS^{OE}/Tp53^{KO} HCC. Wild-type KRAS activation represses the intrinsic and extrinsic IFN responses in the tumour cells and the TIME. This includes the downregulation of the MHC-I expression in tumour cells, diminished APC functions and suppression of T cell infiltration and activation.

Mechanistically, the overexpression of wild-type KRAS activates the downstream ERK signalling in the c-Myc-lucOS^{OE}/Tp53^{KO}/Kras HCC mouse model. To validate whether Kras-induced immune evasion is mediated through MEK/ERK signalling, we employed the CRISPR/Cas9 system to target *in vivo* MEK1/2 in a novel platform. The CRISPR/Cas9 system, derived from a microbial clustered regularly interspaced short palindromic repeats adaptive immune system, enables genome engineering using a 20-nt sequence of sgRNA (Ran et al., 2013). The sgRNA forms a hairpin structure resembling the tracrRNA-crRNA complex, along with a short fragment complementary to the targeted DNA sequence. Subsequently, the Cas9 endonuclease binds to the targeted locus and creates a double-stranded break. Compared to other *in vivo* genome editing technologies such as zinc finger nucleases (ZFNs) or transcription activator-like effector nucleases (TALENS), the CRISPR/Cas system offers easy customisation, high efficiency and specific cleavage pattern (Gaj et al., 2013; Wang et al., 2016).

Multiplexed genome engineering using the CRISPR/Cas9 vector system to edit several genes simultaneously has been applied in mammalian cells for functional studies (Cong et al., 2013; Sakuma et al., 2014; Zhou et al., 2014). This all-in-one CRISPR/Cas9 vector system has been reported to enhance editing efficiency. In our study, we incorporated sgRNAs targeting the MEK1/2 genes Map2k1 and Map2k2 into the px330-sgTp53 plasmid (Figure 7.1, Appendix 3). The product plasmid px330-sgTp53-sgMap2k1-sgMap2k2 expresses three sgRNA sequences targeting Tp53, Map2k1, and Map2k2. By leveraging the HTVI delivery method, this platform facilitates specific and efficient knockout of Map2k1 and Map2k2 at the tumour site. Upon knockout of MEK1/2, we aim to investigate whether the immunosuppressive effects of wild-type Kras overexpression can be rescued.

7.2 Experiment design

(1) The sgRNA sequences targeting Map2k1 and Map2k2 were retrieved from a mouse sgRNA knockout library (Brie) which consists of 78,637 unique sgRNAs targeting 19,674 genes (Doench et al., 2016). Both sgRNA sequences were checked for on-target efficiency (RuleSet2Score) and for potential mismatch sites. After verification, these two sgRNA sequences were cloned into px330-sgTp53 with the addition of the U6 promoter and gRNA scaffold. A control plasmid was also generated with a non-targeting control sequence (NTC) substituted at the sgRNA sites (Appendix 4). The sequence and size of px330-sgTp53-sgMap2k1-sgMap2k2 were confirmed by DNA sequencing and DNA electrophoresis.

(2) The plasmid px330-sgTp53-sgMap2k1-sgMap2k2, along with the plasmids expressing c-Myc-lucOS, transposase SB13 and Kras were introduced into the hepatocytes of the C57BL/6 mouse via HTVI. Tumour growth was monitored through bioluminescent imaging at specified time points. The tumour tissues were harvested for qPCR, western blot and IHC analysis.

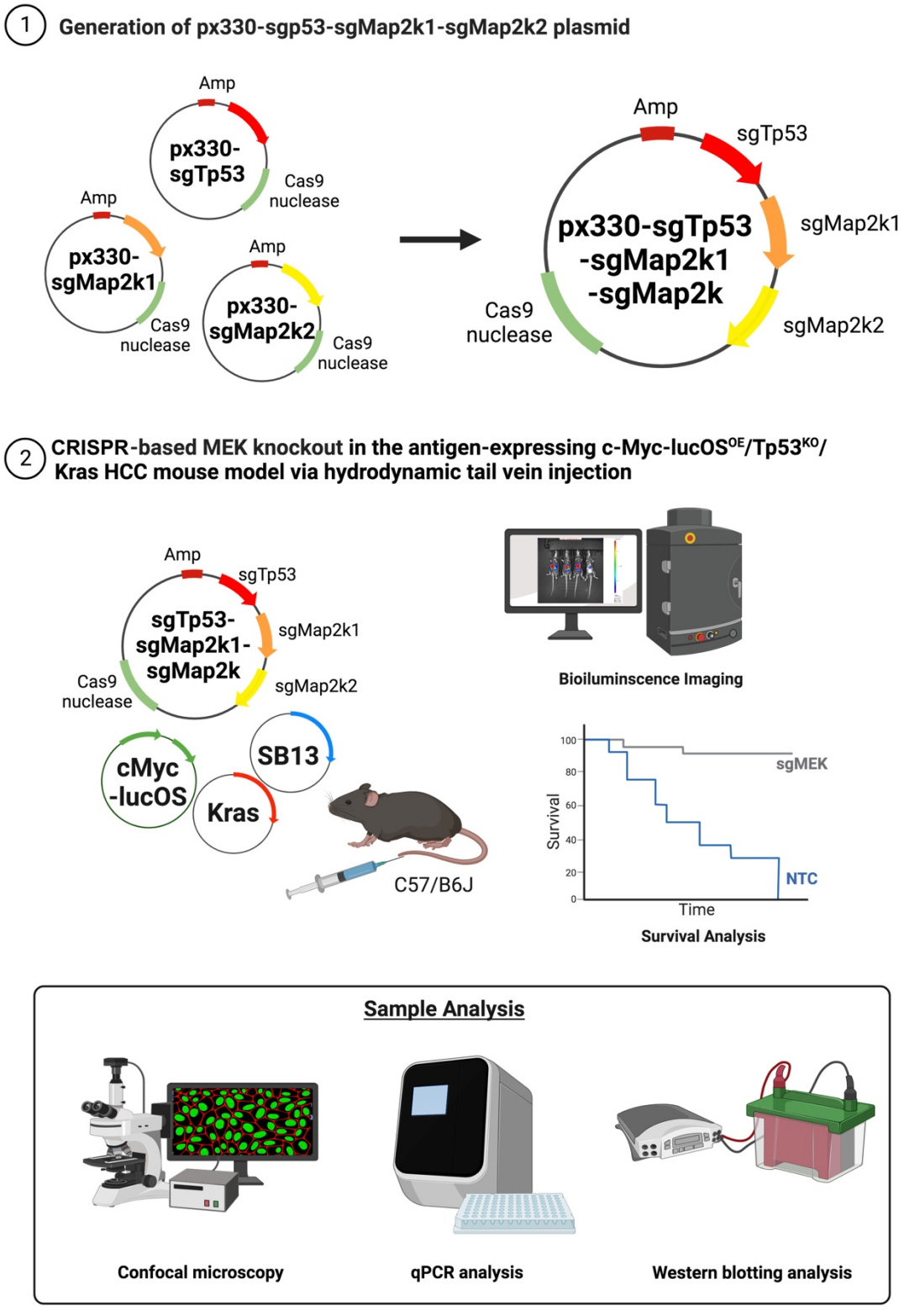

Figure 7.1 An outline of the workflow of generation of px330-sgTp53-sgMap2k1-sgMap2k2 plasmid and the establishment of c-Myc-lucOS^{OE}/Tp53^{KO}/Kras/MEK^{KO} HCC model.

7.3 Results

7.3.1 CRISPR/Cas9-based MEK1/2 knockout rescues the wild-type Kras mediated immune evasion in c-Myc-lucOS^{OE}/Tp53^{KO}/Kras HCC

To evaluate whether MEK1/2 inhibition in tumour cells could rescue the immune escape in wild-type Kras-driven tumours, we tested the effect of model antigens expression in the context of wild-type KRAS activation and MEK1/2 knockout. As described in the Method section, we incorporated the sgRNAs of MEK1/2 genes, Map2k1 and Map2k2, into the plasmid px330-sgTp53 (Appendix 3). The sgRNA sequences targeting Map2k1 and Map2k2 were retrieved from a mouse sgRNA knockout library (Brie) which consists of 78,637 unique sgRNAs targeting 19,674 genes (Doench et al., 2016). The on-target efficiency (RuleSet2Score) for sgMap2k1 and sgMap2k2 are 0.7218 and 0.64 respectively with no potential off-target sites, indicating high specificity of the two sgRNAs (Figure 7.2A&B). DNA electrophoresis confirmed the size of the px330-sgTp53-sgMap2k1-sgMap2k2 plasmid, showing a clear single band at the calculated size of 9kb (Figure 7.2C).

We induced the c-Myc-lucOS^{OE}/Tp53^{KO}/Kras tumours with px330-sgTp53-sgMap2k1-sgMap2k2 or the control px330-sgTp53-NTC. The c-Myc-lucOS^{OE}/Tp53^{KO}/EV group served as a control for immunosurveillance. The luciferase signals of all three groups were comparable on day 5 after HTVI (Figure 7.3A&B), implicating equal transfection efficiency and expression of the c-Myc oncogene in all groups. On day 16, there was a drastic increase in luciferase expression in c-Myc-lucOS^{OE}/Tp53^{KO}/Kras/NTC mice, indicating tumour progression in Kras-overexpressed mice. However, the signals in c-Myc-lucOS^{OE}/Tp53^{KO}/Kras/MEK^{KO} mice were substantially lower compared to those in c-Myc-lucOS^{OE}/Tp53^{KO}/Kras/NTC, and were comparable to those in c-Myc-lucOS^{OE}/Tp53^{KO}/EV mice. This implies that MEK knockout effectively suppressed the tumour growth promoted by Kras. The entire group of c-Myc-lucOS^{OE}/Tp53^{KO}/Kras/NTC mice escaped immunosurveillance and presented gross liver tumours, with a median survival of 21 days (Figure 7.3C&D). All mice were harvested on day 30, the time point at which all NTC mice deceased due to large tumour burden. In the c-Myc-lucOS^{OE}/Tp53^{KO}/Kras/MEK^{KO} group, 6 out of 8 mice developed tumours, while the c-Myc-lucOS^{OE}/Tp53^{KO}/EV mice did not develop any tumours.

A Mouse CRISPR Knockout Pooled Library (Brie)
(Pooled Library #73633)

Map2k1 (NM_008927.3)

Position of Base After Cut (1-based)	Strand	sgRNA Target	Target Context Sequence	PAM Sequence	Exon Number	RuleSet2 score
64193794	sense	CATTCTAGTGAACTCACGTG	CCAACATTCTAGTGAACTC ACGTGGGGAGA	GGG	6	0.7218

Map2k2 (NM_023138.4)

Position of Base After Cut (1-based)	Strand	sgRNA Target	Target Context Sequence	PAM Sequence	Exon Number	RuleSet2 score
81115111	sense	GTGCAACTCGCCCTACATCG	ACGAGTGCAACTCGCCCTA CATCGTGGGCT	TGG	3	0.64

B

sgRNA Off-target Search

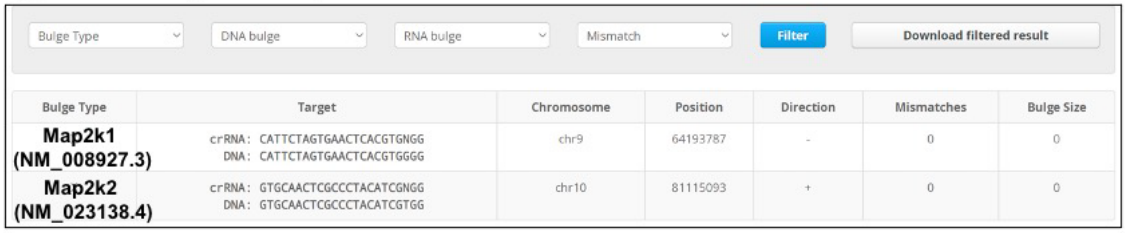

C

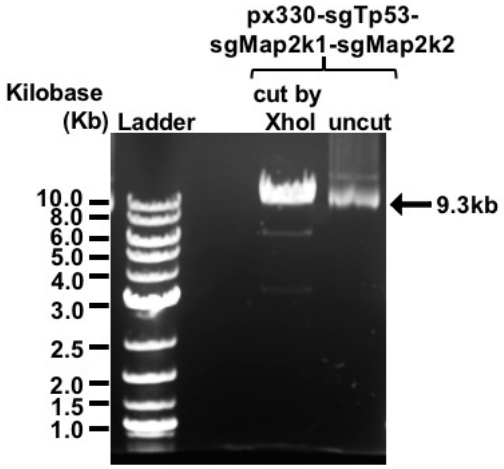

Figure 7.2 Generation of plasmid px330-sgTp53-sgMap2k1-sgMap2k2.
(A) sgRNA sequences targeting Map2k1 and Map2k2 were retrieved from the Mouse CRISPR Knockout Pooled Library (Brie). **(B)** No potential off-target sites were searched in both sgRNA sequences on an online off-target searching tool Cas-OFFinder (http://www.rgenome.net/)(Bae, Park, & Kim, 2014). **(C)** DNA electrophoresis of px330-sgTp53-sgMap2k1-sgMap2k2 plasmid. Lane 1: Ladder, Lane 2: px330-sgTp53-sgMap2k1-sgMap2k2 plasmid digested with XhoI. Lane 3: uncut px330-sgTp53-sgMap2k1-sgMap2k2 plasmid.

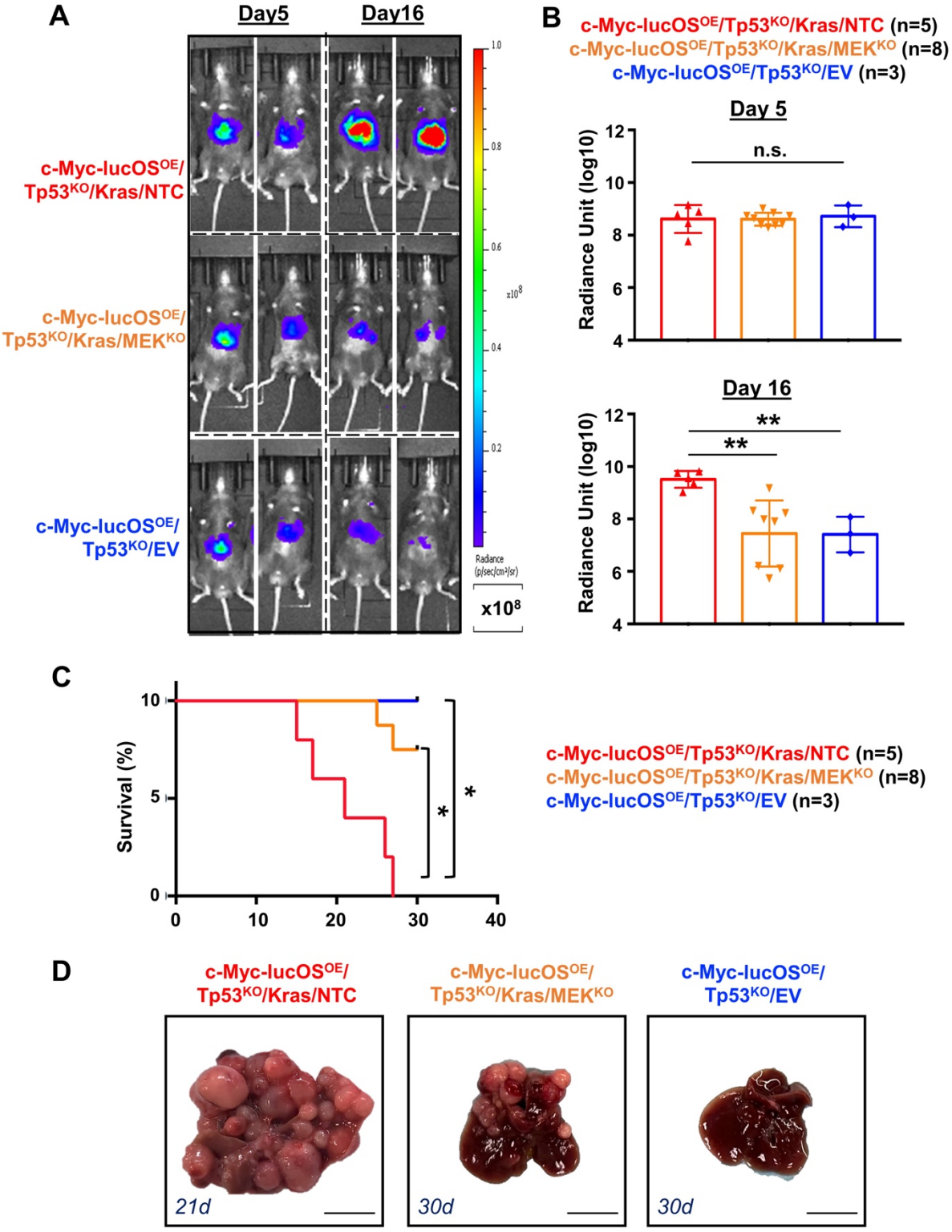

Figure 7.3 MEK1/2 knockout rescues the wild-type Kras-mediated immune evasion in c-Myc-lucOS^{OE}/Tp53^{KO} model

(A) Representative bioluminescence images on days 5 and 16 of c-Myc-lucOS^{OE}/Tp53^{KO}/Kras/NTC, c-Myc-lucOS^{OE}/Tp53^{KO}/Kras/MEK^{KO} and c-Myc-lucOS^{OE}/Tp53^{KO}/EV after HTVI. The scale bar for the luciferase signal is shown. **(B)** Quantification of normalised luciferase signals on days 5 and 16 after HTVI (** $p<0.01$, t-test). **(C)** All c-Myc-lucOS^{OE}/Tp53^{KO}/Kras/NTC mice developed tumours and exploited the survival benefits of T cell-specific antigens. c-Myc-lucOS^{OE}/Tp53^{KO}/Kras/MEK^{KO} mice exhibited significantly improved survival compared to NTC (* $p<0.05$, log-rank test). **(D)** Representative images of the c-Myc-lucOS^{OE}/Tp53^{KO}/Kras/NTC, c-Myc-lucOS^{OE}/Tp53^{KO}/Kras/MEK^{KO}, and c-Myc-lucOS^{OE}/Tp53^{KO}/EV livers.

7.3.2 MEK1/2 knockout enhances the wild-type Kras-mediated suppression of IFN-response and Cxcl9 and Cxcl10 expressions

Western blot (Figure 7.4A) confirmed the successful knockout of MEK1/2 in the protein level, demonstrating downregulation of the downstream pERK1/2 in the MEK^{KO} group. In qPCR analysis (Figure 7.4B), the reduced mRNA levels of KRAS signalling downstream molecules, such as Ccnd1 and dual-specificity phosphatase 6 (Dusp6), in the MEK^{KO} group further confirmed the successful inhibition of KRAS/MEK/ERK signalling.

To investigate the mechanistic link between KRAS signalling and IFN response, we examined the transcription of IFN signalling pathway genes. Intriguingly, MEK1/2 knockout enhanced Kras-mediated suppression of the IFN response. The expression of IFN-associated genes such as Stat1, Irf1, Irf2, Irf7, and Irf9 was upregulated, and thus the IFN-regulated T-cell chemoattractants including Cxcl9 and Cxcl10 (Figure 7.4C). The protein level of CXCL9 was also elevated (Figure 7.4A). These findings suggested a direct crosstalk between KRAS and IFN signalling.

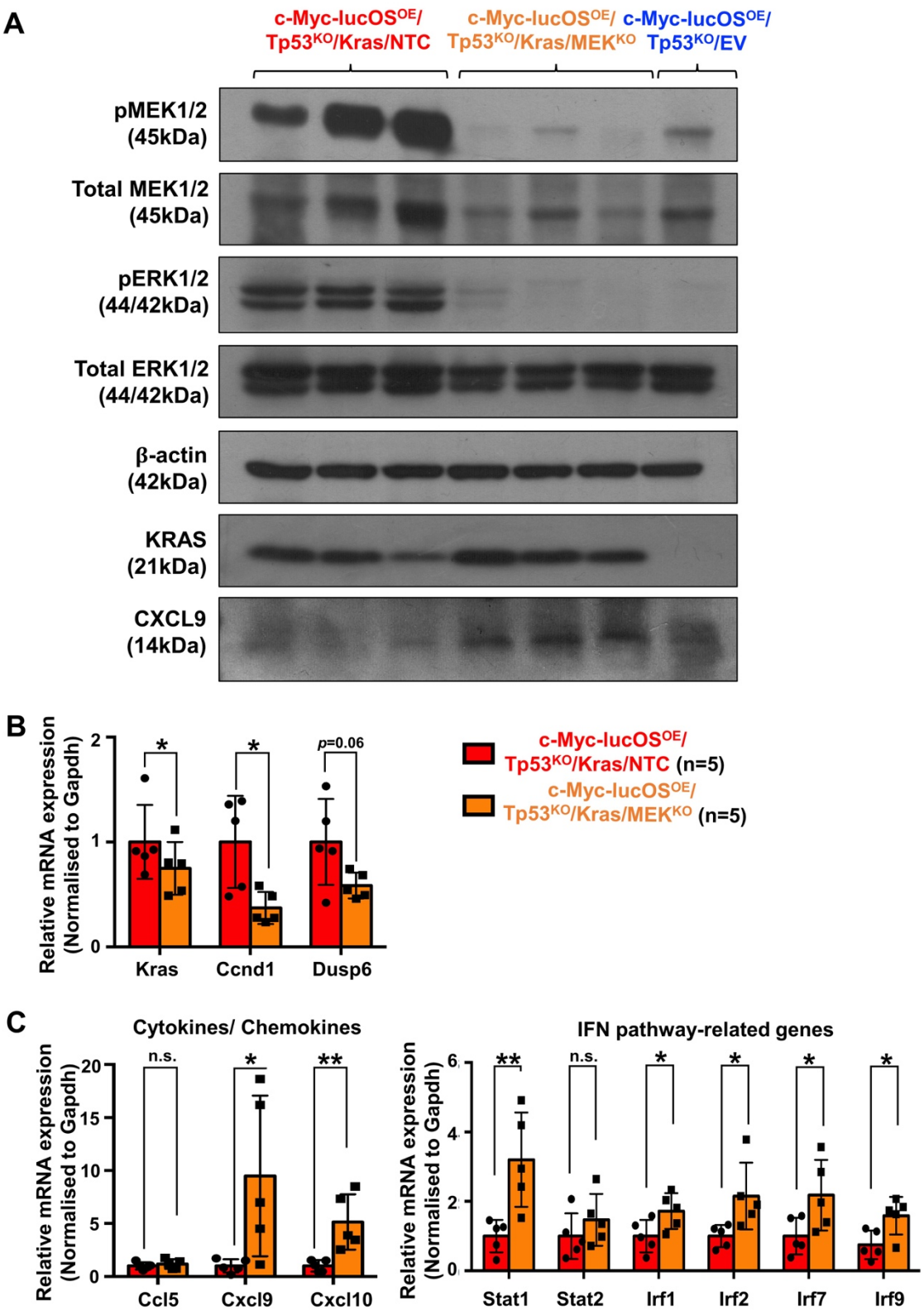
A
c-Myc-lucOS^OE/ Tp53^KO/Kras/NTC
c-Myc-lucOS^OE/ Tp53^KO/Kras/MEK^KO
c-Myc-lucOS^OE/ Tp53^KO/EV
pMEK1/2 (45kDa)
Total MEK1/2 (45kDa)
pERK1/2 (44/42kDa)
Total ERK1/2 (44/42kDa)
β-actin (42kDa)
KRAS (21kDa)
CXCL9 (14kDa)
B
Relative mRNA expression (Normalised to Gapdh)
*
*
p=0.06
Kras
Ccnd1
Dusp6
c-Myc-lucOS^OE/ Tp53^KO/Kras/NTC (n=5)
c-Myc-lucOS^OE/ Tp53^KO/Kras/MEK^KO (n=5)
C
Cytokines/ Chemokines
n.s.
*
**
Ccl5
Cxcl9
Cxcl10
IFN pathway-related genes
**
n.s.
*
*
*
*
Stat1
Stat2
Irf1
Irf2
Irf7
Irf9

Figure 7.4 MEK1/2 knockout enhances the wild-type Kras- suppressed IFN response. **(A)** Western blot validated the successful MEK1/2 knockout and the consequent inhibition of downstream pERK1/2 in the protein level. **(B)** qPCR further confirmed the downregulation of the ERK pathway-associated genes Ccnd1 and Dusp6 upon MEK1/2 knockout (* $p<0.05$, t-test). **(C)** IFN-related pathway genes Stat1, Irf1, Irf2, Irf7 and Irf9, as well as T-cell chemoattractants Cxcl9 and Cxcl10 were upregulated (* $p<0.05$, ** $p<0.01$, t-test).

7.3.3 MEK1/2 inhibition remodels the wild-type Kras-mediated suppressive TIME and increases T cell recruitment to c-Myc-lucOS^{OE}/Tp53^{KO}/Kras tumour

The findings presented above demonstrated the ability of MEK1/2 inhibition to reverse immune evasive mechanisms driven by wild-type Kras, including the upregulation of IFN response and the expression of immunomodulatory factors. Then, we examined how *in vivo* MEK inhibition influences the composition of the TIME in c-Myc-lucOS^{OE}/Tp53^{KO}/Kras tumour.

The immune cell infiltration sites of c-Myc-lucOS^{OE}/Tp53^{KO}/Kras/NTC and c-Myc-lucOS^{OE}/Tp53^{KO}/Kras/MEK^{KO} tumours were compared in Figure 7.5A. Multiplexed immunofluorescence revealed an upregulation of the H-2Kb/SIINFEKL expression in the c-Myc-lucOS^{OE}/Tp53^{KO}/Kras/MEK^{KO} tumours. Notably, CD11c was found to be highly expressed in the MEK^{KO} tumour, indicating an increased infiltration of DCs to the tumour. CXCL9, which is known to be expressed by DCs, is colocalised with CD11c expression (Figure 7.5A&B). The observation of CD8$^+$ T cells in close proximity to CXCL9$^+$ CD11c$^+$ DCs (Figure 7.6A) suggests that MEK blockade enhances CXCL9 production by DCs, facilitating the recruitment of CD8$^+$ T cells within the tumour. Quantification further confirmed the higher presence of CD8$^+$ T cells in the MEK^{KO} tumours (Figure 7.6B). Together, these results supported our hypothesis that wild-type KRAS signalling inhibits T cell recruitment via suppressing DC recruitment and lymphocyte chemotaxis via CXCL9. *In vivo* MEK1/2 inhibition alleviates Kras-induced immunosuppression and leads to a more inflamed TIME, characterised by a substantial increase in activated DCs and T cells.

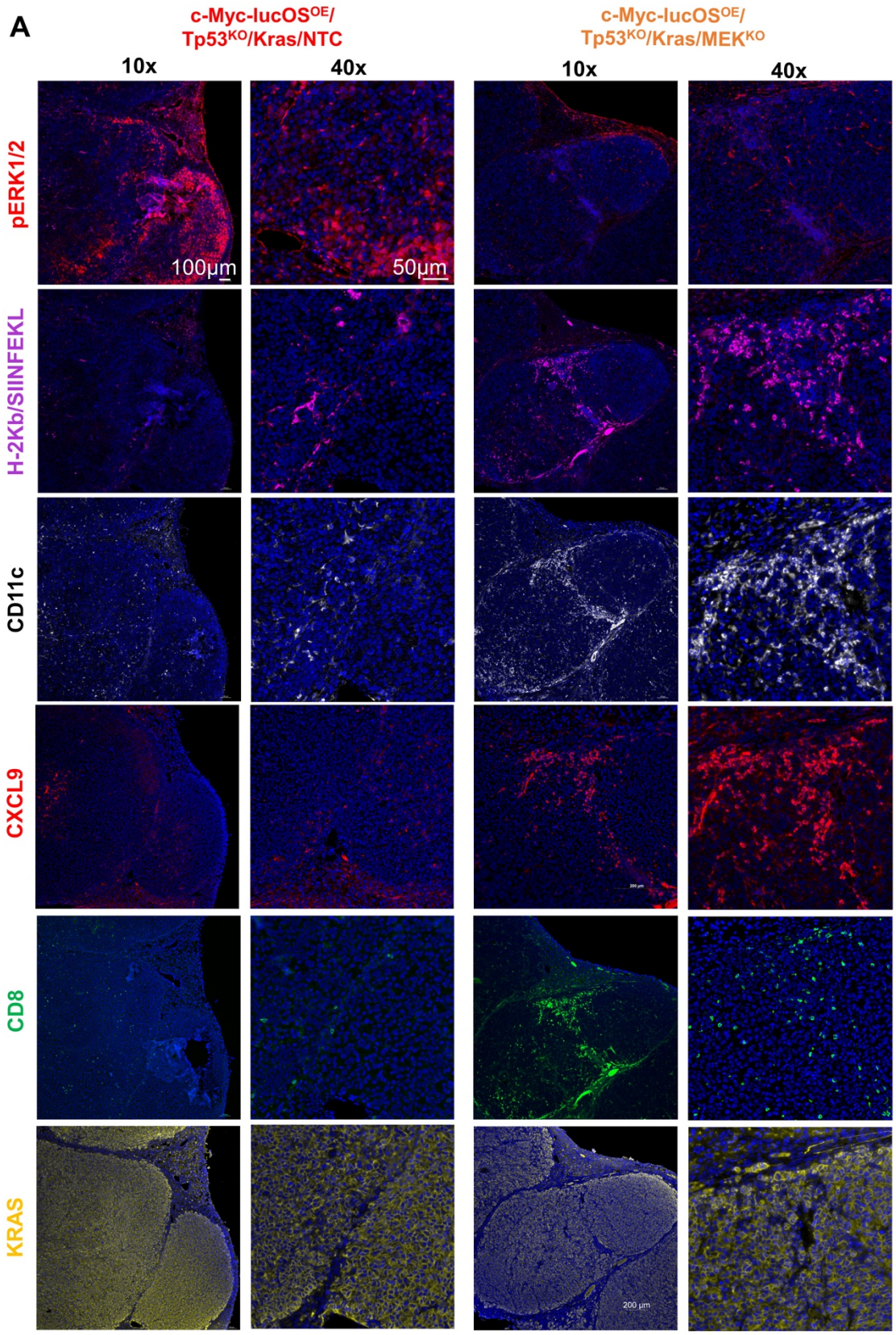
A
c-Myc-lucOS^OE/
Tp53^KO/Kras/NTC
c-Myc-lucOS^OE/
Tp53^KO/Kras/MEK^KO
10x
40x
10x
40x
pERK1/2
H-2Kb/SIINFEKL
CD11c
CXCL9
CD8
KRAS
100μm
50μm
200 μm

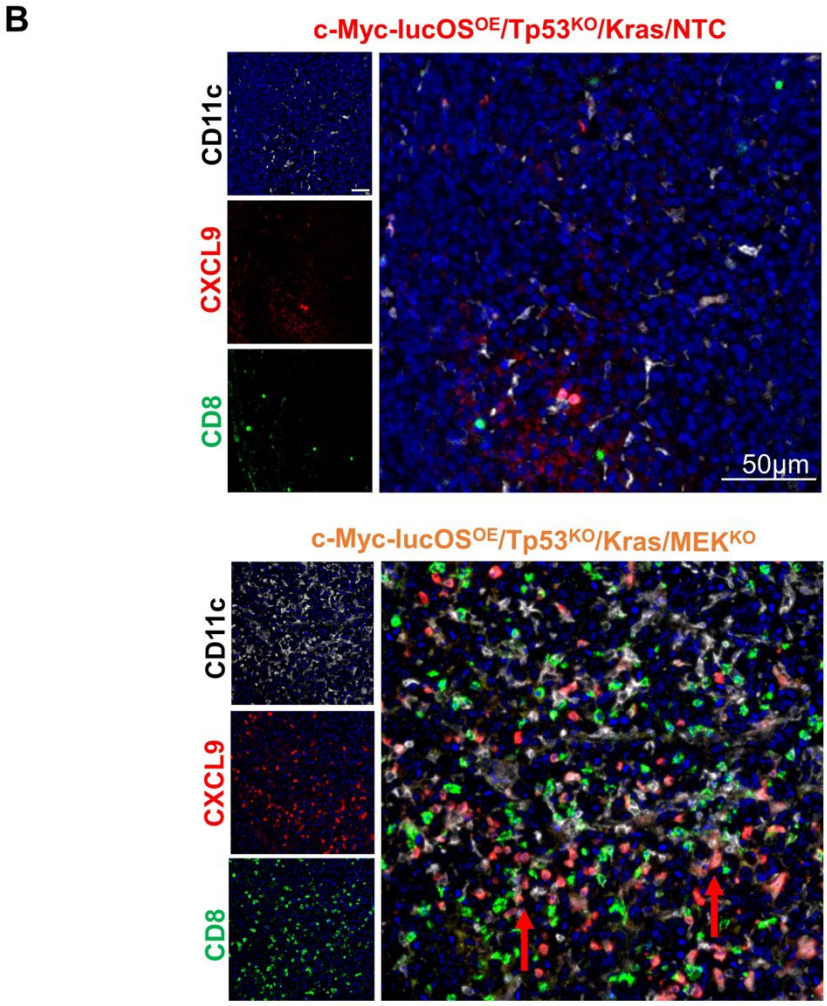

Figure 7.5 MEK1/2 inhibition remodels the wild-type Kras-mediated immunosuppressive TIME in c-Myc-lucOS^{OE}/Tp53^{KO}/Kras tumour.
(A) Representative images of pERK1/2 (red), H-2Kb/SIINFEKL (magenta), CD11c (white), CXCL9 (red), CD8 (green) and KRAS (yellow) in the immune infiltrate of c-Myc-lucOS^{OE}/Tp53^{KO}/Kras/NTC and c-Myc-lucOS^{OE}/Tp53^{KO}/Kras/MEK^{KO} tumours. Scale bar=100μm (left:10x magnification), 50μm (right:40x magnification). **(B)** Representative images of multiplex immunofluorescence of CD11c (white), CXCL9 (red), and CD8 (green) in c-Myc-lucOS^{OE}/Tp53^{KO}/Kras/NTC and c-Myc-lucOS^{OE}/Tp53^{KO}/Kras/MEK^{KO} tumours. Scale bar=50μm.

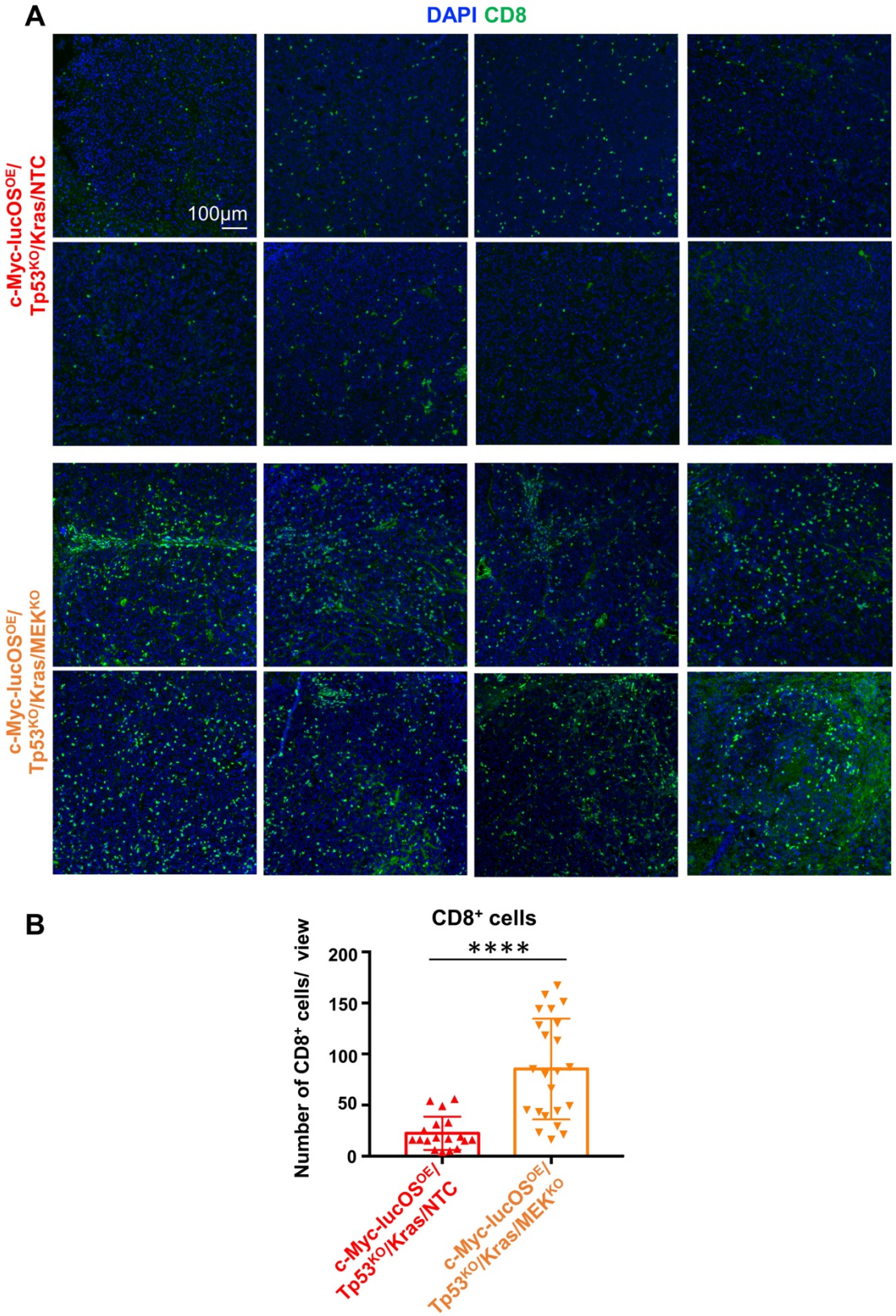

Figure 7.6 MEK1/2 knockout increases T cell recruitment to c-Myc-lucOS^{OE}/Tp53^{KO}/Kras tumour.

(A) Representative images of CD8 (green) staining in c-Myc-lucOS^{OE}/Tp53^{KO}/Kras/NTC and c-Myc-lucOS^{OE}/Tp53^{KO}/Kras/MEK^{KO} tumours. Scale bar=100μm. **(B)** Quantification of tumour-infiltrating CD8^{+} T cells in NTC and MEK^{KO} tumours in multiplex IHC images, regions for images were randomly selected. (NTC: n=18; MEK^{KO}: n=23; **** $p < 0.0001$, t-test)

7.4 Discussion

In this chapter, we established a novel CRISPR/Cas9 system to target MEK1/2 in c-Myc lucOS^{OE}/Tp53^{KO}/Kras HCC. CRISPR technology has been applied in immunotherapy for genetically modification of CAR-T cells in lymphomas and solid tumour cancer research since its first launch in a clinical trial in 2016 (Stefanoudakis et al., 2023). In the development of gene therapy, CRISPR therapeutics provides a simple and efficient alternative to traditional gene therapy, which relies on viral vector delivery.

Our all-in-one CRISPR/Cas9 knockout system offers several advantages from the perspectives of genome editing procedure, efficiency and delivery system. Firstly, designing an all-in-one system is more straightforward than designing and optimising individual constructs for both sgRNAs and Cas9. The convenience of the design can save time and resources in the experimental design phase. However, the integrated expression vector has limitations in optimising dosage. Secondly, the co-expression of Cas9 and sgRNAs in a single vector ensures that each hepatocyte receives both Cas9 and the sgRNAs, enhancing the efficiency and spatial accuracy of genome editing. MEK signalling is pivotal for lymphocyte activation, the germline null deletion of MEK1/2 in a genetically engineered mouse model would cause immune disorder and development defects (Houde et al., 2022). Since the sgRNAs of Map2k1 and Map2k2 were incorporated into the plasmid expressing sgTp53, the expression of sgMap2k1 and sgMap2k2 can precisely target the hepatic tissue with a Tp53^{KO} background. This allowed us to investigate the effects of MEK1/2 inhibition without interrupting immune activation in a mouse model.

Regarding its *in vivo* delivery system, the all-in-one system takes advantage of HTVI and simplifies the delivery process. The MEK1/2 knockout takes effect once the oncogenic c-Myc^{OE}/Tp53^{KO} HCC background is established in the hepatocytes. Thus, this could save time for additional treatment or injection, minimising potential harm to the mice. Compared to viral vectors such as adeno-associated virus vectors (AAVs) and lentivirus vectors, the non-viral CRISPR/Cas9 vector significantly addresses the safety concern including toxicity and

infectious risks (Wang et al., 2016). It also eases the limitations associated with viral vectors such as potential immunogenicity and carcinogenesis (Baum et al., 2006; Bessis et al., 2004). Most importantly, viral vectors are often constrained by their encapsulation capacity (Thomas et al., 2003). AAVs, with a cargo size of about 4.5kb, remain a challenge to embody the large size of the CRISPR/Cas9 system, which is about 4.2kb. The limited cargo size of AAVs provides minimal space for multiplexed engineered expression in delivering the CRISPR/Cas9 system, potentially affecting delivery efficiency. Taken together, the all-in-one CRISPR/Cas9 system provides a convenient and effective *in vivo* knockout mouse model for HCC study.

The role of MEK1/2 in oncogenic Kras-mediated suppression of the type I/II IFN response has been implicated in pancreatic and lung cancers (Kemp et al., 2023; Mugarza et al., 2022; Muthalagu et al., 2020). Our findings in the MEK^{KO} model provided evidence that tumour-specific MEK1/2 inhibition reverses wild-type Kras-mediated immune evasion. The enhanced anti-tumour response could be attributed to the ameliorated IFN response and the remodelling of the immunosuppressive TIME. The increase in the IFN-related inflammatory gene profiles augmented the antigen presentation function, as evidenced by an upregulation in DC recruitment together with an increase in MHC-I molecules H-2Kb/SIINFEKL. Additionally, the expression of T cell chemoattractants Cxcl9 and Cxcl10 was also significantly upregulated. CXCL9 and CXCL10 are produced by both APCs and tumour cells. They represent one of the critical components for bringing the 'heat' to the tumour and generating a T cell-inflamed microenvironment (Reschke & Gajewski, 2022). In our MEK^{KO} model, Cxcl9 expression was found to colocalise with DCs, adjacent to tumour-infiltrating $CD8^+$ T cells. These results provide an insight into the intricate interplay between MEK1/2 modulation and immune components, particularly DCs and T cells, to boost the adaptive immune response, highlighting the multifaceted effects of MEK1/2 inhibition on the tumour microenvironment.

In the immunogenomic classification of HCC (Figure 7.7), the non-inflamed class (including the intermediate and excluded subclasses) is characterised by decreased TIL infiltration, reduction in IFN-γ signature, and decreased expression of CXCL9, CXCL10, and CXCL11 (Montironi et al., 2023). This non-inflamed HCC class is insufficient to respond to ICI.

Clinical studies have highlighted an association between an IFN gene signature and the efficacy of the ICI treatment (Keenan et al., 2019). The efficacy of anti-PD-1 treatment relies on the presence of at least a modest level of pre-existing IFN-γ-mediated inflammation within the

tumour microenvironment (Rodig et al., 2018). Additionally, the presence of an IFN-mediated signature has shown predictive value in anticipating treatment response (Ayers et al., 2017). In our findings, two prominent ISGs, Irf1 and Irf2, were found to be upregulated in MEK^{KO} tumours. These genes have been identified to play a regulatory role in the expression of PD-L1 in HCC and are favourable for responsiveness to anti-PD-L1/PD-1 therapy (Yan et al., 2021; Yan et al., 2020). Moreover, IRF1 has been reported to mediate $CD8^+$ T cells, NK and NKT cells migration and activate anti-tumour immunity via CXCL10/CXCR3 axis in HCC (Yan et al., 2021).

Litchfield et al. (2021) analysed the whole-exome and transcriptomic data for more than 1,000 ICI-treated patients and found that, apart from tumoral mutation burden, CXCL9 expression serves as a robust indicator for a favourable response to ICI treatment. Moreover, lower serum CXCL9 levels have been reported to predict HCC patients with early progressive disease undergoing treatment with atezolizumab and bevacizumab (Hosoda et al., 2023). However, the correlation between serum CXCL9 levels and the HCC immune milieu remains unclear, a preliminary analysis of two patients reveals a correlation between high serum CXCL9 levels, elevated CXCL9 expression in HCC, and increased CD8 expression (Hosoda et al., 2023).

In a recent study, the presence of DCs and CXCR3-dependeant migration has been identified as a key event for predicting the response to atezolizumab (Iwai et al., 2021). The combination therapy of atezolizumab and bevacizumab was reported to promote the CTL infiltration in tumours and enhance the anti-tumour effect, including non-inflamed tumours, even though the monotherapy with anti-PDL1 or anti-VEGF antibody did not enhance the CTL infiltration into tumours (Ishikura et al., 2022; Kudo, 2022). Combination therapy is likely to trigger the immune cycle by promoting IFN-γ/CXCL9 production and consequently augment $CD8^+$ T cell infiltration (Reschke & Gajewski, 2022). This mechanism could elucidate the effectiveness of combining atezolizumab and bevacizumab in clinical settings.

Similar to the clinical observation of atezolizumab and bevacizumab, our MEK^{KO} model also demonstrated an augmented IFN signalling and anti-tumour $CD8^+$ T cell response, suggesting the potential synergistic value of targeting RAS signalling and anti-PD-1 treatment in HCC. This also opens up the possibility of developing a combinational therapy that targets KRAS signalling and anti-PD-1 treatment.

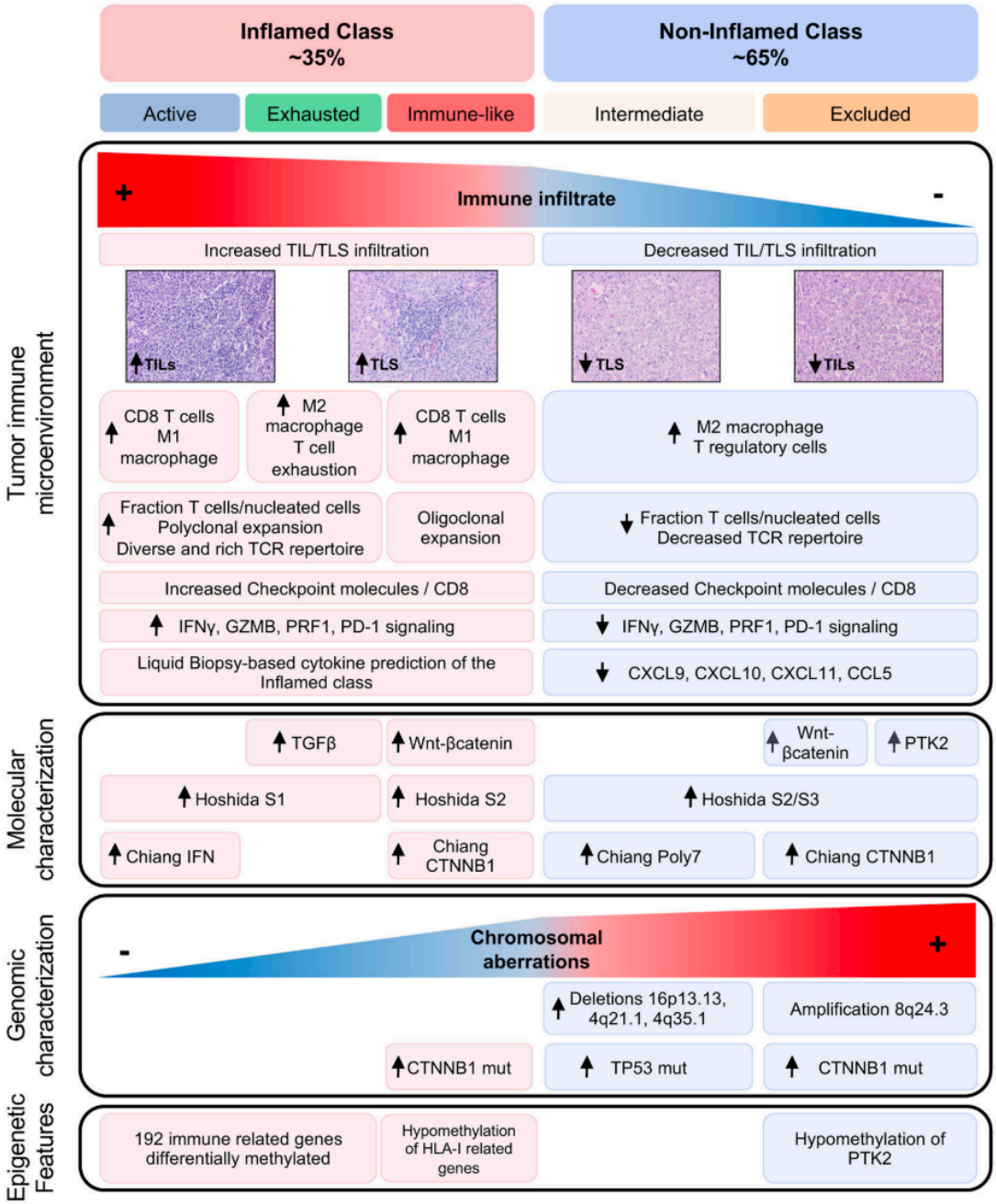

Figure 7.7 Immunogenomic classification of HCC patients. (Montironi et al., 2023)

Chapter 8. Therapeutic development: Targeting ‘undruggable’ Kras in combination with anti-PD1 treatment

8.1 Introduction

In this chapter, we focused on a more in-depth investigation of the relationship between wild-type KRAS activation and anti-PD-1 treatment in different HCC models. Since the ultimate objective of this project is to enhance the therapeutic efficacy of the current immune checkpoint therapy, we also explored the potential of targeting wild-type KRAS signalling in combination with ICI.

For more than 30 years, KRAS has been 'undruggable' in therapeutics due to its high affinity to GTP and unique protein structure (Ostrem & Shokat, 2016; Zhu et al., 2022). One challenge lies in the fact that RAS and GTP exhibit an affinity at the pM level, whereas the cellular GTP concentration remains at 0.5μM (Papke & Der, 2017). It is difficult to develop an effective antagonist, such as a protein kinase inhibitor, to compete with Kras effectively. On the other hand, RAS proteins have a spherical structure which lacks a hydrophobic binding pocket for drug binding (Malumbres & Barbacid, 2003). In 2013, Shokat et al. (2013) identified a new allosteric switch II pocket of $KRAS^{G12C}$ and pioneered the development of a direct covalent KRAS inhibitor.

In 2021, the U.S. The Food and Drug Administration (FDA) approved the first Kras inhibitor, AMG510 (sotorasib), to treat NSCLC patients with Kras G12C mutation (Canon et al., 2019). Sotorasib has shown remarkable clinical responses in advanced solid $KRAS^{G12C}$ tumours including colorectal, pancreatic, and endometrial cancers, and melanoma (Hong et al., 2020). The advance in targeting $KRAS^{G12C}$ also led to the opportunities for small molecule inhibitors to target other KRAS mutants, for example, $KRAS^{G12D}$ (MRTX1133), $KRAS^{G12R}$, $KRAS^{G12S}$ and $KRAS^{G13C}$ (Schulze et al., 2022; Wang et al., 2022; Zhang, Guiley, & Shokat, 2022).

With the launch of direct-targeting drugs, studies on KRAS in cancer have transited from druggable therapy to addressing drug resistance. Multiple acquired drug resistance, such as on-targeted concurrent KRAS alterations and off-targeted vertical signalling alterations, have been observed in cancers treated with Kras inhibitors. After treatment of $KRAS^{G12C}$ inhibitor, a decrease in ERK-related negative regulators e.g. DUSP, SPRY, and PHLDA family genes and an increase in the phosphorylation level of RTKs, which reactivates the wild-type KRAS pathway, were observed (Hallin et al., 2020; Ryan et al., 2020). This has led to the development of pan-KRAS inhibitors to complement mutant KRAS inhibitors.

There are several approaches to develop pan-KRAS inhibitors to halt KRAS activation (Corcoran, 2023). The discovery of the switch I/II pocket in KRAS has presented the possibility of targeting all RAS isoforms, including both wild-type and mutant, by blocking the nucleotide (Maurer et al., 2012). BI-2852, a nanomolar inhibitor, was developed to block both active and inactive forms of RAS (Kessler et al., 2019). Currently, researchers are working on improving the selectivity of pan-RAS inhibitors to target specific RAS isoforms, as triple RAS knockout is lethal in mice (Kim et al., 2023; Nakamura et al., 2008).

Another approach for targeting KRAS is to inhibit the activity of SOS1, a RAS-GEF protein that catalyses KRAS nucleotide exchange. MRTX00902 is an orally active and potent SOS1-KRAS inhibitor that is currently undergoing Phase I/II clinical trial (NCT05578092) in combination with adagrasib (MRTX849) for solid tumours (Ketcham et al., 2022). MRTX0902 monotherapy showed anti-tumour effects with satisfactory pharmacokinetic properties in mouse model (Ketcham et al., 2022). The combinational treatment of MRTX0902 and the EGFR inhibitor Osimertinib exhibited prolonged and augmented inhibition of ERK and PI3K/AKT signalling pathways in NSCLC (Khare et al., 2023). Canon et al. (2019) also reported that the combination of sotorasib ($Kras^{G12C}$ inhibitor) and an MEK inhibitor resulted in enhanced efficacy and good tolerance in a lung cancer mouse model. This suggests the possibility of the combined vertical inhibition of RTK/ERK signalling in targeted cancer therapy.

In our study, we explored the potential of combining MRTX0902 and the MEK inhibitor trametinib with anti-PD-1 treatment in a c-Myc-lucOS^{OE}/Tp53^{KO}/Kras HCC model.

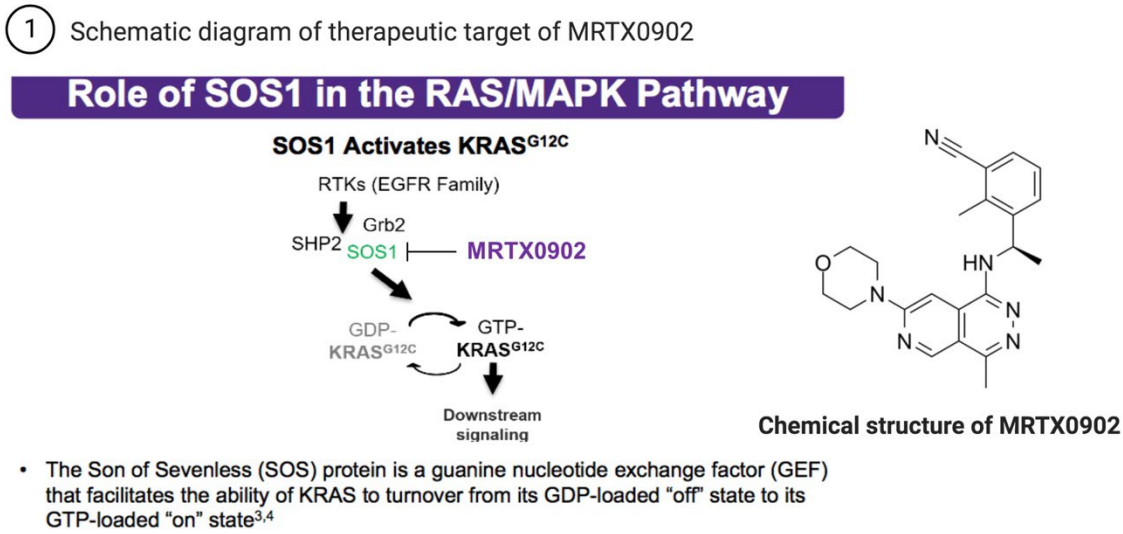

Figure 8.1 Therapeutic target of the SOS1 inhibitor MRTX0902.(Ketcham et al., 2022)

8.2 Experiment design

(1) The c-Myc-lucOS^{OE}/Tp53^{KO}/Kras HCC mouse model was induced via HTVI as previously described. The two-week treatment commenced 6 days after HTVI. The mice were administered the SOS1 inhibitor MRTX0902 (5 mg/kg q.d.) via IV injection, coupled with a daily oral administration of trametinib (0.2 mg/kg b.i.d.), and anti-PD-1 (200μg t.i.w.) through IP injection. Tumour growth was monitored using bioluminescence imaging at specific time points. The tumour tissues were harvested for gene and protein expression analyses.

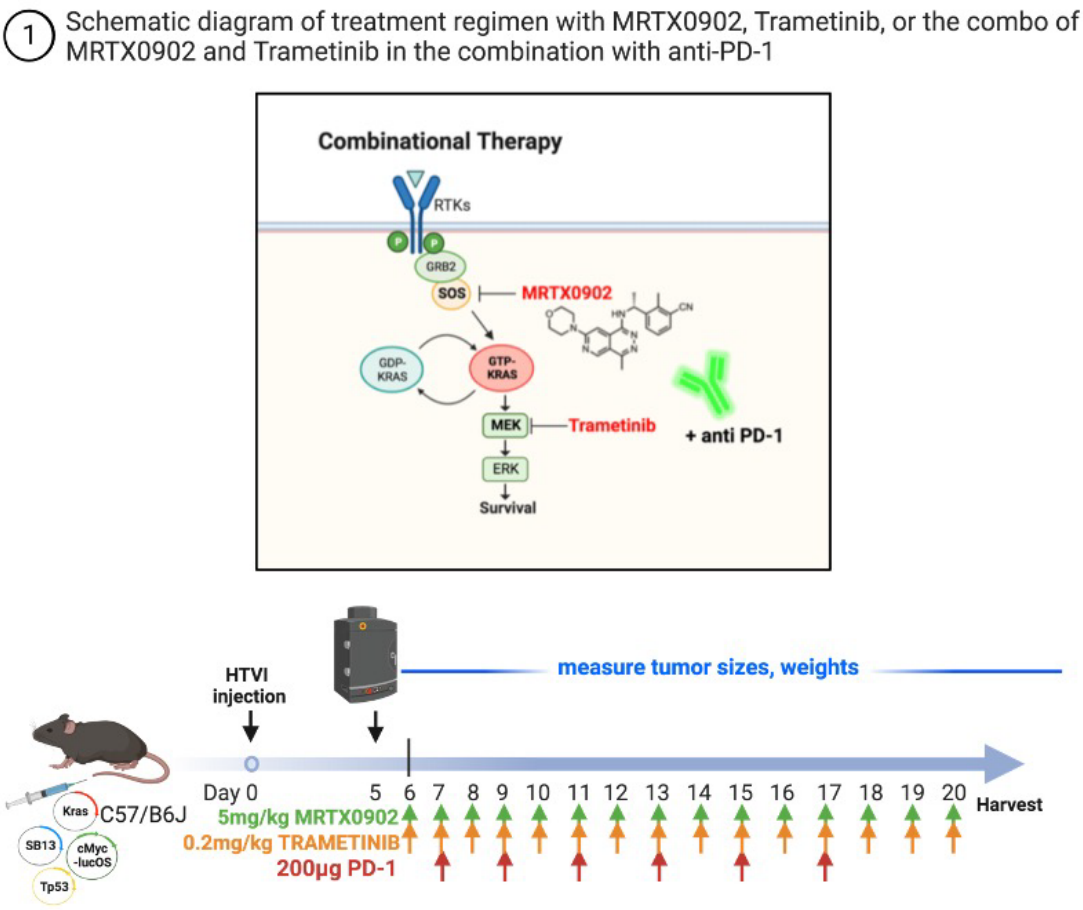

Figure 8.1 Schematic diagram of combinational therapy of KRAS inhibitor MRTX0902, trametinib and anti-PD-1 treatment

Schematic diagram illustrating the therapeutic design of SOS1 inhibitor MRTX0902, trametinib, and anti-PD-1 treatment targeting KRAS signalling in the c-Myc-lucOS^{OE}/Tp53^{KO}/Kras model.

8.3 Results

8.3.1 Activation of EGFR/KRAS/ ERK signalling pathway in anti-PD-1 resistant HCC models

The c-Myc^{OE}/Tp53^{KO} mouse HCC model is a mildly immunogenic HCC model that has been previously reported to be refractory to anti-PD-1 treatment (Chiu et al., 2020). Despite the expansion of effector memory CD8^{+} T cells induced by anti-PD-1 treatment, no significant reduction in tumour size or improvement in survival was observed in this model. We repeated anti-PD-1 treatment in the c-Myc^{OE}/Tp53^{KO} mouse HCC model. Consistent with the previous report, there was no significant difference in tumour size between the control IgG and anti-PD-1 treated groups (Figure 8.2A). Interestingly, we observed an upregulation of pEGFR and pERK1/2 levels in the irresponsive anti-PD-1 treated tumours, yet there was no significant increase in wild-type Kras expression (Figure 8.2B). In another immunogenic NAFLD-induced RIL-175 HCC model, we also observed activation of the EGFR/KRAS/ERK and Akt signalling pathways in irresponsive PD-1 treated tumours (Figure 8.3). These findings led us to hypothesise that the activation of KRAS signalling may contribute to resistance to anti-PD-1 treatment.

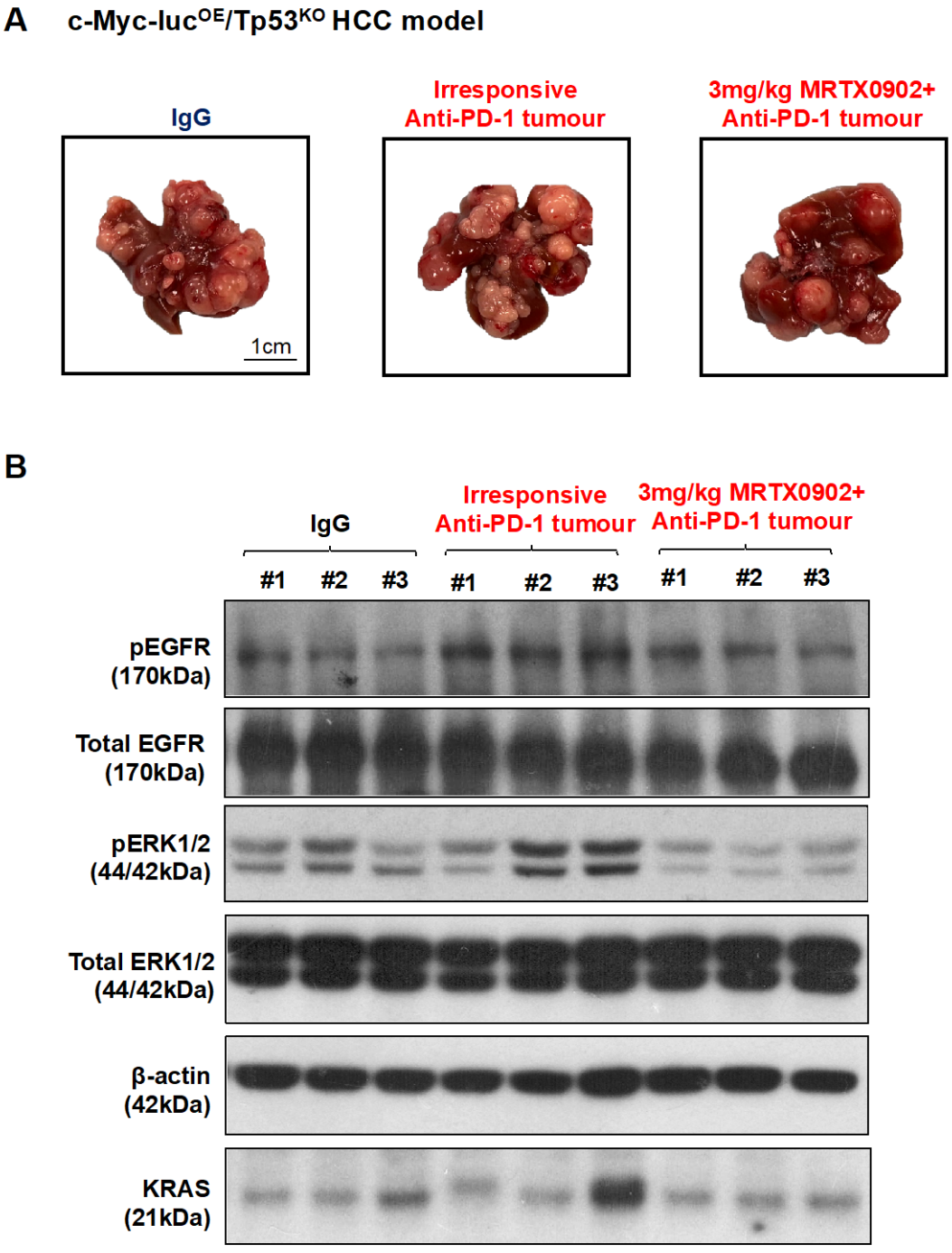

Figure 8.2 Activation of KRAS signalling pathways upon anti-PD-1 treatment in c-Myc-luc^{OE}/Tp53^{KO} HCC mice model.
(A) Representative images of c-Myc-luc^{OE}/Tp53^{KO} HCC tumours after anti-PD-1 treatment. **(B)** Western blot showed activation of KRAS signalling pathways in irresponsive anti-PD-1 treated tumours and a reduction of pERK1/2 expression in MRTX0902-treated unresponsive anti-PD-1 treated tumours.

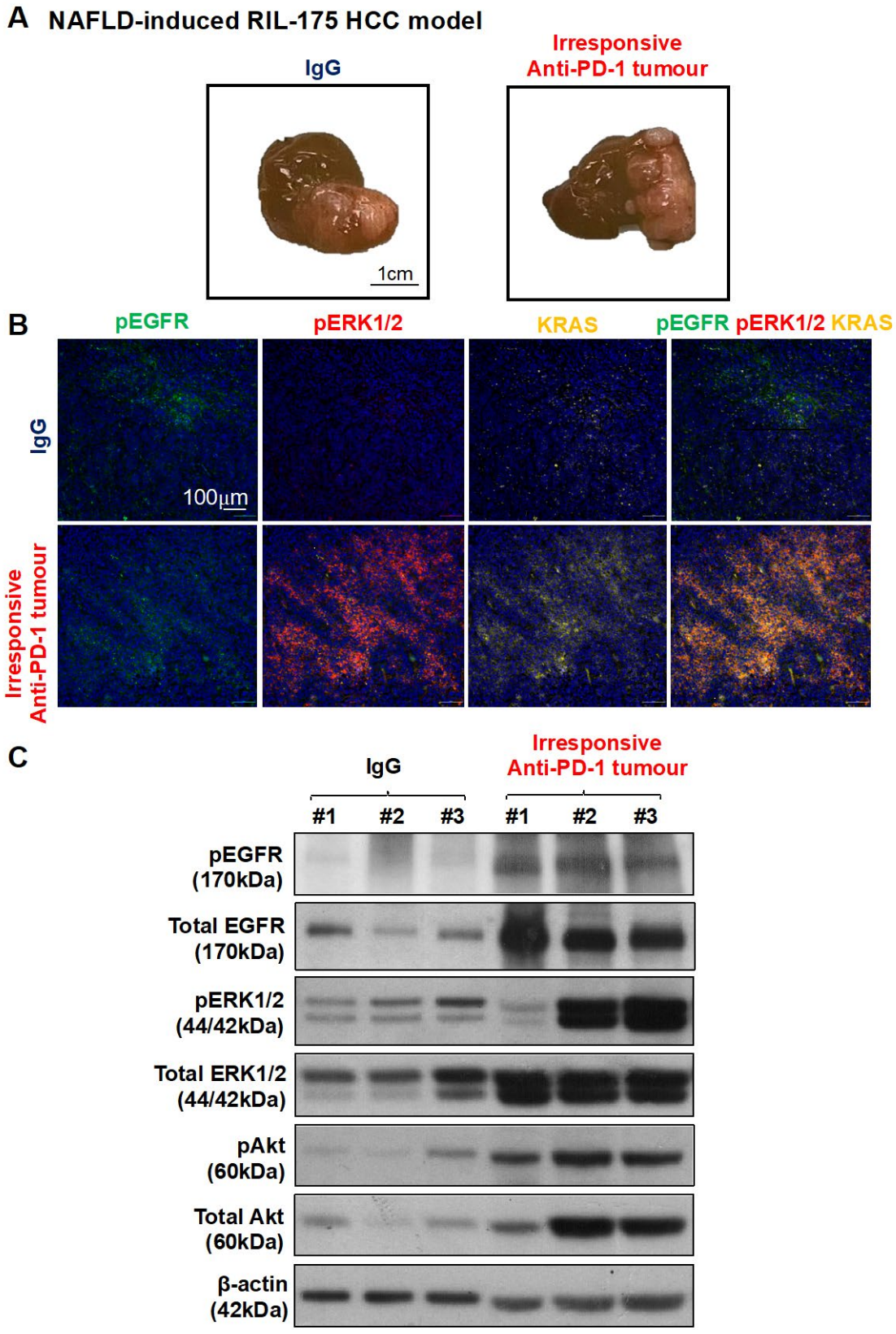

Figure 8.3 Activation of KRAS signalling pathways upon PD-1 treatment in NAFLD-induced RIL-175 HCC mouse model.
(A) Representative images of orthotopic RIL-175 HCC tumours with NAFLD background. **(B&C)** Multiplexed immunofluorescence and western blot showed activation of ERK and Akt signalling pathways in unresponsive anti-PD-1 treated tumours.

8.3.2 Combinational therapy of MRTX0902 and trametinib with anti-PD-1 treatment suppresses tumour growth and improves survival of c-Myc-lucOS^{OE}/Tp53^{KO}/Kras mouse model

With the exogenous expression of the tumour antigens, the lucOS model was reported to sensitise the c-Myc-lucOS^{OE}/Tp53^{KO} tumour to anti-PD-1 therapy (de Galarreta et al., 2019). Given the observed upregulation of EGFR/KRAS/ERK signalling in irresponsive anti-PD-1 treated HCCs, we examined the therapeutic relevance of wild-type Kras-driven immune evasion in response to anti-PD-1 treatment. Consistent with our hypothesis, c-Myc-lucOS^{OE}/Tp53^{KO}/Kras was not responsive to anti-PD-1 treatment, proving that wild-type KRAS activation promotes resistance to immunotherapy in our model (Figure 8.4A&B).

To address Kras-driven resistance to anti-PD-1 therapy, we explored the therapeutic potential of targeting KRAS signalling using the KRAS inhibitor MRTX0902 and the MEK inhibitor trametinib. To evaluate the effectiveness of MRTX0902 in modulating pERK1/2 in the HCC model, we administered 3 mg/kg MRTX0902 via IV injection to c-Myc-luc^{OE}/Tp53^{KO} mice. Tumour tissues were harvested for pERK1/2 measurement an hour after IV injection due to its short half-life in mice ($t_{1/2}$ = 1.3 hour) (Ketcham et al., 2022). Western blot showed downregulated pERK1/2 levels in MRTX0902-treated irresponsive anti-PD-1 tumours (Figure 8.2B).

After confirming the effect of MRTX0902 on pERK1/2modulation, we explored the possibility of combinational therapeutic strategies involving trametinib and anti-PD-1 treatment in our immune escaped Kras model. Based on the short half-life of the compound and the dosing reported in a previous publication (Ketcham et al., 2022), 5 mg/kg q.d. of MRTX0902 was selected for 14-day treatment. MRTX0902 was administered along with anti-PD-1 treatment or in a combination regimen of MRTX0902 (5 mg/kg q.d.), trametinib (0.2 mg/kg b.i.d.) and anti-PD-1 treatment. During the treatment period, no adverse events or side effects were observed in the mice subjected to the combination treatment (MRTX0902 + Trametinib + anti-PD-1), indicating that the combinational therapeutic approach was well tolerated with no enhanced toxicity.

Among all groups, the MRTX0902+PD-1, Trametinib+PD-1 and combo groups showed reduced luciferase signals and improved survival (Figure 8.4A&B). Surprisingly, the luciferase signals of the MRTX0902+PD-1 group were significantly reduced compared with those of the

MRTX0902+IgG-treated group, correlating with improved survival. This suggests that MRTX0902 sensitised the tumour to anti-PD-1 treatment, conferring a survival benefit. Western blot (Figure 8.4C) also demonstrated significant suppression of pERK1/2 levels upon MRTX0902 and trametinib treatment, confirming that targeting KRAS signalling enhances the therapeutic efficacy of anti-PD-1 therapy.

Finally, we investigated the impact of the pharmacological inhibition of KRAS signalling on the T cell compartment. Interestingly, multiplexed immunofluorescence showed an upregulation of $CD8^+$ T cells in anti-PD-1 treated tumours, compared to the IgG control group (Figure 8.4D). Treatment with MRTX0902 alone (MRTX0902+IgG) did not increase the number of $CD8^+$ T cells. However, the combined targeting of wild-type Kras and PD-1 (MRTX0902+PD-1) resulted in a significant increase in $CD8^+$ T cells. Similar to the earlier findings in Figure 7.6, MEK inhibition by trametinib further enhanced the number of $CD8^+$ T cells when combined with anti-PD-1 treatment. In the combo group, the abundance of $CD8^+$ T cells was similar to that in the trametinib-treated group.

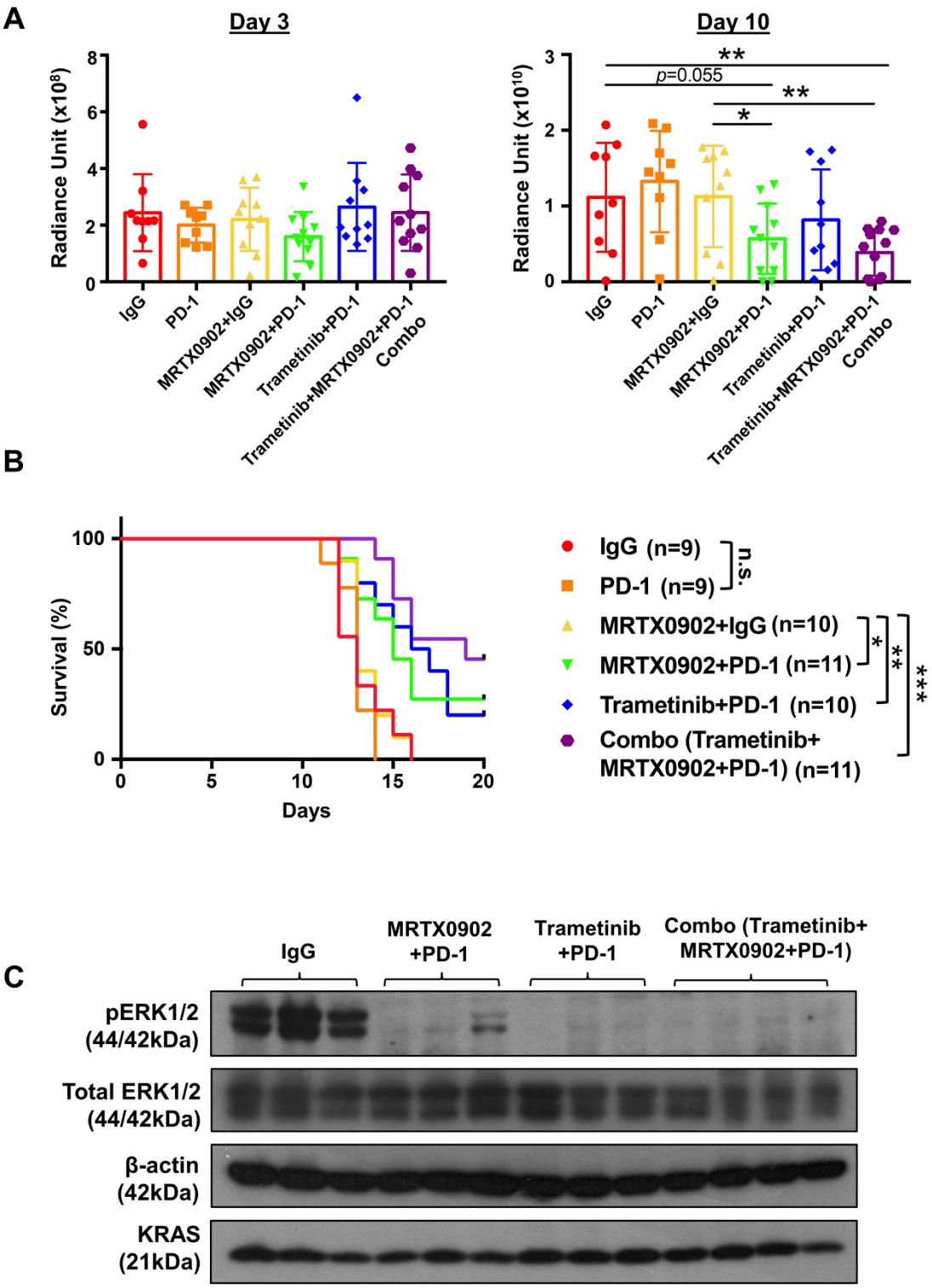
A
Day 3
Day 10
Radiance Unit (x10⁸)
Radiance Unit (x10¹⁰)
p=0.055
**
**
*
IgG
PD-1
MRTX0902+IgG
MRTX0902+PD-1
Trametinib+PD-1
Trametinib+MRTX0902+PD-1
Combo
B
Survival (%)
Days
IgG (n=9)
PD-1 (n=9)
MRTX0902+IgG (n=10)
MRTX0902+PD-1 (n=11)
Trametinib+PD-1 (n=10)
Combo (Trametinib+ MRTX0902+PD-1) (n=11)
n.s.
*
**
***
C
IgG
MRTX0902 +PD-1
Trametinib +PD-1
Combo (Trametinib+ MRTX0902+PD-1)
pERK1/2 (44/42kDa)
Total ERK1/2 (44/42kDa)
β-actin (42kDa)
KRAS (21kDa)

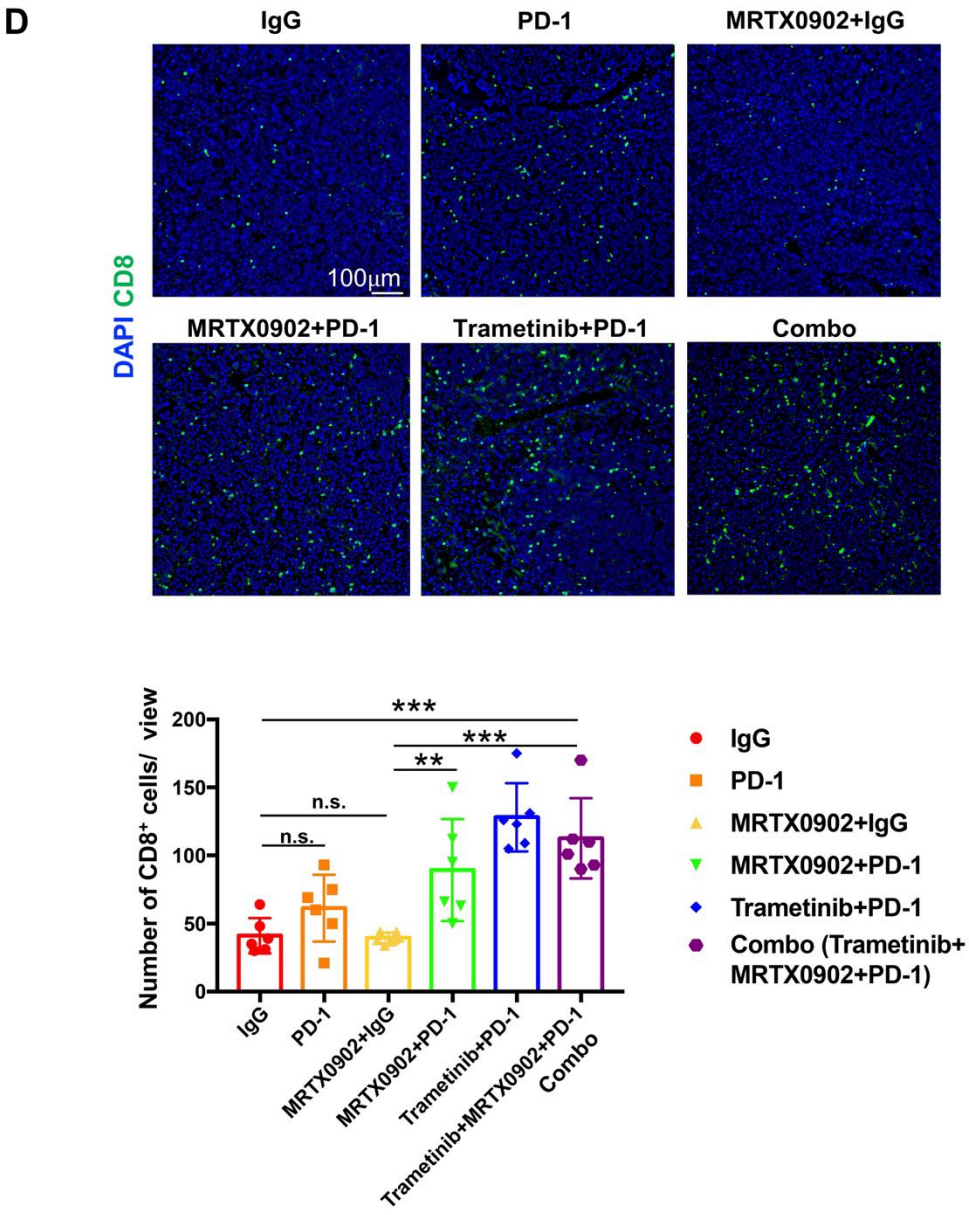

Figure 8.4 Combinational therapy with MRTX0902, trametinib, and anti-PD-1 treatment suppresses tumour growth and improves survival of c-Myc-lucOS^{OE}/Tp53^{KO}/Kras mice. **(A)** Quantification of the normalised luciferase signal in c-Myc-lucOS^{OE}/Tp53^{KO}/Kras mice on days 3 and 10 after HTVI. (* $p<0.05$, ** $p<0.01$, t-test). **(B)** The survival of c-Myc-lucOS^{OE}/Tp53^{KO}/Kras mice after treatment with vehicle, MRTX0902 5 mg/kg, trametinib 0.2 mg/kg (with IgG control or anti-PD-1) (* $p<0.05$, ** $p<0.01$, *** $p<0.001$, log-rank test). **(C)** Western blot demonstrated a decrease in pERK1/2 level following treatment with MRTX0902 and trametinib. **(D)** Representative images and quantification of intra-tumoral CD8 (green) staining for IgG, PD-1, MRTX0902+IgG, MRTX0902+PD-1, Trametnib+PD-1 and MRTX0902+ Trametnib+PD-1 tumours. Scale bar=100μm. (** $p<0.01$, *** $p<0.001$, t-test).

8.4 Discussion

The clinical response to anti-PD-1/PD-L1 treatment in HCC is highly variable, with most patients experiencing disease progression. Although the targets of ICIs are known, a complete understanding of the downstream therapeutic mechanisms is still elusive. Several factors contribute to the failure of anti-PD-1 treatment, including lack of tumour immunogenicity, T cell dysfunction, expression of other immune checkpoint markers, and an immunosuppressive tumour microenvironment. Currently, none of these markers is robust enough to guide the clinical management of HCC or improve the efficacy of ICI. As a consequence, the development of novel combinational therapies to improve ICI outcomes is essential.

In this chapter, we observed the activation of EGFR/KRAS/ERK signalling in irresponsive anti-PD-1 treated tumours in two HCC mouse models: c-Myc^{OE}/Tp53^{KO} and NAFLD-induced RIL-175 HCC models. The c-Myc^{OE}/Tp53^{KO} mouse model is mildly immunogenic and has previously been reported to be resistant to anti-PD-1 therapy (Chiu et al., 2020). Although an increase in effector memory CD8^{+} T cells was observed in the anti-PD-1 treated c-Myc^{OE}/Tp53^{KO} tumour, this expansion did not lead to tumour reduction. Nevertheless, blockade of another immune checkpoint, TIGIT, was found to enhance the response to anti-PD-1 treatment (Chiu et al., 2020). Moreover, the addition of exogenous antigens to the lucOS model enhances the immunogenicity of the model and sensitises it to anti-PD-1 treatment (de Galarreta et al., 2019). Notably, we characterised this escaped c-Myc-lucOS^{OE}/Tp53^{KO} tumour with the activation of KRAS signalling in Chapter 3.

The immunological RIL-175 cell line HCC model is responsive to anti-PD-1 treatment. Previous findings from our lab and other researchers have demonstrated that NASH limits anti-tumour surveillance in anti-PD-1 treated HCC (Pfister et al., 2021). An expansion of PD1^{+} effector CD8^{+} T cells was observed upon anti-PD-1 treatment in the NASH-induced RIL-175 model. Based on the immune-mediated cancer field (ICF) signature published by Llovet et al. (2019), preventive anti-PD-1 treatment was associated with the immunosuppressive ICF signature. The immunosuppressive ICF signature was characterised by the mediator of immune tolerance and inhibition, such as the activation of TGF-β signalling, T cell exhaustion, the presence of M2 macrophages, and CD4^{+} memory resting cells. Intriguingly, this immunosuppressive subtype was also characterised by the enrichment of KRAS signalling (Moeini et al., 2019). Based on our observation of activated EGFR/KRAS/ERK signalling in

unresponsive anti-PD-1 treated HCC models and the aforementioned evidence in the literature, we deduced that KRAS signalling plays a role in conferring resistance to anti-PD-1 treatment.

Oncogenic RAS signalling has been documented to promote immune suppression, allowing cancer cells to evade the anti-tumour immune response (Ward et al., 2020). Our study provides new insights into the role of wild-type KRAS signalling in resistance to immunotherapy, and highlights the therapeutic potential of targeting Kras to enhance the efficacy of immunotherapy in HCC. Interestingly, anti-PD-1 treatment also led to an increase in the intra-tumoral infiltration of $CD8^+$ T cells although it did not improve the survival of the c-Myc-lucOS^{OE}/Tp53^{KO}/Kras mice. This observation suggests the presence of other immunosuppressive factors mediated by wild-type KRAS activation, affecting the efficacy of anti-PD-1 treatment. Despite reports of pharmacological MEK inhibition affecting the lymphocyte activation and proliferation (Vella et al., 2014; Yamaguchi et al., 2012), our combinational therapeutics of Kras or MEK inhibition with PD-1 blockade demonstrated an enhancement in $CD8^+$ T cell-mediated anti-tumour immunity and the response to immunotherapy. Immunologically, the introduction of Kras or MEK inhibition exerts an additional impact on $CD8^+$ T cell infiltration, complementing the effect of anti-PD-1. The combination of the triple treatments also exhibited a good response in survival outcomes as well as the intra-tumoral $CD8^+$ T cell infiltration. To alleviate the suppressive effect of Kras/MEK inhibition on T cell activation, pulsatile treatment with these inhibitors was suggested to enhance T cell activity, which led to an enhanced anti-tumour effect when combined with the ICI (Choi et al., 2019).

The synergistic effect of KRAS/MEK inhibition on immunotherapy was also evident in other KRAS-mutated cancers (Canon et al., 2019; Mugarza et al., 2022; Ward et al., 2020). In NSCLC, the Kras^{G12C} inhibitor sotorasib created a “hot” TIME with an increase in T-cell infiltration via CXCL10/11, synergising the effect of immunotherapy in an immunocompetent mouse model (Canon et al., 2019). Another lung cancer model showed an increased population of exhausted T cells and enhanced IFN responses upon MRTX1257 (Kras^{G12C} inhibitor) treatment, sensitizing the tumour to ICI (Mugarza et al., 2022). Trametinib, in combination with ICI, shifted the TIME to become more proinflammatory with an increased presence of tumour-infiltrating lymphocytes (Liu et al. 2015).

Nevertheless, the synergised response of KRAS inhibition with immunotherapy is limited to immunogenic models (Mugarza et al., 2022). Although KRAS inhibition enhanced the infiltration of cytotoxic T cells, it failed to synergise with the response to immunotherapy in intrinsically non-immunogenic models, which lack neoantigens or exhibit T cell exclusion with MHC-I downregulation (Boumelha et al., 2022). Tumour immunogenicity is correlated to the capability of the T cells to recognise tumour cells, which is crucial for the effectiveness of PD-1/PD-L1 blockade (Sun et al., 2020). The lack of tumour antigen significantly hinders T cells from recognising tumour cells, eventually resulting in the failure of immunotherapy. This observation emphasises the importance of an intact tumour intrinsic IFN signalling in responding to immunotherapy, even when KRAS inhibition alleviates the immunosuppressive TIME.

Together, this study highlights that inhibiting KRAS signalling by ameliorating the immunosuppressive TIME synergises with anti-PD-1 treatment. Moreover, it uncovers the potential clinical application of combined vertical inhibition of Kras/ERK signalling using trametinib and MRTX0902.

Chapter 9. Conclusion and Future Perspectives

9.1 Conclusion

In the recent decade, therapeutic advances have dramatically altered the systemic treatment landscape of advanced HCC. Combination therapy such as atezolizumab-bevacizumab or durvalumab-tremelimumab has become the central focus of the current treatment regimen. However, ICI therapies exhibit highly heterogeneous efficacies among patients with advanced HCC. There is an urgent need to identify effective biomarkers to select patients who could benefit the most from well-established treatments and predict the response outcomes. Taking into account these questions, there is a need to understand better the immune evasive mechanisms of HCC.

Increasing evidence indicates that activation of the oncogenic pathways is associated with generating an unfavourable tumour microenvironment with consequent immunotherapy resistance. Therefore, targeting the oncogenic pathways may be a promising strategy to overcome ICI resistance in HCC patients. In this study, we aimed to identify the oncogenic pathway that modulates immune evasion in HCC and understand the underlying molecular mechanisms. Finally, we evaluated the therapeutic efficacy of targeting this oncogenic pathway in enhancing the effectiveness of the ICI.

Utilising the immunogenic c-Myc-lucOS^{OE}/Tp53^{KO} HCC mouse model, we have demonstrated that wild-type KRAS activation in HCC tumour cells is an important immune escape mechanism. Unlike other cancer types, KRAS mutation is rare in liver cancer. This rarity has contributed to a gap in our understanding of the functional role of KRAS in HCC and its potential impact on the immune response. Recognising this knowledge gap and building upon our previous observations in immune-evaded c-Myc-lucOS^{OE}/Tp53^{KO} tumours, we focused on wild-type Kras in this study.

In human HCCs, wild-type KRAS expression is upregulated in mRNA and protein levels and is correlated with poor prognosis. Endogenous wild-type Kras overexpression modulates immune escape via the activation of oncogenic Kras/MEK/ERK signalling in the c-Myc-lucOS^{OE}/Tp53^{KO} model, leading to an increase in tumour burden with a shorter survival time in mice. EGF, upregulated in the c-Myc-lucOS^{OE}/Tp53^{KO} model, activates wild-type KRAS signalling and phosphorylates the upstream EGFR. This differential activation mechanism sheds light on the unique role of wild-type Kras in driving oncogenic signalling pathways in HCC.

Our investigations delved into the intricate molecular mechanisms by which wild-type Kras promotes immune evasion in HCC. Wild-type Kras reprogrammes the TIME into a more immunosuppressive milieu, by dampening the IFN responses, both intrinsically and extrinsically. The suppressed tumour-intrinsic IFN response downregulates surface MHC-I expression on the tumour cells. Extrinsically, wild-type Kras suppresses the recruitment of DCs and T cells to the tumour site, hinders antigen presentation and dampens T cell activation. All these findings consolidated our hypothesis that wild-type Kras, via the activation of its downstream MEK/ERK signalling, acts as a crucial immune evasive mechanism in HCC and contributes to resistance to anti-PD-1 therapy.

In the clinical cohort, wild-type Kras expression is negatively associated with IFN response and MHC-I–related genes. This clinical correlation aligns with our laboratory results, further reinforcing the link between wild-type Kras expression and compromised immune responses in HCC. The convergence of evidence from both experimental models and clinical data emphasises the clinical relevance and potential translational impact of our study.

We also established a novel *in vivo* CRISPR/Cas9 system to target MEK1/2 in c-Myc lucOS^{OE}/Tp53^{KO}/Kras HCC. MEK1/2 knockout reverses the immunosuppressive effects of wild-type Kras overexpression, enhancing IFN responses, antigen presentation function, and MHC-I expression. Regarding the immune compartments, MEK1/2 knockout increased the recruitment of CD8^{+} T cells into tumours through elevated T cell chemoattractants Cxcl9 and Cxcl10.

Lastly, our study provided new insights into the therapeutic potential of targeting wild-type Kras to enhance the efficacy of immunotherapy in HCC. The combination therapy of the Kras inhibitor MRTX0902, MEK inhibitor trametinib and anti-PD1 treatment successfully enhanced intra-tumoral CD8^{+} T cell infiltration as well as exhibited a favourable response in survival outcome. This finding highlighted the synergistic impact of targeting wild-type KRAS signalling on the efficacy of anti-PD-1 treatment. Moreover, it elucidated the possibility of combined vertical inhibition of Kras and MEK in HCC.

In summary, this study has elucidated a novel signalling axis in immune evasion in HCC. The role of wild-type Kras in HCC has been unveiled, and its role in developing resistance to anti-

PD-1 treatment. It also shed light on the potential of the combination therapy targeting KRAS signalling and anti-PD-1 in HCC, providing a foundation for further exploration and potential clinical applications.

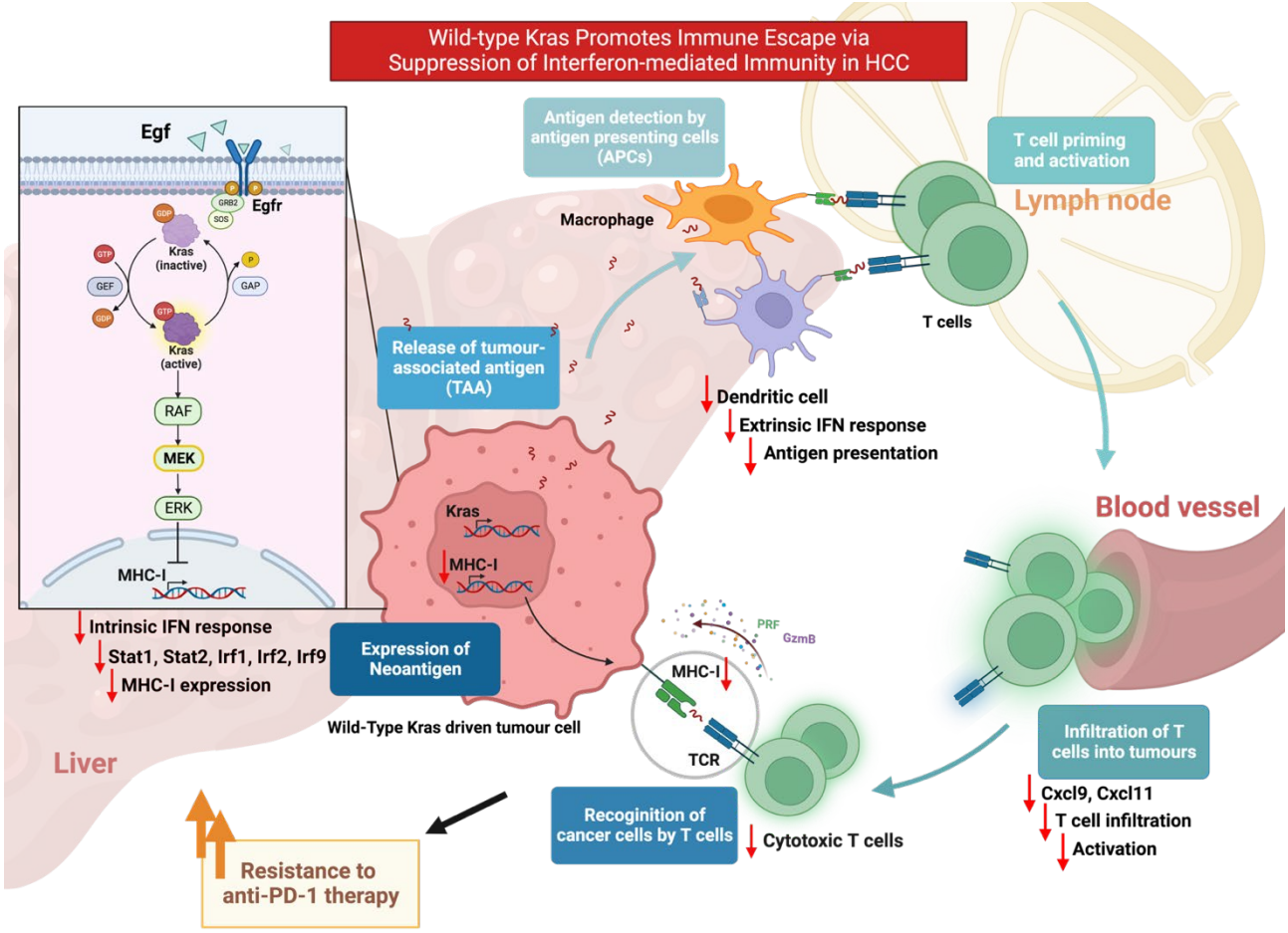

Figure 9.1 Graphical summary of wild-type Kras promoting immune evasion via suppression of the IFN responses in HCC.
In the context of HCC with c-Myc^{OE}/Tp53^{KO} background, wild-type KRAS activation shaped an immunosuppressive TIME via suppression of IFN responses, resulting in downregulation of antigen presentation function and impaired T cell infiltration into the tumour. The suppression of tumour intrinsic IFN response further resulted in a reduction in MHC-I expression on the tumour cells. Collectively, these mechanisms orchestrated a deficit anti-tumour T cell response, resulting in immune evasion and conferring resistance to anti-PD-1 treatment.

9.2 Future Perspectives

9.2.1 To investigate the source of EGF expression in c-Myc-lucOS^{OE}/Tp53^{KO} HCC

In the c-Myc-lucOS^{OE}/Tp53^{KO} HCC, we observed an elevated EGF level compared to c-Myc-luc^{OE}/Tp53^{KO} HCC. Upon wild-type Kras overexpression, we hypothesised that the upregulation of EGF expression leads to the activation of the EGFR, and subsequently activates the downstream KRAS signalling, resulting in the phosphorylation of ERK1/2. EGF is highly expressed in HCC tumour cells or from TAMs (Goswami et al., 2005; Liu et al., 2018). Flow cytometry results indicate that the expression of exogenous antigens enhances tumour immunogenicity, and induces immune infiltration, including TAMs, DCs and T cells. In addition, DIA-MS data exhibited an increase in macrophage marker gene Itgam, suggesting that enhancing the immunogenicity of the tumours may activate the RTK signalling via the recruitment of TAMs. Further investigations, for example, IHC analysis of the -Myc-lucOS^{OE}/Tp53^{KO}/Kras tissue will be executed to confirm the source of EGF.

9.2.2 To modify the combinational therapeutic scheme of Kras inhibitor MRTX0902, MEK inhibitor trametinib and anti-PD-1 therapy

We examined the efficacy of combinational therapy of Kras inhibitor MRTX0902, MEK inhibitor trametinib and anti-PD-1 therapy on c-Myc-lucOS^{OE}/Tp53^{KO}/Kras HCC. To improve treatment outcomes, we propose some modifications. Given that MRTX0902 is an orally active drug, the next step involves testing its oral bioavailability in the mouse model. Moreover, to alleviate the suppressive effect of Kras/MEK inhibition on T cell activation, a pulsatile treatment approach was suggested to enhance T cell activity (Choi et al., 2019). For instance, a 5-day-on and 2-day-off schedule of trametinib with MRTX0902 via oral gavage will be administered to the mice.

9.2.3 To investigate the correlation of wild-type KRAS signalling and CD8$^+$ T cell infiltration in anti-PD-1 treated clinical samples

We suggested that the observed correlation between wild-type KRAS activation, reduced intra-tumoral CD8$^+$ T cell infiltration and resistance to anti-PD-1 treatment in the c-Myc-lucOS^{OE}/Tp53^{KO} HCC mouse model. It is crucial to examine whether this observation also occurs in human HCC. To validate our findings, we will analyse HCC clinical samples post anti-PD-1 treatment, comparing the expression of EGFR/KRAS/ERK signalling in anti-PD-1-sensitive and resistant tissues. Subsequently, we will explore the correlation between Kras

expression and $CD8^+$ T cell abundance in HCC tissue. Given the activation of EGFR/KRAS/ERK signalling in the HCC mouse model upon anti-PD-1 treatment, examining this signalling in HCC tissues from patients before and after receiving anti-PD-1 treatment would be valuable.

Appendices

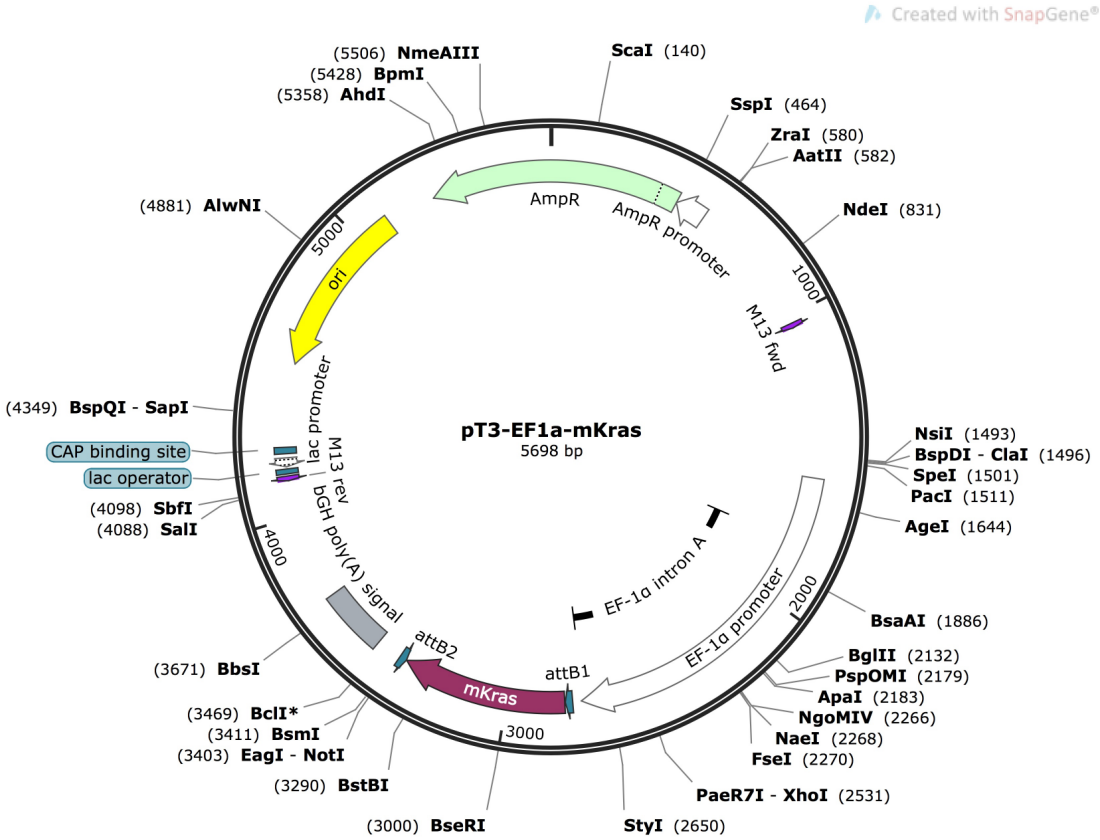

Appendix 1. The plasmid map of pT3-EF1a-Kras.

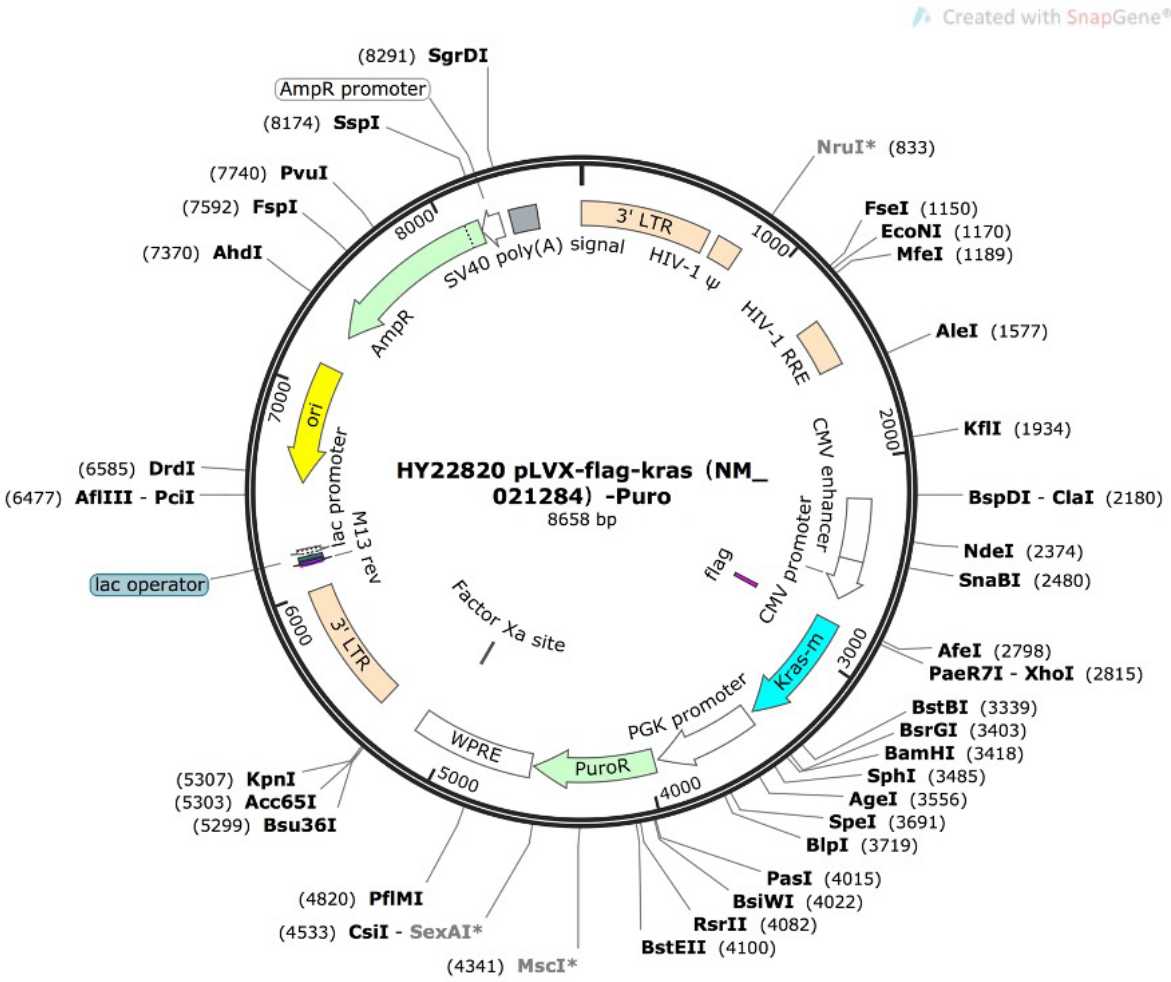

Appendix 2. The plasmid map of pLVX-flag-Kras-Puro.

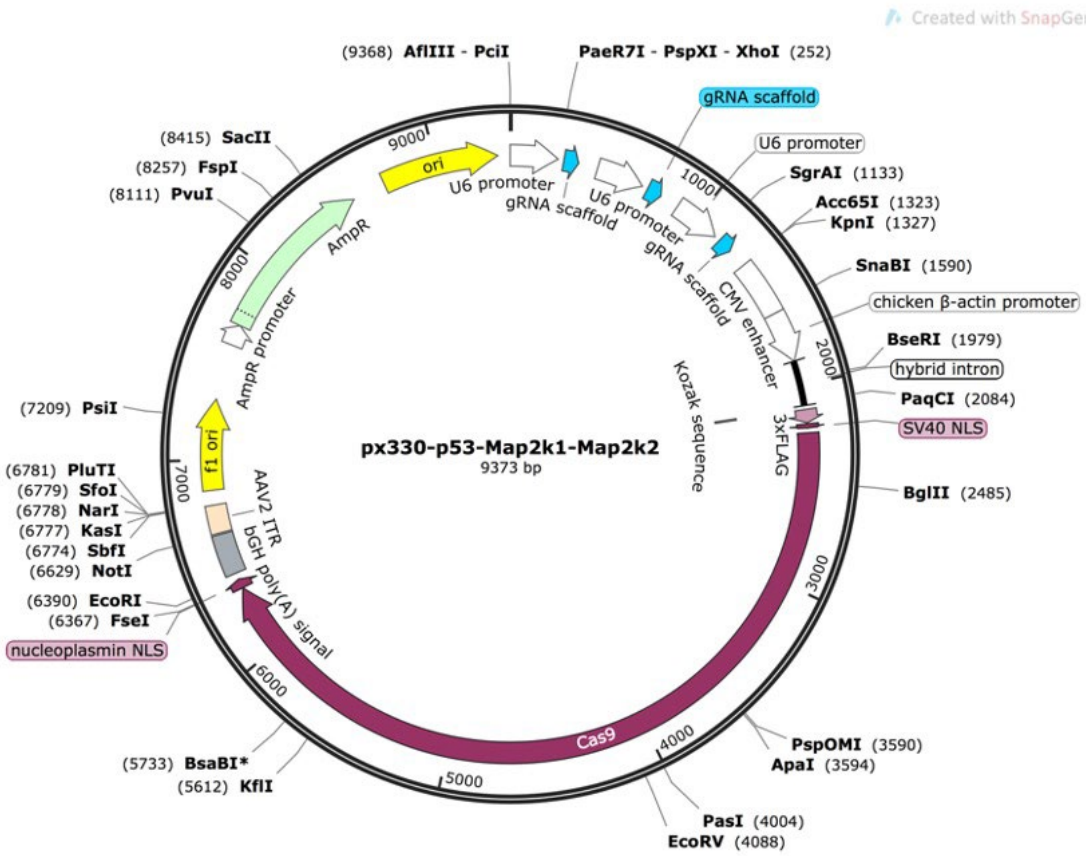

Appendix 3. The plasmid map of px330-sgTp53-sgMap2k1-sgMap2k2.

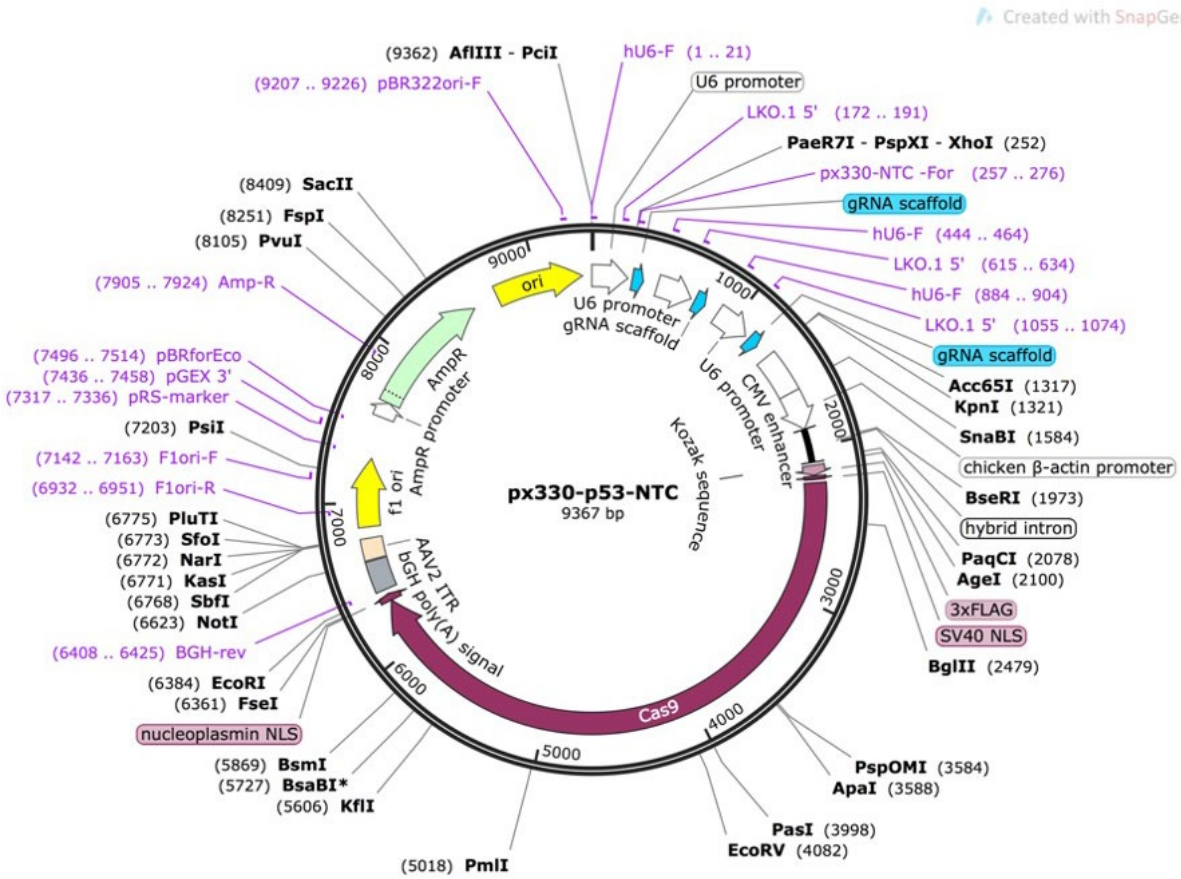

Appendix 4. The plasmid map of px330-sgTp53-NTC.

References

1. Ambrogio, C., Köhler, J., Zhou, Z. W., Wang, H., Paranal, R., Li, J., … Jänne, P. A. (2018). KRAS Dimerization Impacts MEK Inhibitor Sensitivity and Oncogenic Activity of Mutant KRAS. *Cell*, *172*(4), 857-868.e15. https://doi.org/10.1016/j.cell.2017.12.020
2. Atkins, D., Breuckmann, A., Schmahl, G. E., Binner, P., Ferrone, S., Krummenauer, F., … Seliger, B. (2004). MHC class I antigen processing pathway defects, ras mutations and disease stage in colorectal carcinoma. *International Journal of Cancer*, *109*(2), 265–273. https://doi.org/10.1002/ijc.11681
3. Ayers, M., Lunceford, J., Nebozhyn, M., Murphy, E., Loboda, A., Albright, A., … Kang, S. P. (2017). IFN-γ–related mRNA profile predicts clinical response to PD-1 blockade. *Journal of Clinical Investigation*, *127*(8). https://doi.org/10.1172/jci91190
4. Bae, S., Park, J., & Kim, J. S. (2014). Cas-OFFinder: A fast and versatile algorithm that searches for potential off-target sites of Cas9 RNA-guided endonucleases. *Bioinformatics*, *30*(10), 1473–1475. https://doi.org/10.1093/bioinformatics/btu048
5. Baum, C., Kustikova, O., Modlich, U., Li, Z., & Fehse, B. (2006). Mutagenesis and oncogenesis by chromosomal insertion of gene transfer vectors. *Human Gene Therapy*, *17*(3), 253–263. https://doi.org/10.1089/hum.2006.17.253
6. Berasain, C., & Avila, M. A. (2014). The EGFR signalling system in the liver: From hepatoprotection to hepatocarcinogenesis. *Journal of Gastroenterology*, *49*(1), 9–23. https://doi.org/10.1007/s00535-013-0907-x
7. Bessis, N., GarciaCozar, F. J., & Boissier, M. C. (2004). Immune responses to gene therapy vectors: Influence on vector function and effector mechanisms. *Gene Therapy*, *11*, S10–S17. https://doi.org/10.1038/sj.gt.3302364
8. Bezzi, M., Seitzer, N., Ishikawa, T., Reschke, M., Chen, M., Wang, G., … Pandolfi, P. P. (2018). Diverse genetic-driven immune landscapes dictate tumor progression through distinct mechanisms. *Nature Medicine*, *24*(2), 165–175. https://doi.org/10.1038/nm.4463
9. Bichmann, L., Gupta, S., Rosenberger, G., Kuchenbecker, L., Sachsenberg, T., Ewels, P., … Röst, H. (2021). DIAproteomics: A Multifunctional Data Analysis Pipeline for Data-Independent Acquisition Proteomics and Peptidomics. *Journal of Proteome Research*, *20*(7), 3758–3766. https://doi.org/10.1021/acs.jproteome.1c00123
10. Billiau, A., & Matthys, P. (2009). Interferon-γ: A historical perspective. *Cytokine and Growth Factor Reviews*, *20*(2), 97–113. https://doi.org/10.1016/j.cytogfr.2009.02.004
11. Blagih, J., Buck, M. D., & Vousden, K. H. (2020). P53, Cancer and the Immune Response. *Journal of Cell Science*, *133*(5). https://doi.org/10.1242/jcs.237453
12. Boumelha, J., de Carné Trécesson, S., Law, E. K., Romero-Clavijo, P., Coelho, M. A., Ng, K. W., … Downward, J. (2022). An Immunogenic Model of KRAS-Mutant Lung Cancer Enables Evaluation of Targeted Therapy and Immunotherapy Combinations. *Cancer Research*, *82*(19), 3435–3448. https://doi.org/10.1158/0008-5472.CAN-22-0325
13. Brown, Z. J., Yu, S. J., Heinrich, B., Ma, C., Fu, Q., Sandhu, M., … Greten, T. F. (2018). Indoleamine 2,3-dioxygenase provides adaptive resistance to immune checkpoint inhibitors in hepatocellular carcinoma. *Cancer Immunology, Immunotherapy*, *67*(8), 1305–1315. https://doi.org/10.1007/s00262-018-2190-4
14. Burgess, M. R., Eugene Hwang, Mroue, R., Bielski, C. M., Wandler, A. M., Huang, B., … Kevin Shannon. (2017). KRAS Allelic Imbalance Enhances Fitness and Modulates MAP Kinase Dependence In Cancer. *Physiology & Behavior*, *176*(3), 139–148. https://doi.org/10.1016/j.cell.2017.01.020.KRAS
15. Canon, J., Rex, K., Saiki, A. Y., Mohr, C., Cooke, K., Bagal, D., … Lipford, J. R. (2019). The clinical KRAS(G12C) inhibitor AMG 510 drives anti-tumour immunity. *Nature*, *575*(7781), 217–223. https://doi.org/10.1038/s41586-019-1694-1

16. Carvalho, P. D., Guimarães, C. F., Cardoso, A. P., Mendonça, S., Costa, Â. M., Oliveira, M. J., & Velho, S. (2018). KRAS oncogenic signaling extends beyond cancer cells to orchestrate the microenvironment. *Cancer Research*, *78*(1), 7–14. https://doi.org/10.1158/0008-5472.CAN-17-2084
17. Castillo, J., Erroba, E., Perugorría, M. J., Santamaría, M., Lee, D. C., Prieto, J., … Berasain, C. (2006). Amphiregulin contributes to the transformed phenotype of human hepatocellular carcinoma cells. *Cancer Research*, *66*(12), 6129–6138. https://doi.org/10.1158/0008-5472.CAN-06-0404
18. Cauwels, A., Van Lint, S., Paul, F., Garcin, G., De Koker, S., Van Parys, A., … Tavernier, J. (2018). Delivering type i interferon to dendritic cells empowers tumor eradication and immune combination treatments. *Cancer Research*, *78*(2), 463–474. https://doi.org/10.1158/0008-5472.CAN-17-1980
19. Census and Statistics Department. (2022). Liver Cancer.
20. Cerami, E., Gao, J., Dogrusoz, U., Gross, B. E., & Sumer, O. S. (2012). The cBio Cancer Genomics Portal: An Open Platform for Exploring Multidimensional Cancer Genomics Data. *Cancer Discov.*, *2*(5), 1–7. https://doi.org/10.1158/2159-8290.CD-12-0095.The
21. Chang, C. H., Hammer, J., Loh, J. E., Fodor, W. L., & Flavell, R. A. (1992). The activation of major histocompatibility complex class I genes by interferon regulatory factor-1 (IRF-1). *Immunogenetics*, *35*(6), 378–384. https://doi.org/10.1007/BF00179793
22. Chauvin, J. M., & Zarour, H. M. (2020). TIGIT in cancer immunotherapy. *Journal for ImmunoTherapy of Cancer*, *8*(2), 1–7. https://doi.org/10.1136/jitc-2020-000957
23. Chen, D. S., & Mellman, I. (2013). Oncology meets immunology: The cancer-immunity cycle. *Immunity*, *39*(1), 1–10. https://doi.org/10.1016/j.immuni.2013.07.012
24. Chen, D. S., & Mellman, I. (2017). Elements of cancer immunity and the cancer-immune set point. *Nature*, *541*(7637), 321–330. https://doi.org/10.1038/nature21349
25. Chen, J., Ji, T., Zhao, J., Li, G., Zhang, J., Jin, R., … Cai, X. (2016). Sorafenib-resistant hepatocellular carcinoma stratified by phosphorylated ERK activates PD-1 immune checkpoint. *Oncotarget*, *7*(27), 41274–41284. https://doi.org/10.18632/oncotarget.8978
26. Chen, N., Fang, W., Lin, Z., Peng, P., Wang, J., Zhan, J., … Zhang, L. (2017). KRAS mutation-induced upregulation of PD-L1 mediates immune escape in human lung adenocarcinoma. *Cancer Immunology, Immunotherapy*, *66*(9), 1175–1187. https://doi.org/10.1007/s00262-017-2005-z
27. Cheng, Y. H., Ko, Y. C., Ku, H. J., Huang, C. C., Yao, Y. C., Liao, Y. T., … Huang, L. R. (2022). Novel Paired Cell Lines for the Study of Lipid Metabolism and Cancer Stemness of Hepatocellular Carcinoma. *Frontiers in Cell and Developmental Biology*, *10*(May), 1–16. https://doi.org/10.3389/fcell.2022.821224
28. Chiu, D. K. C., Yuen, V. W. H., Cheu, J. W. S., Wei, L. L., Ting, V., Fehlings, M., … Wong, C. C. L. (2020). Hepatocellular Carcinoma Cells Up-regulate PVRL1, Stabilizing PVR and Inhibiting the Cytotoxic T-Cell Response via TIGIT to Mediate Tumor Resistance to PD1 Inhibitors in Mice. *Gastroenterology*, *159*(2), 609–623. https://doi.org/10.1053/j.gastro.2020.03.074
29. Choi, H., Deng, J., Li, S., Silk, T., Dong, L., Brea, E. J., … Wolchok, J. D. (2019). Pulsatile MEK Inhibition Improves Anti-tumor Immunity and T Cell Function in Murine Kras Mutant Lung Cancer. *Cell Reports*, *27*(3), 806-819.e5. https://doi.org/10.1016/j.celrep.2019.03.066
30. Coelho, M. A., de Carné Trécesson, S., Rana, S., Zecchin, D., Moore, C., Molina-Arcas, M., … Downward, J. (2017). Oncogenic RAS Signaling Promotes Tumor Immunoresistance by Stabilizing PD-L1 mRNA. *Immunity*, *47*(6), 1083-1099.e6. https://doi.org/10.1016/j.immuni.2017.11.016
31. Cong, L., Ran, F. A., Cox, D., Lin, S., Barretto, R., Habib, N., … Zhang, F. (2013).

Multiplex genome engineering using CRISPR/Cas systems. *Science*, *339*(6121), 819–823. https://doi.org/10.1126/science.1231143
32. Corcoran, R. B. (2023). A single inhibitor for all KRAS mutations. *Nature Cancer*, *4*(8), 1060–1062. https://doi.org/10.1038/s43018-023-00615-x
33. Cox, A. D., Fesik, S. W., Kimmelman, A. C., Luo, J., & Der, C. J. (2014). Drugging the undruggable RAS: Mission Possible? *Nature Reviews Drug Discovery*, *13*(11), 828–851. https://doi.org/10.1038/nrd4389
34. Cremer, I., Ghysdael, J., & Vieillard, V. (2002). A non-classical ISRE/ISGF3 pathway mediates induction of RANTES gene transcription by type I IFNs. *FEBS Letters*, *511*(1–3), 41–45. https://doi.org/10.1016/S0014-5793(01)03276-8
35. de Galarreta, M. R., Bresnahan, E., Molina-Sánchez, P., Lindblad, K. E., Maier, B., Sia, D., … Lujambio, A. (2019). β-catenin activation promotes immune escape and resistance to anti–PD-1 therapy in hepatocellular carcinoma. *Cancer Discovery*, *9*(8), 1124–1141. https://doi.org/10.1158/2159-8290.CD-19-0074
36. Degirmenci, U., Wang, M., & Hu, J. (2020). Targeting Aberrant RAS/RAF/MEK/ERK Signaling for Cancer Therapy. *Cells*, *9*, 1–33.
37. Denkert, C., Loibl, S., Noske, A., Roller, M., Müller, B. M., Komor, M., … Von Minckwitz, G. (2010). Tumor-associated lymphocytes as an independent predictor of response to neoadjuvant chemotherapy in breast cancer. *Journal of Clinical Oncology*, *28*(1), 105–113. https://doi.org/10.1200/JCO.2009.23.7370
38. Dietrich, P., Koch, A., Fritz, V., Hartmann, A., Bosserhoff, A. K., & Hellerbrand, C. (2018). Wild type Kirsten rat sarcoma is a novel microRNA- 622-regulated therapeutic target for hepatocellular carcinoma and contributes to sorafenib resistance. *Gut*, *67*(7), 1328–1341. https://doi.org/10.1136/gutjnl-2017-315402
39. Doench, J. G., Fusi, N., Sullender, M., Hegde, M., Vaimberg, E. W., Donovan, K. F., … Root, D. E. (2016). Optimized sgRNA design to maximize activity and minimize off-target effects of CRISPR-Cas9. *Nature Biotechnology*, *34*(2), 184–191. https://doi.org/10.1038/nbt.3437
40. Dong, H., & Bullock, T. N. J. (2014). Metabolic influences that regulate dendritic cell function in tumors. *Frontiers in Immunology*, *5*(JAN), 1–7. https://doi.org/10.3389/fimmu.2014.00024
41. Dong, L., Peng, L., Ma, L. jie, Liu, D. bing, Zhang, S., Luo, S. zhen, … Gao, Q. (2020). Heterogeneous immunogenomic features and distinct escape mechanisms in multifocal hepatocellular carcinoma. *Journal of Hepatology*, *72*(5), 896–908. https://doi.org/10.1016/j.jhep.2019.12.014
42. Dong, N., Shi, X., Wang, S., Gao, Y., Kuang, Z., Xie, Q., … Li, J. L. (2019). M2 macrophages mediate sorafenib resistance by secreting HGF in a feed-forward manner in hepatocellular carcinoma. *British Journal of Cancer*, *121*(1), 22–33. https://doi.org/10.1038/s41416-019-0482-x
43. Dong, Z. Y., Zhong, W. Z., Zhang, X. C., Su, J., Xie, Z., Liu, S. Y., … Wu, Y. L. (2017). Potential predictive value of TP53 and KRAS mutation status for response to PD-1 blockade immunotherapy in lung adenocarcinoma. *Clinical Cancer Research*, *23*(12), 3012–3024. https://doi.org/10.1158/1078-0432.CCR-16-2554
44. DuPage, M., Cheung, A. F., Mazumdar, C., Winslow, M. M., Bronson, R., Schmidt, L. M., … Jacks, T. (2011). Endogenous T cell responses to antigens expressed in lung adenocarcinomas delay malignant tumor progression. *Cancer Cell*, *19*(1), 72–85. https://doi.org/10.1016/j.ccr.2010.11.011
45. Dupage, M., Mazumdar, C., Schmidt, L. M., Cheung, A. F., & Jacks, T. (2012). Expression of tumour-specific antigens underlies cancer immunoediting. *Nature*, *482*(7385), 405–409. https://doi.org/10.1038/nature10803

46. El-Jawhari, J. J., El-Sherbiny, Y. M., Scott, G. B., Morgan, R. S. M., Prestwich, R., Bowles, P. A., … Cook, G. P. (2013). Blocking oncogenic RAS enhances tumour cell surface MHC class I expression but does not alter susceptibility to cytotoxic lymphocytes. *Molecular Immunology*, *58*(2), 160–168. https://doi.org/10.1016/j.molimm.2013.11.020
47. El-Serag, H. B. (2012). Epidemiology of Viral Hepatitis and Hepatocellular Carcinoma. *Gastroenterology.*, *142*(6), 71–97. https://doi.org/10.1142/9789814299794_0003
48. Elcheva, I. A., Gowda, C. P., Bogush, D., Gornostaeva, S., Fakhardo, A., Sheth, N., … Spiegelman, V. S. (2023). IGF2BP family of RNA-binding proteins regulate innate and adaptive immune responses in cancer cells and tumor microenvironment. *Frontiers in Immunology*, *14*(July), 1224516. https://doi.org/10.3389/fimmu.2023.1224516
49. Feng, X. C., Liu, F. C., Chen, W. Y., Du, J., & Liu, H. (2023). Lipid metabolism of hepatocellular carcinoma impacts targeted therapy and immunotherapy. *World Journal of Gastrointestinal Oncology*, *15*(4), 617–631. https://doi.org/10.4251/wjgo.v15.i4.617
50. Fenton, S. E., Saleiro, D., & Platanias, L. C. (2021). Type i and ii interferons in the anti-tumor immune response. *Cancers*, *13*(5), 1–19. https://doi.org/10.3390/cancers13051037
51. Finn, R. S., Qin, S., Ikeda, M., Galle, P. R., Ducreux, M., Kim, T.-Y., … Cheng, A.-L. (2020). Atezolizumab plus Bevacizumab in Unresectable Hepatocellular Carcinoma. *New England Journal of Medicine*, *382*(20), 1894–1905. https://doi.org/10.1056/nejmoa1915745
52. Flecken, T., Schmidt, N., Hild, S., Gostick, E., Drognitz, O., Zeiser, R., … Thimme, R. (2014). Immunodominance and functional alterations of tumor-associated antigen-specific CD8+ T-cell responses in hepatocellular carcinoma. *Hepatology*, *59*(4), 1415–1426. https://doi.org/10.1002/hep.26731
53. Forero, A., Ozarkar, S., Li, H., Lee, C. H., Hemann, E. A., Nadjsombati, M. S., … Savan, R. (2019). Differential Activation of the Transcription Factor IRF1 Underlies the Distinct Immune Responses Elicited by Type I and Type III Interferons. *Immunity*, *51*(3), 451-464.e6. https://doi.org/10.1016/j.immuni.2019.07.007
54. Franklin, D. A., James, J. L., Axelrod, M. L., & Balko, J. M. (2020). MEK inhibition activates STAT signaling to increase breast cancer immunogenicity via MHC-I expression. *Cancer Drug Resistance*, *3*(3), 603–612. https://doi.org/10.20517/cdr.2019.109
55. Freed-Pastor, W. A., Lambert, L. J., Ely, Z. A., Pattada, N. B., Bhutkar, A., Eng, G., … Jacks, T. (2021). The CD155/TIGIT axis promotes and maintains immune evasion in neoantigen-expressing pancreatic cancer. *Cancer Cell*, *39*(10), 1342-1360.e14. https://doi.org/10.1016/j.ccell.2021.07.007
56. Fu, X. T., Song, K., Zhou, J., Shi, Y. H., Liu, W. R., Shi, G. M., … Fan, J. (2019). Tumor-associated macrophages modulate resistance to oxaliplatin via inducing autophagy in hepatocellular carcinoma. *Cancer Cell International*, *19*(1), 1–11. https://doi.org/10.1186/s12935-019-0771-8
57. Gaj, T., Guo, J., Kato, Y., Sirk, S. J., & Barbas Iii, C. F. (2013). Targeted gene knockout by direct delivery of ZFN proteins HHS Public Access. *Nat Methods*, *9*(8), 805–807. https://doi.org/10.1038/nmeth.2030.Targeted
58. Gallage, S., García-Beccaria, M., Szydlowska, M., Rahbari, M., Mohr, R., Tacke, F., & Heikenwalder, M. (2021). The therapeutic landscape of hepatocellular carcinoma. *Med*, *2*(5), 505–552. https://doi.org/10.1016/j.medj.2021.03.002
59. Gao, Qiang, Wang, X. Y., Qiu, S. J., Yamato, I., Sho, M., Nakajima, Y., … Fan, J. (2009). Overexpression of PD-L1 significantly associates with tumor aggressiveness and postoperative recurrence in human hepatocellular carcinoma. *Clinical Cancer Research*, *15*(3), 971–979. https://doi.org/10.1158/1078-0432.CCR-08-1608
60. Gao, Qun, Wang, S., Chen, X., Cheng, S., Zhang, Z., Li, F., … Zhang, Y. (2019). Cancer-cell-secreted CXCL11 promoted CD8 + T cells infiltration through docetaxel-induced-

release of HMGB1 in NSCLC. *Journal for ImmunoTherapy of Cancer*, *7*(1), 1–17. https://doi.org/10.1186/s40425-019-0511-6
61. Garrido, F., Romero, I., Aptsiauri, N., & Garcia-Lora, A. M. (2016). Generation of MHC class i diversity in primary tumors and selection of the malignant phenotype. *International Journal of Cancer*, *138*(2), 271–280. https://doi.org/10.1002/ijc.29375
62. Garris, C. S., Arlauckas, S. P., Kohler, R. H., Trefny, M. P., Garren, S., Piot, C., … Pittet, M. J. (2018). Successful Anti-PD-1 Cancer Immunotherapy Requires T Cell-Dendritic Cell Crosstalk Involving the Cytokines IFN-γ and IL-12. *Immunity*, *49*(6), 1148-1161.e7. https://doi.org/10.1016/j.immuni.2018.09.024
63. Gessani, S., Conti, L., Del Cornò, M., & Belardelli, F. (2014). Type I interferons as regulators of human antigen presenting cell functions. *Toxins*, *6*(6), 1696–1723. https://doi.org/10.3390/toxins6061696
64. Gettinger, S., Choi, J., Hastings, K., Truini, A., Datar, I., Sowell, R., … Politi, K. (2017). Impaired HLA class I antigen processing and presentation as a mechanism of acquired resistance to immune checkpoint inhibitors in lung cancer. *Cancer Discovery*, *7*(12), 1420–1435. https://doi.org/10.1158/2159-8290.CD-17-0593
65. Ghafouri-Fard, S., Shirvani-Farsani, Z., Hussen, B. M., Taheri, M., & Jalili Khoshnoud, R. (2022). Emerging role of non-coding RNAs in the regulation of KRAS. *Cancer Cell International*, *22*(1), 1–15. https://doi.org/10.1186/s12935-022-02486-1
66. Glorieux, C., Xia, X., He, Y. Q., Hu, Y., Cremer, K., Robert, A., … Huang, P. (2021). Regulation of PD-L1 expression in K-ras-driven cancers through ROS-mediated FGFR1 signaling. *Redox Biology*, *38*, 101780. https://doi.org/10.1016/j.redox.2020.101780
67. Golabi, P., Fazel, S., Otgonsuren, M., Sayiner, M., Locklear, C. T., & Younossi, Z. M. (2017). Mortality assessment of patients with hepatocellular carcinoma according to underlying disease and treatment modalities. *Medicine (United States)*, *96*(9). https://doi.org/10.1097/MD.0000000000005904
68. Goswami, S., Sahai, E., Wyckoff, J. B., Cammer, M., Cox, D., Pixley, F. J., … Condeelis, J. S. (2005). Erratum: Macrophages promote the invasion of breast carcinoma cells via a colony-stimulating factor-1/epidermal growth factor paracrine loop (Cancer Research (June 15, 2005) 65 (5278-5283)). *Cancer Research*, *65*(15), 7031. https://doi.org/10.1158/0008-5472.CAN-65-15-COR
69. Gu, C. Y., & Lee, T. K. W. (2022). Preclinical mouse models of hepatocellular carcinoma: An overview and update. *Experimental Cell Research*, *412*(2). https://doi.org/10.1016/j.yexcr.2022.113042
70. Hallberg, B., Rayter, S. I., & Downward, J. (1994). Interaction of Ras and Raf in intact mammalian cells upon extracellular stimulation. *Journal of Biological Chemistry*, *269*(6), 3913–3916. https://doi.org/10.1016/s0021-9258(17)41718-2
71. Hallin, J., Engstrom, L. D., Hargi, L., Calinisan, A., Aranda, R., Briere, D. M., … Christensen, J. G. (2020). The KRASG12C inhibitor MRTX849 provides insight toward therapeutic susceptibility of KRAS-mutant cancers in mouse models and patients. *Cancer Discovery*, *10*(1), 54–71. https://doi.org/10.1158/2159-8290.CD-19-1167
72. Harding, J. J., Nandakumar, S., Armenia, J., Khalil, D. N., Albano, M., Ly, M., … Abou-Alfa, G. K. (2019). Prospective genotyping of hepatocellular carcinoma: Clinical implications of next-generation sequencing for matching patients to targeted and immune therapies. *Clinical Cancer Research*, *25*(7), 2116–2126. https://doi.org/10.1158/1078-0432.CCR-18-2293
73. Herber, D. L., Cao, W., Nefedova, Y., Novitskiy, S. V., Nagaraj, S., Tyurin, V. A., … Gabrilovich, D. I. (2010). Lipid accumulation and dendritic cell dysfunction in cancer. *Nature Medicine*, *16*(8), 880–886. https://doi.org/10.1038/nm.2172
74. Hong, D. S., Fakih, M. G., Strickler, J. H., Desai, J., Durm, G. A., Shapiro, G. I., … Kuboki,

Y. (2020). KRASG12C Inhibition with Sotorasib in Advanced Solid Tumors. *N Engl J Med.*, *383*(13), 1207–1217. https://doi.org/10.1056/NEJMoa1917239
75. Hosoda, S., Suda, G., Sho, T., Ogawa, K., Kimura, M., Yang, Z., … Sakamoto, N. (2023). Low Baseline CXCL9 Predicts Early Progressive Disease in Unresectable HCC with Atezolizumab Plus Bevacizumab Treatment. *Liver Cancer*, *12*(2), 156–170. https://doi.org/10.1159/000527759
76. Houde, N., Beuret, L., Bonaud, A., Fortier-Beaulieu, S. P., Truchon-Landry, K., Aoidi, R., … Charron, J. (2022). Fine-tuning of MEK signaling is pivotal for limiting B and T cell activation. *Cell Reports*, *38*(2). https://doi.org/10.1016/j.celrep.2021.110223
77. Huang, D. Q., El-Serag, H. B., & Loomba, R. (2021). Global epidemiology of NAFLD-related HCC: trends, predictions, risk factors and prevention. *Nat Rev Gastroenterol Hepatol*, *18*(4), 223–238. https://doi.org/10.1038/s41575-020-00381-6.Global
78. Huang, L., Guo, Z., Wang, F., & Fu, L. (2021). KRAS mutation: from undruggable to druggable in cancer. *Signal Transduction and Targeted Therapy*, *6*(1), 1–20. https://doi.org/10.1038/s41392-021-00780-4
79. Hulseberg, P. D., Zozulya, A., Chu, H. H., Triccas, J. A., Fabry, Z., & Sandor, M. (2010). The same well-characterized T cell epitope SIINFEKL expressed in the context of a cytoplasmic or secreted protein in BCG induces different CD8+ T cell responses. *Immunology Letters*, *130*(1–2), 36–42. https://doi.org/10.1016/j.imlet.2009.12.004
80. Ibrahim, J., Nguyen, A. H., Rehman, A., Ochi, A., Jamal, M., Graffeo, C. S., … Miller, G. (2012). Dendritic cell populations with different concentrations of lipid regulate tolerance and immunity in mouse and human liver. *Gastroenterology*, *143*(4), 1061–1072. https://doi.org/10.1053/j.gastro.2012.06.003
81. International Agency for Research on Cancer, W. (2022). Global Cancer Observatory. Retrieved from https://gco.iarc.fr/today/online-analysismap?v=2020&mode=population&mode_population=continents&population=900&populations=900&key=total&sex=0&cancer=39&type=1&statistic=5&prevalence=0&population_group=0&ages_group%5B%5D=17&nb_items=10&group_cancer=1&inclu
82. Ishikura, N., Sugimoto, M., Yorozu, K., Kurasawa, M., & Kondoh, O. (2022). Anti-VEGF antibody triggers the effect of anti-PD-L1 antibody in PD-L1low and immune desert-like mouse tumors. *Oncology Reports*, *47*(2), 1–10. https://doi.org/10.3892/or.2021.8247
83. Ito, Y., Takeda, T., Sakon, M., Tsujimoto, M., Higashiyama, S., Noda, K., … Matsuura, N. (2001). Expression and clinical significance of erb-B receptor family in hepatocellular carcinoma. *British Journal of Cancer*, *84*(10), 1377–1383. https://doi.org/10.1054/bjoc.2000.1580
84. Iwai, T., Sugimoto, M., Patil, N. S., Bower, D., Suzuki, M., Kato, C., … Kondoh, O. (2021). Both T cell priming in lymph node and CXCR3-dependent migration are the key events for predicting the response of atezolizumab. *Scientific Reports*, *11*(1), 13912. https://doi.org/10.1038/s41598-021-93113-y
85. Jhunjhunwala, S., Hammer, C., & Delamarre, L. (2021). Antigen presentation in cancer: insights into tumour immunogenicity and immune evasion. *Nature Reviews Cancer*, *21*(5), 298–312. https://doi.org/10.1038/s41568-021-00339-z
86. Jiang, D. K., Sun, J., Cao, G., Liu, Y., Lin, D., Gao, Y. Z., … Yu, L. (2013). Genetic variants in STAT4 and HLA-DQ genes confer risk of hepatitis B virus-related hepatocellular carcinoma. *Nature Genetics*, *45*(1), 72–75. https://doi.org/10.1038/ng.2483
87. Jilg, N., Lin, W., Hong, J., Schaefer, E. A., Wolski, D., Meixong, J., … Chevaliez, S. (2014). Kinetic Differences in the Induction of Interferon Stimulated Genes by Interferon-α and IL28B are altered by Infection with Hepatitis C Virus. *Hepatology*, *59*(4), 1250–1261. https://doi.org/10.1002/hep.26653.
88. Jongsma, M. L. M., Neefjes, J., & Spaapen, R. M. (2021). Playing hide and seek: Tumor

cells in control of MHC class I antigen presentation. *Molecular Immunology*, *136*(April), 36–44. https://doi.org/10.1016/j.molimm.2021.05.009
89. Kan, Z., Zheng, H., Liu, X., Li, S., Barber, T. D., Gong, Z., … Mao, M. (2013). Whole-genome sequencing identifies recurrent mutations in hepatocellular carcinoma. *Genome Research*, *23*(9), 1422–1433. https://doi.org/10.1101/gr.154492.113
90. Kanwal, F., Kramer, J., Asch, S. M., Chayanupatkul, M., Cao, Y., & El-Serag, H. B. (2017). Risk of Hepatocellular Cancer in HCV Patients Treated With Direct-Acting Antiviral Agents. *Gastroenterology*, *153*(4), 996-1005.e1. https://doi.org/10.1053/j.gastro.2017.06.012
91. Kaplan, D. H., Shankaran, V., Dighe, A. S., Stockert, E., Aguet, M., Old, L. J., & Schreiber, R. D. (1998). Demonstration of an interferon γ-dependent tumor surveillance system in immunocompetent mice. *Proceedings of the National Academy of Sciences of the United States of America*, *95*(13), 7556–7561. https://doi.org/10.1073/pnas.95.13.7556
92. Kawate, S., Fukusato, T., Ohwada, S., Akira, M., & Yasuo, W. (1999). Amplification of c-myc in Hepatocellular Carcinoma: Correlation with Clinicopathologic Features, Proliferative Activity and p53 Overexpression. *Oncology*, *57*(2), 157–163. https://doi.org/10.1159/000012024
93. Keenan, T. E., Burke, K. P., & Van Allen, E. M. (2019). Genomic correlates of response to immune checkpoint blockade. *Nature Medicine*, *25*(3), 389–402. https://doi.org/10.1038/s41591-019-0382-x
94. Kemp, S. B., Cheng, N., Markosyan, N., Sor, R., Kim, I. K., Hallin, J., … Stanger, B. Z. (2023). Efficacy of a Small-Molecule Inhibitor of KrasG12D in Immunocompetent Models of Pancreatic Cancer. *Cancer Discovery*, *13*(2), 298–311. https://doi.org/10.1158/2159-8290.CD-22-1066
95. Kessler, D., Gmachl, M., Mantoulidis, A., Martin, L. J., Zoephel, A., Mayer, M., … McConnell, D. B. (2019). Drugging an undruggable pocket on KRAS. *Proceedings of the National Academy of Sciences of the United States of America*, *116*(32), 15823–15829. https://doi.org/10.1073/pnas.1904529116
96. Ketcham, J. M., Haling, J., Khare, S., Bowcut, V., Briere, D. M., Burns, A. C., … Marx, M. A. (2022). Design and Discovery of MRTX0902, a Potent, Selective, Brain-Penetrant, and Orally Bioavailable Inhibitor of the SOS1:KRAS Protein-Protein Interaction. *Journal of Medicinal Chemistry*, *65*(14), 9678–9690. https://doi.org/10.1021/acs.jmedchem.2c00741
97. Ketcham, J. M., Khare, S., Sudhakar, N., Briere, D. M., Yan, L., Laguer, J., … Haling, J. R. (2022). Abstract ND02: MRTX0902: A SOS1 inhibitor for therapeutic intervention of KRAS-driven cancers. *Cancer Research*, *82*(12_Supplement).
98. Khare, S., Sudhakar, N., Laguer, J., Briere, D. M., Yan, L., Hebbert, A., … Haling, J. R. (2023). Abstract 3499: Inhibition of SOS1 by MRTX0902 augments the anti-tumor response of the targeted EGFR inhibitor osimertinib in NSCLC. *Cancer Res*, *87*(7_Supplement), 3499. Retrieved from https://doi.org/10.1158/1538-7445.AM2023-3499
99. Kim, C. G., Kim, C., Yoon, S. E., Kim, K. H., Choi, S. J., Kang, B., … Lim, H. Y. (2021). Hyperprogressive disease during PD-1 blockade in patients with advanced hepatocellular carcinoma. *Journal of Hepatology*, *74*(2), 350–359. https://doi.org/10.1016/j.jhep.2020.08.010
100. Kim, D., Herdeis, L., Rudolph, D., Zhao, Y., Böttcher, J., Vides, A., … Lito, P. (2023). Pan-KRAS inhibitor disables oncogenic signalling and tumour growth. *Nature*, *619*(7968), 160–166. https://doi.org/10.1038/s41586-023-06123-3
101. Klampfer, L., Huang, J., Corner, G., Mariadason, J., Arango, D., Sasazuki, T., … Augenlicht, L. (2003). Oncogenic Ki-Ras Inhibits the Expression of Interferon-responsive

Genes through Inhibition of STAT1 and STAT2 Expression. *Journal of Biological Chemistry*, *278*(47), 46278–46287. https://doi.org/10.1074/jbc.M304721200
102. Kohli, K., Pillarisetty, V. G., & Kim, T. S. (2022). Key chemokines direct migration of immune cells in solid tumors. *Cancer Gene Therapy*, *29*(1), 10–21. https://doi.org/10.1038/s41417-021-00303-x
103. Kortlever, R. M., Sodir, N. M., Wilson, C. H., Burkhart, D. L., Pellegrinet, L., Brown Swigart, L., … Evan, G. I. (2017). Myc Cooperates with Ras by Programming Inflammation and Immune Suppression. *Cell*, *171*(6), 1301-1315.e14. https://doi.org/10.1016/j.cell.2017.11.013
104. Kriegsman, B. A., Vangala, P., Chen, B. J., Meraner, P., Brass, A. L., Garber, M., & Rock, K. L. (2019). Frequent Loss of IRF2 in Cancers Leads to Immune Evasion through Decreased MHC Class I Antigen Presentation and Increased PD-L1 Expression. *The Journal of Immunology*, *203*(7), 1999–2010. https://doi.org/10.4049/jimmunol.1900475
105. Kudo, M. (2022). Combination Immunotherapy with Anti-PD-1/PD-L1 Antibody plus Anti-VEGF Antibody May Promote Cytotoxic T Lymphocyte Infiltration in Hepatocellular Carcinoma, Including in the Noninflamed Subclass. *Liver Cancer*, *11*(3), 185–191. https://doi.org/10.1159/000524977
106. Kurebayashi, Y., Ojima, H., Tsujikawa, H., Kubota, N., Maehara, J., Abe, Y., … Sakamoto, M. (2018). Landscape of immune microenvironment in hepatocellular carcinoma and its additional impact on histological and molecular classification. *Hepatology*, *68*(3), 1025–1041. https://doi.org/10.1002/hep.29904
107. Lacaze, L., & Scotté, M. (2015). Surgical treatment of intra hepatic recurrence of hepatocellular carcinoma. *World Journal of Hepatology*, *7*(13), 1755–1760. https://doi.org/10.4254/wjh.v7.i13.1755
108. Lal, N., White, B. S., Goussous, G., Pickles, O., Mason, M. J., Beggs, A. D., … Middleton, G. W. (2018). KRAS mutation and consensus molecular subtypes 2 and 3 are independently associated with reduced immune infiltration and reactivity in colorectal cancer. *Clinical Cancer Research*, *24*(1), 224–233. https://doi.org/10.1158/1078-0432.CCR-17-1090
109. Lauko, A., Kotecha, R., Barnett, A., Li, H., Tatineni, V., Ali, A., … Ahluwalia, M. S. (2021). Impact of KRAS mutation status on the efficacy of immunotherapy in lung cancer brain metastases. *Scientific Reports*, *11*(1), 1–8. https://doi.org/10.1038/s41598-021-97566-z
110. Lee, J. H., Shklovskaya, E., Lim, S. Y., Carlino, M. S., Menzies, A. M., Stewart, A., … Rizos, H. (2020). Transcriptional downregulation of MHC class I and melanoma de-differentiation in resistance to PD-1 inhibition. *Nature Communications*, *11*(1), 1–12. https://doi.org/10.1038/s41467-020-15726-7
111. Lei, W. Y., Hsiung, S. C., Wen, S. H., Hsieh, C. H., Chen, C. L., Wallace, C. G., … Liao, S. K. (2018). Total HLA class I antigen loss with the downregulation of antigen-processing machinery components in two newly established sarcomatoid hepatocellular carcinoma cell lines. *Journal of Immunology Research*, *2018*. https://doi.org/10.1155/2018/8363265
112. Leonardi, G. C., Candido, S., Cervello, M., Nicolosi, D., Raiti, F., Travali, S., … Libra, M. (2012). The tumor microenvironment in hepatocellular carcinoma. *International Journal of Oncology*, *40*(6), 1733–1747. https://doi.org/10.3892/ijo.2012.1408
113. Leone, P., Shin, E. C., Perosa, F., Vacca, A., Dammacco, F., & Racanelli, V. (2013). MHC class i antigen processing and presenting machinery: Organization, function, and defects in tumor cells. *Journal of the National Cancer Institute*, *105*(16), 1172–1187. https://doi.org/10.1093/jnci/djt184
114. Li, N., Wang, J., Zhang, N., Zhuang, M., Zong, Z., Zou, J., … Shi, Y. (2018). Cross-

talk between TNF-α and IFN-γ signaling in induction of B7-H1 expression in hepatocellular carcinoma cells. *Cancer Immunology, Immunotherapy*, *67*(2), 271–283. https://doi.org/10.1007/s00262-017-2086-8
115. Li, Y., Li, F., Bai, X., Li, Y., Ni, C., Zhao, X., & Zhang, D. (2021). ITGA3 Is Associated With Immune Cell Infiltration and Serves as a Favorable Prognostic Biomarker for Breast Cancer. *Frontiers in Oncology*, *11*(May), 1–16. https://doi.org/10.3389/fonc.2021.658547
116. Liao, W., Overman, M. J., Boutin, A. T., Shang, X., Zhao, D., Dey, P., … DePinho, R. A. (2020). KRAS-IRF2 axis drives immune suppression and immune therapy resistance in colorectal cancer, *38*(2), 279–296. https://doi.org/10.1016/j.ccell.2019.02.008.KRAS-IRF2
117. Lin, C. L., & Kao, J. H. (2021). Prevention of hepatitis b virus-related hepatocellular carcinoma. *Hepatoma Research*, *7*. https://doi.org/10.20517/2394-5079.2020.125
118. Litchfield, K., Reading, J. L., Puttick, C., Thakkar, K., Abbosh, C., Bentham, R., … Swanton, C. (2021). Meta-analysis of tumor- and T cell-intrinsic mechanisms of sensitization to checkpoint inhibition. *Cell*, *184*(3), 596-614.e14. https://doi.org/10.1016/j.cell.2021.01.002
119. Liu, H., Liang, Z., Cheng, S., Huang, L., Li, W., Zhou, C., … Kang, L. (2023). Mutant KRAS Drives Immune Evasion by Sensitizing Cytotoxic T-Cells to Activation-Induced Cell Death in Colorectal Cancer. *Advanced Science*, *10*(6), 1–15. https://doi.org/10.1002/advs.202203757
120. Liu, L., Mayes, P. A., Eastman, S., Shi, H., Yadavilli, S., Zhang, T., … Hoos, A. (2015). The BRAF and MEK inhibitors dabrafenib and trametinib: Effects on immune function and in combination with immunomodulatory antibodies targeting PD-1, PD-L1, and CTLA-4. *Clinical Cancer Research*, *21*(7), 1639–1651. https://doi.org/10.1158/1078-0432.CCR-14-2339
121. Liu, M., Chen, S., Zhang, A., Zheng, Q., & Fu, J. (2021). Plaur as a potential biomarker associated with immune infiltration in bladder urothelial carcinoma. *Journal of Inflammation Research*, *14*(September), 4629–4641. https://doi.org/10.2147/JIR.S326559
122. Liu, P., Wang, Y., & Li, X. (2019). Targeting the untargetable KRAS in cancer therapy. *Acta Pharmaceutica Sinica B*, *9*(5), 871–879. https://doi.org/10.1016/j.apsb.2019.03.002
123. Liu, X. S., Yang, J. W., Zeng, J., Chen, X. Q., Gao, Y., Kui, X. Y., … Pei, Z. J. (2022). SLC2A1 is a Diagnostic Biomarker Involved in Immune Infiltration of Colorectal Cancer and Associated With m6A Modification and ceRNA. *Frontiers in Cell and Developmental Biology*, *10*(March), 1–18. https://doi.org/10.3389/fcell.2022.853596
124. Liu, Y. T., Tseng, T. C., Soong, R. S., Peng, C. Y., Cheng, Y. H., Huang, S. F., … Huang, L. R. (2018). A novel spontaneous hepatocellular carcinoma mouse model for studying T-cell exhaustion in the tumor microenvironment. *Journal for ImmunoTherapy of Cancer*, *6*(1), 1–14. https://doi.org/10.1186/s40425-018-0462-3
125. Liu, Z., Chen, D., Ning, F., Du, J., & Wang, H. (2018). EGF is highly expressed in hepatocellular carcinoma (HCC) and promotes motility of HCC cells via fibronectin. *Journal of Cellular Biochemistry*, *119*(5), 4170–4183. https://doi.org/10.1002/jcb.26625
126. Llovet, J. M., Kelley, R. K., Villanueva, A., Singal, A. G., Pikarsky, E., Roayaie, S., … Finn, R. S. (2021). Hepatocellular carcinoma. *Nature Reviews Disease Primers*, *7*(1). https://doi.org/10.1038/s41572-020-00240-3
127. Loi, S., Dushyanthen, S., Beavis, P. A., Salgado, R., Denkert, C., Savas, P., … Balko, J. M. (2016). RAS/ERK activation is associated with reduced tumor-infiltrating lymphocytes in triple-negative breast cancer: Therapeutic cooperation between MEK and PD-1/PD-L1 immune checkpoint inhibitors. *Clinical Cancer Research*, *22*(6), 1499–1509. https://doi.org/10.1158/1078-0432.CCR-15-1125
128. López, M. D. la F., Landskron, G., Parada, D., Dubois-Camacho, K., Simian, D.,

Martinez, M., … Hermoso-R, M. A. (2018). The relationship between chemokines CCL2, CCL3, and CCL4 with the tumor microenvironment and tumor-associated macrophage markers in colorectal cancer. *Tumor Biology*, *40*(11), 1–12. https://doi.org/10.1177/1010428318810059

129. Lorenzi, S., Forloni, M., Cifaldi, L., Antonucci, C., Citti, A., Boldrini, R., … Fruci, D. (2012). IRF1 and NF-kB Restore MHC Class I-Restricted Tumor Antigen Processing and Presentation to Cytotoxic T Cells in Aggressive Neuroblastoma. *PLoS ONE*, *7*(10), 1–8. https://doi.org/10.1371/journal.pone.0046928
130. Lu, L. G., Zhou, Z. L., Wang, X. Y., Liu, B. Y., Lu, J. Y., Liu, S., … Chen, Y. (2022). PD-L1 blockade liberates intrinsic antitumourigenic properties of glycolytic macrophages in hepatocellular carcinoma. *Gut*, 2551–2560. https://doi.org/10.1136/gutjnl-2021-326350
131. Ma, L., Hernandez, M. O., Zhao, Y., Mehta, M., Tran, B., Kelly, M., … Wang, X. W. (2019). Tumor Cell Biodiversity Drives Microenvironmental Reprogramming in Liver Cancer. *Cancer Cell*, *36*(4), 418-430.e6. https://doi.org/10.1016/j.ccell.2019.08.007
132. Makarova-Rusher, O. V., Medina-Echeverz, J., Duffy, A. G., & Greten, T. F. (2015). The yin and yang of evasion and immune activation in HCC. *Journal of Hepatology*, *62*(6), 1420–1429. https://doi.org/10.1016/j.jhep.2015.02.038
133. Malumbres, M., & Barbacid, M. (2003). RAS oncogenes: The first 30 years. *Nature Reviews Cancer*, *3*(6), 459–465. https://doi.org/10.1038/nrc1097
134. Martinelli, E., Morgillo, F., Troiani, T., & Ciardiello, F. (2017). Cancer resistance to therapies against the EGFR-RAS-RAF pathway: The role of MEK. *Cancer Treatment Reviews*, *53*, 61–69. https://doi.org/10.1016/j.ctrv.2016.12.001
135. Maurer, T., Garrenton, L. S., Oh, A., Pitts, K., Anderson, D. J., Skelton, N. J., … Fang, G. (2012). Small-molecule ligands bind to a distinct pocket in Ras and inhibit SOS-mediated nucleotide exchange activity. *Proceedings of the National Academy of Sciences of the United States of America*, *109*(14), 5299–5304. https://doi.org/10.1073/pnas.1116510109
136. McFarland, B. J., Sant, A. J., Lybrand, T. P., & Beeson, C. (1999). Ovalbumin(323-339) peptide binds to the major histocompatibility complex class II I-A(d) protein using two functionally distinct registers. *Biochemistry*, *38*(50), 16663–16670. https://doi.org/10.1021/bi9913931
137. Moeini, A., Torrecilla, S., Tovar, V., Montironi, C., Andreu-Oller, C., Peix, J., … Llovet, J. M. (2019). An Immune Gene Expression Signature Associated With Development of Human Hepatocellular Carcinoma Identifies Mice That Respond to Chemopreventive Agents. *Gastroenterology.*, *157*(5), 1383–1397. https://doi.org/10.1053/j.gastro.2019.07.028.An
138. Mohammadian, M., Mahdavifar, N., Mohammadian-Hafshejani, A., & Salehiniya, H. (2018). Liver cancer in the world: epidemiology, incidence, mortality and risk factors. *World Cancer Research Journal*, *5*(2), e1082. Retrieved from https://www.wcrj.net/wp-content/uploads/sites/5/2018/06/e1082-Liver-cancer-in-the-world-Epidemiology-incidence-mortality-and-risk-factors.pdf
139. Mohr, R., Jost-Brinkmann, F., Özdirik, B., Lambrecht, J., Hammerich, L., Loosen, S. H., … Roderburg, C. (2021). Lessons From Immune Checkpoint Inhibitor Trials in Hepatocellular Carcinoma. *Frontiers in Immunology*, *12*(March), 1–8. https://doi.org/10.3389/fimmu.2021.652172
140. Montironi, C., Castet, F., Haber, P. K., Pinyol, R., Torres-Martin, M., Torrens Fontanals, L., … Llovet, J. M. (2023). Inflamed and non-inflamed classes of HCC: a revised immunogenomic classification. *Gut*, *72*(1), 129–140. https://doi.org/10.1136/gutjnl-2021-325918
141. Moon, W. S., Park, H. S., Yu, K. H., Park, M. Y., Kim, K. R., Jang, K. Y., … Cho, B.

H. (2006). Expression of betacellulin and epidermal growth factor receptor in hepatocellular carcinoma: implications for angiogenesis. *Human Pathology*, *37*(10), 1324–1332. https://doi.org/10.1016/j.humpath.2006.04.022

142. Mugarza, E., van Maldegem, F., Boumelha, J., Moore, C., Rana, S., Sopena, M. L., … Downward, J. (2022). Therapeutic KRASG12C inhibition drives effective interferon-mediated antitumor immunity in immunogenic lung cancers. *Science Advances*, *8*(29). https://doi.org/10.1126/sciadv.abm8780
143. Muthalagu, N., Monteverde, T., Raffo-Iraolagoitia, X., Wiesheu, R., Whyte, D., Hedley, A., … Murphy, D. J. (2020). Repression of the type i interferon pathway underlies MYC- and KRAS-dependent evasion of NK and B cells in pancreatic ductal adenocarcinoma. *Cancer Discovery*, *10*(6), 872–887. https://doi.org/10.1158/2159-8290.CD-19-0620
144. Nakamura, K., Ichise, H., Nakao, K., Hatta, T., Otani, H., Sakagami, H., … Katsuki, M. (2008). Partial functional overlap of the three ras genes in mouse embryonic development. *Oncogene*, *27*(21), 2961–2968. https://doi.org/10.1038/sj.onc.1210956
145. Neel, N. F., Martin, T. D., Stratford, J. K., Zand, T. P., Reiner, D. J., & Der, C. J. (2011). The RalGEF-ral effector signaling network: The road less traveled for anti-ras drug discovery. *Genes and Cancer*, *2*(3), 275–287. https://doi.org/10.1177/1947601911407329
146. Nevzorova, Y. A., Hu, W., Cubero, F. J., Haas, U., Freimuth, J., Tacke, F., … Liedtke, C. (2013). Overexpression of c-myc in hepatocytes promotes activation of hepatic stellate cells and facilitates the onset of liver fibrosis. *Biochimica et Biophysica Acta - Molecular Basis of Disease*, *1832*(10), 1765–1775. https://doi.org/10.1016/j.bbadis.2013.06.001
147. Nguyen, P. H. D., Wasser, M., Tan, C. T., Lim, C. J., Lai, H. L. H., Seow, J. J. W., … Chew, V. (2022). Trajectory of immune evasion and cancer progression in hepatocellular carcinoma. *Nature Communications*, *13*(1), 1–13. https://doi.org/10.1038/s41467-022-29122-w
148. Ning, Y., Li, Y., & Wang, H. (2023). ANXA2 is a potential biomarker for cancer prognosis and immune infiltration: A systematic pan-cancer analysis. *Frontiers in Genetics*, *14*(January), 1–16. https://doi.org/10.3389/fgene.2023.1108167
149. Ogawa, K., Kanzaki, H., Chiba, T., Ao, J., Qiang, N., Ma, Y., … Kato, N. (2022). Effect of Atezolizumab plus Bevacizumab in Patients with Hepatocellular Carcinoma Harboring CTNNB1 Mutation in Early Clinical Experience. *Journal of Cancer*, *13*(8), 2656–2661. https://doi.org/10.7150/jca.71494
150. Ostrem, Jonathan M., Peters, U., Sos, M. L., Wells, J. A., & Shokat, K. M. (2013). K-Ras(G12C) inhibitors allosterically control GTP affinity and effector interactions. *Nature*, *503*(7477), 548–551. https://doi.org/10.1038/nature12796
151. Ostrem, Jonathan ML, & Shokat, K. M. (2016). Direct small-molecule inhibitors of KRAS: From structural insights to mechanism-based design. *Nature Reviews Drug Discovery*, *15*(11), 771–785. https://doi.org/10.1038/nrd.2016.139
152. Ozga, A. J., Chow, M. T., & Luster, A. D. (2021). Chemokines and the immune response to cancer. *Immunity*, *54*(5), 859–874. https://doi.org/10.1016/j.immuni.2021.01.012
153. Papke, B., & Der, C. J. (2017). Drugging RAS: Know the enemy. *Science*, *355*(6330), 1158–1163. https://doi.org/10.1126/science.aam7622
154. Paulson, K. G., Voillet, V., McAfee, M. S., Hunter, D. S., Wagener, F. D., Perdicchio, M., … Chapuis, A. G. (2018). Acquired cancer resistance to combination immunotherapy from transcriptional loss of class I HLA. *Nature Communications*, *9*(1). https://doi.org/10.1038/s41467-018-06300-3
155. Peng, W., Chen, J. Q., Liu, C., Malu, S., Creasy, C., Tetzlaff, M. T., … Hwu, P. (2016). Loss of PTEN promotes resistance to T cell–mediated immunotherapy. *Cancer Discovery*, *6*(2), 202–216. https://doi.org/10.1158/2159-8290.CD-15-0283

156. Petty, A. J., Dai, R., Lapalombella, R., Baiocchi, R. A., Benson, D. M., Li, Z., … Yang, Y. (2021). Hedgehog-induced PD-L1 on tumor-associated macrophages is critical for suppression of tumor-infiltrating CD8+ T cell function. *JCI Insight*, *6*(6). https://doi.org/10.1172/jci.insight.146707
157. Pfister, D., Núñez, N. G., Pinyol, R., Govaere, O., Pinter, M., Szydlowska, M., … Heikenwalder, M. (2021). *NASH limits anti-tumour surveillance in immunotherapy-treated HCC*. *Nature* (Vol. 592). https://doi.org/10.1038/s41586-021-03362-0
158. Pinyol, R., Sia, D., & Llovet, J. M. (2019). Immune exclusion-WNT/CTNNB1 class predicts resistance to immunotherapies in HCC. *Clinical Cancer Research*, *25*(7), 2021–2023. https://doi.org/10.1158/1078-0432.CCR-18-3778
159. Platanitis, E., Demiroz, D., Schneller, A., Fischer, K., Capelle, C., Hartl, M., … Decker, T. (2019). A molecular switch from STAT2-IRF9 to ISGF3 underlies interferon-induced gene transcription. *Nature Communications*, *10*(1), 1–17. https://doi.org/10.1038/s41467-019-10970-y
160. Prior, I. A., Hood, F. E., & Hartley, J. L. (2020). The frequency of ras mutations in cancer. *Cancer Research*, *80*(14), 2669–2974. https://doi.org/10.1158/0008-5472.CAN-19-3682
161. Pylayeva-Gupta, Y., Lee, K. E., Hajdu, C. H., Miller, G., & Bar-Sagi, D. (2012). Oncogenic Kras-Induced GM-CSF Production Promotes the Development of Pancreatic Neoplasia. *Cancer Cell*, *21*(6), 836–847. https://doi.org/10.1016/j.ccr.2012.04.024
162. Qiu, L.-W., Liu, Y.-F., Cao, Xiao-Qing, C., Yan, W., Cui, X.-H., Ye, X., … Zhang, H.-J. (2020). Annexin A2 promotion of hepatocellular carcinoma tumorigenesis via the immune microenvironment. *World Journal of Gastroenterology*, *9327*(18).
163. Ran, F. A., Hsu, P. D., Wright, J., Agarwala, V., Scott, D. A., & Zhang, F. (2013). Genome engineering using the CRISPR-Cas9 system. *Nature Protocols*, *8*(11), 2281–2308. https://doi.org/10.1038/nprot.2013.143
164. Rebouissou, S., & Nault, J. C. (2020). Advances in molecular classification and precision oncology in hepatocellular carcinoma. *Journal of Hepatology*, *72*(2), 215–229. https://doi.org/10.1016/j.jhep.2019.08.017
165. Reig, M., Forner, A., Rimola, J., Ferrer-Fàbrega, J., Burrel, M., Garcia-Criado, Á., … Bruix, J. (2022). BCLC strategy for prognosis prediction and treatment recommendation: The 2022 update. *Journal of Hepatology*, *76*(3), 681–693. https://doi.org/10.1016/j.jhep.2021.11.018
166. Reschke, R., & Gajewski, T. F. (2022). CXCL9 and CXCL10 bring the heat to tumors. *Science Immunology*, *7*(73), 7–10. https://doi.org/10.1126/sciimmunol.abq6509
167. Rodig, S. J., Gusenleitner, D., Jackson, D. G., Gjini, E., Giobbie-Hurder, A., Jin, C., … Hodi, F. S. (2018). MHC proteins confer differential sensitivity to CTLA-4 and PD-1 blockade in untreated metastatic melanoma. *Science Translational Medicine*, *10*(450), 1–14. https://doi.org/10.1126/scitranslmed.aar3342
168. Rötzschke, O., Falk, K., Stevanovic, S., Jung, G., Walden, P., & Rammensee, H. -G. (1991). Exact prediction of a natural T cell epitope. *European Journal of Immunology*, *21*(11), 2891–2894. https://doi.org/10.1002/eji.1830211136
169. Ryan, M. B., de la Cruz, F. F., Phat, S., Myers, D. T., Wong, E., Shahzade, H. A., … Corcoran, R. B. (2020). Vertical pathway inhibition overcomes adaptive feedback resistance to KrasG12C inhibition. *Clinical Cancer Research*, *26*(7), 1617–1643. https://doi.org/10.1158/1078-0432.CCR-19-3523
170. Sade-Feldman, M., Jiao, Y. J., Chen, J. H., Rooney, M. S., Barzily-Rokni, M., Eliane, J. P., … Hacohen, N. (2017). Resistance to checkpoint blockade therapy through inactivation of antigen presentation. *Nature Communications*, *8*(1). https://doi.org/10.1038/s41467-017-01062-w

171. Sakuma, T., Nishikawa, A., Kume, S., Chayama, K., & Yamamoto, T. (2014). Multiplex genome engineering in human cells using all-in-one CRISPR/Cas9 vector system. *Scientific Reports*, *4*, 4–9. https://doi.org/10.1038/srep05400
172. Salaroglio, I. C., Mungo, E., Gazzano, E., Kopecka, J., & Riganti, C. (2019). ERK is a pivotal player of chemo-immune-resistance in cancer. *International Journal of Molecular Sciences*, *20*(10), 1–31. https://doi.org/10.3390/ijms20102505
173. Schmid, M. C., Khan, S. Q., Kaneda, M. M., Pathria, P., Shepard, R., Louis, T. L., … Varner, J. A. (2018). Integrin CD11b activation drives anti-tumor innate immunity. *Nature Communications*, *9*(1), 1–14. https://doi.org/10.1038/s41467-018-07387-4
174. Schulze, C. J., Cregg, J., Seamon, K. J., Yang, Y. C., Wang, Z., Garrenton, L. S., … Smith, J. A. (2022). Abstract 3598: a first-in-class tri-complex KRASG13C(ON) inhibitor validates therapeutic targeting of KRASG13Cand drives tumor regressions in preclinical models. *Cancer Research*, *3958*. Retrieved from https://doi.org/10.1158/%0A1538-7445.AM2022-3598
175. Seidel, J. A., Otsuka, A., & Kabashima, K. (2018). Anti-PD-1 and anti-CTLA-4 therapies in cancer: Mechanisms of action, efficacy, and limitations. *Frontiers in Oncology*, *8*(MAR), 1–14. https://doi.org/10.3389/fonc.2018.00086
176. Sharma, P., Hu-Lieskovan, S., Wargo, J. A., & Ribas, A. (2017). Primary, Adaptive, and Acquired Resistance to Cancer Immunotherapy. *Cell*, *168*(4), 707–723. https://doi.org/10.1016/j.cell.2017.01.017
177. Shi, F., Shi, M., Zeng, Z., Qi, R. Z., Liu, Z. W., Zhang, J. Y., … Wang, F. S. (2011). PD-1 and PD-L1 upregulation promotes CD8+ T-cell apoptosis and postoperative recurrence in hepatocellular carcinoma patients. *International Journal of Cancer*, *128*(4), 887–896. https://doi.org/10.1002/ijc.25397
178. Sia, D., Jiao, Y., Martinez-Quetglas, I., Kuchuk, O., Villacorta-Martin, C., Castro de Moura, M., … Llovet, J. M. (2017). Identification of an Immune-specific Class of Hepatocellular Carcinoma, Based on Molecular Features. *Gastroenterology*, *153*(3), 812–826. https://doi.org/10.1053/j.gastro.2017.06.007
179. Sivan, A., Corrales, L., Hubert, N., Williams, J. B., Aquino-Michaels, K., Earley, Z. M., … Gajewski, T. F. (2015). Commensal Bifidobacterium promotes antitumor immunity and facilitates anti-PD-L1 efficacy. *Science*, *350*(6264), 1084–1089. https://doi.org/10.1126/science.aac4255
180. Specht, K., Harbeck, N., Smida, J., Annecke, K., Reich, U., Naehrig, J., … Hoefler, H. (2009). Expression profiling identifies genes that predict recurrence of breast cancer after adjuvant CMF-based chemotherapy. *Breast Cancer Research and Treatment*, *118*(1), 45–56. https://doi.org/10.1007/s10549-008-0207-y
181. Spranger, S., & Gajewski, T. F. (2018). Impact of oncogenic pathways on evasion of antitumour immune responses. *Nature Reviews Cancer*, *18*(3), 139–147. https://doi.org/10.1038/nrc.2017.117
182. Stefanoudakis, D., Kathuria-Prakash, N., Sun, A. W., Abel, M., Drolen, C. E., Ashbaugh, C., … Drakaki, A. (2023). The Potential Revolution of Cancer Treatment with CRISPR Technology. *Cancers*, *15*(6). https://doi.org/10.3390/cancers15061813
183. Subramanian, A., Tamayo, P., Mootha, V. K., Mukherjee, S., Ebert, B. L., Gillette, M. A., … Mesirov, J. P. (2005). Gene set enrichment analysis: A knowledge-based approach for interpreting genome-wide expression profiles. *Proceedings of the National Academy of Sciences of the United States of America*, *102*(43), 15545–15550. https://doi.org/10.1073/pnas.0506580102
184. Sumimoto, H., Takano, A., Teramoto, K., & Daigo, Y. (2016). RAS-mitogen-activated protein kinase signal is required for enhanced PD-L1 expression in human lung cancers. *PLoS ONE*, *11*(11), 1–18. https://doi.org/10.1371/journal.pone.0166626

185. Sun, J., Althoff, K. N., Jing, Y., Horberg, M. A., Buchacz, K., Gill, M. J., … Kirk, G. D. (2021). Trends in Hepatocellular Carcinoma Incidence and Risk among Persons with HIV in the US and Canada, 1996-2015. *JAMA Network Open*, *4*(2), 1–15. https://doi.org/10.1001/jamanetworkopen.2020.37512
186. Sun, J. Y., Zhang, D., Wu, S., Xu, M., Zhou, X., Lu, X. J., & Ji, J. (2020). Resistance to PD-1/PD-L1 blockade cancer immunotherapy: Mechanisms, predictive factors, and future perspectives. *Biomarker Research*, *8*(1), 1–10. https://doi.org/10.1186/s40364-020-00212-5
187. Sung, H., Ferlay, J., Siegel, R. L., Laversanne, M., Soerjomataram, I., Jemal, A., & Bray, F. (2021). Global Cancer Statistics 2020: GLOBOCAN Estimates of Incidence and Mortality Worldwide for 36 Cancers in 185 Countries. *CA: A Cancer Journal for Clinicians*, *71*(3), 209–249. https://doi.org/10.3322/caac.21660
188. Suyama, T., Furuya, M., Nishiyama, M., Kasuya, Y., Kimura, S., Ichikawa, T., … Ishikura, H. (2005). Up-regulation of the interferon γ (IFN-γ)-inducible chemokines IFN-inducible T=cell α chemoattractant and monokine induced by IFN-γ and of their receptor CXC receptor 3 in human renal cell carcinoma. *Cancer*, *103*(2), 258–267. https://doi.org/10.1002/cncr.20747
189. Takahashi, A., Umemura, A., Yano, K., Okishio, S., Kataoka, S., Okuda, K., … Itoh, Y. (2021). Tyrosine Kinase Inhibitors Stimulate HLA Class I Expression by Augmenting the IFNγ/STAT1 Signaling in Hepatocellular Carcinoma Cells. *Frontiers in Oncology*, *11*(August), 1–12. https://doi.org/10.3389/fonc.2021.707473
190. Tan, Y., Xu, Q., Wu, Z., Zhang, W., Li, B., Zhang, B., … Yan, L. (2022). Overexpression of PD-L1 is an Independent Predictor for Recurrence in HCC Patients Who Receive Sorafenib Treatment After Surgical Resection. *Frontiers in Oncology*, *11*(January), 1–11. https://doi.org/10.3389/fonc.2021.783335
191. Taylor, B. C., & Balko, J. M. (2022). Mechanisms of MHC-I Downregulation and Role in Immunotherapy Response. *Frontiers in Immunology*, *13*(February), 1–11. https://doi.org/10.3389/fimmu.2022.844866
192. Thomas, C. E., Ehrhardt, A., & Kay, M. A. (2003). Progress and problems with the use of viral vectors for gene therapy. *Nature Reviews Genetics*, *4*(5), 346–358. https://doi.org/10.1038/nrg1066
193. Turhal, N. S., Savaş, B., Çoşkun, Ö., Baş, E., Karabulut, B., Nart, D., … Artaç, M. (2015). Prevalence of K-Ras mutations in hepatocellular carcinoma: A Turkish Oncology Group pilot study. *Molecular and Clinical Oncology*, *3*(6), 1275–1279. https://doi.org/10.3892/mco.2015.633
194. Umemoto, Y., Okano, S., Matsumoto, Y., Nakagawara, H., Matono, R., Yoshiya, S., … Maehara, Y. (2015). Prognostic impact of programmed cell death 1 ligand 1 expression in human leukocyte antigen class I-positive hepatocellular carcinoma after curative hepatectomy. *Journal of Gastroenterology*, *50*(1), 65–75. https://doi.org/10.1007/s00535-014-0933-3
195. Vella, L. J., Pasam, A., Dimopoulos, N., Andrews, M., Knights, A., Puaux, A. L., … Cebon, J. S. (2014). MEK inhibition, alone or in combination with BRAF inhibition, affects multiple functions of isolated normal human lymphocytes and dendritic cells. *Cancer Immunology Research*, *2*(4), 351–360. https://doi.org/10.1158/2326-6066.CIR-13-0181
196. Vergnes, L., Argus, J. P., Marbois, B. N., Komisopoulou, E., Osborne, T. F., Graeber, T. G., … Program, D. (2013). The sterol regulatory element binding proteins are essential for the metabolic programming of effector T cells and adaptive immunity Yoko, *14*(5), 489–499. https://doi.org/10.1038/ni.2570.The
197. Wabitsch, S., Tandon, M., Ruf, B., Zhang, Q., McCallen, J. D., McVey, J. C., … Greten, T. F. (2021). Anti–PD-1 in Combination With Trametinib Suppresses Tumor Growth and

Improves Survival of Intrahepatic Cholangiocarcinoma in Mice. *Cmgh*, *12*(3), 1166–1178. https://doi.org/10.1016/j.jcmgh.2021.05.011
198. Wang, B., Niu, D., Lai, L., & Ren, E. C. (2013). P53 increases MHC class i expression by upregulating the endoplasmic reticulum aminopeptidase ERAP1. *Nature Communications*, *4*. https://doi.org/10.1038/ncomms3359
199. Wang, C. Y., & Li, S. (2019). Clinical characteristics and prognosis of 2887 patients with hepatocellular carcinoma : A single center 14 years experience from China. *Medicine (United States)*, *98*(4). https://doi.org/10.1097/MD.0000000000014070
200. Wang, H., Franco, F., Tsui, Y. C., Xie, X., Trefny, M. P., Zappasodi, R., … Ho, P. C. (2020). CD36-mediated metabolic adaptation supports regulatory T cell survival and function in tumors. *Nature Immunology*, *21*(3), 298–308. https://doi.org/10.1038/s41590-019-0589-5
201. Wang, L., Li, F., Dang, L., Liang, C., Wang, C., He, B., … Zhang, G. (2016). In Vivo delivery systems for therapeutic genome editing. *International Journal of Molecular Sciences*, *17*(5). https://doi.org/10.3390/ijms17050626
202. Wang, X., Allen, S., Blake, J. F., Bowcut, V., Briere, D. M., Calinisan, A., … Marx, M. A. (2022). Identification of MRTX1133, a Noncovalent, Potent, and Selective KRASG12D Inhibitor. *J Med Chem*, *65*(4), 3123–3133. https://doi.org/10.1021/acs.jmedchem.1c01688.
203. Wang, Y., Guo, Z., Isah, A. D., Chen, S., Ren, Y., & Cai, H. (2023). Lipid metabolism and tumor immunotherapy. *Frontiers in Cell and Developmental Biology*, *11*(May), 1–13. https://doi.org/10.3389/fcell.2023.1187989
204. Ward, A. B., Keeton, A. B., Chen, X., Mattox, T. E., Coley, A. B., Maxuitenko, Y. Y., … Piazza, G. A. (2020). Enhancing anticancer activity of checkpoint immunotherapy by targeting RAS. *MedComm*, *1*(2), 121–128. https://doi.org/10.1002/mco2.10
205. Westcott, P. M. K., Sacks, N. J., Schenkel, J. M., Ely, Z. A., Smith, O., Hauck, H., … Jacks, T. (2021). *Low neoantigen expression and poor T-cell priming underlie early immune escape in colorectal cancer*. *Nature Cancer* (Vol. 2). https://doi.org/10.1038/s43018-021-00247-z
206. Whiting, D., Hsieh, G., Yun, J. J., Banerji, A., Yao, W., Fishbein, M. C., … Bonavida, B. (2007). Chemokine Monokine Induced by IFN-γ/CXC Chemokine Ligand 9 Stimulates T Lymphocyte Proliferation and Effector Cytokine Production. *J Immunol*, *178*(4), 2278–2286.
207. World Health Organisation. (2020). *Immunization Agenda 2030: A Global Strategy to Leave No One Behind*. *World Health Organisation.* Geneva, Switzerland.
208. Wu, J., Zhang, X. J., Shi, K. Q., Chen, Y. P., Ren, Y. F., Song, Y. J., … Tang, K. F. (2014). Hepatitis B surface antigen inhibits MICA and MICB expression via induction of cellular miRNAs in hepatocellular carcinoma cells. *Carcinogenesis*, *35*(1), 155–163. https://doi.org/10.1093/carcin/bgt268
209. Xu, A., Wang, B., Fu, J., Qin, W., Yu, T., Yang, Z., … Wang, H. (2019). Diet-induced hepatic steatosis activates Ras to promote hepatocarcinogenesis via CPT1α. *Cancer Letters*, *442*(October 2018), 40–52. https://doi.org/10.1016/j.canlet.2018.10.024
210. Yamaguchi, T., Kakefuda, R., Tanimoto, A., Watanabe, Y., & Tajima, N. (2012). Suppressive effect of an orally active MEK1/2 inhibitor in two different animal models for rheumatoid arthritis: A comparison with leflunomide. *Inflammation Research*, *61*(5), 445–454. https://doi.org/10.1007/s00011-011-0431-5
211. Yan, W., Liu, X., Ma, H., Zhang, H., Song, X., Gao, L., … Ma, C. (2015). Tim-3 fosters HCC development by enhancing TGF-β-mediated alternative activation of macrophages. *Gut*, *64*(10), 1593–1604. https://doi.org/10.1136/gutjnl-2014-307671
212. Yan, Y., Zheng, L., Du, Q., Cui, X., Dong, K., Guo, Y., & Geller, D. A. (2021). Interferon regulatory factor 1 (IRF-1) downregulates Checkpoint kinase 1 (CHK1) through

miR-195 to upregulate apoptosis and PD-L1 expression in Hepatocellular carcinoma (HCC) cells. *British Journal of Cancer*, *125*(1), 101–111. https://doi.org/10.1038/s41416-021-01337-6

213. Yan, Y., Zheng, L., Du, Q., Yan, B., & Geller, D. A. (2020). Interferon regulatory factor 1 (IRF-1) and IRF-2 regulate PD-L1 expression in hepatocellular carcinoma (HCC) cells. *Cancer Immunology, Immunotherapy*, *69*(9), 1891–1903. https://doi.org/10.1007/s00262-020-02586-9
214. Yan, Y., Zheng, L., Du, Q., Yan, B., & Geller, D. A. (2021). Interferon Regulatory Factor 1(IRF-1) activates anti-tumor immunity via CXCL10/CXCR3 axis in Hepatocellular Carcinoma (HCC). *Cancer Lett.*, *506*(1), 95–106. https://doi.org/10.1016/j.canlet.2021.03.002.Interferon
215. Yang, C., Zhang, H., Zhang, L., Zhu, A. X., Bernards, R., Qin, W., & Wang, C. (2023). Evolving therapeutic landscape of advanced hepatocellular carcinoma. *Nature Reviews Gastroenterology and Hepatology*, *20*(4), 203–222. https://doi.org/10.1038/s41575-022-00704-9
216. Yau, T., Park, J. W., Finn, R. S., Cheng, A.-L., Mathurin, P., Edeline, J., … Sangro, B. (2019). CheckMate 459: A randomized, multi-center phase III study of nivolumab (NIVO) vs sorafenib (SOR) as first-line (1L) treatment in patients (pts) with advanced hepatocellular carcinoma (aHCC). *Annals of Oncology*, *30*(October), v874–v875. https://doi.org/10.1093/annonc/mdz394.029
217. Yoshihama, S., Cho, S. X., Yeung, J., Pan, X., Lizee, G., Konganti, K., … Kobayashi, K. S. (2021). NLRC5/CITA expression correlates with efficient response to checkpoint blockade immunotherapy. *Scientific Reports*, *11*(1), 1–12. https://doi.org/10.1038/s41598-021-82729-9
218. Yoshihama, S., Roszik, J., Downs, I., Meissner, T. B., Vijayan, S., Chapuy, B., … Kobayashi, K. S. (2016). NLRC5/MHC class I transactivator is a target for immune evasion in cancer. *Proceedings of the National Academy of Sciences of the United States of America*, *113*(21), 5999–6004. https://doi.org/10.1073/pnas.1602069113
219. Yu, S., Zi, X., Zhu, Q., Zheng, Y., Wu, C., Ren, H., … Zheng, Y. J. (2022). Accelerating Decreases in the Incidences of Hepatocellular Carcinoma at a Younger Age in Shanghai Are Associated With Hepatitis B Virus Vaccination. *Frontiers in Oncology*, *12*(April), 1–8. https://doi.org/10.3389/fonc.2022.855945
220. Zaretsky, J. M., Garcia-Diaz, A., Shin, D. S., Escuin-Ordinas, H., Hugo, W., Hu-Lieskovan, S., … Ribas, A. (2016). Mutations Associated with Acquired Resistance to PD-1 Blockade in Melanoma. *New England Journal of Medicine*, *375*(9), 819–829. https://doi.org/10.1056/nejmoa1604958
221. Zender, L., Xue, W., Cordón-Cardo, C., Hannon, G. J., Lucito, R., Powers, S., … Lowe, S. W. (2005). Generation and analysis of genetically defined liver carcinomas derived from bipotential liver progenitors. *Cold Spring Harbor Symposia on Quantitative Biology*, *70*, 251–261. https://doi.org/10.1101/sqb.2005.70.059
222. Zhang, W., Liu, Y., Yan, Z., Yang, H., Sun, W., Yao, Y., … Jiang, R. (2020). IL-6 promotes PD-L1 expression in monocytes and macrophages by decreasing protein tyrosine phosphatase receptor type O expression in human hepatocellular carcinoma. *Journal for Immunotherapy of Cancer*, *8*(1), 1–14. https://doi.org/10.1136/jitc-2019-000285
223. Zhang, Z., Guiley, K. Z., & Shokat, K. M. (2022). Chemical acylation of an acquired serine suppresses oncogenic signaling of K-Ras(G12S). *Nature Chemical Biology*, *18*(11), 1177–1183. https://doi.org/10.1038/s41589-022-01065-9
224. Zhao, Y., Cao, Y., Chen, Y., Wu, L., Hang, H., Jiang, C., & Zhou, X. (2021). B2M gene expression shapes the immune landscape of lung adenocarcinoma and determines the response to immunotherapy. *Immunology*, *164*(3), 507–523.

https://doi.org/10.1111/imm.13384
225. Zheng, Y., Wang, T., Tu, X., Huang, Y., Zhang, H., Tan, D., … Fang, W. (2019). Gut microbiome affects the response to anti-PD-1 immunotherapy in patients with hepatocellular carcinoma. *Journal for ImmunoTherapy of Cancer*, *7*(1), 1–7. https://doi.org/10.1186/s40425-019-0650-9
226. Zhou, J., Wang, J., Shen, B., Chen, L., Su, Y., Yang, J., … Huang, X. (2014). Dual sgRNAs facilitate CRISPR/Cas9-mediated mouse genome targeting. *FEBS Journal*, *281*(7), 1717–1725. https://doi.org/10.1111/febs.12735
227. Zhu, C., Guan, X., Zhang, X., Luan, X., Song, Z., Cheng, X., … Qin, J. J. (2022). Targeting KRAS mutant cancers: from druggable therapy to drug resistance. *Molecular Cancer*, *21*(1), 1–19. https://doi.org/10.1186/s12943-022-01629-2
228. Zhu, K., Wang, J., Zhu, J., Jiang, J., Shou, J., & Chen, X. (1999). p53 induces TAP1 and enhances the transport of MHC class I peptides. *Oncogene*, *18*(54), 7740–7747. https://doi.org/10.1038/sj.onc.1203235
229. Zong, Z., Zou, J., Mao, R., Ma, C., Li, N., Wang, J., … Shi, Y. (2019). M1 macrophages induce PD-L1 expression in hepatocellular carcinoma cells through IL-1β signaling. *Frontiers in Immunology*, *10*, 1–12. https://doi.org/10.3389/fimmu.2019.01643
230. Zou, H., Li, M., Lei, Q., Luo, Z., Xue, Y., Yao, D., … Hu, H. (2022). Economic Burden and Quality of Life of Hepatocellular Carcinoma in Greater China: A Systematic Review. *Frontiers in Public Health*, *10*(April). https://doi.org/10.3389/fpubh.2022.801981